Genomic Profiling Of Metastatic Castration-Resistant Prostate Cancer

Naoual Menssouri

THESE DE DOCTORAT

NNT : 2022UPASL099

université PARIS-SACLAY

Genomic Profiling Of Metastatic Castration-Resistant Prostate Cancer

Profilage génomique du cancer de la prostate résistant à la castration

Thèse de doctorat de l'université Paris-Saclay

École doctorale n° 582 : Cancérologie : biologie - médecine - santé (CBMS)
Spécialité de doctorat : Sciences de la vie et de la santé
Graduate School : Life Sciences and Health. Référent : Faculté de médecine

Thèse préparée dans l'unité de reherche :
Prédicteurs moléculaires et nouvelles cibles en oncologie (Université Paris-Saclay, Institut Gustave Roussy, Inserm),
sous la direction de **Karim FIZAZI**, PU-PH et la co-direction de **Yohann LORIOT**, Médecin des centres

Thèse soutenue à Villejuif, le 21 décembre 2022, par

Naoual MENSSOURI

Composition du Jury

Membres du jury avec voix délibérative

Stéphane OUDARD PU-PH, Université Paris Descartes. Paris, FR	Président & Rapporteur
Gabriel MALOUF PU-PH, Université de Strasbourg. Strasbourg, FR	Rapporteur & Examinateur
Antoine THIERY-VUILLEMIN MCU-PH, Université de Besançon. Besançon, FR	Examinateur
Géraldine PIGNOT Médecin des centres. Marseille, FR	Examinatrice

ACKNOWLEDGEMENTS

Mes premiers remerciements vont à mon Directeur de thèse le Professeur Karim Fizazi et à mon superviseur le Docteur Yohann Loriot qui m'ont permis d'accomplir ce projet dans les meilleures conditions. Ce doctorat m'a donné la possibilité de découvrir la profession de chercheur ainsi que d'allier des concepts cliniques, biologiques, statistiques et informatiques au service d'un sujet de recherche innovant et passionnant.

Je remercie tout particulièrement le Docteur Yohann Loriot, de m'avoir toujours poussée à me surpasser, depuis le début, et jusqu'à ce jour. Je me rends compte maintenant des progrès que j'ai réalisés grâce à lui, moi qui ne connaissais que peu la recherche translationnelle à mon arrivée à Gustave Roussy.

Je remercie également le Directeur de l'unité INSERM U981 le Professeur Fabrice André et le Directeur de la plateforme bioinformatique le Docteur Marc Deloger de m'avoir accueillie au sein de leurs laboratoires et permis d'interagir avec leurs équipes.

Un grand merci au programme « dons et legs » de Gustave Roussy d'avoir financé mon doctorat.

Je tiens également à remercier tous les patients et leurs familles pour leur participation à notre recherche.

Par ailleurs, je tiens à remercier tous nos collaborateurs pour leur précieuse contribution.

Je tiens à remercier les membres du jury de ma soutenance de thèse, qui ont accepté d'évaluer ce projet et d'être présents à sa réalisation, à savoir le Président du jury et rapporteur, le Professeur Stéphane Oudard ; le Professeur Gabriel Malouf, rapporteur de ce manuscrit ; et les Docteurs Géraldine Pignot et Antoine Thiery Vuilllemin, examinateurs.

J'adresse ma gratitude aux membres du comité de suivi de ma thèse, le Professeur Ivan Bièche, le Professeur Yves Allory et le Docteur Céline Lefebvre pour leurs commentaires constructifs afin de mener à bien mon projet de recherche.

Je souhaite aussi exprimer ma gratitude à Madame Léa Poisot de l'École doctorale de Cancérologie: Biologie, Médecine, Santé (CBMS-ED418), pour avoir facilité mes démarches administratives.

Je tiens également à remercier l'ensemble de mes collègues de l'unité U980, de la plateforme de bioinformatique, et d'autres collègues, de qui j'ai beaucoup appris, non seulement sur le plan professionnel, mais aussi sur le plan personnel.

Une pensée particulière pour tous mes amis, proches ou éloignés, qui m'ont apporté beaucoup de soutien et de bonheur ces dernières années, particulièrement difficiles sur le plan personnel, au-delà des épisodes d'enfermement liés au covid. Vous avez contribué tous directement ou indirectement à la réalisation de mon doctorat, je vous en remercie infiniment.

Ce travail ne serait jamais envisageable sans l'aide et la patience de mes proches et notamment mes parents et mes sœurs qui m'ont soutenue de leur amour inconditionnel et qui m'ont accordé leur confiance au cours de cette longue et incroyable aventure universitaire.

« An expert is a man who has made all the mistakes that can be made in a very narrow field »

— ***Niels Bohr*** —

PUBLICATIONS AND PRESENTATIONS INCLUDED IN THIS THESIS

Publications

Naoual Menssouri, Loïc Poiraudeau, Carole Hellisey, Ludovic Bigot, Jonathan Sabio, Tony Ibrahim, Cédric Pobel, Claudio Nicotra, Maud Ngo-Camus, Ludovic Lacroix, Etienne Rouleau, Lambros Tselikas, Anne Chauchereau, Félix Blanc-Durand, Alice Bernard-Tessier, Anna Patrikidou, Natacha Naoun, Ronan Flippot, Emeline Colomba, Alina Fuerea, Laurence Albiges, Pernelle Lavaud, Paul van de Wiel, Eveline den Biezen-Timmermans, Yvonne Wesseling-Rozendaal, Stefan Michiels, Christophe Massard, Fabrice Barlesi, Fabrice André, Benjamin Besse, Jean-Yves Scoazec, Luc Friboulet, Karim Fizazi, and Yohann Loriot. **Genomic profiling of metastatic castration-resistant prostate cancer samples resistant to androgen-receptor pathway inhibitors**. *Submitted to Cancer Discovery,* 2022

Posters

Naoual Menssouri, Yvonne Wesseling-Rozendaal, Loïc Poiraudeau, Carole Helissey, Ludovic Bigot, Jonathan Sabio,Tony Ibrahim, Claudio Nicotra, Lambros Tselikas, Emeline Colomba, Pernelle Lavaud, Benjamin Besse, Jean-Yves Scozec, Eveline den Biezen-Timmermans, Sigi Neerken, Karim Fizazi, Daniel Gautheret, Paul van de Wiel, and Yohann Loriot. **High Sonic Hedgehog (Hh) signaling activity, low androgen receptor activity and clonal evolution are associated with resistance to androgen receptor axis inhibitors in patients with metastatic prostate cancer**. *Annals of Oncology*, *33*, S1173, 2022 (European Society for Medical Oncology (ESMO))

Naoual Menssouri, Loïc Poiraudeau, Carole Helissey, Ludovic Bigot, Jonathan Sabio, Tony Ibrahim, Claudio Nicotra, Maud Ngocamus, Lambros Tselikas, Thierry De Baere,

Etienne Rouleau, Ludovic Lacroix, Anne Chauchereau, Luc Friboulet, Ronan Flippot, Giulia Baciarello, Laurence Albiges, Emeline Colomba, Pernelle Lavaud, Stefan Michiels, Aline Maillard, Antoine Italiano, Fabrice Barlesi, Jean-Charles Soria, Jean-Yves Scoazec, Christophe Massard, Benjamin Besse, Fabrice André, Karim Fizazi, Daniel Gautheret, and Yohann Loriot. **A prospective study of prostate cancer metastases identifies an androgen receptor activity-low, stemness program associated with resistance to androgen receptor axis inhibitors and unveils mechanisms of clonal evolution**. *Cancer Research*, 81(13_Supplement), 358-358, 2021 (American Association for Cancer Research (AACR) and French Open Days in Biology, Computer Science and Mathematics (JOBIM))

Naoual Menssouri, Karim Fizazi, Fabrice André, and Yohann Loriot. **Mechanisms of resistance to therapies targeting the androgen receptor pathway in prostate cancer**. Curie Institute, Worksop on computational systems biology of cancer, 2019

Oral presentations

Naoual Menssouri. **Genomic Profiling Of Metastatic Castration-Resistant Prostate Cancer**. Association of Young Researchers of Gustave Roussy ("Association des Jeunes Chercheurs de Gustave Roussy (AJC)"), Gustave Roussy, 2022

Naoual Menssouri. **Genomic profiling of metastatic castration-resistant prostate cancer samples resistant to androgen-receptor pathway inhibitors**. Genitourinary scientific committee, Gustave Roussy, 2022

Naoual Menssouri. **Genomic characterisation of lethal forms of metastatic castration-resistant prostate cancer and its mechanisms of resistance to therapies targeting the androgen receptor pathway**. Molecular predictors and new targets in oncology, INSERM U981 seminars, Gustave Roussy, 2022

Naoual Menssouri. **Genomic characterisation of metastatic prostate cancer**. Gustave Roussy Bioinformatics Platform Club, 2021-2022

Naoual Menssouri. **Prostate cancer research projects**. Molecular predictors and new targets in oncology, INSERM U981, Gustave Roussy, donor day of Gustave Roussy, 2019-2022

Contribution to other publications

Ludovic Bigot, Jonathan Sabio, Loïc Poiraudeau, Maxime Annereau, **Naoual Menssouri**, Carole Hellisey, Olivier Déas, Marine Aglave, Tony Ibrahim, Cédric Pobel, Claudio Nicotra, Maud Ngo-Camus, Ludovic Lacroix, Etienne Rouleau, Lambros Tselikas, Jean-Gabriel Judde, Anne Chauchereau, Alice Bernard-Tessier, Anna Patrikidou, Natacha Naoun, Ronan Flippot, Emeline Colomba, Alina Fuerea, Laurence Albiges, Pernelle Lavaud, Christophe Massard, Luc Friboulet, Karim Fizazi, Benjamin Besse, Jean-Yves Scoazec, and Yohann Loriot. **Development of novel models of aggressive variants of castrate-resistant prostate cancer**. *Submitted to Clinical Cancer Research, 2022*

Igor Duquesne, **Naoual Menssouri**, Noemie Pata-Merci, R. Tang, Maud Ngo-Camus, Claudio Nicotra, Jean-Yves Scoazec, Christophe Massard, Benjamin Besse, Etienne Rouleau, and Yohann Loriot. **Concordance of plasmatic circulating DNA and matched metastatic tissue in metastatic urothelial carcinoma**. *European Urology Open Science,* 19: e200, 2020

Contribution to other oral presentations

Ludovic Bigot, Jonathan Sabio, Tony Ibrahim, **Naoual Menssouri**, Loïc Poiraudeau, Carole Helissey, Jean-Yves Scoazec, Zahira Merabet, Thierry De Baere, Frederic

Deschamps, Maud Ngocamus, Claudio Nicotra, Etienne Rouleau, Ludovic Lacroix, Olivier Deas, Luc Friboulet, Gilles Vassal, Eric Solary, Jean-Charles Soria, Karim Fizazi, Fabrice André, Christophe Massard, Benjamin Besse, Yohann Loriot. **Novel preclinical models of aggressive variants of castration-resistant prostate cancer**. *Cancer Research*, 80(16_Supplement), 1114-1114, 2020 (AACR)

Futur related projects and collaborations

Yohann Loriot, Maud Kamal, Laurene Syx, Remy Nicolle, Celia Dupain, **Naoual Menssouri**, Igor Duquesne, Claudio Nicotra, Maud Ngocamus, Ludovic Lacroix, Lambros Tselikas, Gilles Créhange, Francesco Ricci,Yann Neuzillet, Edith Borcomann, Philippe Beuzeboc, Patricia Tresca, Tom Gutman, Jennifer Wong, Jean-Charles Soria, Francois Radvanyi, Jean-Yves Scoazec, Christophe Massard, Nicolas Servant, Yves Allory, Christophe Le Tourneau, Fabrice André, and Ivan Bièche. **The Genomic and immune landscape of metastatic urothelial Cancers**. *In preparation*

Loïc poiraudeau, **Naoual Menssouri**, Ludovic Bigot, Jonathan Sabio, Tony Ibrahim, Anne Chauchereau, Lambros Tselikas, Claudio Nicotra, Benjamin Besse, Karim Fizazi, Jean-Yves Scoazec, Bauchet AL, and Yohann Loriot. **CEACAM-5 as a new therapeutic target in neuroendocrine prostate cancer**. *In preparation*

TABLE OF CONTENTS

LIST OF FIGURES

LIST OF TABLES

ABBREVIATIONS

3D	3 dimensions
5ADHT	5-α-dihydrotestosterone
AA	Abiraterone acetate
AD	Androstenedione
ADK	Adenocarcinoma
ADP-ribose	Adenosine diphosphate ribose
ADT	Androgen-deprivation therapy
AE	Adverse events
AJCC	American joint committee on cancer
AMP	Amplification
APOBEC	Apolipoprotein B mRNA editing enzyme
array-CGH	Array comparative genomic hybridization
AR	Androgen receptor
ARE	Androgen response element
AR-FL	Full-length androgen receptor
ARPI	Androgen receptor pathway inhibitor
AR-V7	Androgen receptor splicing variant 7
AR-Vs	Androgen receptor splicing variants
ASR	Age-standardized rates
BAF	B allele frequency
BH	Benjamini hochberg
bp	Base pair
BPH	Benign prostate hyperplasia
BWA	Burrows-wheeler aligner
CAFs	Cancer-associated fibroblasts
CBS	Circular binary segmentation
CCF	Cancer cell fraction
cfDNA	Cell free DNA
CI	Confidence interval
CNV	Copy number variation
COAs	Co-activators
CPI	Checkpoint inhibitor
CPM	Counts per million mapped reads
CR	Complete response
CRPC	Castration-resistant prostate cancer
CT	Computed tomography
CTAT	Cancer transcriptome analysis toolkit
CYP17A1	Cytochrome P450 17A1
DBD	DNA-binding domain
dbGaP	Database of genotypes and phenotypes
DDR	DNA damage repair
DEG	Differentially expressed genes

DEL	Deletion
DFS	Disease-free survival
DGE	Differential gene expression
DHEA/S	Dehydroepiandrosterone/sulphate
DHT	Dihydrotestosterone
DMEM	Dulbecco's modified eagle's medium
dMMR	Mismatch repair deficiency
DMSO	Dimethyl sulfoxide
DNA	Deoxyribo nucleic acid
DRE	Digital rectal examination
DSS	Disease-specific survival
EBRT	External beam radiotherapy
ECM	Extracellular matrix
edgeR	Empirical analysis of digital gene expression data in R
EMA	European medicines agency
EMT	Epithelial–mesenchymal transition
ESCAT	ESMO scale for clinical actionability of molecular targets
FAA	Fraction of chromosome arms altered
FAG	Fraction of altered genome
FDA	Food and drug administration
FDR	False discovery rate
FPKM	Fragments per kilo base/million mapped reads
GAP	Genome alteration print
GATK	Genome analysis toolkit
GGs	Grade group
GO	Gene ontology
GRCh38	Homo sapiens (human) genome assembly *GRCh38* (hg38)
GSEA	Gene set enrichment analysis
GY	Gray, dose unit of ionizing radiation
H&E	Hematoxylin and eosin
Hh	Sonic hedgehog signaling pathway
HRR	Homologous recombination repair
HR	Hinge region
HR	Hazard ratio
IC50	Half maximal inhibitory concentration
IGV	Integrative genomics viewer
IHC	Immunohistochemistry
IMRT	Intensity modulated conformal radiotherapy
indel	Insertion/deletion
IQR	Interquartile range
IRB	Institutional review board
ISUP	International society of urological pathology
Kb	Kilobase
LBD	Ligand-binding domain
LHRH	Luteinizing hormone releasing hormone
LIMMA	Linear models for microarray data

lincRNA	Long noncoding RNA
LNCaP	Lymph node carcinoma of the prostate cell line
LOH	Loss of heterozygosity
LRR	Log R ratio
mCRPC	Metastatic castration-resistant prostate cancer
mCSPC	Metastatic castration-sensitive prostate cancer
MFS	Metastasis-free survival
mHSPC	Metastatic hormone-sensitive prostate cancer
MMR	Mismatch-Repair
mPC	Metastatic prostate cancer
mpMRI	Multi-parametric magnetic resonance imaging
MRI	Magnetic resonance imaging
mRNA	Messenger ribonucleic acid
MSI/H	Microsatellite instability/high
MsigDB	Molecular signatures database
NE/PC	Neuroendocrine/prostate cancer
NES	Normalized enrichment score
NGS	New generation sequencing
NK cells	Natural killer cells
nmCRPC	non-metastatic castration-resistant prostate cancer
NTD	N-terminal domain
OS	Overall survival
PCA	Principal components analysis
PCR	Polymerase chain reaction
PDO	Patient-derived organoid
PDX	Patient derived xenografts
PDXO	Patient-derived xenograft organoid
PET	Positron emission tomography
PFS	Progression free survival
PolyPhen	Polymorphism phenotyping
PR	Partial response
PRAC	Pharmacovigilance risk assessment committee
PSA	Prostate specific antigen
PSMA	Prostate-specific membrane antigen
QC	Quality control
QPCR	Quantitative polymerase chain reaction
QSS	Sum of base quality scores for each allele
RECIST	Response evaluation criteria in solid tumors
RIN	RNA integrity number
RNA	Ribonucleic Acid
RNA Pol II	RNA polymerase II
RNA-seq	RNA sequencing
rRNA	Ribosomal RNA
RSEM	RNA-seq by expectation-maximization
RTA	Real-time analysis
SCC	Small cell carcinoma

scRNA-seq	Single cell RNA sequencing
SD	Stable response
SNP	Single nucleotide polymorphism
SNV	Single nucleotide variant
SIFT	Sorting intolerant from tolerant
TCGA	The cancer genome atlas
TMB	Tumor mutational burden
TME	Tumor microenvironment
TMM	Trimmed mean of M-values
TNM	Tumor-nodes-metastasis
TPM	Transcripts per kilobase million
Tregs	Regulatory T cells
t-SCNC	Treatment emergent small cell neuroendocrine prostate cancer
UMAP	Uniform manifold approximation and projection space
UMI	Unique molecular identifier
VAF	Variant allele fraction
VEP	Ensembl variant effect predictor
WES	Whole exome sequencing
WGS	Whole genome sequencing

LIST OF GENES AND PROTEINS

3β-HSD	3β-Hydroxysteroid dehydrogenase
ADAMTS8	ADAM Metallopeptidase With Thrombospondin Type 1 Motif 8
AKR1C3	Aldo-Keto Reductase Family 1 Member C3
AKT/1	AKT Serine/Threonine Kinase 1
APC	Adenomatosis Polyposis Coli Tumor Suppressor
APLP2	Amyloid Beta Precursor Like Protein 2
AR	Androgen receptor
ARID2/4A	ARID Domain-Containing Protein 2/AT-Rich Interactive Domain-Containing Protein 4A
ATM	Ataxia Telangiectasia Mutated
ATR	Ataxia Telangiectasia And Rad3-Related Protein
AURKA	Aurora kinase A
AXIN1/2	Axin 1/2
BAG1	BAG Cochaperone 1
BARD1	BRCA1 Associated RING Domain 1
BRCA1/2	Breast And Ovarian Cancer Susceptibility Protein 1/2
BRIP1	BRCA1 Interacting Helicase 1
BRAF	B-Raf Proto-Oncogene
BRN2	alias of POU3F2: POU Class 3 Homeobox 2
CBP	alias of CREBBP: CREB Binding Protein
CCND1/E1	Cyclin D1/E1
CD56	alias of NCAM1: Neural Cell Adhesion Molecule 1
CD4	T-Cell Surface Glycoprotein CD4
CDH1/6/7/12	Cadherin 1/6/7/12
CDK6/12	Cyclin Dependent Kinase 6/12
CHD6/7	Chromodomain Helicase DNA Binding Protein 6/7
CHEK1/2	Checkpoint Kinase 1/2
CHGA	Chromogranin A
CK5/8/14/18	Keratin 5/8/14/18
COL5A1	Collagen Type V Alpha 1 Chain
CSMD1	CUB And Sushi Multiple Domains 1
CTLA-4	Cytotoxic T-Lymphocyte Associated Protein 4
CTNNB1	Catenin Beta 1
CYP17A1/11A1	Cytochrome P450 Family 17/11 Subfamily A Member 1
DHEA-S	dehydroepiandrosterone sulfate
DHT	5-alpha-dihydrotestosterone
DLL3	Delta Like Canonical Notch Ligand 3
E2F	E2F family of transcription factors
ER	Estrogen Receptor 1
ERF	ETS2 Repressor Factor
ERG	ETS Transcription Factor ERG
ETV3	ETS Variant Transcription Factor 3
EZH2	Enhancer Of Zeste 2 Polycomb Repressive Complex 2 Subunit
FANCL	FA Complementation Group L
FLI1	Fli-1 Proto-Oncogene, ETS Transcription Factor
FOXA1	Forkhead Box A1
GEMIN5	Gem Nuclear Organelle Associated Protein 5
GLI1/3	GLI Family Zinc Finger 1/3
GnRH/R	Gonadotropin Releasing Hormone 1/Receptor

GPC6	Glypican 6
GR	Glucocorticoid Receptor, alias of NR3C1: Nuclear Receptor Subfamily 3 Group C Member 1
HOXB5/6	Homeobox B5/6
HSP	Heat Shock Protein
IFNα/γ	Interferon alpha/gamma
IGF1R/2R	Insulin Like Growth Factor 1/2 Receptor
IL6	Interleukin 6
ITSN1	Intersectin 1
JAK/1	Janus Kinase 1
KAT6B	Lysine Acetyltransferase 6B
KLK2/3	Kallikrein Related Peptidase 2/3
KMT2A/2C/2D	Lysine Methyltransferase 2A/2C/2D
LH	Luteizing Hormone
MAPK	Mitogen-activated protein kinase
MATN4	Matrilin 4
MED12	Mediator Complex Subunit 12
MEK1	Mitogen-Activated Protein Kinase Kinase 1
MLH1	MutL Homolog 1
MR	alias of NR3C2: Nuclear Receptor Subfamily 3 Group C Member 2
MSH2/6	MutS Homolog 2/6
MTOR	Mechanistic Target Of Rapamycin Kinase
MYC	MYC Proto-Oncogene, BHLH Transcription Factor
MYCN	MYCN Proto-Oncogene, BHLH Transcription Factor
NCOR1/2	Nuclear Receptor Corepressor 1/2
NF1	Neurofibromin 1
NOTCH	NOTCH gene family
NFκB1/2	Nuclear Factor Kappa B Subunit ½
NR1D2	Nuclear Receptor Subfamily 1 Group D Member 2
NSE	alias of ENO2: Enolase 2
ONECUT2	One Cut Homeobox 2
P63	Tumor Protein P63
PALB2	Partner And Localizer Of BRCA2
PARP1/2	Poly(ADP-Ribose) Polymerase 1/2
PD-1/L1	Programmed Cell Death 1/Ligand 1
PEG10	Paternally Expressed 10
PGR	Progesterone Receptor
PIK3CA/CB/R1	Phosphatidylinositol-4,5-Bisphosphate 3-Kinase Catalytic Subunit Alpha/Beta/ Phosphoinositide-3-Kinase Regulatory Subunit 1
PMS1/2	PMS1/2 Homolog 1/2, Mismatch Repair System Component
PPP2R2A	Protein Phosphatase 2 Regulatory Subunit Balpha
PSA	alias of KLK3: Kallikrein Related Peptidase 3
PTCH1	Patched 1
PTEN	Phosphatase And Tensin Homolog
RAD51 B/C/D	RAD51 Paralog B/C/D
RAD54L	RAD54 Like
RB1	RB Transcriptional Corepressor 1
RH	Rh Blood Group CcEe Antigens
RNF43	Ring Finger Protein 43
RPRD2	Regulation Of Nuclear Pre-MRNA Domain Containing 2
SETD2/DB1	SET Domain Containing 2, Histone Lysine Methyltransferase / alias of VEZF1: Vascular Endothelial Zinc Finger 1
SF3B1	Splicing Factor 3b Subunit 1
SMAD3	SMAD Family Member 3

SMARCA1	SWI/SNF Related, Matrix Associated, Actin Dependent Regulator Of Chromatin Subfamily A, Member 1
SOC2	alias SHOC2 Leucine Rich Repeat Scaffold Protein
SOX2	SRY-Box Transcription Factor 2
SPEN	Spen Family Transcriptional Repressor
SRD5A	Steroid 5 Alpha-Reductase
SRRM4	Serine/Arginine Repetitive Matrix 4
STAB2	Stabilin 2
STAT1-2	Signal Transducer And Activator Of Transcription 1-2
STS	Steroid Sulfatase
SULT2A1	Sulfotransferase Family 2A Member 1
SYP	Synaptophysin
SYT11	Synaptotagmin 11
TAF1L	TATA-Box Binding Protein Associated Factor 1 Like
TBP	TATA-Box Binding Protein
TCERG1	Transcription Elongation Regulator 1
TGF-β	Transforming Growth Factor beta
TMPRSS2	Transmembrane Serine Protease 2
TNF-α	Tumor Necrosis Factor alpha
TP53	Tumor Protein P53
UNC13D	Unc-13 Homolog D
USP28	Ubiquitin Specific Peptidase 28
VIM	Vimentin
WNT	WNT gene family
ZMYM3	Zinc Finger MYM-Type Containing 3
ZNF292	Zinc Finger Protein 292
ZNRF3	Zinc And Ring Finger 3
α-SMA	Alpha Smooth Muscle Actin

LIST OF AMINO ACIDS

Ala	A	Alanine
Arg	R	Arginine
Asn	N	Asparagine
Asp	D	Aspartic acid
Cys	C	Cysteine
Gln	Q	Glutamine
Glu	E	Glutamic acid
Gly	G	Glycine
His	H	Histidine
Ile	I	Isoleucine
Leu	L	Leucine
Lys	K	Lysine
Met	M	Methionine
Phe	F	Phenylalanine
Pro	P	Proline
Pyl	O	Pyrrolysine
Ser	S	Serine
Sec	U	Selenocysteine
Thr	T	Threonine
Trp	W	Tryptophan
Tyr	Y	Tyrosine

OVERALL INTRODUCTION

INTRODUCTION

1. Epidemiology of prostate cancer

Prostate cancer (PCa) is the most prevalent cancer in men worldwide. In 2020, 1.4 million new cases were diagnosed and PCa was the fifth leading cause of cancer death among men (**Figure 1**). Incidence varies between 6.3 to 83.4 per 100,000 men depending on geographic location, but PCa remains the most frequently diagnosed cancer in men in over one-half (112 of 185) of the countries of the world (**Figure 2**). Established risk factors are represented by age, ethnicity, fat rich diet, obesity, smoke, family history, genetic alterations in susceptibility genes (e.g. *BRCA1* and *BRCA2*) and predisposing conditions (e.g. Lynch syndrome)[1].

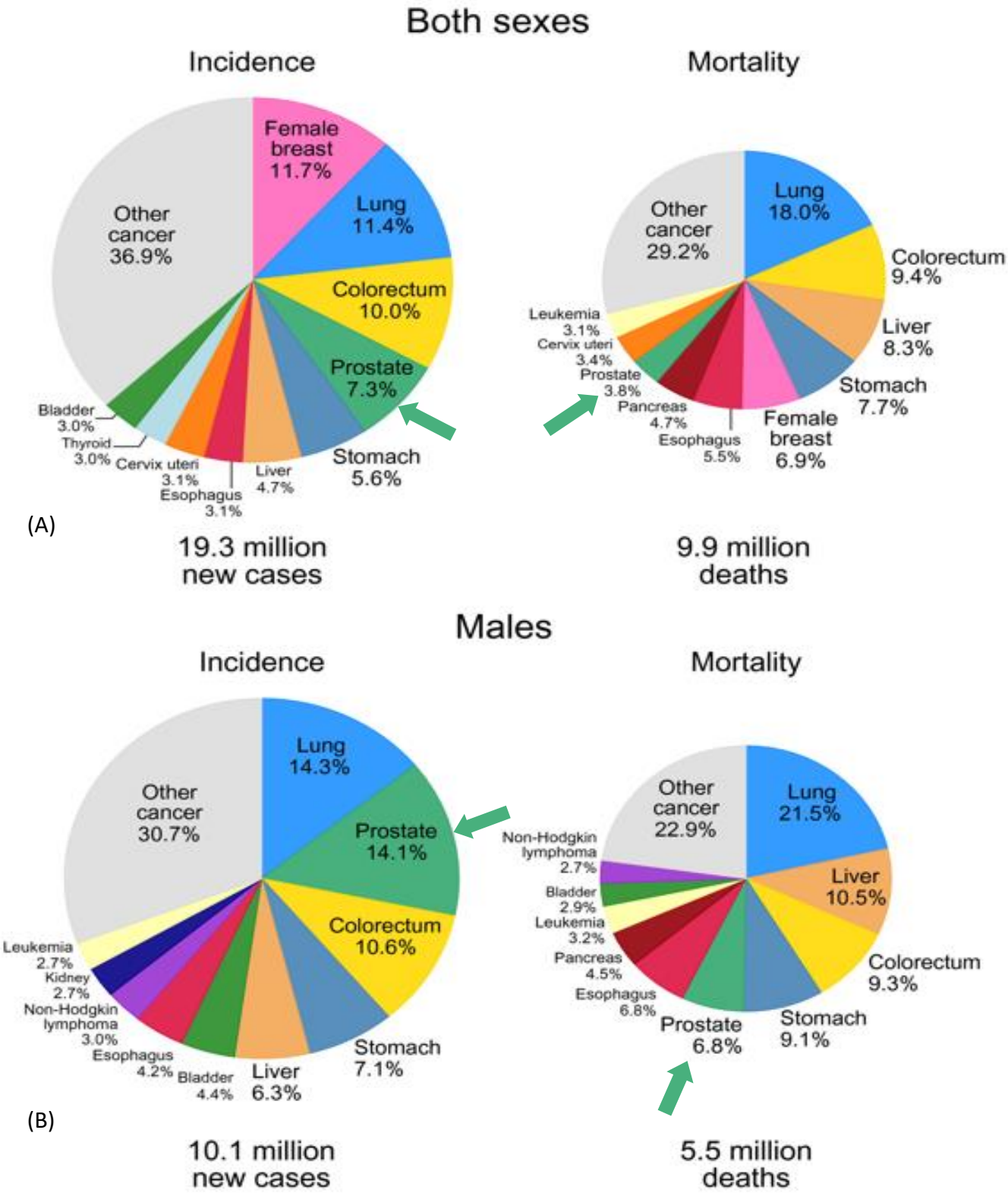

Figure 1: Top 10 most common cancers in 2020 by cases and deaths for (A) both sexes and (B) men[1].

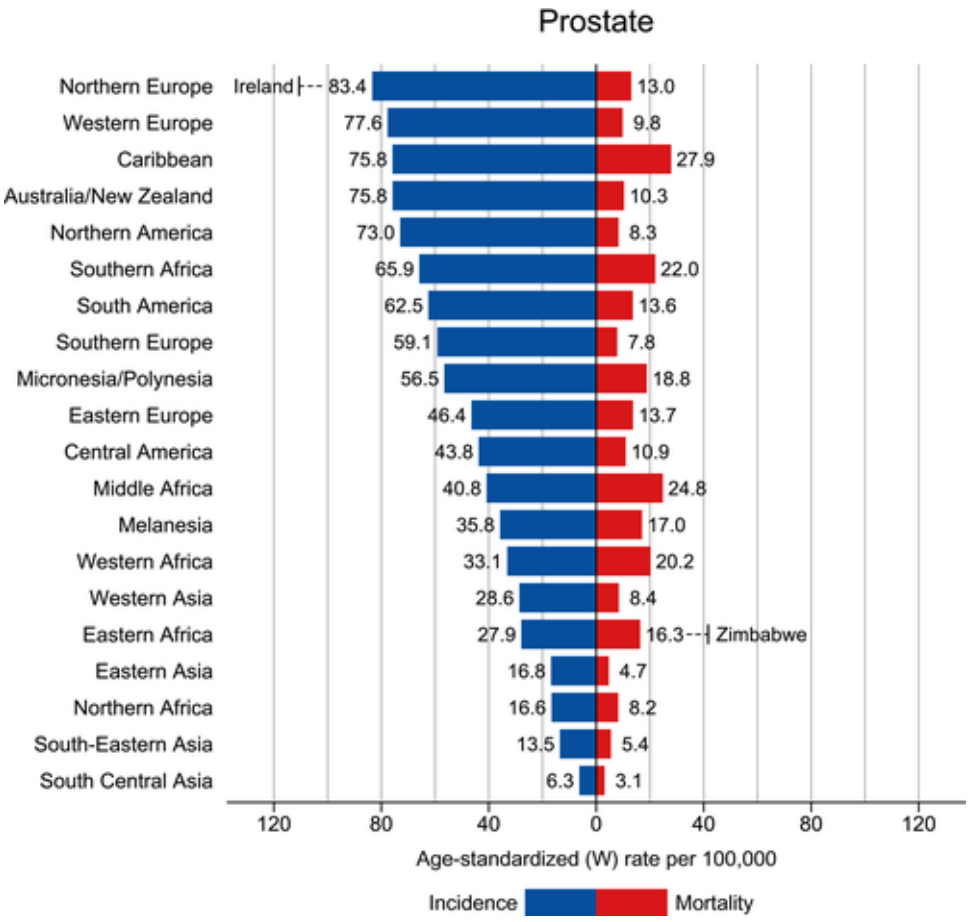

Figure 2: **PCa in 2020 by region-specific incidence and mortality age-standardized rates**[1]**.** Rates are shown in descending order of the world (W) age-standardized incidence rate, and the highest national age-standardized rates for incidence and mortality are superimposed.

Incidence, prevalence and mortality of PCa in the European Union are similar to those observed worldwide: in 2018 the estimated absolute number of diagnosis, incidence and mortality was 449.8 cases (21.8% of the total), 92.5 and 19.4 cases per 100,000 men/year (age-standardized rates (ASR)), respectively[2]. Similar rates of incidence and mortality were confirmed in 2020 and PCa remains the main cancer in males and one of the leading causes of cancer-related death. Mortality rates have been declining since the 1990s in Western and Northern European countries; thus, the geographical variability in rates across those European areas has been reducing somewhat[3]. Of all cases of PCa, 77% are diagnosed at localized stage, 11% with regional involvement, 5% with metastatic disease and 7% of unknown stage[4]. Although the long-term survival of

localized PCa is high, metastatic PCa (mPC) is an incurable and lethal disease, despite the different therapeutic regimens that are nowadays available[5]. Incidence and mortality of PCa proceed at different rates: by 2040 if it is estimated that there will be 2.21 million new cases of PCa worldwide with exponential increase in incidence rates, while the number of deaths is expected to show only a slight increase between 2020 (375 304) and 2040 (720 661) (**Figure 3**)[6].

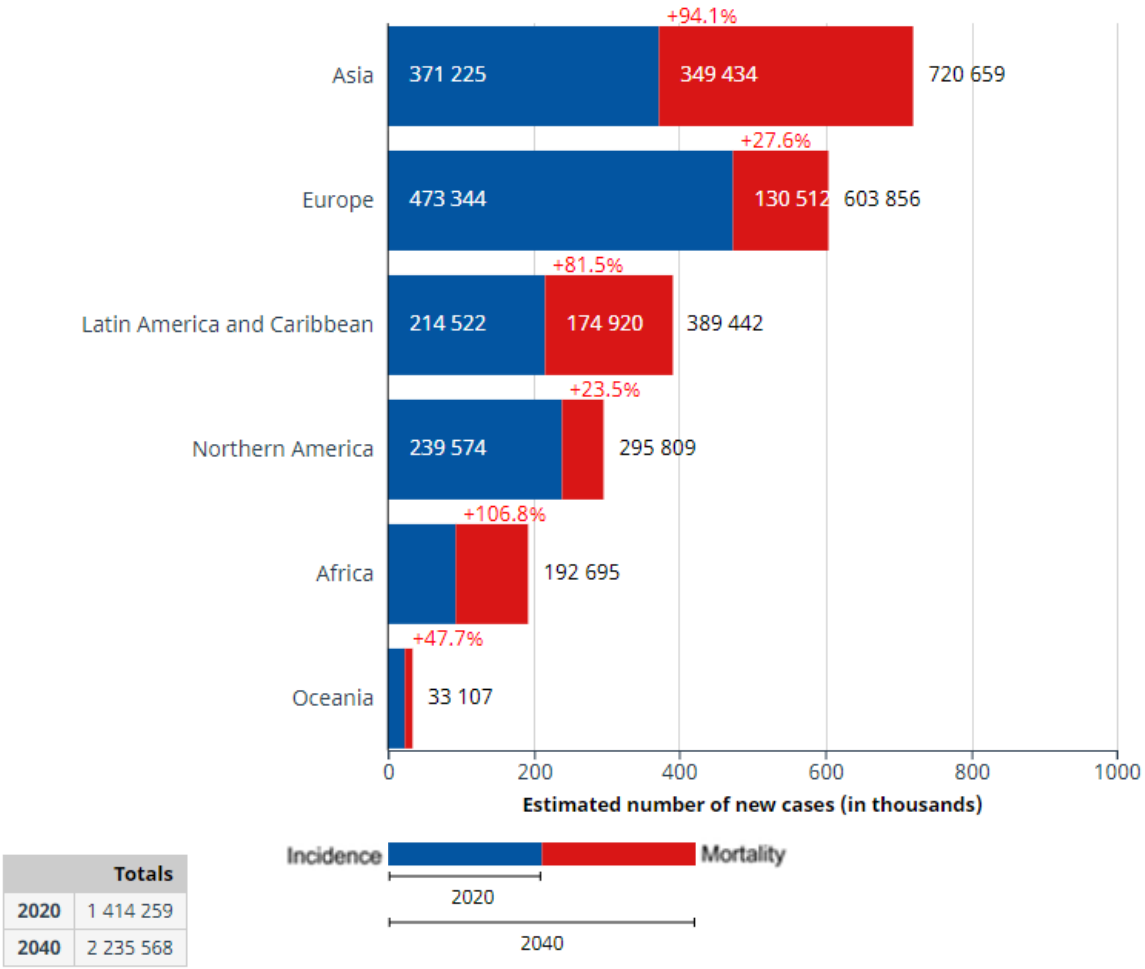

Figure 3: **Estimated number of new cases of PCa worldwide between 2020 and 2040**[5]**.**

Despite its prevalence, there are still many unresolved questions about the diagnosis and treatment of PCa.

2. Prostate: anatomy and function

The prostate is a male sex gland bounded above by the bladder, below by the urogenital diaphragm, in front by the pubic symphysis, and behind by the rectum. The prostate gland surrounds the urethra in a triangular shape. This organ consists of 5 anatomical regions: the central zone, the periurethral region, the transitional zone, the peripheral zone, and the fibromuscular region (or stroma) (**Figure 4A**). The microscopic cellular architecture is detailed in **Figure 4B**.

From a clinical point of view, the prostate is generally composed of two lateral lobes divided by a central groove palpable on rectal examination, and a middle lobe that may extend into the bladder in older men. The lobes do not represent histologically specified structures in the normal prostate, but are usually associated with pathologic enlargement of the lateral transition zone and medial periurethral glands[7]. In contrast, the prostate is typically walnut-sized in young men, but continues to enlarge over time in men over 40 years of age[8].

About 75% of prostatic tumors arise in the peripheral zone, 20% in the transitional zone, and 5% in the central zone[9,10,11]. The disease spreads mainly by direct dissemination, lymphatic drainage, and hematogenous spread.

The main glandular functions of the prostate are to supply sperm with vital secretions (by producing the seminal fluid that, consists of enzymes such as acid phosphatase and prostate specific antigen (PSA), involved in sperm liquefaction), which form the ejaculate and maintain sperm viability and motility, which also enables their nutrition

and transport[7,12]. In particular, the stromal compartment of the prostate provides the appropriate microenvironment for the epithelial compartment. It contributes numerous supportive signals to maintain or restore glandular homeostasis under healthy conditions or in regenerative stages. The epithelium of the prostate gland produces the prostatic fluid, which, like other accessory glandular secretions of the male, plays an important role in male fertility.

The stroma and epithelium influence each other under the action of androgens and through various signaling pathways that control differentiation, cell activity, and apoptosis, as well as the action of growth factors and vitamins, the normal development and homeostasis of the prostate[11]. The prostate, in fact, has no hormonal function of its own, but is hormone-dependent. Its development depends on stimulation by testosterone (a fuel or driver for PCa growth via ligand-mediated activation of the androgen receptor (AR)), since the prostate contains receptors for dihydrotestosterone, the active form of testosterone. The conversion of testosterone to dihydrotestosterone in the prostate occurs under the enzymatic control of 5-alpha-reductase.

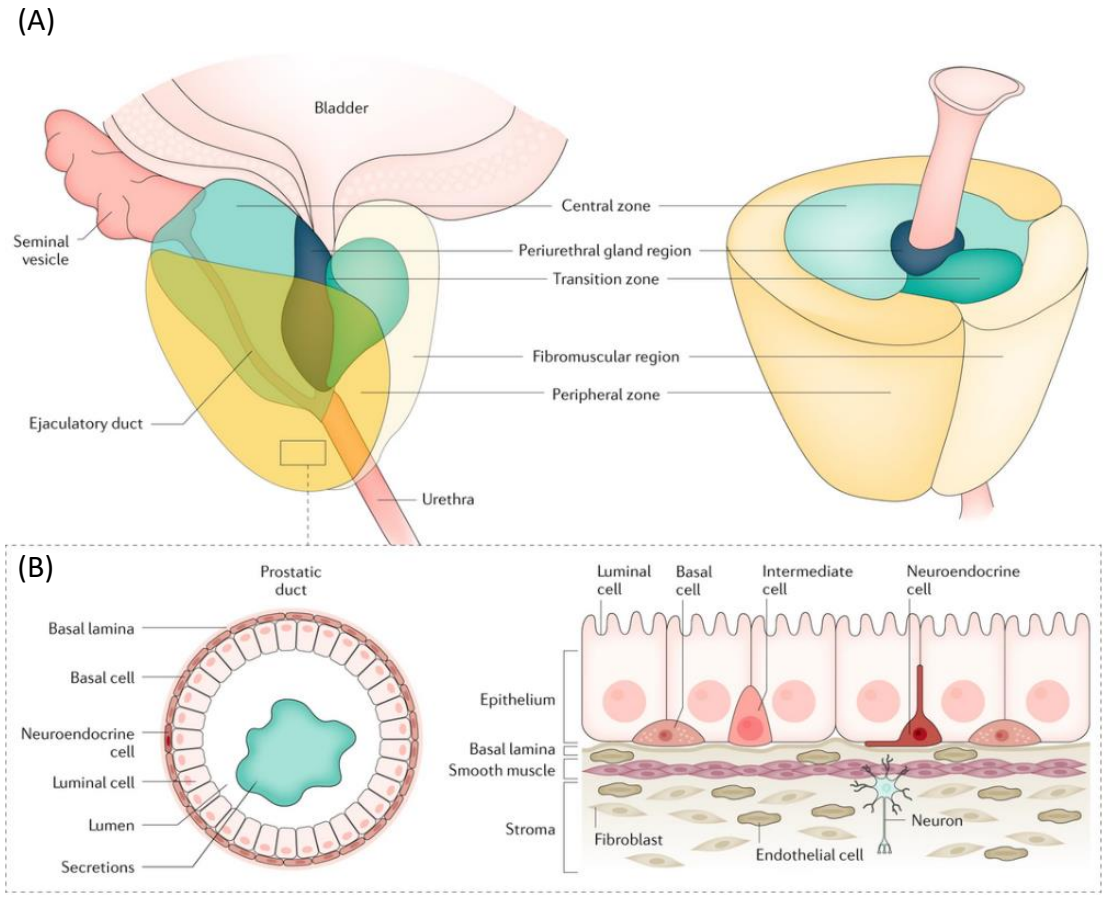

Figure 4: The anatomy of prostate[8,13]**.** A) 3D structure of the prostate. B) The composition of the prostate tissue. Each region consists of ducts and acini embedded in the stroma, which contains different cell types, mainly smooth muscle cells but also fibroblasts. The ducts and acini consist of a single layer of columnar epithelium (AR +, CK8+, CK18+, PSA+) surrounded by a layer of basal epithelial cells (CK5+, CK14+, p63+) that form the basement membrane, a layer of extracellular matrix anchored to the stromal cells (α- SMA +, vimentin+). Neuroendocrine cells (Syn+, CHGA+, NSE+) are also present in the duct. The epithelium is formed by 2 histologically distinct layers. The luminal secretory layer consists of large columnar cells that produce the PSA that is secreted into the seminal fluid. This cell layer is underlain by a basal layer of ulnar epithelial cells and neuroendocrine cells. This layer is in turn covered by a basal wall of extracellular matrix that separates the basal cells from the stroma.

3. Clinical overview of management of prostate cancer

3.1. Diagnosis and staging

Clinically, several factors can be used to confirm the diagnosis of suspect PCa, such as PSA, age, ethnicity, family history, and digital rectal examination (DRE)[14]. However, the definitive diagnosis of PCa relies on histological evaluation of either biopsies or surgical sample obtained via radical prostatectomy. PSA screening was introduced since 1990s for diagnosis of PCa and has led to a decrease in mortality[15]. However it is less than perfect at the diagnosis, as there are reports of aggressive cancers with no increase in PSA[15]. Conversely, PSA screening has been associated with overdiagnosis and resulting overtreatment and therefore its clinical application has evolved in recent years[16]. Recently, ESMO clinical practice guidelines for diagnosis, treatment and follow-up of PCa have recommended the use of PSA screening according to different scenarios with the above mentioned features depending on the diagnostic work-up and stage of the PCa[17]. Staging of PCa relies on several imaging techniques (computed tomography (CT) and multi-parametric magnetic resonance imaging (mpMRI)) and nuclear medicine imaging techniques (positron emission tomography (PET) using different tracers such as coline or prostate-specific membrane antigen (PSMA)).

The definition of the three main known stages of PCa (localized, regional or distant stage) and the elaboration of the Tumor-Nodes-Metastasis (TNM) are based on the results of the stratification tests (CT, MRI) (**Table 1**). Recently the histopathological classification of PCa has been modified and the International Society of Urological Pathology (ISUP) Grade Group (GGs), an articulation of the Gleason score, replaced it[18]. Then, integration of the TNM with the ISUP Grade Group and the PSA level provides the PCa risk category. Based on the characteristics evaluated several classifications of PCa are currently in use used (**Table 2**).

T category	T criteria	
TX	Primary tumour cannot be assessed	
T0	No evidence of primary tumour	
T1	Clinically inapparent tumour that is not palpable	
	T1a	Tumour incidental histological finding in 5% or less of tissue resected
	T1b	Tumour incidental histological finding in more than 5% of tissue resected
	T1c	Tumour identified by needle biopsy found in one or both sides, but not palpable
T2	Tumour is palpable and confined within prostate	
	T2a	Tumour involves one-half of one lside or less
	T2b	Tumour involves more than one-half of one side but not both sides
	T2c	Tumour involves both lobes
T3	Extraprostatic tumour that is not fixed or does not invade adjacent structures	
	T3a	Extraprostatic extension (unilateral or bilateral)
	T3b	Tumour invades seminal vesicle(s)
T4	Tumour is fixed or invades adjacent structures other than seminal vesicles such as external sphincter, rectum, bladder, levator muscles, and/or pelvic wall	
N category	**N criteria**	
NX	Regional lymph nodes cannot be assessed	
N0	No positive regional lymph nodes	
N1	Metastases in regional node(s)	
cM0	No distant metastasis	
cM1	Distant metastasis	
	cM1a	Nonregional lymph node(s)
	cM1b	Bone(s)
pM1	Distant metastasis, microscopically confirmed	
	pM1a	Nonregional lymph node(s), microscopically confirmed
	pM1b	Bone(s), microscopically confirmed
	pM1c	Other site(s) with or without bone disease, microscopically confirmed

Table 1: Summary of PCa staging from eighth edition of the American Joint Committee on Cancer (AJCC) cancer staging Manual[17,19]**.**

Clinical classification	Histological classification
TNM classification (localized/loco-regional/metastatic)	Adenocarcinoma (ADK)
Low/intermediate/high grade (Gleason score and ISUP)	Neuroendocrine (NE)
Low/intermediate/high risk (PSA, TNM and Gleason score)* for nmPC	ADK-NE (Mixte)
Non metastatic/metastatic/*de novo* metastatic (anatomy and recurrence)	
Hormone naïve/sensitive/resistant to castration	
Visceral/ bone diseases (metastatic sites)	
Low/high-volume (tumor volume) for mPC	
Low/high risk (Gleason and metastatic site) for mPC	
Hereditary PCa	

*Each of these categories of risk can be subdivided into two categories to better stratify patients based on their clinical characteristics: Very low/low/favorable intermediate/unfavorable intermediate/high/very high risk

Table 2: Main PCa states. Classifications based on genomic (genetic alterations) or immune (presence of immune cells) criteria can also be used (not shown). nmPC: non metastatic PCa.

3.2. Natural history of prostate cancer

The natural history of PCa is still ambiguous and in evolution (**Figure 5**). This is partly due to the biological and clinical heterogeneity of the disease, and to the emergence of new systemic therapies for advanced PCa. Knowledge of the natural history of early PCa allows for better clinical management of the disease, by selecting which patients can benefit from screening and treatment. Indeed, in some patients, specific treatment may not be necessary and its possible side effects avoided, since concomitant comorbidities may be the cause of mortality.

Low-risk PCa is associated with a very low cancer-related mortality: during the first 15 years after diagnosis mortality rate is 33 per 1000 person-years which further declines to 18 per 1000 person-years after 15 years of follow-up. Furthermore, the PCa annual

mortality rate remains unchanged for patients managed with either observation or androgen deprivation therapy (ADT). Globally, these results do not suggest the need for invasive treatment of localized low-risk PCa when expected patients survival is under 10-15 years. Conversely, the risk of dying from PCa increases gradually for intermediate and high grade PCa and patients who develop high-grade PCa are highly likely to die of PCa in the 10 years after diagnosis[20].

Since in the long term, there is a possibility for local tumor progression and development of aggressive and incurable metastatic disease, early radical treatment, especially in men whose life expectancy is estimated to be more than 15 years, is the preferred course of action. In the absence of initial treatment, there are few patients diagnosed with early-stage cancer who die of PCa within 10 to 15 years following diagnosis[21].

Even in patients who receive primary treatment for PCa, the natural history of the disease can be indolent: after radical prostatectomy or radiotherapy, only a fraction of patients, mainly those at higher risk at the moment of diagnosis, will experience a biochemical recurrence. After biochemical recurrence, 8 years is the median time to development of metastases, and the median time to death is 5 years after the occurrence of clinically significant metastatic disease[22]. Approximately 15 to 30% of men receiving curative local treatment for early-stage disease have a recurrence, and 5% of the men will ultimately die due to metastatic disease[22].

Usually patients who experience biochemical progression after primary treatment are treated with ADT. Among these men a small, but non-negligible, proportion will experience a biochemical progression while on hormone therapy without any radiological sign of metastatic disease a condition known as non-metastatic castration-resistant PCa (nmCRPC). These patients can present a very heterogeneous natural history: some have very indolent evolution with a median metastatic free survival (MFS) estimated to be 2.5 years[23]; however after two years, 33% of patients have bone

metastasis, implying that resistance to castration inevitably leads to disease progression and an increased risk of mortality[23,24].

Metastatic castration-resistant PCa (mCRPC), is a clinical condition that appears during ADT treatment and is defined by the following criteria[25]: castrate serum testosterone < 50 ng/dL or 1.7 nmol/L in combination with both: (i) biochemical progression (3 consecutive rises in PSA at least 1 week apart leading to two 50% increases over the nadir, and a PSA > 2 ng/mL); (ii) and radiological progression (the presence of new lesions: either ≥ 2 new bone lesions on bone scan or a soft tissue lesion using RECIST (Response Evaluation Criteria in Solid Tumors).

The most frequent sites of metastasis from PCa are bone (for 80-90% of men with mPC[26,27]) and regional lymph nodes, whereas other sites of metastasis are uncommon. Nevertheless, liver metastases can occur in 10% of men with mPC as an initial site of metastasis[26]. Nowadays, visceral metastases are more common (40% of patients) in comparison to the past (26%). This increase in the prevalence of visceral metastatic disease should be considered in the clinical management of the disease (surveillance with systematic imaging) and in the development of new therapeutic approaches that focus on visceral metastases[28].

Following the introduction of PCa screening using PSA the proportion of patients presenting with *de novo* metastatic disease as gradually reduced over time. In the 1990s, only 3.4% of patients had metastasis at diagnosis, and much less (1.6%) in the period 1998-2003, whereas prior to 1990 the rate was around 20%[29,30].

Standard of care for the treatment of metastatic hormone-sensitive PCa (mHSPC), both *de novo* or recurrent, is ADT combined with either chemotherapy or next generation androgen receptor pathway inhibitor (ARPI). Median overall survival (OS) in one of the first trial evaluating ADT vs bilateral orchiectomy was 24 months[31]. In the last two decades, the natural history of newly diagnosed mPC has evolved, and median OS has improved from 22 to 42 months[32,32,33,34] with the use of new active drugs such as

taxane-based chemotherapy and ARPIs. In addition, the survival of men with mCRPC[35], has been improved. In retrospective analyses, median OS since development of mCRPC is currently between 20 and 30 months[36,37].

In conclusion, PCa is a very heterogeneous disease encompassing both low-risk tumors that have low cancer-specific mortality rate and tumors that develop as metastatic from the diagnosis. The natural history of this disease is therefore dependent on both the biological characteristics and presentation of disease at diagnosis. The introduction of several new treatment has radically modified both the natural history and the prognosis of PCa. Globally, PCa patients have a better prognosis, both in localized and metastatic forms, when compared to other cancers. In spite of these impressive accomplishments, PCa is still a major cause of cancer mortality in the world.

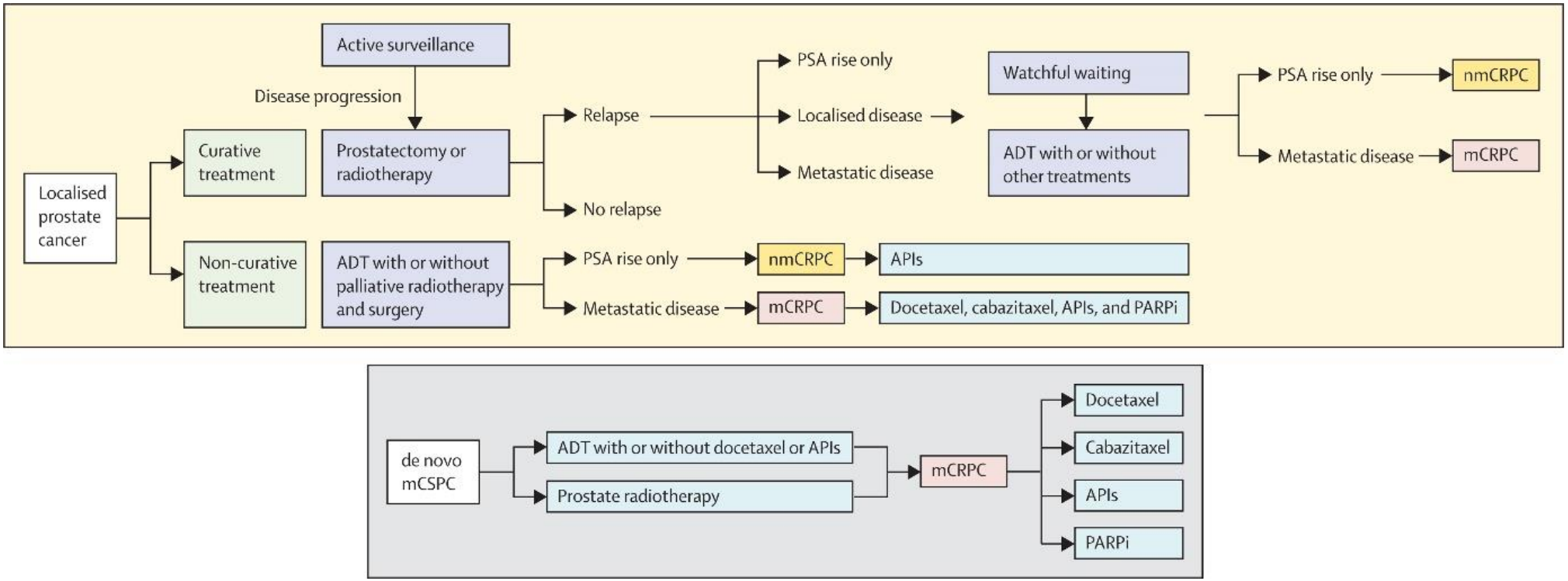

Figure 5: Natural history of PCa from localized to metastatic PCa with therapeutic option according to stage of disease[38]**.** APIs: androgen pathway inhibitors; mCSPC: metastatic castration-sensitive PCa PARPi: poly(ADP) polymerase inhibitors. (Treatment details in the following section)

3.3. Treatments of prostate cancer

The treatment landscape of PCa has evolved considerably every two decades and it is still growing with new therapeutics, advanced functional imaging, next generation sequencing and combinations of existing therapies (**Figure 6**). PCa can be treated in different ways depending on its characteristics. Different treatment modalities can be used depending on the stage (non-metastatic or metastatic), histological subtype (the type of cells involved), and grade (degree of aggressiveness). These characteristics are determined by the aforementioned diagnostic workup findings[19]. Several modalities can be proposed, alone or in combination: active surveillance, surgery, radiotherapy, brachytherapy, hormone therapy, chemotherapy, immunotherapy, radiopharmaceuticals, and targeted therapy based on specific molecular alteration. Depending on the clinical situation, the objective(s) is (are) to: monitor the evolution of the disease to delay the initiation of treatment, eliminate or reduce the tumor and/or metastases, reduce the risk of recurrence, slow the development of the tumor or metastases, treat the symptoms caused by the disease to ensure the best possible quality of life, and improve survival. These different options of treatment have advantages and disadvantages. The frequency, durability, and gravity of these side effects varies between treatments. The best treatment outcomes comprise improved OS, disease-specific survival (DSS) and MFS, reduced adverse events (AE), optimized quality of life and reduced costs.

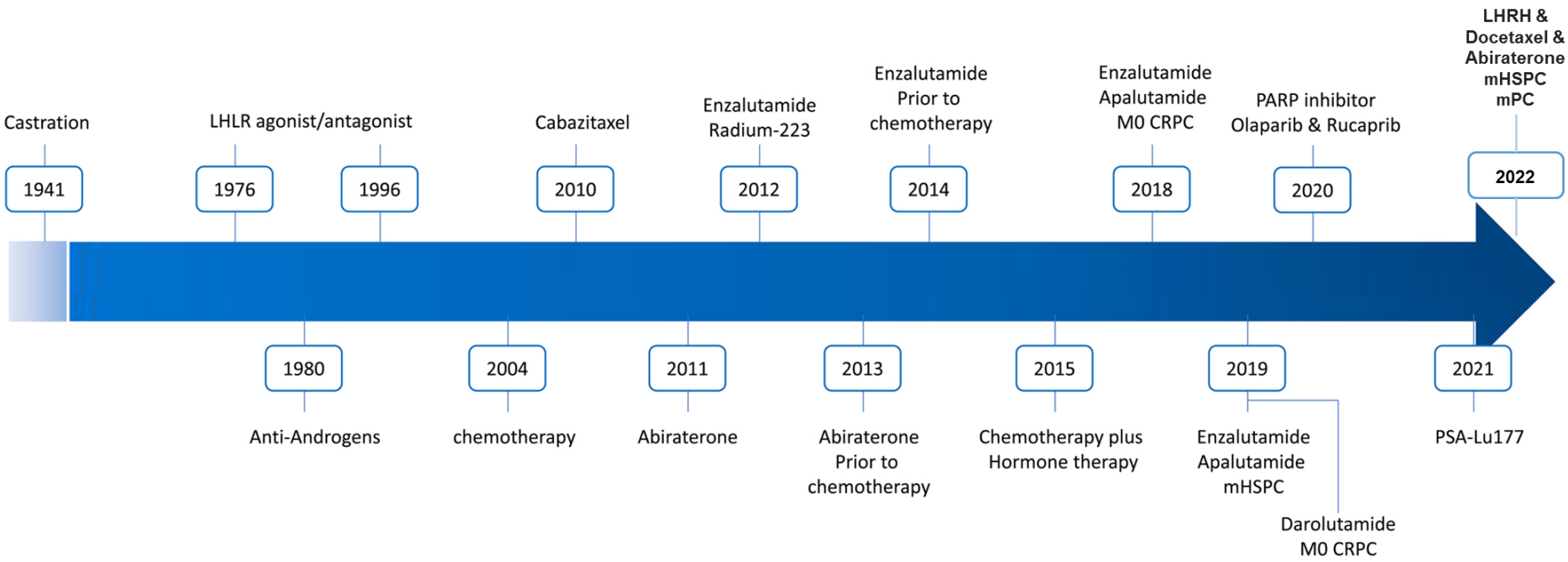

Figure 6: Timeline with the key milestones in historical development of treatments for PCa (adapted from Zoubeidi et al, 2021)[39,40].

3.3.1 Active surveillance

A surveillance strategy is recommended in the case of a very low and low risk localised PCa that does not cause any symptoms. The goal is to delay treatment, and the AE that accompany it, until it is necessary. Active surveillance relies on a specific, periodic protocol that allows performing curative treatment in case of disease evolution[41]. This monitoring strategy is based on regular examinations, using PSA, repeated biopsies and magnetic resonance imaging (MRI). Although there are several methods of active surveillance to reduce overtreatment in patients with low-risk PCa, standardized active surveillance is not yet available[42,43]. Indeed, some prostate cancers evolve slowly and sometimes for a long time. Usually active surveillance continues throughout life or until the disease progresses.

3.3.2 Surgery

Surgery is one of the standard treatments for localized PCa[44,45]. The proposed procedure is a total prostatectomy, also known as radical prostatectomy[46]. It aims to remove the entire prostate as well as the seminal vesicles, two small glands located on either side of the prostate. In some cases, the neighboring lymph nodes are also removed; this is called lymph node dissection. The surgery can be offered for patients with tumors at low and intermediate risk and in some cases at high risk of recurrence. After the prostate has been removed, the urethra is attached to the bladder to ensure the flow of urine through the natural channels. The nerves and blood vessels that allow erection pass on each side of the prostate. They form the two neurovascular bands. Whenever possible, these strips are preserved by a nerve-sparing technique. However, they may be damaged during the procedure. In some cases, when the cancer cells are very close, it is necessary to remove them. The most common AE specific to prostatectomy are urinary incontinence and erectile dysfunction. It should also be noted that total prostatectomy results in a permanent inability to ejaculate. In the long term, a narrowing of the urethra may occur. The symptoms include a decrease in the strength of the urine stream, pain when urinating and even blood in the urine.

Furthermore, complications common to all surgery can occur: pain in the operated area; accumulation of blood or lymph in the operated area; infection in the scar; venous thrombosis or phlebitis and fatigue. Fatigue can be caused by anesthesia, blood loss or anxiety generated by the operation and or other AE.

3.3.3 Radiotherapy

Radiotherapy can be used to treat all localized prostate cancers and, depending on the initial risk, may be combined with hormone therapy of different duration[47,48,49]. Finally, external beam radiotherapy (EBRT) can also sometimes be used to complement surgical treatment in certain cases of high-risk cancers or to treat bone metastases[50,51,52]. It uses ionizing radiation to destroy cancer cells by preventing them from multiplying. The radiation is precisely directed at the prostate to reach the tumor and nearby lymph nodes through the skin, while preserving as much healthy tissue and nearby organs as possible, called organs at risk (especially the bladder and the last segment of the digestive system: rectum and anal canal).

Before the actual treatment, a radiation therapy involves a simulation step to identify the area to be treated and a dosimetry step to calculate the dose distribution. During the simulation phase, a scanner is performed to obtain a three dimensional (3D) simulation of these areas. Then, the types of radiation to be used, the size of the beams and their orientation are determined in order to irradiate the tumor while sparing the surrounding healthy organs. At the dosimetry stage, the irradiation is optimized by a computerized study to best treat the tumor or, after surgery, the area where the prostate was located, while sparing the surrounding healthy tissue. The final treatment plan establishes the total dose of radiation and the way it is delivered (e.g. dose per session, number of sessions, spacing of sessions). The total doses usually delivered during EBRT for PCa are 70 to 80 Gray (Gy).

For PCa, 3D conformal radiotherapy is used. This technique consists of matching the volume on which the radiations will be directed as closely as possible to the volume of

the prostate. It uses 3D images of the tumor and surrounding organs. These images can be acquired by CT scan or by merging CT images with MRI images. Software simulates, in 3D, the shape of the irradiation beams to be used to best adapt to the volume of the tumor and calculates the dose distribution. In some situations, radiation techniques with modulated beam intensity are used. This is known as intensity modulated conformal radiotherapy (IMRT)[53]. When irradiating a tumor, one cannot completely avoid irradiating and thus altering healthy tissues located nearby. This explains the appearance of undesirable effects. They vary depending on the area treated, the dose of radiation delivered, the sensitivity and general health of the patient, as well as the associated treatments.

A distinction is made between: (i) the immediate, acute or early AE, which occur during treatment and the few weeks that follow. They are often temporary; the most frequent are: urinary disorders, inflammation of the rectum and anus, skin reactions, intestinal disorders, fatigue. And (ii) the late AE, complications, which can appear several months or even years after the end of the treatment. They can be long-lasting. Advances in irradiation techniques have made late AE less frequent and less severe. However, some symptoms may appear several months or years after the end of treatment. They are sometimes favored by certain treatments. They can be: pain in the irradiated area; inflammation of the mucous membrane of the rectum; urinary problems; erectile dysfunction; the risk of a second cancer. After treatment of prostate cancers with EBRT, there is a very small risk (estimated to be less than 1%) of developing rectal or bladder cancer. This risk is statistically higher than that of a person who has not been treated for a first cancer.

3.3.4 Brachytherapy

Brachytherapy is a local treatment for cancer that involves placing radioactive sources inside the affected organ. It improves the radiotherapy performance providing the

most anatomically correct dose to the prostate and not to the neighboring tissue than would be a possibility with EBRT. The radioactive elements emit radiation that destroys the cancer cells. The dose of radiation decreases very quickly as one moves away from these radioactive sources, which limits the undesirable effects on the surrounding healthy tissues. There are two forms of brachytherapy: (i) by permanent implants of iodine 125 seeds; (ii) by temporary implants, generally of iridium 192 sources. This is also called the high dose rate technique. Brachytherapy has a very localized action on the prostate and is usually used to treat localized prostate cancers. In high risk PCa, brachytherapy can be combined with EBRT and androgen suppression[54,55].

In order to implant the material necessary for brachytherapy (whether it is performed with permanent or temporary implants), a general anesthesia or spinal anesthesia (anesthesia of the abdomen and legs) is performed. After the anesthesia, a urinary catheter and endorectal ultrasound probe are inserted. The purpose of this probe is to visualize the prostate, the urethra and the rectum; and to acquire the images in the computer. These elements allow for real-time planning and dosimetry in 3D. The objective is to optimize the radiation, so as to treat the tumor as well as possible while sparing the surrounding healthy organs. Ultrasound is used to guide the implantation of the needles used to introduce the radioactive sources. These needles are introduced through the perineum through an implantation grid.

The AE of brachytherapy depend on the type of implants, the volume of the area treated, the dose of radiation that may have reached nearby organs, which is usually very low, and the total dose received. Some AE may occur immediately after the procedure or a few weeks later. In general, they are temporary. Others appear long after the treatment and may last for a long. Overall, the side effects observed are urinary disorders, sexual dysfunction, rectal troubles, perineal haematoma, venous thrombosis, fatigue and pain.

3.3.5 Hormone therapy

PCa is a hormonal disease and its growth depends on activation of the AR by endogenous ligands (such as testosterone and dihydrotestosterone). Therefore hormone therapy was developed to block testosterone production and that this can be achieved by using either luteinizing hormone releasing hormone (LHRH) or anti-androgens.

Hormone therapy drugs are administered orally, injected under the skin or intramuscularly. More rarely, testosterone production is suppressed by surgical removal of the testicles. The hormone therapy drugs used are LHRH analogues or antagonists, which block the production of testosterone by the testicles (**Figure 7a**). This is termed chemical castration. In addition to LHRH analogues, AR inhibitors (oral) are usually prescribed at the beginning of treatment. Their purpose is to avoid a transient rise in testosterone that sometimes occurs with this type of medication. AR inhibitors act as anti-hormones by taking the place of testosterone at the hormone receptors of the cells. The most common are flutamide, bicalutamide, nilutamide and cyproterone acetate. LHRH analogues and antagonists are administered by injection. The most commonly used drugs are leuprorelin, goserelin, buserelin, triptorelin and histrelin as LHRH analogues; and degarelix, relugolix as LHRH antagonist. Overall, androgen suppression approaches have similar overall efficacy and toxity profile, except of the new oral LHRH antagonist, relugolix, is related to a reduction in cardiovascular events by comparison with leuprolide[56]. If the tumor becomes resistant to a first treatment based on hormone therapy, another molecule can usually be proposed. This may include two new generation ARPIs: abiraterone acetate (AA) or enzalutamide.

Hormone therapy, combined with EBRT, is the standard treatment for locally advanced PCa and is one of the possible treatments for localized high-risk forms. Hormone therapy is usually started before radiation therapy and continued after radiation therapy for up to 3 years. In some cases of intermediate-risk localized cancers, short-term hormone therapy (up to 6 months) may be combined with EBRT. Long-term

hormone therapy is the standard of care for mPC[57]. In some clinical situations, hormone therapy may be prescribed in combination with chemotherapy.

Androgen deprivation therapy (ADT), which involves decreasing testosterone levels by surgical or medical castration, remains the backbone therapy for the treatment of mHSPC.

In recent years, for different types of PCa, including mCRPC, several treatments, comprising docetaxel, AA plus prednisone, enzalutamide, darolutamide and apalutamide, have each been shown to demonstrate survival benefit when used upfront along with ADT. However, not all patients benefit from these combinations and treatment selection for an individual patient remains a challenge[58,59,60,61,62].

Future changes may incorporate molecular markers that might select patients who require more intensive treatment due to higher risk of progression and death.

All forms of hormone therapy can cause AE. The occurrence and intensity of these symptoms depend on each individual, as well as on the medication used. The following AE are common to all types of hormone therapy: hot flashes, erectile dysfunction, decreased libido, weight gain, decreased bone mass and density, breast swelling and tenderness, and irritability. Other drug-specific AE may also occur.

3.3.6 ARPIs: mechanisms of action and clinical effectiveness

Currently, two classes of ARPIs have been developed: CYP17A1 inhibitors and AR inhibitors.

AA, a small-molecule inhibitor of cytochrome CYP17A1 (cytochrome P450 family 17 subfamily A polypeptide 1, key enzyme in androgen synthesis), inhibits androgen biosynthesis by the adrenal glands and by tumor cells (**Figure 7b**)[63,64].

To substitute cortisol and prevent adverse reactions, prednisone, one of the steroids, is given together with AA. In mCRPC, the randomized phase 3 COU-AA-301 and COU-AA-302 trials, have demonstrated OS benefits for patients treated with AA plus

prednisone versus placebo plus prednisone[65,66] in pre and post chemotherapy settings. Following the results of these studies, AA in combination with prednisone has been approved by the Food and Drug Administration (FDA) [67] for the treatment of mCRPC. AEs of AA/prednisone are notably fatigue, hypokalemia, hypertension, and hepatotoxicity[68].

Enzalutamide, a powerful AR antagonist, was approved by the FDA in 2012 to treat mCRPC patients after treatment with docetaxel according to the findings of AFFIRM study[69,70]. Subsequently, the efficacy of enzalutamide was demonstrated even in chemotherapy-naïve patients by the phase 3 PREVAIL study[71,72]. To reduce AR transcriptional activity, Enzalutamide acts in 3 steps: (1) inhibition of binding of androgens to the AR, (2) translocation of the AR to the nucleus, (3) and inhibition of AR binding to DNA (**Figure 7c**)[73]. Other AR inhbitors have been developed and improved for patients with metastatic PCa: apalutamide and darolutamide.

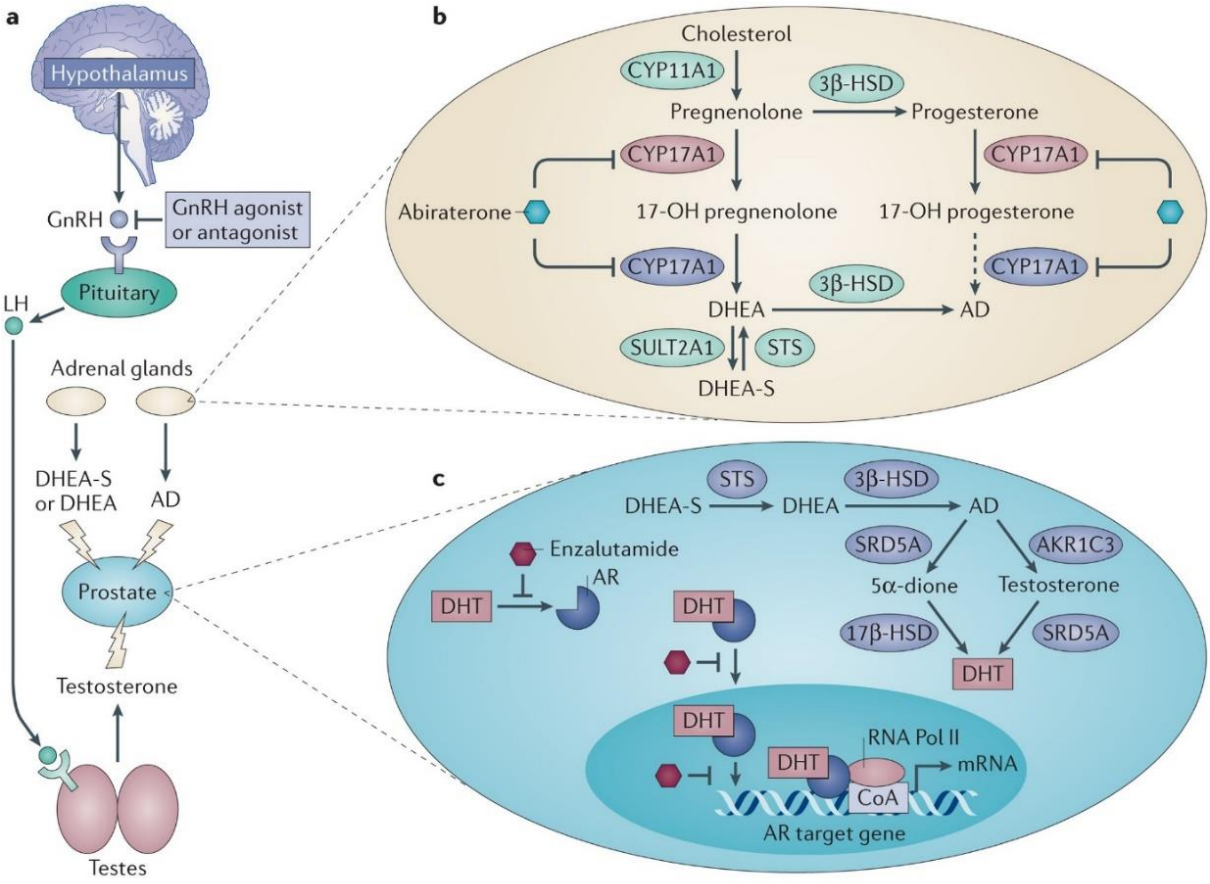

Figure 7: Mechanisms of actions of AR inhibitors in PCa[74].
Androgen synthesis is regulated by the hypothalamic-pituitary-testicular axis. **a)** The binding of the hormones gonadotropin (GnRH) and LH to their corresponding receptors induces the Leydig cells of the testes to produce testosterone. Continuous use of GnRH agonists results in down-regulation of the GnRH receptor (GnRH-R), whereas antagonists immediately block the GnRH receptor. Both agents inhibit the production of LH, and thus the amount of serum testosterone decreases to castration levels. In parallel, the androgens dehydroepiandrosterone sulphate (DHEA-S; mainly), DHEA and androstenedione (AD) are produced by the adrenal glands. **b)** *De novo* steroidogenesis of adrenal androgens (enzymes in ovals). AA inhibits both CYP17A1 activities: 17α-hydroxylation in red and 17,20-lyase in blue.The slight effect is indicated by a dotted arrow. **c)** The conversion of adrenal androgens to dihydrotestosterone (DHT) by the prostate is represented in the upper right part of the cell. In the cytoplasm, DHT-AR binding leads to a conformational change that results in nuclear translocation. To activate or repress the expression of the AR target gene, in the nucleus, DHT-bound AR homodimerises and, together with co-activators (CoAs) and RNA polymerase II (RNA Pol II) or co-repressors (not represented), links to DNA at the cis-androgen response elements. Inhibition of AR by enzalutamide is competitive with DHT for binding. It prevents both nuclear translocation and binding between DNA and cofactors.

3.3.6 Chemotherapy

Chemotherapy, in combination with continuous ADT, is one of the therapeutic options for treatment of both mHSPC and mCRPC. Chemotherapy is a systemic treatment that employs antitumor agents targeting mechanisms of cell division common to both cancer and normal cell.

The two main drugs used to treat PCa are: docetaxel and cabazitaxel, both administered by infusion and usually combined with oral corticosteroids (prednisone or prednisolone). Docetaxel and cabazitaxel, both belonging to the taxane class, were the first and second drugs approved by the FDA for mCRPC, due to an OS benefit shown in Phase 3 of (TAX327 and SWOG9916 trials) and (TROPIC trial), respectively[75,76,77]. Although cabazitaxel has shown benefit after docetaxel, it should not be used in place of docetaxel as first-line chemotherapy, according to the phase 3 FIRSTANA trial[78]. When PCa progresses after a first treatment with hormone therapy, a chemotherapy molecule and different hormone therapy molecules may be prescribed. Platinum-based chemotherapy is often used to treat the neuroendocrine PCa (NEPC), an aggressive histological variant of advanced PCa that appears as a hormonal treatment

resistant form of castration-resistant PCa (CRPC) or may arise *de novo*[79]. The treatment plan is determined on a case-by-case basis, as the drugs used, the doses administered, as well as the schedule of the courses and the total duration of the treatment, vary from person to person, depending on the characteristics of the cancer and the tolerance to the treatment, in relation to the predefined doses and schedule. Chemotherapy drugs often have AE on the blood and bone marrow: a decrease in white blood cells, red blood cells, haemoglobin and platelets, which respectively leads to an increased risk of infection, because the body's defences are reduced, anaemia, and an increased risk of bruising and bleeding. This may be accompanied by fever or severe chills, diarrhoea or vomiting. Both docetaxel and cabazitaxel can have a toxic effect on the nerves and cause sensation disorders (paresthesia).

3.3.7 Immunotherapy

Immunotherapy aims to stimulate and strengthen the body's natural defences to better identify cancer cells and destroy them more effectively, without directly targeting the "host" cells. The premise of this strategy is that every patient has an intrinsic response to cancer, but the cancer manages to escape the immune system, which does not identify the cell as abnormal and goes into tolerance[80]. Recently there has been a trend towards the use of immune checkpoint inhibitors, and the main pathways of clinical interest in oncology, have involved cytotoxic T lymphocyte-related antigen 4 (CTLA-4) and Programmed Cell Death 1 (PD-1) receptors with its ligand Programmed death-ligand 1 (PD-L1).

Immunotherapy with sipuleucel-T, a dendritic cell-based therapeutic vaccine, can be used to treat mCRPC (with no or very few cancer symptoms and usually no chemotherapy), by manipulating the immune system. Sipuleucel-T was the first cancer vaccine approved by FDA in 2010 following results of the IMPACT trial[81]. It has been shown to increase survival by 4.1 months with little or no symptoms. Ethnicity and certain prognostic factors may be independently linked to longer OS. These data

suggest racial differences in mCRPC tumors to be considered in terms of treatment[82]. Some additional emerging agents may also enhance immune-mediated tumor destruction[83]. However, we still need to develop reliable PCa biomarkers to help determine which future immunotherapy will offer the most benefit for each individual patient[84,85].

Subsequently, the immune checkpoint inhibitor pembrolizumab was approved by the FDA, since 2017, for all mismatch repair deficiency (dMMR) cancers or in those with high-level microsatellite instability status (MSI-H) or non resectable or metastatic solid tumors resistants to standard care or solid tumors with tumor mutational burden (TMB) ≥ 10 mutations/megabase[86,87]. In all other PCa patients, immune checkpoints inhibitors are not approved due to limited antitumor activity[88]. Combination immunotherapy with other treatments is also an area of active investigation. Combining PCa vaccines with immune checkpoint inhibitors has great potential for improving clinical outcomes in PCa, by creating and then recruiting tumor-specific T cells while increasing their effector function[83]. Common immunotherapy AE include skin reactions, flulike symptoms, diarrhoea, and weight changes.

3.3.8 Radiopharmaceutical therapy

Nuclear medicine provides a new treatment option to treat cancer. Radium-223 is an alpha emitting bone-seeking radioisotope and recommended for patients with mCRPC and symptomatic bone metastases[89]. In advanced PCa, 40-50% of patients have bone metastases only[90]. Radium-223 is a calcium mimetic, targeting the bone tissue cells of mPC, which take up calcium. Alpha particles cause double-strand DNA breaks in tumor cells, which induce tumor cell death and suppresses pathological bone formation. Based on the ALSYMPCA trial, Radium-223 was approved by FDA in 2013 for men with mCRPC have symptomatic bone metastases and not visceral metastasis[89,91]. Radium-223 increased median OS by 3.6 months and time to first skeletal-related event by 5.8 months compared with placebo[92]. Nowadays, the application of radium-223 is limited

for patients pre-treated with at least 2 lines of CRPC systemic treatment or patient unselected for these therapies, by the pharmacovigilance Risk Assessment Committee (PRAC) of the European Medicines Agency (EMA)[93]. The combination of radium-223 with AA and prednisone/prednisolone is not indicated, because of the higher number of fractures and deaths with the combination therapies[94]. Some of the AEs reported with radium-223 use are: bone pain, anemia, spinal cord compression and fractures[95].

3.3.9 PSMA-radioligand therapy

Molecular imaging is an innovative approach that is emerging to identify patients suitable for drugs coupled to a radioisotope targeting prostate-specific membrane antigen (PSMA). PSMA is a cell membrane-specific marker highly expressed by PCa cells, which can be visualised by positron emission tomography PET-imaging using specific radiotracers[96]. PSMA PET-imaging was approved by the FDA for disease localization for high risk localized and biochemical recurrent PCa.

In addition, recent phase 2 studies have shown that ^{177}Lu and PSMA-617 based therapies may have interesting antitumor activity[97]. Subsequently, mCRPC patients treated with ^{177}Lu-PSMA-617 had a significant improvement in PSA progression-free survival (PFS) compared with the cabazitaxel arm in randomised phase 2 trial[98]. Recently, the phase 3 VISION trial showed improved radiographic PFS and OS for the ^{177}Lu-PSMA-617 plus standard of care arm compared to the standard of care control arm alone (median rPFS, 8.7 vs 3.4 months; median OS, 15.3 vs 11.3 months respectively), in mCRPC patients previously treated with at least one hormone therapy drug and at least one but not more than two agents of chemotherapy[99]. The most common AE observed in the study were dry mouth and thrombocytopenia. In summer 2021, ^{177}Lu-PSMA-617 was granted breakthrough designation by the FDA. Several approaches are underway to test the efficacy of combinations of ^{177}Lu-PSMA-617 with other therapeutic agents (such as the engagement of bispecific T-cell antibodies

directed against PSMA and the immune system), and to design new drugs targeting PSMA[100,101].

3.3.10 Targeted therapy

Targeted therapy is based on the unraveling of cancer biology allowing, according to the genetic and molecular alterations of each tumor, to adopt the best choice of targeted molecules to be used for a specific treatment at a given time, and for a given patient. This approach is designed to block identified molecular abnormalities in the tumor in order to block cancer progression by overcoming intra and inter-patient tumor heterogeneity and resistance mechanisms. Indeed, regardless of the type of cancer, patients have different biological characteristics and respond differently to treatment. Therefore, targeted therapy permits to adapt the treatment to each patient according to the molecular profile of his cancer (also called personalized medicine). From biopsies of solid or liquid tumors, the genetic material of patient is analysed to identify the presence of pathogenic alterations using next-generation sequencing (NGS). Targeted therapeutic approaches can be applied for metastatic cancer, regardless of its location. A significant number of targeted agents are still being developed, either in clinical trials or approved by drug regulatory authorities to treat specific types of PCa.

Olaparib and rucaparib, drugs targeting poly(ADP-ribose) polymerase (*PARP*), were FDA approved in 2020, to treat mCRPC with genomic alterations in homologous recombination (HR) DNA repair genes (*BRCA1*, *BRCA2*, *ATM*, *BARD1*, *BRIP1*, *CDK12*, *CHEK1/2*, *FANCL*, *PALB2*, *PPP2R2A*, RAD51 B/C/D and *RAD54L*). HR defects are observed in up to 20% of mCRPC patients with somatic or germline mutations[102]. The *BRCA2* gene is the most commonly altered of the other HR genes in PCa, with loss of function resulting from mutation or deletion. In particular, germline *BRCA* mutations are associated with a poor clinical outcomes[103]. *BRCA* mutated mCRPC may be more likely responsive to PARP inhibition, a synthetic lethality phenomenon (the loss of

function of both genes simultaneously results in cell death, whereas the defect in any one gene only has a minor impact on cell viability), than other HR genes[104]. Recently, a phase 3 trial showed that in men with mCRPC who had disease progression while receiving enzalutamide or abiraterone and who had alterations in genes with a role in HR repair, olaparib was associated with longer OS and PFS[105].

PARP inhibitors are also being tested in association with AR pathway inhibitors in mCRPC (e.g. TALAPRO-2, a phase 3 randomized study of enzalutamide plus talazoparib (PARP inhibitor) vs placebo)[106]. In addition to PARP inhibitors, platinum-based chemotherapy can also be proposed for tumors with HR gene deficiency[107].

The PI3K-AKT-mTOR pathway is one of most frequently activated among the several regulatory pathways involved in PCa. This signaling network is involved in a large number of essential biological processes including cell cycle, proliferation, growth, survival, metabolism, motility, genomic instability and remodeling of the cancer microenvironment[108]. AKT activation is associated with PTEN loss which may induce inhibition of AR transcriptional activity in PCa and is commonly implicated in advanced disease with unfavorable clinical outcomes[109]. Ipatasertib is a potent AKT inhibitor, which has shown to improve PFS in combination with AA in patients with PTEN loss tumors[110]. Likewise, the MSI-H/dMMR disease is observed in around in 3.1% of PCa patients[111]. Furthermore, CDK12 alterations appear to correlate with the efficiency of immunotherapies in mCRPC[112].

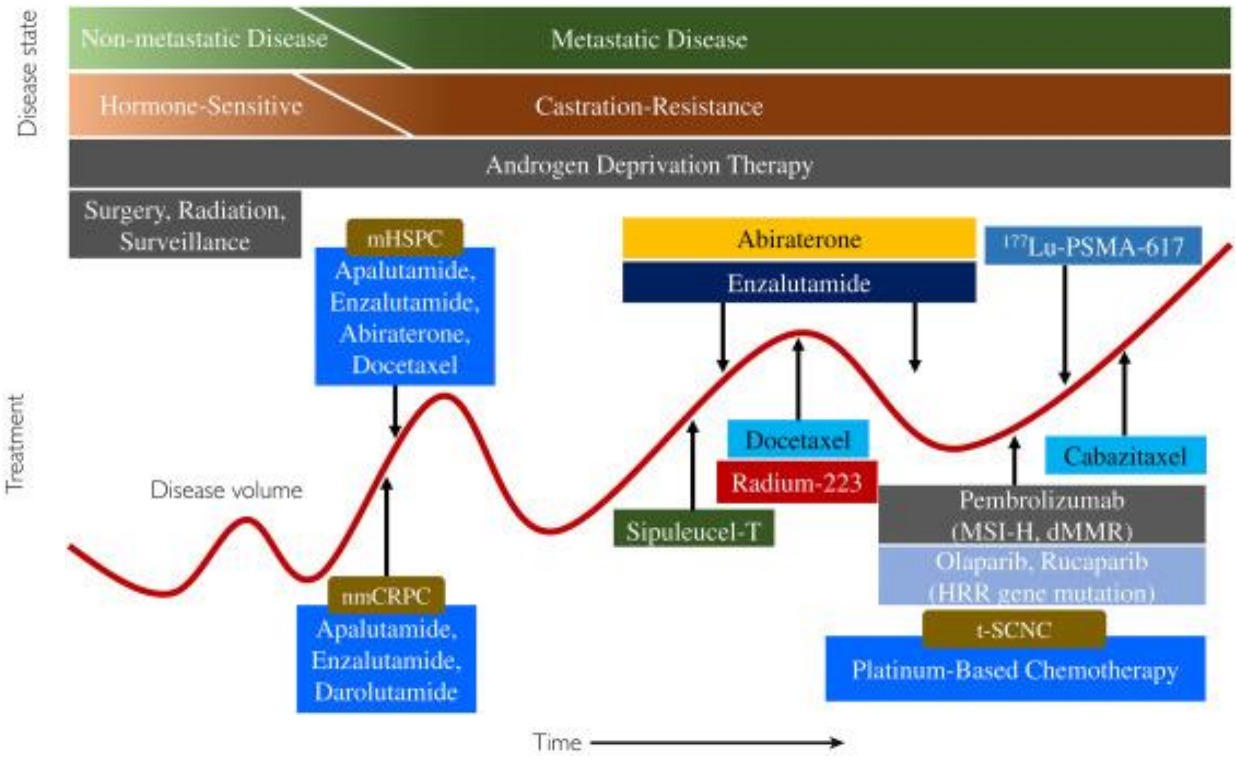

Figure 8: The current management landscape of systemic therapies in PCa. HRR: homologous recombination repair; t-SCNC: treatment-emergent small-cell neuroendocrine PCa[113].

Overall, this section showed that many drugs have been approved recently and are currently used for the management of patients with metastatic PCa. One major issue is that these novel agents (ARPIs, chemotherapy, radioligands) that are now in widespread clinical use prolong survival of patients with metastatic PCa but are not curative. Especially, an abundance of data has made it clear that AR pathway itself remain central both to the progression to CRPC and to its continued growth. Despite the success of these second-generation ARPIs, inherent or acquired resistance remains a major clinical challenge in daily practice. Indeed, ARPIs are now used in several settings (high-risk localized prostate cancer, non-metastatic CRPC, castration-sensitive prostate cancer, metastatic castration-resistant prostate cancer) and the identification of mechanisms of resistance will allow better patient selection and envision new strategies to overcome resistance.

4. Mechanisms of resistance to ARPIs

4.1 AR function in the prostate

Prostatic development takes place through fetal and postnatal processes of epithelial budding and branching. During early development there is rapid growth and differentiation of the prostate[114]. The process of development of the prostate has 6 main phases: (1) specification, (2) emergence of solid prostatic epithelial buds from the urogenital sinus epithelium, (3) elongation and branching of the buds, (4) canalization of the solid epithelial strands, (5) differentiation of the luminal and basal epithelial cells, and (6) secretory cytodifferentiation[115]. The last two steps are achieved during puberty in response to increased secretion of androgens. The adult prostate shows a considerable capacity for regeneration, with the possibility of regaining its initial size even after several castration and androgen treatments. This ability to regenerate in a controlled manner led to the investigation of an androgen-independent epithelial progenitor in benign prostate hyperplasia (BPH) and PCa. Indeed, the advanced PCa can be delayed by androgen withdrawal, but resistance develops, which may point to the presence of an independent progenitor of androgens. New findings suggest that there are several castration-insensitive epithelial cell types in the proximal zone of the prostate, but not all of them function as progenitor cells in both prostate development and regeneration[114].

The detection of adult stem cells in human prostate is mainly based on the identification of populations with the expression of putative stem cell markers in combination with the assessment of their proliferative potential both *in vitro* and in xenografts[116,117,118,119,120,121]. These studies propose the cell population with stem-like characteristics is both small and dispersed across the glandular epithelium. This population is mainly localized in the basal cell compartment, even though recent

studies show that luminal cells also have significant latent regenerative capacity and contribute to all prostate epithelial cell types[122,13].

The normal prostate epithelium is composed by three main epithelial cell types: basal, luminal and neuroendocrine (NE) in an approximate ratio of 60, 40 and 1%[123]. These cells can be classified based on their shape, gene expression, surface antigens and their respective localization in the glandular acini[124,125].

Based on gene expression, basal prostate cells express cytokeratin 5 (CK5), CK14, transcription factor p63, and very low amounts of AR. While the luminal cell markers include CK8, CK18, AR and androgen-regulated secretory proteins such as KLK3 or PSA[126,127] (**Figure 4**). However, upon the common expression of basal and luminal cytokeratins, a putative intermediate cell state between basal and luminal lineages was identified. They are derived from the cellular differentiation of basal cells to become luminal cells. Intermediate cells may play an important role in normal growth and neoplastic transformation, and also in the early stages of prostate development and regulation[128,129].

Normally, AR is highly expressed by luminal cells of the prostate, which may lead to increased cell proliferation in neoplasia[130]. Through the luminal epithelium of the normal prostate, binding of androgens, such as DHT, induces a cytoplasmic to nuclear translocation of the AR where it links to target genes (those with an androgen response element (ARE)) to trigger a transcriptional response[131]. Whereas, NE cells represent a rare population of endocrine-paracrine cells, scattered between the basal and luminal cells, and characterized by expression of NE markers (Synaptophysin (SYP), Chromogranin A (CHGA)[132] and neuron-specific enolase (NSE)), but not expressing AR[126]. They are sensorial and endocrine cells, which share structural, functional, and metabolic properties with prostate neuronal cells, and produce NE peptides by promoting the epithelial growth and viability[133].

In parallel, stromal cells express Alpha Smooth Muscle Actin (α-SMA), and VIM (vimentin)[8]. They surround the glandular structures of the prostate to control and support the growth and differentiation of the epithelium. Stromal cells consist of fibroblasts, myofibroblasts, and smooth muscle cells derived from mesenchyme[13].

4.2 AR structure

The development, growth, maintenance and function of prostate cells is driven by androgen hormone stimulation. This hormonal dependency is maintained by cancer cells, notably in the early stages of malignancy development.

The AR is the key molecule for moderating androgenic function and the oncogenic target for endocrine therapy of PCa. Furthermore, the AR axis is mainly involved in the mechanisms of resistance to therapies in PCa and tumor progression.

The *AR* gene is located on the long arm of the X chromosome (locus: Xq11-Xq12). Gene transcription produces an mRNA containing 8 exons that code for the AR protein, composed of 920 amino acids (**Figure 9A**). The AR protein has 3 main functional domains: the N-terminal domain (NTD), the DNA-binding domain (DBD) and the ligand-binding domain (LBD); with 5-α-dihydrotestosterone (5ADHT) as ligand (**Figure 9B**).

The nuclear receptor protein AR acts as a transcription factor triggered by steroid hormones, that regulate cellular proliferation and differentiation. Without activating ligands, AR is sequestered through a complex of heat shock protein (HSP) chaperones12 and their co-chaperones, like the BAG-1 family of molecular chaperones regulator (BAG-1), in the cytoplasm. When the hormone ligand is bound, the cascade of transcription factor activation steps is induced: the receptor cleaves from the complex proteins, translocates into the nucleus, dimerizes, and thus stimulates transcription of *AR* target genes (**Figure 9C**).

Alternative splicing (the alternative inclusion and exclusion of exons and introns via the splicesome regulation) of AR mRNA leads to many transcript variants which code for different isoforms.

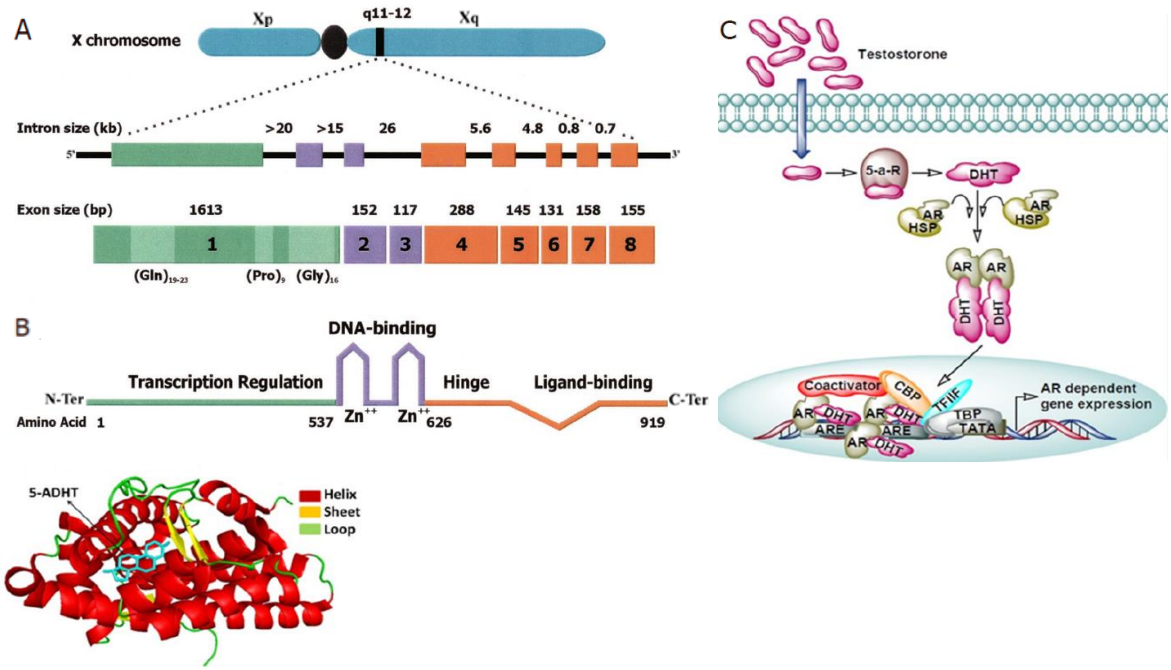

Figure 9: AR nuclear (A) and protein structures (B) and signaling pathway (C)[134,135]**.**

4.3 Current knowledge of mechanisms of resistance to ARPIs

Multiple mechanisms of resistance to ARPIs have been identified (*AR* overexpression with or without amplification, AR mutations, AR splice variants (AR-Vs), intratumoral DHT synthesis, Glucocorticoid Receptor (GR) overexpression and loss of AR) and others undoubtedly remain to be discovered (**Figure 10**). Due to the multiclonal and heterogeneous nature of PCa, it is plausible that multiple mechanisms of resistance may be operating concurrently in any given patient, and these may also change temporally in response to sequential treatments.

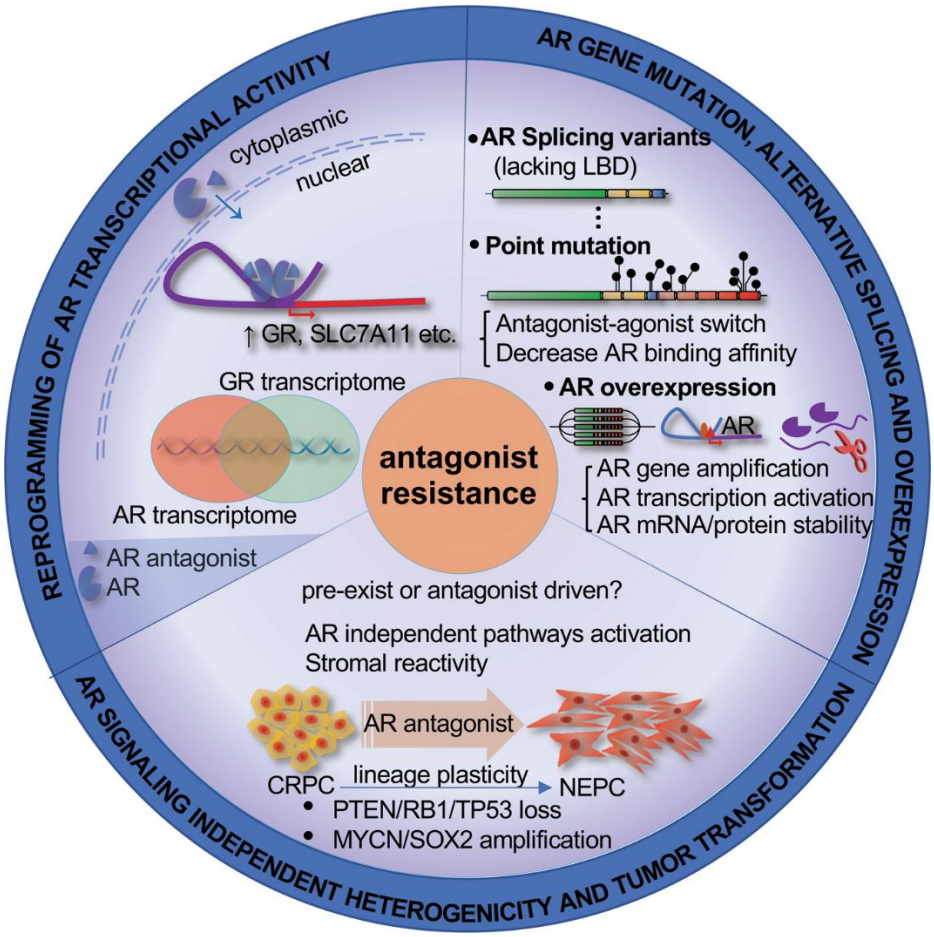

Figure 10: Mechanisms of resistance to ARPIs in PCa[136]**.** Direct AR pathway signaling mechanisms (e.g. alternative splicing, mutation and overexpression) and indirect mechanisms (e.g. oncogenic genes' expression, especially the glucocorticoid receptor (GR), loss of function of *PTEN*/*TP53*/*RB1* and amplification of *MYCN*/*SOC2*), contributing to tumor progression and resistance to ARPIs.

AR Ligand Binding Domain Mutations: recurrent *AR* mutants are present in ~15–20% of CRPC cases, a frequency that grows to greater than 60% when combined with *AR* gene amplification[137,102]. F877L mutation in the ligand-binding domain causes enzalutamide and apalutamide to play as AR agonists and confers drug resistance across multiple models both *in vitro* and *in vivo*[138]. Using circulating cell-free DNA (cfDNA), F877L was identified in a small number of CRPC patients at the time of progression with apalutamide or enzalutamide[139]. However, current evidence suggests they may be infrequent[102]. Another group of mutations in the ligand-binding domain, H875Y, T878A, and L702H, were found in patients progressing on abiraterone[139]. These

mutations share the property of promiscuous activation by non-canonical steroid ligands such as adrenal androgens, estrogen, progesterone or, in the case of L702H, by glucocorticoids. The frequent identification of L702H, H875Y and T878A mutations in contemporary patient cohorts may be a consequence of promiscuity towards other steroid ligands rather than antiandrogen resistance (**Figure 11**)[140,136,141].

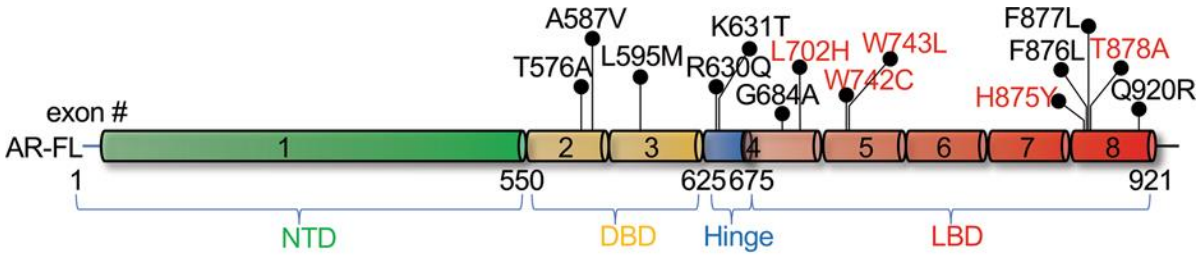

Figure 11: *AR* resistance mutations responsible for resistance to *AR* antagonists. In red: the most frequent mutations in patients. In black: mutations that result in resistance to enzalutamide and apalutamide[140,136,141].

AR Splice Variants: alternative splicing of *AR* mRNA is another mechanism implicated in progression to CRPC as well as in resistance to abiraterone and enzalutamide. Although expression of AR-Vs is clearly increased in resistant tumors, the evidence that AR-Vs play a causal role in resistance remains somewhat controversial. All AR-Vs share the common structural feature of truncation or exon skipping of the complete carboxy-terminal LBD, typically with a small, variant-specific in-frame sequence added as a consequence of alternative splicing (**Figure 12**)[142]. Importantly, all AR-Vs retain the amino-terminal transactivation and DNA binding domains. These structural properties could confer constitutive, androgen independent activity to all AR isoforms. However, overexpression of AR-V7 in AR-negative LNCaP cells did not confer resistance to enzalutamide *in vitro* and *in vivo*, even though AR-V7 promoted tumor growth in mice treated with castration alone[143]. The confusion about the role of AR-V7 (and other AR-Vs) in resistance will only be resolved through carefully executed prospective studies

in human. First reports in pioneer cohorts of men with heavily pre-treated CRPC (post-docetaxel, multiple lines of hormonal therapies) showed that AR-V7 expression correlated with primary resistance to abiraterone or enzalutamide[144,145] (**Figure 13**).

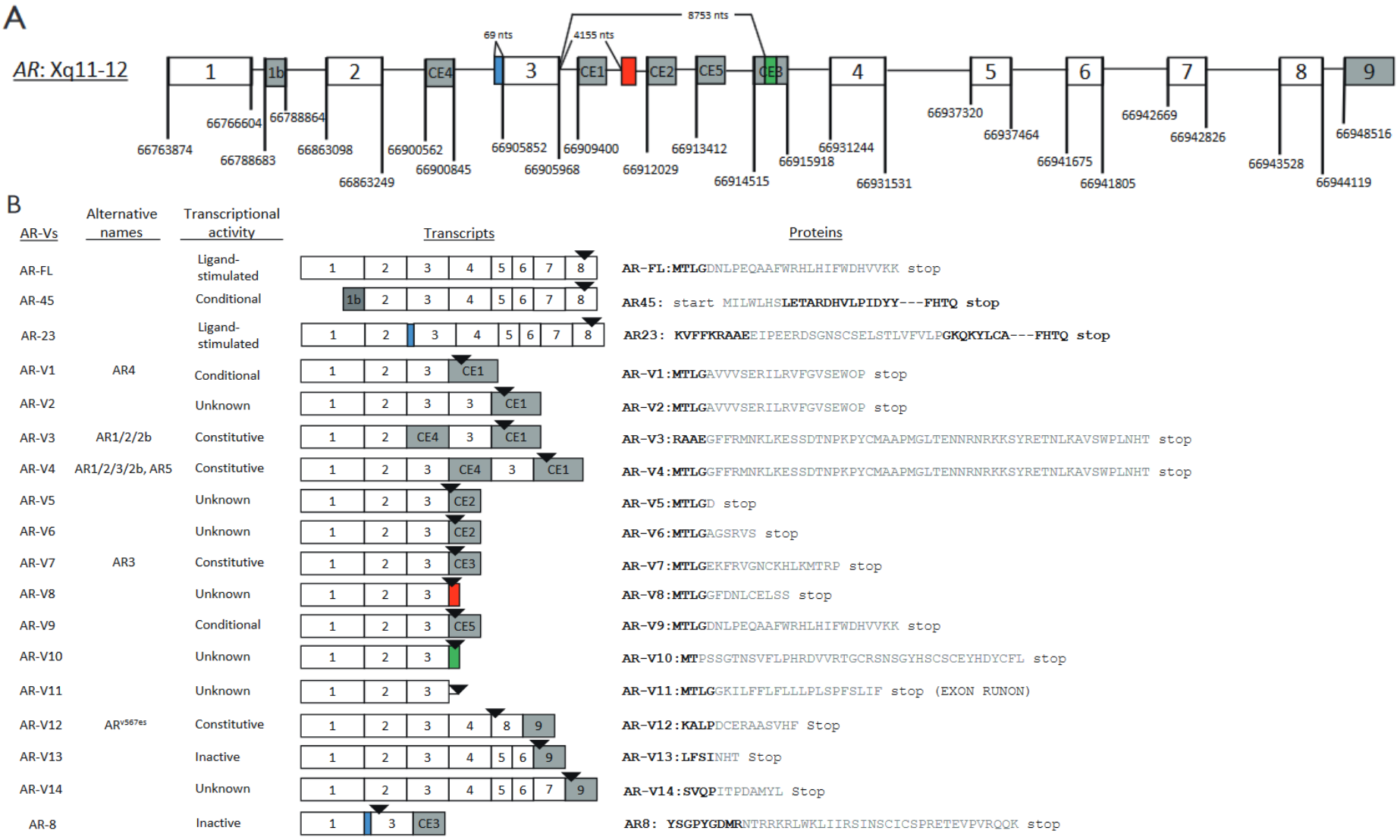

Figure 12: *AR* gene and the majority of AR splicing transcripts' structures. A: *AR* gene structure with canonical and cryptic exon splice junctions mapped to GRCh37/hg19 human genome sequences (non-scaled). **B:** Variant-specific nomenclature, functional annotation, exon composition, and mRNA sequences (coloured according to A) and peptides (grey)[142].

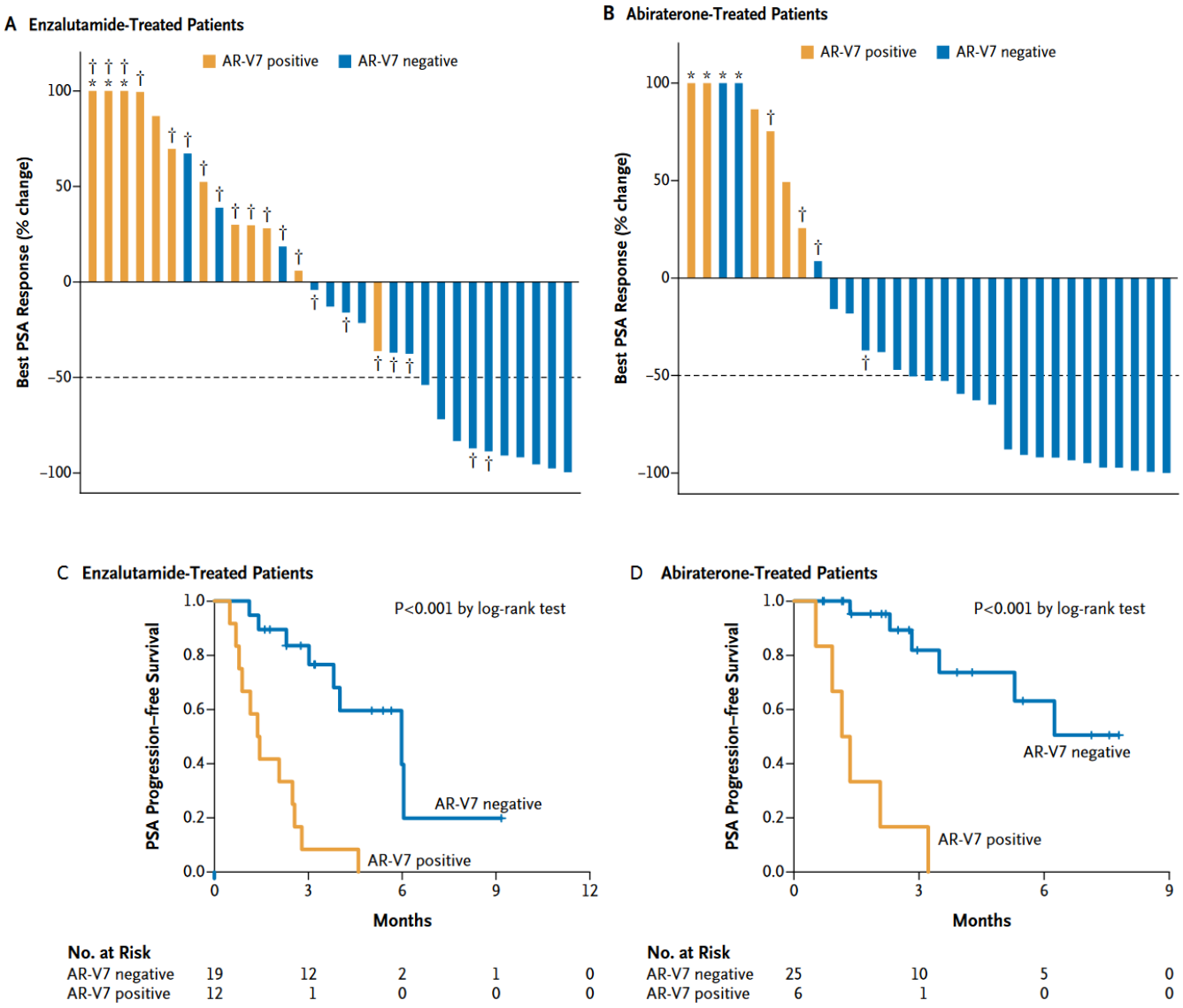

Figure 13: Waterfall plots of the best PSA change responses and Kaplan–Meier analysis of PSA PFS, all based on AR-V7 status[144]**.** In all, 31 patients receiving enzalutamide (A and C) and 31 patients receiving abiraterone were included in the study (B and D). The dotted line represents the cut-off to define a PSA response (≥ 50% reduction in PSA level from baseline). Asterisks correspond to an increment of ≥ 100% of the best PSA response. Daggers show abiraterone-pretreated patients in the enzalutamide cohort and enzalutamide-pretreated patients in the abiraterone cohort. C: median PSA PFS in enzalutamide-treated patients was 1.4 months (95% CI, 0.9 to not reached) and 6.0 months (95% CI, 3.8 to not reached) in AR-V7–positive and negative patients respectively. Hazard ratio = 7.4; (95% CI, 2.7 to 20.6; P < 0.001 by the log-rank test) for PSA progression with AR-V7 positive. D: median PSA PFS in abiraterone-treated patients was 1.3 months (95% CI, 0.9 to not reached) versus ≥ 5.3 months (95% CI, 5.3 to not reached) in AR-V7–positive and negative patients, respectively. Hazard ratio = 16.1 (95% CI, 3.9 to 66.0; P < 0.001 by the log-rank test) for PSA progression with AR-V7 positive.

AR Bypass Signaling: this refers to mechanisms in which downstream hormone receptor pathway signaling remains important but through activation by a different hormone receptor. Preclinical studies reported that by acquiring expression of the glucocorticoid receptor, PCa cells were shown to evade the antiproliferative effects of enzalutamide or apalutamide by utilizing this related steroid hormone receptor to cross regulate a subset of *AR* regulated target genes[146]. In addition to GR, the progesterone receptor (PGR) and the mineralocorticoid receptor (MR) are also steroid hormone nuclear receptor family members structurally related to AR, sharing substantial homology within the DNA binding domain. As with GR, it is plausible that PGR or MR could transcriptionally regulate a subset of AR target genes in PCa, and thereby bypass AR.

Lineage plasticity: with the daily use of abiraterone and enzalutamide, it is well recognized that some patients can have disease progression with clinically aggressive variants of PCa with reduced or absent AR expression. While the histological classification of these subtypes continues to be refined, they are often found to express markers of NE differentiation (CHGA and SYP). Adding further complexity, tumor cells with NE differentiation can often be found mixed with usual adenocarcinoma cells. Molecular profiling of PCa with NE differentiation has revealed loss of *RB1, PTEN, and TP53* mutations as well as amplification of *MYCN* and *AURKA*[147]. Evidence supporting transdifferentiation comes from multiple studies showing the presence of the AR-regulated *TMPRSS2-ERG* genomic translocation in AR-negative tumor at a frequency akin to that seen in AR-positive adenocarcinoma[147]. Another study of 101 cases of CRPC resistant to abiraterone or enzalutamide reported that only 33% displayed typical adenocarcinoma histology, with 12% small cell carcinoma (SCC) and an intermediate histology distinct from either in 27% of cases[148]. Non genetic mechanisms of NE differentiation includes activation of transcriptional factors such as SOX2, BRN2, ONECUT2, SRRM4, and PEG10[149].

SCIENTIFIC CONTEXT

Most data on the mechanisms of resistance to ARPI stem from preclinical studies or from retrospectives studies in human samples. A few studies to date have prospectively examined samples from men with mCRPC to identify determinants of response or resistance to ARPIs. However, these studies have largely been restricted to mutational profiling, were small in size, or focused on primary —rather than acquired—resistance. Thus, predictors and determinants of both *de novo* and acquired ARPIs resistance in CRPC remain largely unknown.

To summarize, ARPIs include CYP17A1 inhibitors and AR inhibitors have dramatically changed the management of patients with PCa in early and late stage disease. While these therapies are active in most patients, 20-25% of patients experience primary (or *de novo*) resistance and most patients who benefit from these therapies eventually experience subsequent disease progression due to acquired resistance. Current data from preclinical and clinical studies suggest that these mechanisms are diverse. Few reports on resistance mechanisms are available to date and limited hints on strategies to overcome resistance have been proposed yet.

Furthermore, there is a lack of biomarkers and treatments, in spite of the progress of precision medicine treatments, including for advanced PCa (**Table 3**)[150]. In addition, not all cancers benefit from precision medicine options in the absence of reliable biomarkers or approved targeted therapies. The use of large gene panels to test patients' tumors is often expensive and long; because it is still difficult to prove the efficacy of drugs targeting these pathways given the low prevalence of these same alterations[150]. At times, although an oncogenic alteration is recognized, developing drugs to target it can be a challenge because of its molecular structure, location and function in cells. In prostate cancer, it is still difficult to identify new biomarkers compared to other tumors. Hence, it is essential to pursue studies aimed at elucidating

the mechanisms of resistance to next-generation AR inhibitors in mCRPC, and then develop biomarkers predictive of treatment response at very early stages of cancer, which will optimize the relevance of existing drugs, as well as develop new ones or discover new biomarkers, leading to better patient outcomes.

Gene	Alteration	Prevalence	ESCAT	References
BRCA1/2	Somatic mutations/deletions	9%	IA	De Bono J, et al. *NEJM*. 2020[105]
	MSI-H	1%	IC	Cortes-Ciriano I, et al. *Nat Commun*. 2017[151]
				Abida W, et al. *Clin Oncol*. 2018[152]
				Marcus L, et al. *Clin Cancer Res*. 2019[86]
PTEN	Deletions/mutations	40%	IIA[a]	Abida W, et al. *Proc Natl Acad Sci*. 2019[153]
				De Bono J, et al. *Clin Cancer Res*. 2019[154]
				Kotani N, et al. *Cancer Chemother. Pharmacol. 2022*[155]
ATM	Mutations/deletions	5%	IIA	De Bono J, et al. *NEJM*. 2020[105]
PALB2	Mutations	1%	IIB	Mateo J, et al. *NEJM*. 2015[156]
				De Bono J, et al. *NEJM*. 2020[105]
PIK3CA	Hotspot mutations	3%	IIIA	Crumbaker M, et al. *Cancers*. 2017[157]
AKT1^{E17K}	Mutations	1%	IIIA	Crumbaker M, et al. *Cancers*. 2017[157]

Table 3. The ESCAT list of level I/II/III genomic alterations in advanced PCa[150]. ESCAT: ESMO Scale for Clinical Actionability of molecular Targets. a: AKT inhibitors may be effective for *PTEN*-mutant PCa specifically. Depending on the extent of the benefits and the evaluation of the report by peers, PTEN could be reclassified as an IA.

THESIS AIMS

The objectives of my PhD project are to define the molecular mechanisms responsible for resistance to ARPIs in patients suffering from mCRPC. The analysis of the molecular findings, derived from both baseline and post-progression tissue biopsies represent the ultimate objective in this work. The source of clinical samples is MATCH-R, an institutional study (NCT02517892) set up at Gustave Roussy Cancer Campus by my PhD director, Dr Loriot, in 2015, aiming to identify molecular mechanisms of acquired resistance across targeted treatments. In addition to perform high-throughput molecular analyses, the MATCH-R study aims to establish patient-derived xenografts (PDX) and cell lines (**Figure 14**).

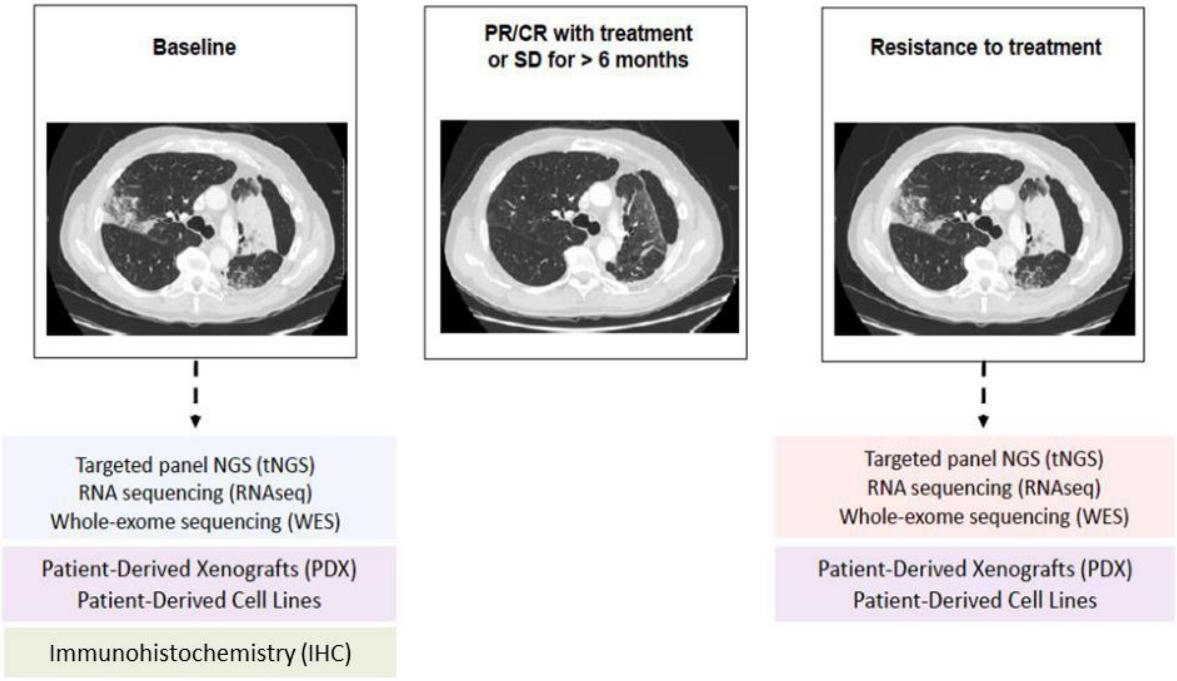

Figure 14: MATCH-R trial design[158]**.** Patients had either an initial response, described as a partial response (PR) or complete response (CR) according to RECIST 1.1, or a stable response (SR) within at least 24 weeks, and experienced disease progression during active treatment with molecular targeted therapy or immunotherapy.

At the beginning of this project, the initial idea was to report resistance to ARPIs in the two different stories, one for mechanisms of primary resistance and the second for

mechanisms of acquired resistance. However, we eventually decided to report our study within the same story here proposed emphasizing similarities and differences. This decision came from both pragmatical, "editorial" reasons (it would have been challenging to report the information in a two papers from the same data set) as well as for scientific reasons.

SPECIFIC AIMS (MANUSCRIPT 1)

CHAPTER 1	**Aim 1: To decipher the genomic and transcriptomic landscapes of metastatic prostate cancer resistant to castration and androgen receptor pathway inhibitors** (1) To statistically describe the clinical and biopsy data of patients in the whole cohort (2) To assess patient survival stratified by response status and monitor the response at time of baseline and progression (3) To characterize a genomic and transcriptomic metastatic prostate tumors (4) To evaluate mCRPC tumor histology characteristics
CHAPTER 2	**Aim 2: To study molecular mechanisms of primary resistance to ARPIs** (1) To identify genomic aberrations associated with primary resistance (2) To determine gene expression alterations and alternative oncogenic signaling leading to primary resistance (3) To highlight clonal evolution of mCRPC at primary resistance
CHAPTER 3	**Aim 3: To explore molecular mechanisms and acquired resistance** (1) To detect genomic alterations related to acquired resistance (2) To elucidate biological signaling pathways involved in acquired resistance (3) To investigate tumor clonal architecture driving the acquired resistance from patients treated with ARPIs

OVERALL METHODOLOGY

Data sources

In this thesis, we exploited multidisciplinary data sources, including clinical, molecular and tissue data from patients in the MATCH-R cohort (NCT02517892). All participants provided informed consent and the study was approved by the independent ethics committees or institutional review boards at each site.

MATCH-R is a French, prospective, multicentre clinical trial conducted mainly by the Gustave Roussy Cancer Campus. It includes studies on numerous solid cancers, such as lung and melanoma with the specific objectives of assessing predictive factors of resistance to anticancer agents and studying the evolution of the clonal architecture of patients' tumors.

Between 01/2015 and 11/2019, 90 patients with mCRPC were enrolled in MATCH-R. From which 59 patients were recruited in the current analysis. Of these, 30 patients were excluded due to insufficient tumor cells or DNA/RNA quantity and 1 patient was excluded due to unknown response status. The ultimate goal is to discover novel mechanisms of primary and acquired resistance to hormone therapies with a new generation of agents that inhibit the AR signaling axis (e.g. abiraterone, enzalutamide), among mCRPC patients. Other targeted therapies (e.g. olaparib, PDL1 inhibitors) were also investigated but not included in the thesis work.

All patients are followed for several years until disease progression. Data are collected before and after treatment for tumor progression. This data collection includes demographic data, detailed clinical data and treatment data. High-throughput RNA-seq and WES data on matched biopsy samples of tumor lesions at baseline and at disease progression were obtained, where possible. In addition, blood samples were also collected during the first biopsy. Protein data from IHC were provided and validated by pathologists for both biopsies per patient, where possible.

Throughout the work reported here, we have used human data and selected patients according to agreed quality control procedures for each stage of the overall analysis, thereby preventing, reducing and or eliminating bias and confounding factors, to address several clinical and research questions.

Description of overall approaches

Data management and statistical analysis: by considering multilevel data for single and whole patients (all statistical analyses were performed in R)

(1) Data extraction and descriptive statistical analysis of data
(2) Univariate and multivariate survival analysis
(3) Statistical test for comparison between interest groups
(4) Association studies

Genomic analysis (WES): assessment of germline and somatic alterations, tumor mutational load, copy number variations, activated pathway data, mutational signatures and other genomic features that reflect genomic instabilities

(1) Quality control analysis of both raw and processed data
(2) Exploratory or unsupervised analysis (e.g. clustering analysis)
(3) Differential or supervised analysis between groups of interest
(4) Functional analysis: determination of the biological signaling pathways involved
(5) Tumor progression trees reconstruction for matched baseline and resistance samples

Transcriptomic analysis (RNA-seq): exploration of gene expression, splicing variants, pathway analysis, and tumor microenvironment analysis

(1) Quality control analysis of both raw and processed data
(2) Exploratory or unsupervised analysis (e.g. clustering analysis)
(3) Differential analysis or supervised analysis between groups of interests
(4) Functional analysis: determination of the biological signaling pathways involved, computation of transcriptomic scores
(5) Pathway activity analysis: measurement of the oncogenic pathway activity score
(6) Immune analysis based on gene expression to estimate the abundances of immune cell types in tumors

IHC analysis: assessment of the staining intensity of used relevant biomarkers and the histological phenotype subtypes of mCRPC tumors

Omics and clinical data integration analysis and exploration:

(1) Descriptive analysis and the visualisation of the results: Oncoprint and oncogenic trees with genomic, transcriptomic and pathway data, including clinical annotations
(2) Statistical analysis (e.g. calculation of the frequency of multiple types of alterations and proportions of mutational signatures for each patient)

Contribution and involvement of the PhD student

All major assignments were carried out by MSc Naoual Menssouri, PhD student:

- Design and administration of the projects
- Data management of the database
- Define appropriate solutions to exploit and interpret data, by developing and adapting bioinformatics algorithms in R, Bash and Python
- Searching for funding
- Build and maintain collaborations with national and international actors in the field
- Processing to submit and present results at scientific events
- Writing and reviewing manuscripts
- Delivery of results for publication

OVERALL RESULTS

RESULTS

The paper here presented, I report the clinical outcomes and the molecular correlates of resistance to ARPIs in 59 patients with mCRPC. The findings obtained in tissue has served as the basis for suggesting which alterations could be responsible for both primary and acquired resistance. First, I analysed the genomic landscape of mCRPC samples we obtained from baseline and resistant samples. In the second part, we correlated WES and RNA-seq data with outcome. In the last part of the paper, we aimed to characterize the clonal evolution of mCRPC under the exposure to ARPIs taking advantage of paired biopsies. Finally, we compared the transcriptomic landscape of baseline and resistant samples to study potential transcriptional programs involved in acquired resistance. Of note, one mechanism of resistance of secondary resistance was lineage plasticity with acquisition of NE differentiation. My work did not focus on exploring the precise mechanisms of lineage plasticity. Another PhD student in the lab aims to figure out these machanisms of NE differentiation. I am involved in this project by doing several bioinformatics analysis. In addition, another goal of MATCH-R study is to develop preclinical models of agressive prostate cancers such as NEPC or prostate cancers with specific genetic alterations. I have been also involved in this project by performing additional bioinformatics analysis. The paper related to this project is currently under revision in the *Clinical Cancer Research* journal and can be found in the appendix.

MANUSCRIPT 1: Genomic profiling of metastatic castration-resistant prostate cancer samples resistant to androgen-receptor pathway inhibitors

Authors

Naoual Menssouri[1], Loïc Poiraudeau[1], Carole Hellisey[2], Ludovic Bigot [1], Jonathan Sabio[1], Tony Ibrahim[1], Cédric Pobel[1], Claudio Nicotra[3], Maud Ngo-Camus[3], Ludovic Lacroix[4,5], Etienne Rouleau[4,5], Lambros Tselikas[6], Anne Chauchereau[1], Félix Blanc-Durand[7], Alice Bernard-Tessier[7], Anna Patrikidou[7], Natacha Naoun[7], Ronan Flippot[7], Emeline Colomba[7], Alina Fuerea[7], Laurence Albiges[7], Pernelle Lavaud[7], Paul van de Wiel[8], Eveline den Biezen[8], Yvonne Wesseling-Rozendaal[8], Santiago-Ponce[3], Stefan Michiels[9], Christophe Massard[3], Fabrice Barlesi[1], Fabrice André[1,10], Benjamin Besse[1,7,10], Jean-Yves Scoazec[1,4,5], Luc Friboulet[1], Karim Fizazi[1,7], and Yohann Loriot[1,3,7,10]

Affiliations

[1] Paris-Saclay University, Gustave Roussy Cancer Campus, INSERM U981, Molecular predictors and new targets in oncology, Villejuif, France

[2] Hôpital d'Instruction des Armées BÉGIN, Saint Mandé, France

[3] Drug Development Department (DITEP), Gustave Roussy Cancer Campus, Villejuif, France

[4] Experimental and Translational Pathology Platform (PETRA), Genomic Platform-Molecular Biopathology Unit (BMO) and Biological Resource Center, AMMICA, INSERM US23/CNRS UMS3655, Gustave Roussy Cancer Campus, France

[5] Department of Medical Biology and Pathology, Gustave Roussy Cancer Campus, Villejuif, France

[6] Department of Interventional Radiology, Gustave Roussy Cancer Campus, Villejuif, France

[7] Department of Medical Oncology, Gustave Roussy Cancer Campus, Villejuif, France

[8] InnoSIGN, High Tech Campus 11, 5656 AE Eindhoven, The Netherlands

[9] Oncostat U1018, INSERM, Paris-Saclay University, Labelled Ligue Contre le Cancer, Office of Biostatistics and Epidemiology, Gustave Roussy Cancer Campus, Villejuif, France

[10] PRISM Center for personalized medicine, Gustave Roussy Cancer Campus, Villejuif, France

Funding

MATCH-R prostate cancer study was funded by a grant from Sanofi

Previous presentations

Presented in part at AACR 2021 and at ESMO 2022, Paris

Running title

Mechanisms of resistance to ARPI in mCRPC

Keywords

Resistance, mCRPC, androgen receptor inhibitors, genomics

Publication

Submitted for publication to journal *Cancer Discovery* in November 2022

Abstract

Androgen receptor pathway inhibitors (ARPIs) are cornerstone therapies for men with metastatic castration-resistant prostate cancer (mCRPC). However, primary and acquired resistance mechanisms remain largely unknown. To address this question, we conducted a prospective study (NCT02517892) in 59 men with mCRPC treated with ARPIs, who underwent baseline biopsy and paired biopsy at resistance when feasible. Whole-exome sequencing analysis indicated that no single-gene genomic alterations was associated with primary resistance. RNA-seq analysis showed that *AR* gene alterations and expression levels were similar between responders and non-responders. RNA-based pathway analysis showed increased AR and NOTCH pathway activity in responders and activation of the Hedgehog pathway in non-responders. Subclonal evolution and acquisition of new alterations in AR-related genes or neuroendocrine differentiation are associated with acquired resistance. ARPIs do not induce significant changes in the tumor transcriptome of most patients; however, programs associated with cell proliferation are enriched in resistant samples.

Statement of significance

We analyzed the genomics and transcriptomics of human mCRPC to identify the mechanisms underlying the resistance to AR pathway inhibitors. We observed increased AR and NOTCH pathway activity in responders and Hh pathway activation in non-responders. Subclonal evolution, with new alterations in *AR*-related genes or neuroendocrine differentiation, is associated with acquired resistance.

1. Introduction

Metastatic prostate cancer remains a lethal disease and represents the second leading cause of cancer-related deaths in males in Western countries[1]. Almost all hormone-sensitive prostate cancer patients treated with androgen deprivation therapy (ADT) progress to metastatic castration-resistant prostate cancer (mCPRC)[2]. Activation of the AR is commonly found in mCRPC tumors despite ADT through several mechanisms, including intracrine biosynthesis of androgens[3], *AR* gene amplification[4], expression of AR variants[5], activation of *AR* target genes by alternative steroid receptors[6], and evolution to a neuroendocrine phenotype[7]. Recently, potent AR pathway inhibitors (ARPIs) have been developed to counteract AR-related mechanisms of resistance. ARPIs include abiraterone acetate/prednisone (AA/P), which inhibits the intracrine biosynthesis of androgens by blocking cytochrome P450 17A1 (CYP17A1) activity[8], and newer AR antagonists such as enzalutamide[9,10], apalutamide[11], and darolutamide[12-14]. These new agents have been shown to improve progression-free survival (PFS) and overall survival (OS) in patients with mCRPC, metastatic castration-sensitive prostate cancer, and non-metastatic CRPC.

However, many patients experience rapid disease progression under ARPI therapy, suggesting primary resistance, and the majority of patients with clinical benefits eventually experience "secondary" or "acquired" resistance status. Few analyses using WES and RNA-seq of prospectively collected human samples[15-17] have been conducted to elucidate the mechanisms underlying primary and acquired ARPIs' resistance, which remain largely unknown. We hypothesized that thorough characterization of the genomic landscape of samples from patients with mCRPC treated with ARPIs could identify the determinants of primary and acquired resistance. To address this question, we conducted a prospective clinical trial in men with mCRPC who had metastatic lesions amenable to a pretreatment biopsy. In addition, we aimed to identify the

molecular alterations associated with acquired resistance to ARPIs by analyzing paired biopsies obtained at the time of resistance.

2. Materials and methods

2.1 Patients and samples

The 'MATCH-R' (NCT02517892) study[18] was initiated in 2015 after approval by the Gustave Roussy Institutional Review Board (IRB) and ethics committee. This multicenter prospective study evaluated the predictors of resistance to targeted therapy (including ARPIs, in men with mCRPC). All enrolled patients provided written informed consent to undergo two serial tumor tissue biopsies, which were performed before the initiation of either AA/P or enzalutamide and at the time of disease progression when feasible.

Patients were required to experience disease progression on continuous ADT at the time of enrollment. Patients who were previously treated with other ARPIs were included in this study. Prior to the initiation of ARPIs treatment, the subjects underwent image-guided biopsy of the tumor lesion to obtain tumor tissue for baseline genomic analyses. The subjects then received ARPIs continuously and were assessed for clinical, biochemical, or radiographic progression every eight weeks. Disease progression was defined according to the imaging criteria for soft tissue disease measured by computerized tomography (CT) scan or magnetic resonance imaging and/or the appearance of two or more unequivocal bone lesions on bone scan and/or clinical progression. Prostate-specific antigen (PSA) progression alone was not considered a criterion for discontinuation of study treatment. For the reported analysis, primary resistance was defined as disease progression within the first four months of therapy. These patients were classified as non-responders. Patients with no disease progression within the first four months were classified as responders. When feasible, a second biopsy was performed during disease progression (including in patients with primary

resistance). The primary goal of this study was to identify genomic alterations associated with primary and secondary resistance to ARPIs. The secondary clinical endpoints were PFS and OS, which were measured from the date of ARPI initiation.

2.2 Sequencing and genomic aberration analysis

Tumor cores were later stored in RNA, and the tumor cell content was reviewed by histological control. The tumors were frozen on the same day. WES of both tumor and germline DNA was carried out using the Illumina NextSeq500 and HiSeq2000 systems. RNA-seq was performed on an Illumina NextSeq500 platform using paired-end 75b reads. Details of the sequencing methods, copy number variation (CNV) analysis, and germline and somatic mutation (clonal and subclonal) analyses are provided in the supplementary methods. Genomics parameters (ploidy, fraction of altered genome (FAG), and fraction of allelic alterations (FAA)) were calculated as described in the supplementary methods.

2.3 Transcriptomic analysis - Unsupervised analysis

STAR[19] was used to obtain the number of reads associated with each gene in the Gencode v26 (GRCh38) annotation (restricted to protein-coding genes, antisense RNAs, and lincRNAs). Raw gene counts for each sample were imported into R statistical environment (v.4.0.2). The extracted count matrix was normalized for library size and coding length of genes by computing transcript per million (TPM) expression levels. The Bioconductor edgeR package[20] was used to import raw counts into R statistical software, and normalized log2(counts per million mapped reads (CPM)) were computed using the weighted trimmed mean of M-value (TMM) normalization procedure. The normalized expression matrix from the 1000 most variable genes (based on standard deviation) was used to classify the samples according to their gene

expression patterns using hierarchical (based on the Pearson distance and Ward.D2 clustering method) and consensus clustering. The latter was performed by "ConsensusClusterPlus" R package (v1.54.0) to assess the stability of the clusters. We established consensus partitions of the dataset in k clusters based on 1,000 resampling iterations (80% of genes and 80% of samples) of hierarchical clustering using the Pearson distance and Ward.D2 clustering method.

2.4 Differential expression analysis

Differential expression analysis was performed using the limma package[21] and voom transformation. Only the genes expressed in at least one sample (TPM ≥ 0.1) were considered. A q-value threshold of ≤ 0.05 and a minimum log2(fold change) of 1.2 were used to define differentially expressed genes.

2.5 Pathway enrichment analysis – GSEA

The gene list from differential analysis was ordered by decreasing log2(fold change). Gene set enrichment analysis (GSEA) was performed using the clusterProfiler package with the fgsea method in the GSEA function[22]. Gene sets from the Molecular Signatures Database (MSigDB, Broad Institute)[23] (v7.4) were selected from the hallmark collection, retaining only gene sets defined by 10–500 genes.

2.6 Pathway activity scores

Functional signal transduction pathway activity was determined from RNA-seq data using the OncoSIGNal pathway activity profiling Data Service (InnoSIGN B.V., Eindhoven, The Netherlands)[24]. In total, the activities of 10 oncogenic signal

transduction pathways (Estrogen Receptor, AR, MAPK, Hh, NOTCH, TGFβ, PI3K, NFκB, JAK/STAT1-2, and WNT) were determined as described in reference 24 and Supplementary Methods. OncoSIGNal pathway activity scores range from 0 to 100, with higher values indicating higher pathway activity. A Quality Control (QC) pass/fail judgment was made for each sample based on a multitude of predefined QC criteria (e.g. ratio of mapped reads to the total number of reads, reference gene expression, and transcript integrity number). Samples with poor performance were excluded from further analyses.

2.7 AR and NEPC scores

AR and neuroendocrine prostate cancer (NEPC) scores were calculated as Pearson correlation coefficients between the patient sample and the corresponding reference samples for the expression of each gene of the transcriptomic signatures (70 NE signature genes and 30 *AR* signature genes). A detailed description of the scoring approach is provided in the Supplementary Methods.

2.8 Immunohistochemistry (IHC)

IHC was performed to identify the phenotypes of mCRPC tumors by assessing the expression levels of AR (nuclear vs cytoplasmic expression) and protein markers associated with the neuroendocrine phenotype (e.g. Synaptophysin (SYP), Chromogranin A (CHGA), and CD56). The details are included in the Supplementary Methods section.

2.9 Statistical analysis

Descriptive statistics (median and interquartile range (IQR) for continuous variables; frequencies and percentages for categorical variables) were used to summarize the demographic and clinical data by response group. Statistical tests were performed using Fisher's exact test for categorical variables in two groups, chi-square test ($\chi 2$-test) for categorical variables in more than two groups, and Wilcoxon's test for quantitative variables. The paired t-test was used for paired analysis of the acquired resistance and matched baseline samples. Time-to-event analysis was performed using Kaplan–Meier curves and log-rank tests to evaluate the PFS and OS associations between the response groups. Cox regression models were used to calculate hazard ratios by response group with 95% Confidence Intervals (CIs). These models were also applied to assess the association of gene-based pathway cores with response status for primary resistance. Pearson's correlation coefficient was used to compare two continuous variables. All tests were two-sided, and statistical significance was set at $P < 0.05$. The Benjamini-Hochberg (BH) method was used to obtain adjusted P-values. All statistical analyses were performed using R software (v.3.6.0).

3. Results

3.1 Clinical and histopathologic parameters

Between 2015 and 2019, 90 patients were enrolled in the MATCH-R trial (NCT02517892) (**Figure 1A, Supplementary Figure 1**) at two French centers. The current analysis included 59 evaluable patients with at least one available RNA-seq or WES response status (**Supplementary Figure 2**). The clinical and demographic characteristics of patients for primary resistance analysis are shown in **Figure 1B** and **Suppdata1**. Of the 59 biopsies, 44.1% were prostate, 40.7% were lymph node, 5.1% were bone, 5.1% were lung, and 5.1% were liver biopsies. Following biopsy, the patients were treated with AA/P (25.4%) and enzalutamide (74.6%). Overall, 31 patients

(52.5%) achieved disease response. The median OS from the time of ARPI initiation was 18.2 months (95% CI: 14.1-NA). Median OS was not reached (95% CI: 16.1-NA) for patients with response versus 9.1 months (95% CI: 5-18.2) for patients with primary resistance (P = 0.00042) (**Figure 1C**). A PSA decline of ≥ 50% was achieved in 56% of evaluable patients (**Figure 1D**).

3.2 Landscape of genomic alterations

We first analyzed all samples (from the baseline and resistant samples). In total, there was sufficient DNA to perform WES on 74 samples. In addition, sufficient RNA was used to perform RNA-seq on the 69 samples. Median tumor cell proportion was 0.6 (IQR: 0.4-0.8) and median ploidy was 2.0 (IQR: 2.0-3.0) (**Suppdata2**). The median tumor mutation burden (TMB) was 65.0 clonal mutations (IQR: 38.0-92.0) and 21.5 subclonal mutations (IQR: 15.0-36.8) per tumor exome. The median FAA and FAG were 0.2 (IQR: 0.1-0.5) and 0.4 (IQR: 0.1-0.5) respectively. Overall, the frequency of genomic alterations, including baseline and resistant samples (**Supplementary Figure 3A**), was similar to those reported in prior cohorts[25,26], with *AR* (36.5%), *TP53* (33.8%), and *PTEN* (29.7%) being the most commonly altered genes (**Suppdata2**). Likewise, alterations in biological pathways were also consistent with previous reports[25], with a significant (> 20%) subset of patients harboring at least one alteration in the AR pathway (56.76%), DNA repair pathway (35.14%), PI3K pathway (35.14%), cell cycle pathway (35.14%), or epigenetic pathway (22.97%). The ERG-gene family fusion was found in 16 of the 51 samples (31.4%) (**Suppdata3**). We then extracted the contribution of a predefined set of six signatures (signatures 1 [clock-like], 2 [APOBEC], 3 [BRCAness], 5 [unknown], 6 [MMR], and 13 [APOBEC]) previously reported as significant in prostate cancer[27], and four signatures (15, 20, 21, and 26) associated with Microsatellite Instability (MSI)[28]. The most frequent mutational signatures (defined as the proportion of mutations associated with one signature > 50%) in our series were

signatures 1, 3, 5, and 15, predominant in 29, 15, 3, and 1 of the samples, respectively (**Suppdata4, Supplementary Figure 3**). Three (MR009, MR114, and MR191) out of 52 (5.8%) patients with both tumor and normal WES available harbored *BRCA2* germline deleterious mutations, one patient (MR182) (1.9%) had an *ATM* germline frameshift mutation, and another patient (MR098) (1.9%) had a germline *MSH6* frameshift mutation (**Suppdata5**).

Unsupervised clustering of 69 RNA-seq samples using the 1000 most variable genes identified four clusters. One cluster was associated with high NEPC scores, as previously reported[7] (**Supplementary Figure 4A**). Clustering was mainly driven by biopsy site (**Supplementary Figure 4B**). Samples underwent central histopathological review, revealing a luminal phenotype in 63.4% (26 of 41), NE features in 7.3% (3 of 41), and a mixed phenotype in 29.3% (12 of 41) of evaluable cases (**Suppdata6, Supplementary Figure 4C**).

3.3 Genomic alterations and primary resistance

Overall, 52 patients were included in the analysis of primary resistance (MR042 was excluded because of insufficient clinical data correlating with response). Twenty-four of these patients were non-responders and 28 were responders (**Figure 2A**). Associations between somatic alterations and primary resistance to treatment were evaluated at the single gene and gene pathway/network levels (**Suppdata7**). The number of clonal or subclonal mutations did not differ between responders and non-responders (P = 0.078 and P = 0.58, respectively). Tumor heterogeneity, as reflected by the proportion of subclonal mutations (P = 0.54) (**Figure 2B**), chromosomal instability as measured by FAG (P = 0.36) (**Figure 2C**), and FAA (P = 0.39), was not associated with response. Ploidy was not associated with response (P = 0.44). No statistically significant differences were detected between the two groups for any of the prostate cancer driver genes (for example, *AR* (P = 0.25), *TP53* (P = 0.38), and *RB1* (P = 0.21)) (**Figure 2D**). At

the pathway level, no statistical association was found between alterations in the AR (P = 0.27), cell cycle (P = 1), DNA repair (P = 1), PI3K (P = 1), epigenetic (P = 0.19), or WNT (P = 0.40) pathways. Furthermore, we found no statistically significant difference in mutational signatures between the non-responder and responder groups (**Figure 2E**) (**Suppdata4**).

Next, we determined whether there were differentially expressed genes and pathways in the RNA-seq data of non-responders compared with responders. RNA-seq data were available for 51 patients (29 patients with response and 22 patients with no response, MR042 was excluded from the analysis) (**Suppdata6**). First, we focused on the AR pathway as the main target of ARPI. *AR* gene expression was not associated with response (P = 0.77) (**Figure 3A**). Notably, AR-V7 expression (measured as the ratio of the TPM of AR-V7 divided by the TPM of *AR* long isoforms) was not associated with primary resistance (P = 0.13) (**Figure 3A**). RNA-seq data were analyzed to identify gene expression signatures associated with primary resistance to ARPI. To identify the relevant pathways associated with resistance, we performed GSEA[22] analysis using all candidate gene sets within the hallmark gene set from MSigDB[23]. This analysis determined that baseline tumors from non-responders versus responders had a statistically significant enrichment of 14 pathways (false discovery rate (FDR) q-value < 0.1) (**Figure 3B, Suppdata8**). Immune hallmark pathways were the top gene sets activated in non-responders, including IFN-α, IFN-γ, inflammatory response, complement, and TNF-alpha (TFNα) signaling via NF-κB. In addition, two pathways recently associated with resistance to ARPI were found: epithelial mesenchymal transition[16] (EMT) (NES = 1.72, q-value = 2.04^{-5}) and IL-6/JAK/STAT3[29] (NES = 1.64, q-value = 0.01). The androgen response gene set was the most enriched in responders (NES = -2.73; q-value = 9.34^{-13}). These data suggest that low AR activity and an EMT-like phenotype are associated with ARPI resistance. Low AR activity was associated with EMT and stemness as well as *de novo* enzalutamide resistance, as previous report[16]. Using GSEA, we found that the sonic hedgehog (Hh) pathway was one of the most

activated signaling pathways in non-responders (NES = 1.48, q-value = 0.07). The Hh pathway is associated with EMT and stemness in several tumor types, including prostate cancer[30,31]. To further study which signaling pathways are associated with the response to ARPIs, we used the OncoSIGNal mRNA-based approach that determines the activity of several signal transduction pathways in cancer and immune cells, including the AR and Hh pathway[24,32]. Eight other pathways were quantified (ER, MAPK, NOTCH, TGF-β, PI3K, JAK/STAT1-2, WNT, and NFκB). For this analysis, 46 samples (27 responders and 19 resistant samples) met the quality requirements (**Suppdata9**). The Hh pathway score was negatively correlated with the AR pathway score (Pearson correlation: r = -0.33, 95% CI: -0.57-0.05, P = 0.02) and weakly positively correlated with the NEPC score (Pearson correlation: r = 0.25, 95% CI: 0.05-0.50, P = 0.09) (**Supplementary Figure 5**). Patients with primary resistance had a higher Hh pathway score (P = 0.012), a lower AR pathway score (P = 0.092), and a lower NOTCH pathway score (P = 0.046) than patients with a response (**Figure 3C**) (**Suppdata9**). Low AR activity (defined as lower than the median score, **Supplementary Figure 6**) and high Hh pathway activity (defined as higher than the median score, **Figure 3D**) were associated with shorter PFS (P = 0.097 and P = 0.0021, respectively). Finally, multivariate analysis showed that prior chemotherapy (hazard ratio = 2.26, 95% CI: 1.04-4.91, P = 0.04), high Hh pathway activity (hazard ratio = 2.41, 95% CI: 1.15-5.06, P = 0.02), and low NOTCH pathway activity (hazard ratio = 2.17, 95% CI: 1.05-4.52, P = 0.04) were associated with shorter PFS (**Figure 3E**).

3.4 Genomic mechanisms of acquired resistance

Even if patients have clinical benefits for ARPIs, most eventually experience disease progression (secondary resistance). To determine the mechanisms of acquired resistance, we performed tissue biopsy when feasible in patients with an initial response to ARPIs. Overall, 18 patients underwent at least a second biopsy, 5 patients with

primary resistance, and 13 patients with acquired resistance (**Supplementary Figure 2**). For WES analysis, 21 samples were available: 5 samples from 5 patients with primary resistance (MR036-T2, MR040-T2, MR139RE-T1, MR150-T2, and MR363-T2) and 16 samples from 13 patients with response (MR09RE-T2, MR041-T2, MR116-T2, MR145-T2, MR151-T2, MR153-T1, MR166-T2, MR178-T2, MR182-T2, MR183-T2, MR188-T2, MR217-T2, and MR356-T2). For MR009, four sequential biopsies were performed and four additional WES profiles were obtained. For RNA-seq analysis, 17 samples were available: 5 samples from 5 patients with primary resistance and 12 samples from 9 patients with response.

We first analyzed the genomic landscape of the paired samples (n = 12) (**Figure 4A**). In eight patients, the same lesion was biopsied during progression. All except two (MR041 and MR116) were treated with enzalutamide. The median time to ARPI was 9.9 months (IQR: 4-25.3). At baseline, we identified a median of 63 clonal (IQR: 54.50-87.50) and 27 subclonal (IQR: 18.00-36.75) protein-coding mutations per sample, which was similar to that of the other enrolled patients (**Suppdata10**). Most of these changes are non-synonymous mutations in genes that have not been implicated in cancer, likely representing passenger mutations. At progression, the median number of clonal and subclonal mutations was not significantly different from that of baseline mutations (median: 62 (IQR: 49.75-84.75) and median: 23 (IQR: 20.50-31.75), respectively). Genomic instability readouts were not significantly different between baseline samples (median FAA: 0.36 (IQR: 0.11-0.48) and median FAG: 0.43 (IQR: 0.19-0.50)) and resistant samples (median FAA: 0.44 (IQR: 0.06-0.59), P = 0.57; median FAG: 0.43 (IQR: 0.15-0.59), P = 0.42). No single gene alterations were associated with acquired resistance. The proportion of each mutational signature was not significantly different between baseline and resistant samples (**Figure 4B**). Among the 12 patients with baseline and progression samples (**Figure 4A**), seven displayed acquisition of at least one new driver mutation at progression: *AR* (n = 4, MR009-T2, MR166-T2, MR178-T2, and MR217-T2), *NCOR1/2* (n = 1, MR178-T2), *TP53* (n = 1, MR188-T2), *RB1* (n = 2, MR145-T2 and

MR188-T2), *PTEN* (n = 1, MR145-T2), and *CTNNB1* (n = 1, MR041-T2). Three patients had no additional driver alterations at progression but displayed one or more potent drivers already present in the baseline sample: *AR* (n = 2, MR116-T2 and MR182-T2) and *CDK12* (n = 1, MR183-T2). The remaining two patients (MR151-T1 and MR153-T1) had no identified driver alterations in the progression sample. This progression may be driven by alterations that are undetectable by WES.

We then compared all the resistant samples (n = 13, the 12 paired samples and MR356-T2 for which there was no baseline sample available for WES) with the baseline samples from patients who had never received prior ARPI (n = 24) (**Suppdata10, Figure 4C**). No genomic features or driver genes were associated with secondary resistance.

We further analyzed clonal evolution models to define progression patterns (**Figure 5**). In this analysis, we included all patients (n = 14) for whom at least two sequential samples were collected with sufficient coverage to construct genetic trees (4 patients with primary resistance and 10 with secondary resistance). The median tumor cellularity of the baseline and resistant samples were 0.615 (IQR: 0.47-0.71) and 0.71 (IQR: 0.56-0.86), respectively). Most genomic alterations of known functional importance in prostate cancer (e.g. *TP53* and *PTEN*) are early truncal events and are consequently shared between subclones. We did not find a simple linear molecular evolution, because not all oncogenic or passenger alterations were similar at baseline and progression. As reported in other cancers treated with targeted agents, all our analyzed cases showed evidence of subclonal evolution at progression, with loss of at least one mutation present at baseline and acquisition of additional progression-specific changes. For all patients, at both baseline and progression, potent oncogenic alterations that likely precluded efficient clearance of the baseline clone were found (e.g. *TMPRSS2-ERG* fusion, *TP53,* or *PTEN* alteration). In two of these patients (MR145 and MR188), progression was accompanied by the acquisition of new cooperative alterations (*RB1* loss, *PTEN* loss, and/or *TP53* mutations) associated with NEPC. In five other patients, progression was associated with the acquisition of new AR alterations

(MR040, MR166, MR217, MR009, and MR178). In the other five patients (MR036, MR116, MR041, MR182, and MR363), progression was not associated with NEPC or AR pathway alterations.

Interestingly, MR009, which harbored a germline *BRCA2* mutation, underwent multiple sequential biopsies after failure of enzalutamide (MR009-T2), atezolizumab (MR009-T3), olaparib (MR337-T2), and docetaxel (MR386-T1). Clonal analysis revealed the emergence of two different clones over time. When the patient experienced disease progression on olaparib, a clone with *a BRCA2* reversion mutation and NEPC emerged, probably induced by the acquisition of a *PTEN* mutation that cooperated with the *TP53* mutation.

Collectively, baseline genetic alterations were generally retained in the progression samples and favored the emergence of additional drivers or resistance mutations/alterations (7/12, 58.3%). In cases where an *AR* alteration was found at baseline, it was always found during progression.

3.5 Transcriptomic alterations and acquired resistance

To study the transcriptomic characteristics associated with acquired resistance, we followed the same approaches described in the WES analysis. We first compared paired biopsies of sufficient quality for RNA-seq analysis (nine patients: MR09RE-T2, MR041-T2, MR145-T2, MR166-T2, MR178-T2, MR182-T2, MR183-T2, MR188-T2, and MR356-T2). In seven patients, the same lesion was biopsied during progression. All patients except one (MR041) were treated with enzalutamide. First, consensus clustering (**Figure 6A**) and unsupervised hierarchical clustering (**Figure 6B**) were performed. We found that the nearest neighbor of 7/9 (77%) baseline samples was their matched resistant sample pair, except for MR145 and MR188, suggesting that ARPIs do not induce significant sustained changes in the tumor transcriptome in most patients

(**Figure 6A,B**). To assess whether resistance resulted from lineage plasticity, we determined the NEPC scores derived from Beltran et al.[13] (**suppdata6**). In two (22%) patients (MR145 and MR188), NEPC scores increased in resistant samples, suggesting potential lineage plasticity. Pathway analysis between baseline and resistant samples demonstrated enrichment in several pathways, including E2F targets, G2M checkpoints, MYC targets, oxidative phosphorylation, and IL6/JAK/STAT3, with a loss of androgen response pathway activity in resistant samples (**Suppdata11**).

The second approach compared nine resistant samples with 29 baseline samples from patients who achieved a response. Unsupervised clustering analysis showed that samples clustered mainly by biopsy site, but not all resistant samples clustered together, indicating that the mechanisms of secondary resistance were heterogeneous (**Supplementary Figure 7**). Pathway analysis between baseline and resistant samples revealed enrichment in the following pathways: E2F targets, G2M checkpoint, MYC targets, oxidative phosphorylation, and DNA repair. EMT and inflammatory and androgen responses decreased in resistant samples (**Suppdata12**). When we compared the baseline samples with samples resistant to NEPC (**Suppdata13**), we found that almost the same pathways were enriched. However, the Hh pathway was also enriched in resistant samples (**Figure 6C**), whereas when the baseline samples were compared to resistant samples, excluding NEPC, Hh was not enriched (**Suppdata14**). These results indicated that Hh may be associated with the initiation of NE differentiation.

4. Discussion

Several large randomized phase III trials have demonstrated that ARPIs treatment improves both radiographic PFS and OS in men with mCRPC, as well as in hormone-naïve metastatic prostate cancer[8-11,13,33]. The determinants of primary and acquired ARPIs' resistance in mCRPC patients remain relatively unknown. Our study is one of the

largest prospective clinical trial examining molecular predictors of ARPIs response from metastatic tumor biopsies. This study represents a unique collection of metastatic biopsies using WES and RNA-seq before treatment with ARPIs and upon disease progression, including paired biopsies, providing a useful resource for understanding the mechanisms that contribute to clinical ARPIs' resistance. So far, there are a few prospective studies on mechanism of resistance from human samples owing to the challenge of obtaining biopsy of metastases, especially paired pre and post therapy biopsies. Furthermore, most studies did not include characterization of mechanisms of acquired resistance. Here, we move from global and general findings to more granular data on patients prospectively monitored with a collection of well-annotated human samples. We think that our study can provide a useful clinical-genomic dataset to understand resistance in clinical setting.

We did not detect any statistically significant differences in mutations, fusions, or copy number alterations between the non-responders and responders. A previous study on AA[17] and enzalutamide[16] did not find any consistent DNA alterations associated with *de novo* resistance. A trend toward statistical significance for *TP53* mutations that were more frequent in non-responders was reported, while the mutation frequency of *the* CTNNB1-centered gene network in non-responders was higher than that in responders, suggesting dysregulated WNT/β-catenin signaling in non-responders. In both studies, no copy number alterations were found to be associated with *de novo* resistance. Finally, a large analysis[24] integrating mCRPC genomics with the histology and clinical outcomes of 429 patients identified *RB1* genomic alterations as potent predictors of poor outcomes. This apparent discrepancy may be explained by differences in the assay, timing of analysis, and clinical follow-up. Overall, these data suggested that primary resistance may be related to increased cellular reprogramming efficiency or stemness/lineage plasticity.

Although no difference in AR alterations was observed between patients with response and those with primary resistance, we found that lower AR transcriptional activity was

associated with ARPIs' resistance. This is consistent with previous studies of mCRPC, suggesting that low AR activity was found in non-responders[16,17]. Low AR activity has been linked to lineage plasticity, EMT, and stemness[34,35]. We found that baseline tumors from non-responders versus responders were enriched in several pathways, including IFN-α, IFN-γ, allograft rejection, inflammatory response, complement, EMT, IL-6/JAK/STAT3, and Hh. Interestingly, an important role of the Hh pathway in resistance to ARPIs was also indicated by OncoSIGNal pathway analysis, which showed significantly higher Hh activity in non-responders than in responders. Hh signaling has been implicated in mCRPC through its functional association with AR[36]. Other studies have shown that Hh signaling plays an important role in transforming normal prostate basal/stem cells into prostate cancer stem cells[37] and androgen-negative cell lines with features of both basal prostate tissue and cancer stemness[38]. We found that the Hh pathway was also enriched in samples collected at the time of resistance associated with NE features but not in samples without NE differentiation. This suggests that Hh may be associated with lineage plasticity and NE characteristics, similar to other solid tumors[39]. Hh inhibitors have been shown to inhibit stemness of prostate cancer cells[40,41]. A previous single-arm pharmacodynamic trial did not show significant activity of the Hh inhibitor, vismodegib[42], in prostate cancer. However, the molecular mechanism of Hh activation in prostate cancer is unknown, and patient selection based on Hh activation is likely to be key. The role of NOTCH in prostate cancer remains unclear. A recent study found that the NOTCH pathway was enriched in the luminal A subtype according to the PAM50 classification[43], suggesting that low NOTCH activity may also be associated with low AR activity and resistance to ARPI. OncoSIGNal pathway analysis could be useful for future stratification of mCRPC patients for ARPIs because the profile with low Hh, high AR, and high NOTCH was associated with clinical benefit. Patients with the opposite profile, with more mesenchymal activity (high Hh, low NOTCH, and low AR), may benefit from Hh-targeted therapy because this profile was associated with a short PFS upon therapy with ARPIs.

Our study provides some new understanding on mechanisms of acquired resistance. Limited data are currently available mainly due to the challenge to obtain biopsy at time of resistance. Prior studies were mainly restricted to DNA analysis or compared baseline and progression samples from different patients. Our study addressed these limitations by analyzing paired biopsies from the same patients and did include transcriptome analysis. We showed that most tumors with secondary resistance continue to depend on the AR as most tumors exhibit either *AR* amplification or *AR* mutations in a model of branched evolution where resistant subclones emerge at time of resistance. Recently, in a study of cfDNA in patients with mCRPC treated with ARPIs[44], the only highlighted recurrent changes in CNVs, mutations, or structural rearrangements at the AR locus across all 28 consecutive same-patient cfDNA pairs. Our study focused on tissue and inter-patient heterogeneity, which can explain our outcomes. Reliance on a single tissue biopsy may provide an incomplete picture of the polyclonal mechanisms of treatment resistance or underestimate disease subclonal complexity. Importantly, we showed that most progressive tumors clustered with their baseline pair, and that most tumors did not change their transcriptional program between baseline and progression, regardless of whether a different lesion or tissue type was biopsied. AR activity was not changed in most patients at time of acquire resistance reinforcing the reliance of these tumors on the AR. In two (20%) patients, the tumor underwent lineage transformation with NE differentiation. RNA-seq analysis indicated that the trajectory of these tumors with acquired resistance is characterized by upregulation of genes related to cell cycle progression, including E2F targets, G2M checkpoints, MYC targets, and downregulation of genes involved in androgen response pathway in resistant samples. Pathway analysis of progression versus baseline biopsies from patients with NE features demonstrated upregulation of several inflammatory pathways previously found to be activated in cancer stem cells (e.g. interferon alpha (IFNα), interferon gamma (IFN-γ) response, IL6/JAK/STAT signaling, and Hedgehog pathways). These pathways were also found to be associated with

primary resistance. Several of these pathways, IFNα, IFN-γ response, and TFNα signaling via NFκB, were also significantly activated in the pathway analysis of progression versus baseline biopsies from patients with acquired resistance without NE features, which was recently reported in another study[45]. These results suggest that ARPIs' treatment may contribute to a stem-like phenotype, including tumors without the NE phenotype that did not yet have evidence of lineage plasticity at the time point assessed, which may result in resistance. Most of the patients were heavily pretreated. Whether these pathways are relevant in hormone-sensitive prostate cancers treated with both ADT and ARPIs is unknown and requires further research.

Our study has several limitations. We sought to obtain sufficient high-quality material for all molecular analyses, and thus, biopsied mainly soft tissue, which included a limited number of bone lesions. Moreover, only a single metastatic site was biopsied before treatment because it was difficult to collect biopsies from multiple sites at the same time point. However, the intra-patient heterogeneity was limited, at least for the main drivers[46]. Furthermore, WES of the mutational profiles of a tumor with a known low TMB, such as prostate cancer, is a limitation of this analysis. Therefore, we restricted the analysis to known mutational signatures of prostate cancer, and a *de novo* search for mutational signatures was not possible. Whole-genome sequencing is more effective for addressing this issue. Thus, we cannot rule out that new mutational signature was associated with either primary or secondary resistance to ARPIs. Finally, some patients were treated with another ARPI prior to inclusion in the study. However, because some of these patients may still benefit from subsequent ARPI[47,48], we allowed them to be enrolled in the study.

5. Conclusion

In summary, in this prospective clinical trial that performed genomic and transcriptional profiling of samples from patients with mCRPC treated with ARPI, we identified several targetable pathways that may contribute to *de novo* and acquired resistance. Low AR activity, stemness program, and Hedgehog pathways were associated with primary ARPIs' resistance, whereas most acquired resistance was associated with subclonal evolution, AR-related events, and neuroendocrine differentiation. As ARPIs are now widely used with castration in hormone-sensitive prostate cancer, it is important to assess whether these mechanisms are relevant in this setting. Finally, functional validation and a deep understanding of the molecular and tissue processes that regulate these resistances are important to envision rational combinations with ARPIs.

Acknowledgments

We thank Tina Zaarour for editing the manuscript. We thank the patients, their families, caregivers, all primary investigators, and site staff.

Data availability

Source data are provided with this article. The raw WES and RNA-seq data generated in this study are available upon request.

6. References

1. Siegel RL, Miller KD, Fuchs HE, Jemal A. Cancer statistics, 2022. CA Cancer J Clin. 2022;72(1):7-33.

2. Parker C, Castro E, Fizazi K, Heidenreich A, Ost P, Procopio G, et al: ESMO Clinical Practice Guidelines for diagnosis, treatment and follow-up. Ann Oncol. 2020;31(9):1119-1134.

3. Mostaghel EA, Page ST, Lin DW, Fazli L, Coleman IM, True LD, et al. Intraprostatic androgens and androgen-regulated gene expression persist after testosterone suppression: therapeutic implications for castration-resistant prostate cancer. Cancer Res. 2007;67(10):5033-41.

4. Chen CD, Welsbie DS, Tran C, Baek SH, Chen R, Vessella R, et al. Nat Med. 2004;10(1):33-9.

5. Li Y, Hwang TH, Oseth LA, Hauge A, Vessella RL, Schmechel SC, et al. AR intragenic deletions linked to androgen receptor splice variant expression and activity in models of prostate cancer progression. Oncogene. 2012;31(45):4759-67.

6. Arora VK, Schenkein E, Murali R, Subudhi SK, Wongvipat J, Balbas MD, et al. Glucocorticoid receptor confers resistance to antiandrogens by bypassing androgen receptor blockade. Cell. 2013;155(6):1309-22.

7. Beltran H, Prandi D, Mosquera JM, Benelli M, Puca L, Cyrta J, et al. Divergent clonal evolution of castration-resistant neuroendocrine prostate cancer. Nat Med. 2016;22(3):298-305.

8. De Bono JS, Logothetis CJ, Molina A, Fizazi K, North S, Chu L, et al. Abiraterone and increased survival in metastatic prostate cancer. N Engl J Med. 2011; 364(21):1995-2005.

9. Scher HI, Fizazi K, Saad F, Taplin ME, Sternberg CN, Miller K, et al. Increased survival with enzalutamide in prostate cancer after chemotherapy. N Engl J Med. 2012;367(13):1187-97.

10. Beer TM, Armstrong AJ, Rathkopf DE, Loriot Y, Sternberg CN, Higano CS, et al. Enzalutamide in metastatic prostate cancer before chemotherapy. N Engl J Med. 2014;371(5):424-33.

11. Chi KN, Agarwal N, Bjartell A, Chung BH, Pereira de Santana Gomes AJ, Given R, et al. Apalutamide for Metastatic, Castration-Sensitive Prostate Cancer. N Engl J Med. 2019;381(1):13-24.

12. Fizazi K, Shore N, Tammela TL, Ulys A, Vjaters E, Polyakov S, et al. Nonmetastatic, Castration-Resistant Prostate Cancer and Survival with Darolutamide. N Engl J Med. 2020;383(11):1040-1049.

13. Smith MR, Hussain M, Saad F, Fizazi K, Sternberg CN, Crawford ED, et al. Darolutamide and Survival in Metastatic, Hormone-Sensitive Prostate Cancer. N Engl J Med. 2022;386(12):1132-1142.

14. Fizazi K, Albiges L, Loriot Y, Massard C. ODM-201: a new-generation androgen receptor inhibitor in castration-resistant prostate cancer. Expert Rev Anticancer Ther. 2015;15(9):1007-17.

15. Chen WS, Aggarwal R, Zhang L, Zhao SG, Thomas GV, Beer TM, et al Genomic Drivers of Poor Prognosis and Enzalutamide Resistance in Metastatic Castration-resistant Prostate Cancer. Eur Urol. 2019;76(5):562-571.

16. Alumkal JJ, Sun D, Lu E, Beer TM, Thomas GV, Latour E et al. Transcriptional profiling identifies an androgen receptor activity-low, stemness program associated with enzalutamide resistance. Proc Natl Acad Sci U S A. 2020;117(22):12315-12323.

17. Wang L, Dehm SM, Hillman DW, Sicotte H, Tan W, Gormley M, et al. A prospective genome-wide study of prostate cancer metastases reveals association of wnt pathway activation and increased cell cycle proliferation with primary resistance to abiraterone acetate-prednisone. Ann Oncol. 2018;29(2):352-360.

18. Recondo G, Mahjoubi L, Maillard A, Loriot Y, Bigot L, Facchinetti F, et al. Feasibility and first reports of the MATCH-R repeated biopsy trial at Gustave Roussy. NPJ Precis Oncol. 2020; 4:27.

19. Dobin A, Gingeras TR. Mapping RNA-seq Reads with STAR. Curr Protoc Bioinformatics. 2015; 51:11.14.1-11.14.19.

20. Robinson MD, McCarthy DJ, Smyth GK. edgeR: a Bioconductor package for differential expression analysis of digital gene expression data. Bioinformatics. 2010;26(1):139-40.

21. Ritchie ME, Phipson B, Wu D, Hu Y, Law CW, Shi W, et al. limma powers differential expression analyses for RNA-sequencing and microarray studies. Nucleic Acids Res. 2015; 43(7):e47–e47.

22. Korotkevich G, Sukhov V, Sergushichev A (2019). "Fast gene set enrichment analysis." bioRxiv. doi: 10.1101/060012, http://biorxiv.org/content/early/2016/06/20/060012.

23. Liberzon A, Birger C, Thorvaldsdóttir H, et al. The Molecular Signatures Database (MSigDB) hallmark gene set collection. Cell Syst. 2015;1(6):417-425.

24. Verhaegh W, van Ooijen H, Inda M.A, Hatzis P, Versteeg R, Smid M, et al. Selection of Personalized Patient Therapy through the Use of Knowledge-Based Computational Models That Identify Tumor-Driving Signal Transduction Pathways. Cancer Res. 2014, 74, 2936–2945.

25. Abida W, Cyrta J, Heller G, Prandi D, Armenia J, Coleman I, et al. Genomic correlates of clinical outcome in advanced prostate cancer. Proc Natl Acad Sci U S A. 2019;116(23):11428-11436.

26. Armenia J, Wankowicz SAM, Liu D, et al. The long tail of oncogenic drivers inICH prostate cancer. Nat Genet. 2018;50(5):645-651.

27. Gerhauser C, Favero F, Risch T, et al. Molecular Evolution of Early-Onset Prostate Cancer Identifies Molecular Risk Markers and Clinical Trajectories. Cancer Cell. 2018;34:996-1011.e8.

28. Alexandrov LB, Kim J, Haradhvala NJ, Huang MN, Tian Ng AW, Wu Y, Boot A, Covington KR, Gordenin DA, Bergstrom EN, Islam SMA, Lopez-Bigas N, Klimczak LJ, McPherson JR, et al. The repertoire of mutational signatures in human cancer. Nature. 2020;578(7793):94-101.

29. Chan JM, Zaidi S, Love JR, Zhao JL, Setty M, Wadosky KM, et al. Lineage plasticity in prostate cancer depends on JAK/STAT inflammatory signaling. Science. 2022;377(6611):1180-1191.

30. Zhu R, Gires O, Zhu L, Liu J, Li J, Yang H, Ju G, Huang J, Ge W, Chen Y, Lu Z, Wang H. TSPAN8 promotes cancer cell stemness via activation of sonic Hedgehog signaling. Nat Commun. 2019;10(1):2863.

31. Le V, He Y, Aldahl J, Hooker E, Yu EJ, Olson A, Kim WK, Lee DH, Wong M, Sheng R, Mi J, Geradts J, Cunha GR, Sun Z. Loss of androgen signaling in mesenchymal sonic Hedgehog responsive cells diminishes prostate development, growth, and regeneration. PLoS Genet. 2020; 16(1):e1008588.

32. Van de Stolpe A, Verhaegh W, Blay JY, Ma CX, Pauwels P, Pegram M, Prenen H, De Ruysscher D, Saba NF, Slovin SF, Willard-Gallo K, Husain H. RNA Based Approaches to Profile Oncogenic Pathways From Low Quantity Samples to Drive Precision Oncology Strategies. Front Genet. 2021; 11:598118.

33. Fizazi K, Tran N, Fein L, Matsubara N, Rodriguez-Antolin A, Alekseev BY, Özgüroğlu M, Ye D, Feyerabend S, Protheroe A, De Porre P, Kheoh T, Park YC, Todd MB, Chi KN; LATITUDE Investigators. Abiraterone plus Prednisone in Metastatic, Castration-Sensitive Prostate Cancer. N Engl J Med. 2017; 377(4):352-360.

34. Zhang D, Park D, Zhong Y, Lu Y, Rycaj K, Gong S, Chen X, Liu X, Chao HP, Whitney P, Calhoun-Davis T, Takata Y, Shen J, Iyer VR, Tang DG. Stem cell and neurogenic gene-expression profiles link prostate basal cells to aggressive prostate cancer. Nat Commun. 2016;7:10798.

35. Spratt DE, Alshalalfa M, Fishbane N, Weiner AB, Mehra R, Mahal BA, Lehrer J, Liu Y, Zhao SG, Speers C, Morgan TM, Dicker AP, Freedland SJ, Karnes RJ, Weinmann S, Davicioni E, Ross AE, Den RB, Nguyen PL, Feng FY, Lotan TL, Chinnaiyan AM, Schaeffer EM. Transcriptomic Heterogeneity of Androgen Receptor Activity Defines a *de novo* low AR-Active Subclass in Treatment Naïve Primary Prostate Cancer. Clin Cancer Res. 2019;25(22):6721-6730.

36. Burleson M, Deng JJ, Qin T, Duong TM, Yan Y, Gu X, Das D, Easley A, Liss MA, Yew PR, Bedolla R, Kumar AP, Huang TH, Zou Y, Chen Y, Chen CL, Huang H, Sun LZ, Boyer TG. GLI3 Is Stabilized by SPOP Mutations and Promotes Castration Resistance via Functional Cooperation with Androgen Receptor in Prostate Cancer. Mol Cancer Res. 2022;20(1):62-76.

37. Chang HH, Chen BY, Wu CY, Tsao ZJ, Chen YY, Chang CP, Yang CR, Lin DP. Hedgehog overexpression leads to the formation of prostate cancer stem cells with metastatic property irrespective of androgen receptor expression in the mouse model. J Biomed Sci. 2011;18(1):6.

38. Chauchereau A, Al Nakouzi N, Gaudin C, Le Moulec S, Compagno D, Auger N, Bénard J, Opolon P, Rozet F, Validire P, Fromont G, Fizazi K. Stemness markers characterize IGR-CaP1, a new cell line derived from primary epithelial prostate cancer. Exp Cell Res. 2011;317(3):262-75.

39. Chen C, Breslin MB, Lan MS. Sonic Hedgehog signaling pathway promotes INSM1 transcription factor in neuroendocrine lung cancer. Cell Signal. 2018;46:83-91.

40. Zhang L, Li L, Jiao M, Wu D, Wu K, Li X, Zhu G, Yang L, Wang X, Hsieh JT, He D. Genistein inhibits the stemness properties of prostate cancer cells through targeting Hedgehog-Gli1 pathway. Cancer Lett. 2012;323(1):48-57.

41. Nanta R, Kumar D, Meeker D, Rodova M, Van Veldhuizen PJ, Shankar S, Srivastava RK. NVP-LDE-225 (Erismodegib) inhibits epithelial-mesenchymal transition and human prostate cancer

stem cell growth in NOD/SCID IL2Rγ null mice by regulating Bmi-1 and microRNA-128. Oncogenesis. 2013; 2(4):e42.

42. Maughan BL, Suzman DL, Luber B, Wang H, Glavaris S, Hughes R, et al. Pharmacodynamic study of the oral Hedgehog pathway inhibitor, vismodegib, in patients with metastatic castration-resistant prostate cancer. Cancer Chemother Pharmacol. 2016;78(6):1297-1304.

43. Coleman IM, DeSarkar N, Morrissey C, Xin L, Roudier MP, Sayar E, Li D, Corey E, Haffner MC, Nelson PS. Therapeutic Implications for Intrinsic Phenotype Classification of Metastatic Castration-Resistant Prostate Cancer. Clin Cancer Res. 2022;28(14):3127-3140.

44. Herberts C, Annala M, Sipola J, Ng SWS, Chen XE, Nurminen A, et al. Deep whole-genome ctDNA chronology of treatment-resistant prostate cancer. Nature. 2022;608(7921):199-208.

45. Westbrook TC, Guan X, Rodansky E, Flores D, Liu CJ, Udager AM, et al. Transcriptional profiling of matched patient biopsies clarifies molecular determinants of enzalutamide-induced lineage plasticity. Nat Commun. 2022;13(1):5345.

46. Brady L, Kriner M, Coleman I, Morrissey C, Roudier M, True LD, et al. Inter- and intra-tumor heterogeneity of metastatic prostate cancer determined by digital spatial gene expression profiling. Nat Commun. 2021;12(1):1426.

47. De Wit R, de Bono J, Sternberg CN, Fizazi K, Tombal B, Wülfing C, et al. Cabazitaxel versus Abiraterone or Enzalutamide in Metastatic Prostate Cancer. N Engl J Med. 2019;381(26):2506-2518.

48. Loriot Y, Bianchini D, Ileana E, Sandhu S, Patrikidou A, Pezaro C, et al. Antitumour activity of abiraterone acetate against metastatic castration-resistant prostate cancer progressing after docetaxel and enzalutamide (MDV3100). Ann Oncol. 2013;24(7):1807-1812.

7. Figure legends

Figure 1: MATCH-R clinical data

A. Left panel: Molecular analysis performed in MATCH-R study. One patient (MR009) underwent five sequential biopsies (MR009, MR009-T2, MR009-T3, MR337-T2 and MR386-T1). Right panel: Venn diagrams showing intersection of molecular analysis performed in 59 patients for primary resistance analysis and in the 81 samples of the whole cohort (including baseline and resistant samples). ARPI: Androgen-receptor pathway inhibitor. cfDNA: cell free DNA. PDX: Patient derived xenografts. IHC: Immunohistochemistry. WES: Whole-exome sequencing.

B. Patient demographics for evaluable patients (n = 59) included in the primary resistance analysis. Demographic information for the 59 evaluable patients are shown. PSA: Prostate Specific Antigen.

C. Kaplan–Meier curves stratified by response status. Tick marks indicate censoring events. P-values were determined using the log-rank test to compare outcome measures between non-responders and responders. OS: Probability that patients are still alive during follow-up in months. ARPI: Androgen receptor pathway inhibitor. (The overall survival curves were generated by taking as survival intervals the OS times (date of last news minus date of start of treatment) subtracting each time for each patient 4 months so that the reference date is 4 months and not the date of start of treatment. 9 patients were excluded as 3 had no last news date and 6 patients had a negative duration).

D. PSA waterfall plot. PSA change from baseline for patients by response group (25 non-responders and 30 responders). Each bar represents one patient with patient identification indicated along zero axis. PSA response was determined based on change at 4 months versus the baseline value. ARPI: Androgen receptor pathway inhibitor.

Figure 2: Genomic alterations and primary resistance

A. Oncoprint showing drivers genes between responders (n = 28) and non-responders (n = 24). Associations between somatic alterations and primary resistance to treatment were evaluated at the single gene level and the gene pathway/network level. No genomic alteration reached statistical significance (q < 0.05). FAG: Fraction of altered genome. Treatment response (0: response, 1: primary resistance, 2: secondary resistance).

B. and C. Boxplots of the proportion of subclonal mutations as readout of tumor heterogeneity (B) and FAG (Fraction of altered genome) as readout of genomic instability (C) in non-responders and responders are shown. Wilcoxon rank sum test was used to test the difference between the two groups. ARPI: Androgen receptor pathway inhibitor.

D. Proportion of *AR* alteration (mutation and/or amplification and/or focal gain) between non-responders and responders is shown. Fisher test was used to test the difference between the two groups. AR: Androgen receptor. ARPI: Androgen receptor pathway inhibitor.

E. Pie chart showing the mean of proportion of each mutational signature in non-responders and responders.

Figure 3: Transcriptomic alterations and primary resistance

A. Left Panel: Boxplots of the mRNA expression of the AR in non-responders and responders are shown. Wilcoxon rank sum test was used to test the difference between the two groups. Right panel: Proportions of mRNA expression of AR Full length and AR-V7 isoform in non-responders and responders are shown. Wilcoxon rank sum test

was used to test the difference between the two groups. AR: Androgen receptor. ARPI: Androgen receptor pathway inhibitor. TPM: Transcripts Per Million.

B. Results from the GSEA pathway analysis using the Broad Hallmark pathways are shown. The 18 hallmark pathways activated in the non-responders with FDR q-value < 0.1 are shown.

C. Boxplots of the AR, Hh and NOTCH pathway activity score in non-responders and responders are shown. Functional signal transduction pathway activity was determined from RNA-seq data by the OncoSIGNal pathway activity profiling (InnoSIGN B.V.). In total, the pathway activity of 10 oncogenic signal transduction pathways was determined: ER, AR, MAPK, Hh, NOTCH, TGFβ, PI3K, NFκB, JAK/STAT1-2, and WNT. The AR and two pathways significantly associated with response are shown. Wilcoxon rank sum test was used to test the difference between the two groups. AR: Androgen receptor. Hh: Hedgehog pathway.

D. Kaplan–Meier curves stratified by Hh pathway activity (< median versus ≥ median). Tick marks indicate censoring events. P-values were determined using the log-rank test to compare outcome measures between patients with high versus low Hh activity. PFS: Probability that patients are alive and without evidence of disease progression during follow-up in months. Hh: Hedgehog pathway.

E. Forrest plot of hazard ratio determined from multivariate analyzes of clinical factor and pathway scores' association with ARPIs. AR: Androgen receptor. ARPI: Androgen receptor pathway inhibitor. Hh: Hedgehog pathway.

Figure 4: Genomic alterations and acquired resistance

A. Oncoprint showing drivers genes between baseline samples and paired samples collected at time of acquired resistance. Associations between somatic alterations and primary resistance to treatment were evaluated at the single gene level and the gene

pathway/network level. No genomic alteration reached statistical significance ($q < 0.05$). FAG: Fraction of altered genome. Regarding patient MR153, the paired samples include MR033RE-T1 (baseline biopsy) and MR153-T1 (resistance biopsy). Patient MR226 (baseline biopsy: MR226-T1; resistance biopsy: MR356-T2) was excluded for paired samples analysis because WES from MR226-T1 was not available. Treatment response (0: response, 1: primary resistance, 2: acquired resistance).

B. Pie charts showing the mean of proportion of each mutational signature in baseline versus matched paired samples.

C. Oncoprint showing drivers genes between baseline samples of patients that never received any prior ARPI ($n = 24$) and samples collected at time of acquired resistance ($n = 13$). Associations between somatic alterations and primary resistance to treatment were evaluated at the single gene level and the gene pathway/network level. No genomic alteration reached statistical significance ($q < 0.05$). FAG: Fraction of altered genome. Treatment response (0: response, 1: primary resistance, 2: secondary resistance).

Figure 5: Oncogenetic trees in patients with baseline tumors and resistant samples

Oncogenetic trees reconstructed for 14 patients with baseline tumors and resistant samples analyzed by WES. Driver alterations are indicated. Branch lengths are proportional to the number of mutations acquired, with a color code indicating the contribution of each mutational signature. PCa phenotypes (adenocarcinoma, mixte and neuroendocrine) were estimated from the AR and NEPC scores calculated from the RNA-seq data. OncoSIGNal pathway activity scores of Androgen receptor activity (ARa) and Hedgehog activity (HHa) calculated from RNA-seq data are provided. Samples associated with primary resistance: MR036, MR040, MR150, and MR363. Samples associated with secondary resistance: MR009, MR041, MR116, MR145, MR166, MR178,

MR182, MR183, MR188, and MR217. T1: sample at baseline and T2: sample at resistance. One patient (MR009) underwent five sequential biopsies (MR009, MR009-T2, MR009-T3 (3th biopsy), MR337-T2 (4th biopsy) and MR386-T1 (5th biopsy).

Figure 6: Transcriptomic alterations and acquired resistance

A. and B. Consensus clustering (A) and hierarchical clustering using the 1000 most variable genes (B) of paired samples (including baseline and resistant samples). AR: Androgen receptor. NEPC: Neuroendocrine prostate cancer. Resistance type (0: baseline sample from responding patient, 1: baseline sample from non-responding patient, 2: sample collected at time of resistance).

C. Results from the GSEA pathway analysis using the Broad Hallmark pathways are shown. The hallmark pathways activated and down-regulated in resistant samples with neuroendocrine features are shown.

8. Figures

Figure 1

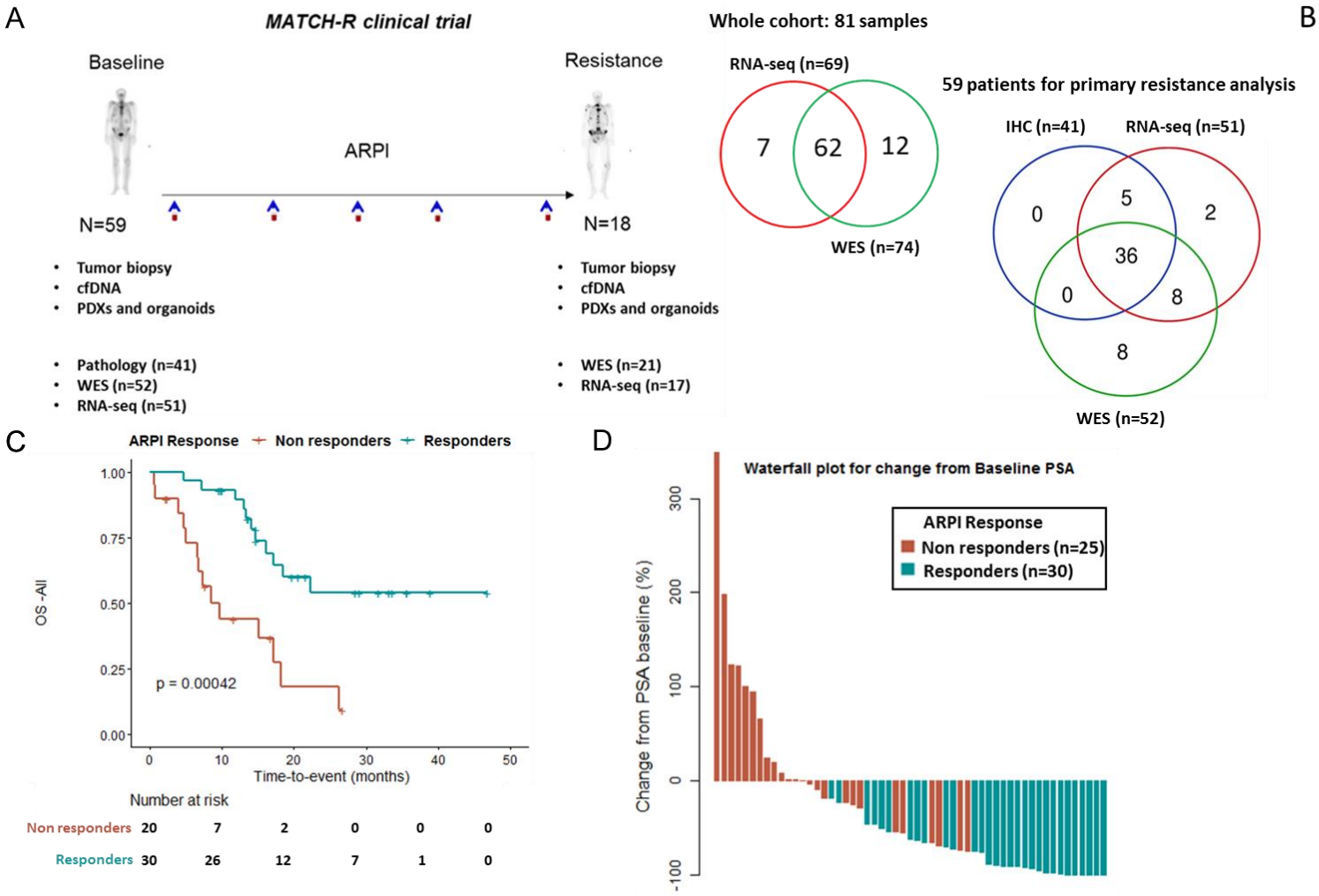

B

Clinical characteristics	Whole cohort (N=59)
Age	
Mean±SD	69.3±10.3
Min–Max	36.0–90.0
Median (IQR)	69.0 (64.0–75.5)
PSA at baseline (ng/ml)	
Mean±SD	142.9±477.2
Min–Max	0.0–3513.0
Median (IQR)	25.0 (8.1–73.0)
PSA at Nadir (ng/ml)	
Mean±SD	153.5±598
Min–Max	0.0–4355.0
Median (IQR)	6.3 (1.2–58.2)
Missing	1
PSA at progression (ng/ml)	
Mean±SD	212.8±664.3
Min–Max	0.0–4250.0
Median (IQR)	26.3 (6.1–87.0)
Missing	9
Prior surgery	
No	37 (62.7)
Yes	22 (37.3)
Prior radiotherapy	
No	24 (40.7)
Yes	35 (59.3)
Prior chemotherapy	
No	32 (54.2)
Yes	27 (45.8)
ARPI pretreated	
No	42 (71.2)
Yes	17 (28.8)
Abiraterone pretreated	
No	49 (83.1)
Yes	10 (16.9)
Enzalutamide pretreated	
No	54 (91.5)
Yes	5 (8.5)
Volume	
High	19 (32.2)
Low	26 (44.1)
Missing	14
De novo metastatic	
No	30 (50.8)
Yes	29 (49.2)
Bone metastatic	
No	19 (32.2)
Yes	40 (67.8)
Lymph node metastatic	
No	15 (25.4)
Yes	44 (74.6)
Visceral metastatic	
No	49 (83.1)
Yes	10 (16.9)
Biopsy site	
Bone	3 (5.1)
Liver	3 (5.1)
Lymph node	24 (40.7)
Lung	3 (5.1)
Prostate	26 (44.1)
Therapy after the biopsy	
Abiraterone	15 (25.4)
Enzalutamide	44 (74.6)

Figure 2

A

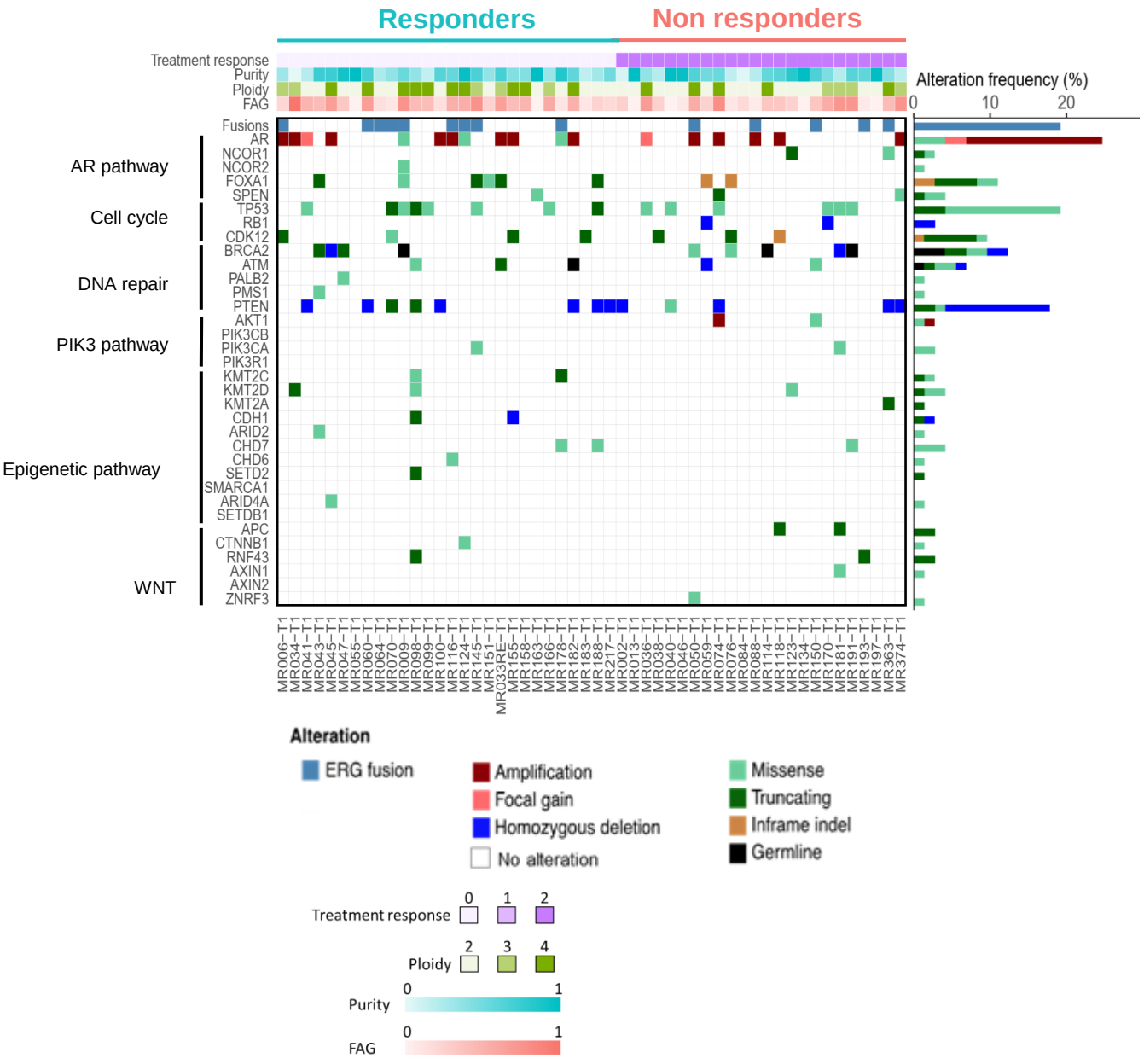
Responders
Non responders
Treatment response
Purity
Ploidy
FAG
Alteration frequency (%)
0
10
20
Fusions
AR
NCOR1
NCOR2
FOXA1
SPEN
TP53
RB1
CDK12
BRCA2
ATM
PALB2
PMS1
PTEN
AKT1
PIK3CB
PIK3CA
PIK3R1
KMT2C
KMT2D
KMT2A
CDH1
ARID2
CHD7
CHD6
SETD2
SMARCA1
ARID4A
SETDB1
APC
CTNNB1
RNF43
AXIN1
AXIN2
ZNRF3
AR pathway
Cell cycle
DNA repair
PIK3 pathway
Epigenetic pathway
WNT
Alteration
ERG fusion
Amplification
Focal gain
Homozygous deletion
No alteration
Missense
Truncating
Inframe indel
Germline
Treatment response
Ploidy
Purity
FAG

B

C

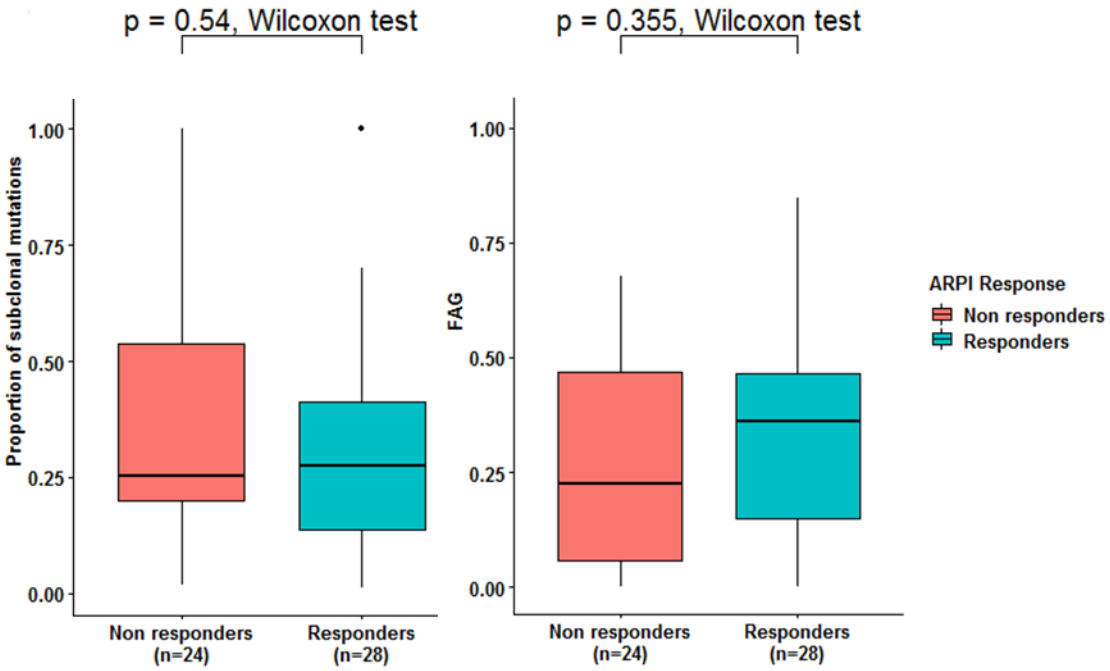
p = 0.54, Wilcoxon test
Proportion of subclonal mutations
1.00
0.75
0.50
0.25
0.00
Non responders (n=24)
Responders (n=28)
p = 0.355, Wilcoxon test
FAG
1.00
0.75
0.50
0.25
0.00
Non responders (n=24)
Responders (n=28)
ARPI Response
Non responders
Responders

D

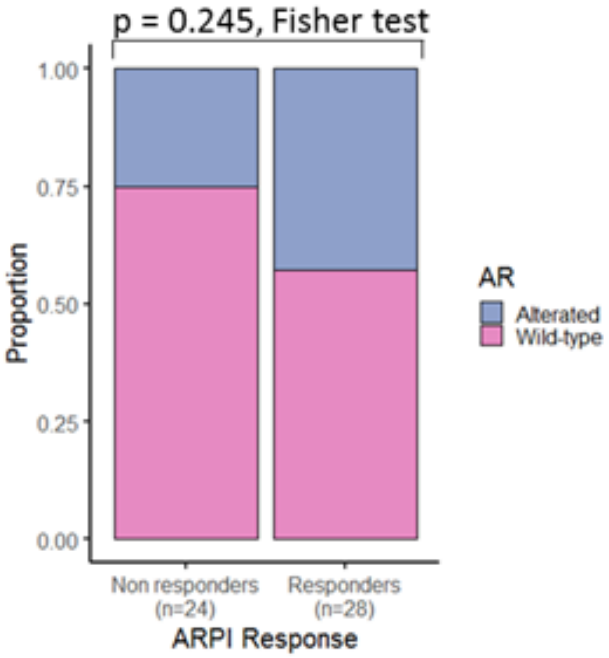
p = 0.245, Fisher test
Proportion
1.00
0.75
0.50
0.25
0.00
Non responders (n=24)
Responders (n=28)
ARPI Response
AR
Alterated
Wild-type

E

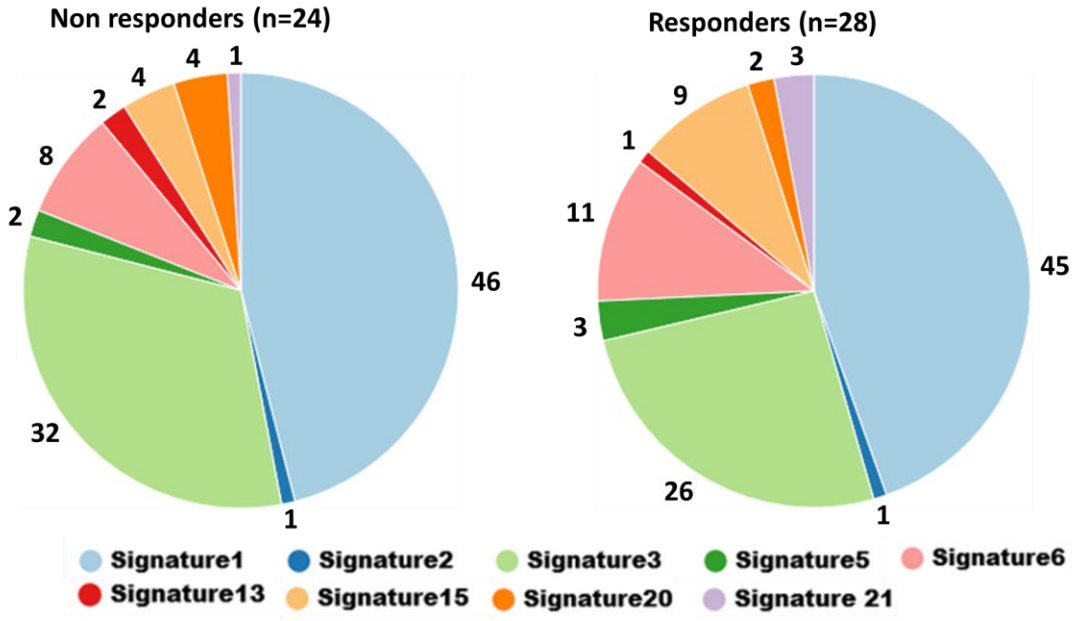

COSMIC Mutational signatures: 1 [clock-like], 2 [APOBEC], 3 [BRCAness], 5 [unknown], 6 [MMR], 13 [APOBEC], 15, 20, 21, 26 [MSI]

Figure 3

A

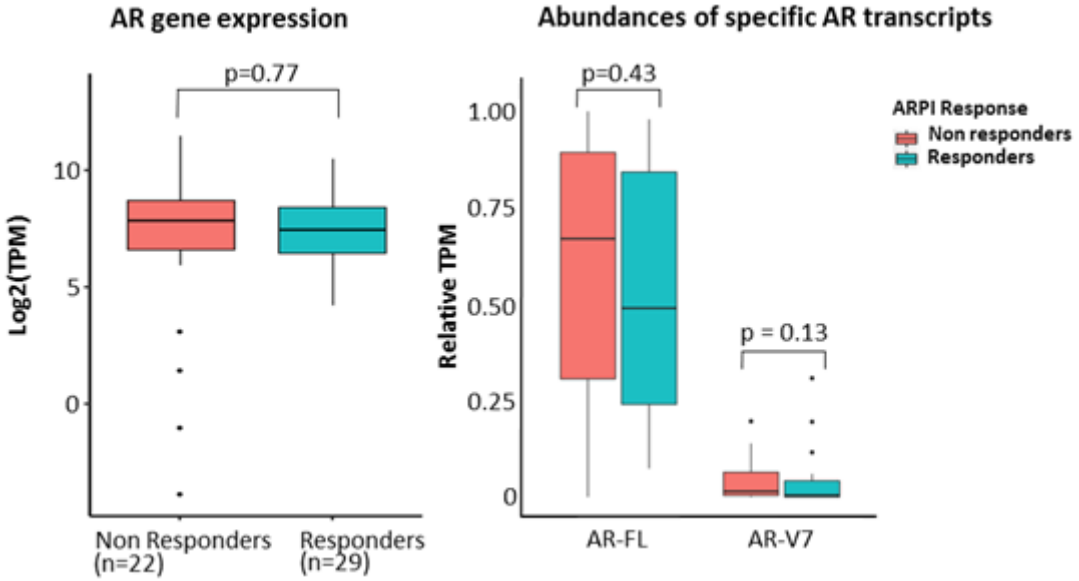
AR gene expression
Abundances of specific AR transcripts
p=0.77
p=0.43
p = 0.13
Log2(TPM)
Relative TPM
10
5
0
1.00
0.75
0.50
0.25
0
Non Responders (n=22)
Responders (n=29)
AR-FL
AR-V7
ARPI Response
Non responders
Responders

B

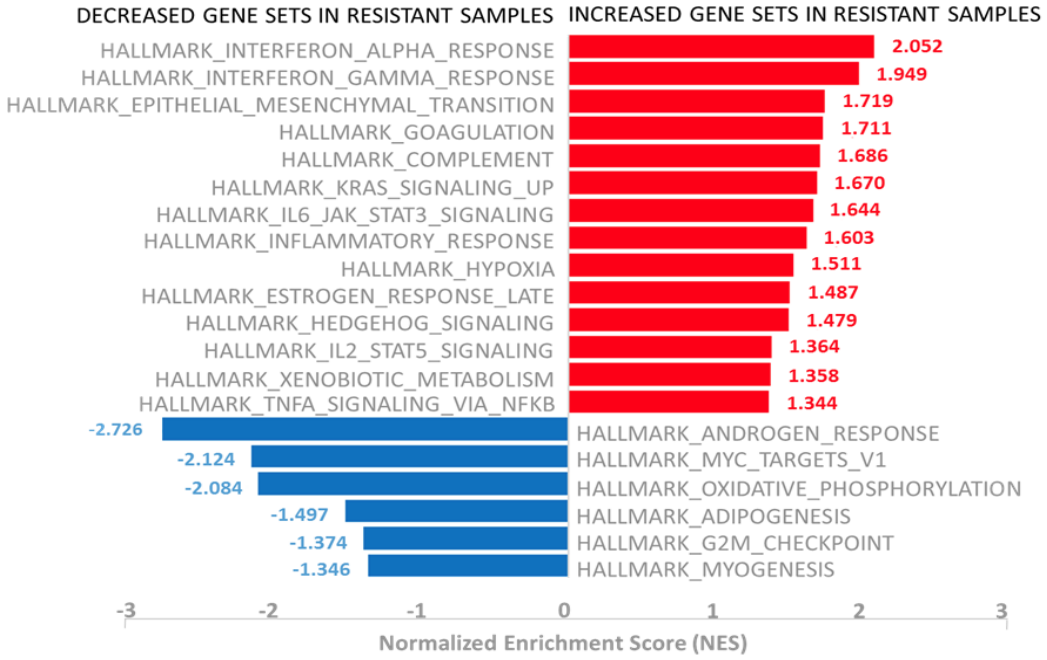
DECREASED GENE SETS IN RESISTANT SAMPLES
INCREASED GENE SETS IN RESISTANT SAMPLES
HALLMARK_INTERFERON_ALPHA_RESPONSE 2.052
HALLMARK_INTERFERON_GAMMA_RESPONSE 1.949
HALLMARK_EPITHELIAL_MESENCHYMAL_TRANSITION 1.719
HALLMARK_COAGULATION 1.711
HALLMARK_COMPLEMENT 1.686
HALLMARK_KRAS_SIGNALING_UP 1.670
HALLMARK_IL6_JAK_STAT3_SIGNALING 1.644
HALLMARK_INFLAMMATORY_RESPONSE 1.603
HALLMARK_HYPOXIA 1.511
HALLMARK_ESTROGEN_RESPONSE_LATE 1.487
HALLMARK_HEDGEHOG_SIGNALING 1.479
HALLMARK_IL2_STAT5_SIGNALING 1.364
HALLMARK_XENOBIOTIC_METABOLISM 1.358
HALLMARK_TNFA_SIGNALING_VIA_NFKB 1.344
-2.726 HALLMARK_ANDROGEN_RESPONSE
-2.124 HALLMARK_MYC_TARGETS_V1
-2.084 HALLMARK_OXIDATIVE_PHOSPHORYLATION
-1.497 HALLMARK_ADIPOGENESIS
-1.374 HALLMARK_G2M_CHECKPOINT
-1.346 HALLMARK_MYOGENESIS
-3
-2
-1
0
1
2
3
Normalized Enrichment Score (NES)

C

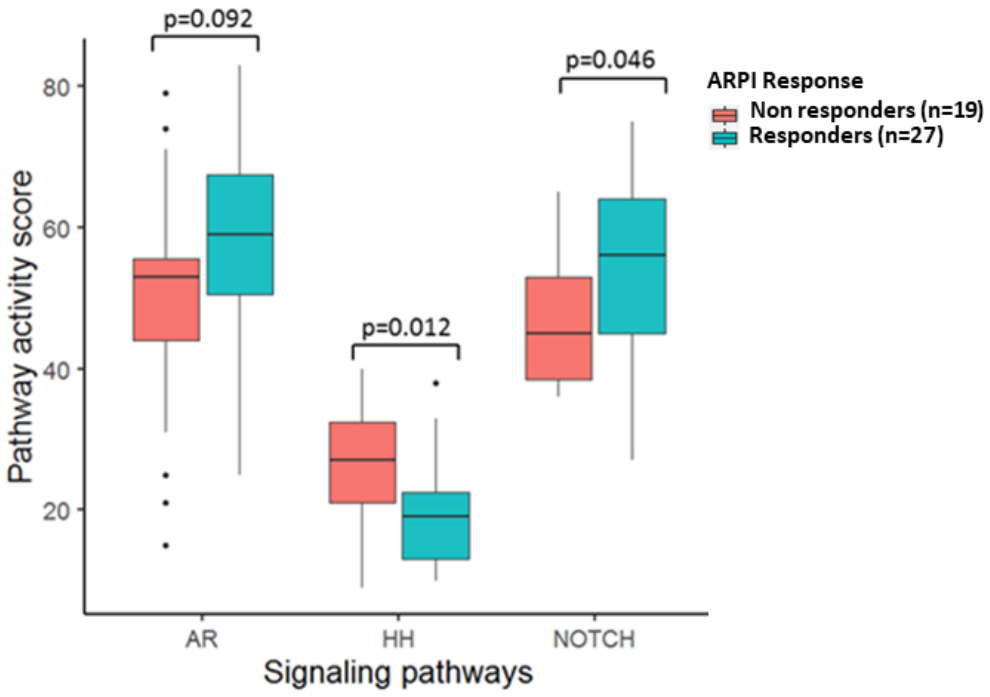
p=0.092
p=0.046
p=0.012
ARPI Response
Non responders (n=19)
Responders (n=27)
Pathway activity score
80
60
40
20
AR
HH
NOTCH
Signaling pathways

D

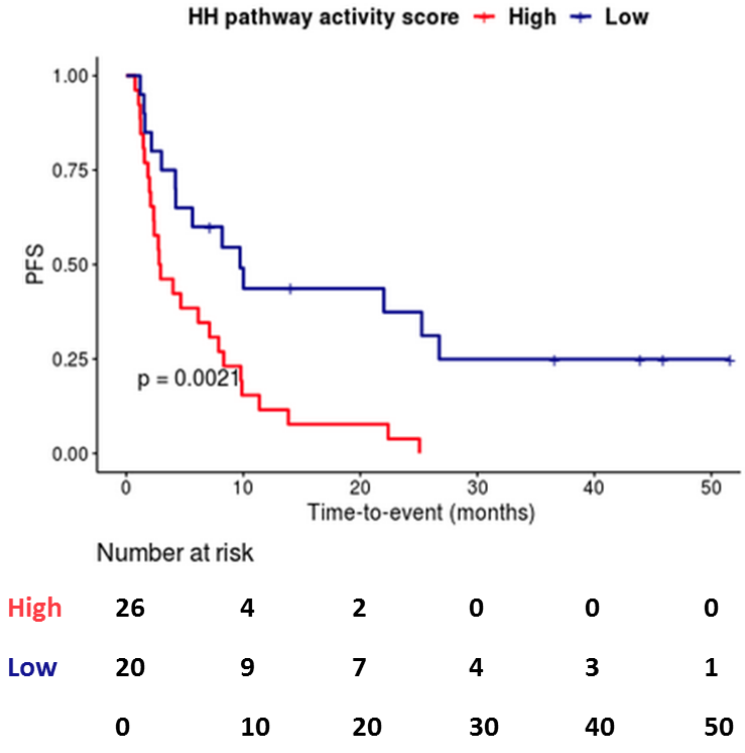
HH pathway activity score
High
Low
PFS
1.00
0.75
0.50
0.25
0.00
p = 0.0021
0
10
20
30
40
50
Time-to-event (months)
Number at risk
High 26 4 2 0 0 0
Low 20 9 7 4 3 1
0 10 20 30 40 50

E

Forest plot for multivariate Cox regression analyses of prognostic factors by PFS

Subgroup	No of Patients (%)	Hazard Ratio(95% CI)	P-value
ARPI_pretreated			
Yes vs No	14 (27.45)	1.850 (0.775 - 4.419)	0.166
Visceral_metastatic			
Yes vs No	9 (17.65)	1.196 (0.360 - 3.975)	0.770
Prior_chemotherapy			
Yes vs No	20 (39.22)	**2.257 (1.037 - 4.914)**	**0.040**
AR_activity			
Low (<54.5 median) vs High	23 (45.1)	1.490 (0.762 - 2.915)	0.244
HH_activity			
High(≥21 median) vs Low	26 (50.98)	**2.413 (1.151 - 5.062)**	**0.020**
NOTCH_activity			
Low (<50 median) vs High	23 (45.1)	**2.173 (1.045 - 4.517)**	**0.038**

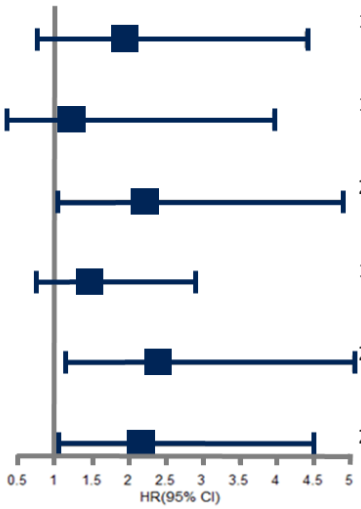

Figure 4

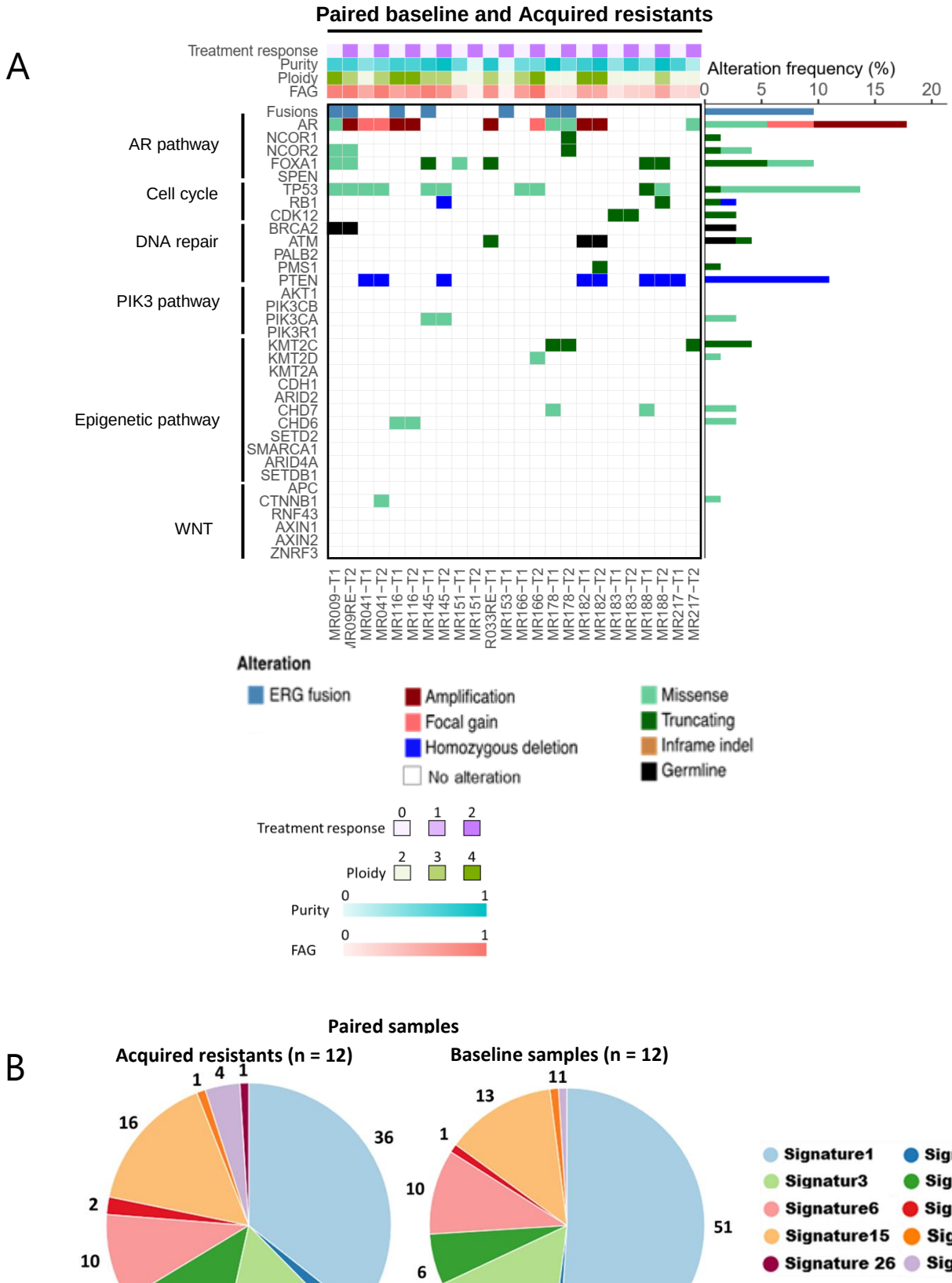
A
Paired baseline and Acquired resistants
Treatment response
Purity
Ploidy
FAG
Alteration frequency (%)
0
5
10
15
20
Fusions
AR
NCOR1
NCOR2
FOXA1
SPEN
TP53
RB1
CDK12
BRCA2
ATM
PALB2
PMS1
PTEN
AKT1
PIK3CB
PIK3CA
PIK3R1
KMT2C
KMT2D
KMT2A
CDH1
ARID2
CHD7
CHD6
SETD2
SMARCA1
ARID4A
SETDB1
APC
CTNNB1
RNF43
AXIN1
AXIN2
ZNRF3
AR pathway
Cell cycle
DNA repair
PIK3 pathway
Epigenetic pathway
WNT
MR009−T1
MR09RE−T2
MR041−T1
MR041−T2
MR116−T1
MR116−T2
MR145−T1
MR145−T2
MR151−T1
MR151−T2
R033RE−T1
MR153−T1
MR166−T1
MR166−T2
MR178−T1
MR178−T2
MR182−T1
MR182−T2
MR183−T1
MR183−T2
MR188−T1
MR188−T2
MR217−T1
MR217−T2
Alteration
ERG fusion
Amplification
Focal gain
Homozygous deletion
No alteration
Missense
Truncating
Inframe indel
Germline
Treatment response
0
1
2
Ploidy
2
3
4
Purity
0
1
FAG
0
1
B
Paired samples
Acquired resistants (n = 12)
Baseline samples (n = 12)
1
4
1
16
36
2
10
13
16
2
11
13
1
10
6
16
1
51
Signature1
Signature2
Signatur3
Signature5
Signature6
Signature13
Signature15
Signature20
Signature 26
Signature 21
COSMIC Mutational signatures:
1 [clock-like], 2 [APOBEC],
3 BRCAness], 5 [unknown],
6 [MMR], 13 [APOBEC],
15, 20, 21, 26 [MSI]

C

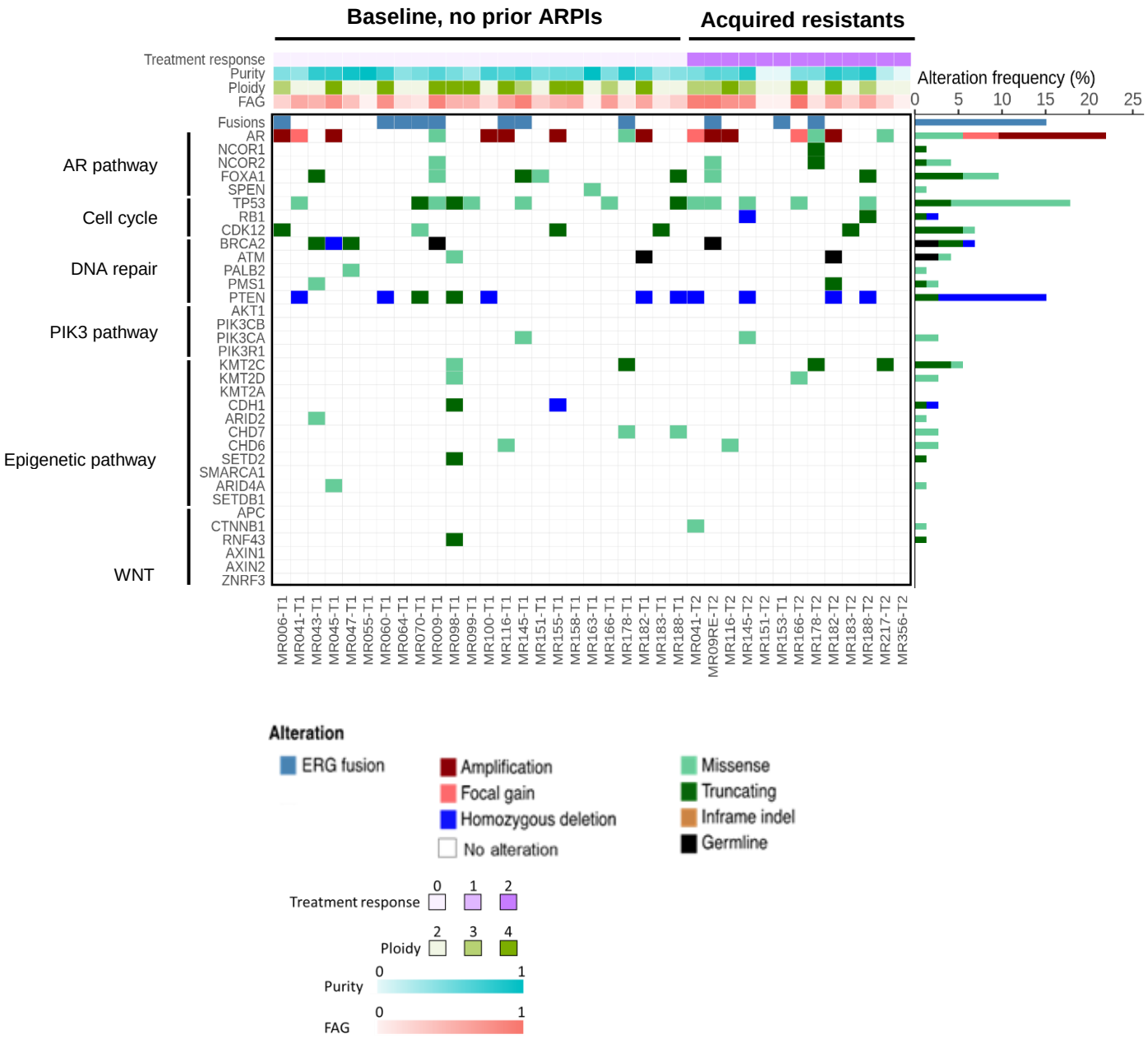
Baseline, no prior ARPIs
Acquired resistants
Treatment response
Purity
Ploidy
FAG
Alteration frequency (%)
0 5 10 15 20 25
Fusions
AR
NCOR1
NCOR2
FOXA1
SPEN
TP53
RB1
CDK12
BRCA2
ATM
PALB2
PMS1
PTEN
AKT1
PIK3CB
PIK3CA
PIK3R1
KMT2C
KMT2D
KMT2A
CDH1
ARID2
CHD7
CHD6
SETD2
SMARCA1
ARID4A
SETDB1
APC
CTNNB1
RNF43
AXIN1
AXIN2
ZNRF3
AR pathway
Cell cycle
DNA repair
PIK3 pathway
Epigenetic pathway
WNT
MR006-T1
MR041-T1
MR043-T1
MR045-T1
MR047-T1
MR055-T1
MR060-T1
MR064-T1
MR070-T1
MR009-T1
MR098-T1
MR099-T1
MR100-T1
MR116-T1
MR145-T1
MR151-T1
MR155-T1
MR158-T1
MR163-T1
MR166-T1
MR178-T1
MR182-T1
MR183-T1
MR188-T1
MR041-T2
MR09RE-T2
MR116-T2
MR145-T2
MR151-T2
MR153-T1
MR166-T2
MR178-T2
MR182-T2
MR183-T2
MR188-T2
MR217-T2
MR356-T2
Alteration
ERG fusion
Amplification
Focal gain
Homozygous deletion
No alteration
Missense
Truncating
Inframe indel
Germline
Treatment response 0 1 2
Ploidy 2 3 4
Purity 0 1
FAG 0 1

Figure 5

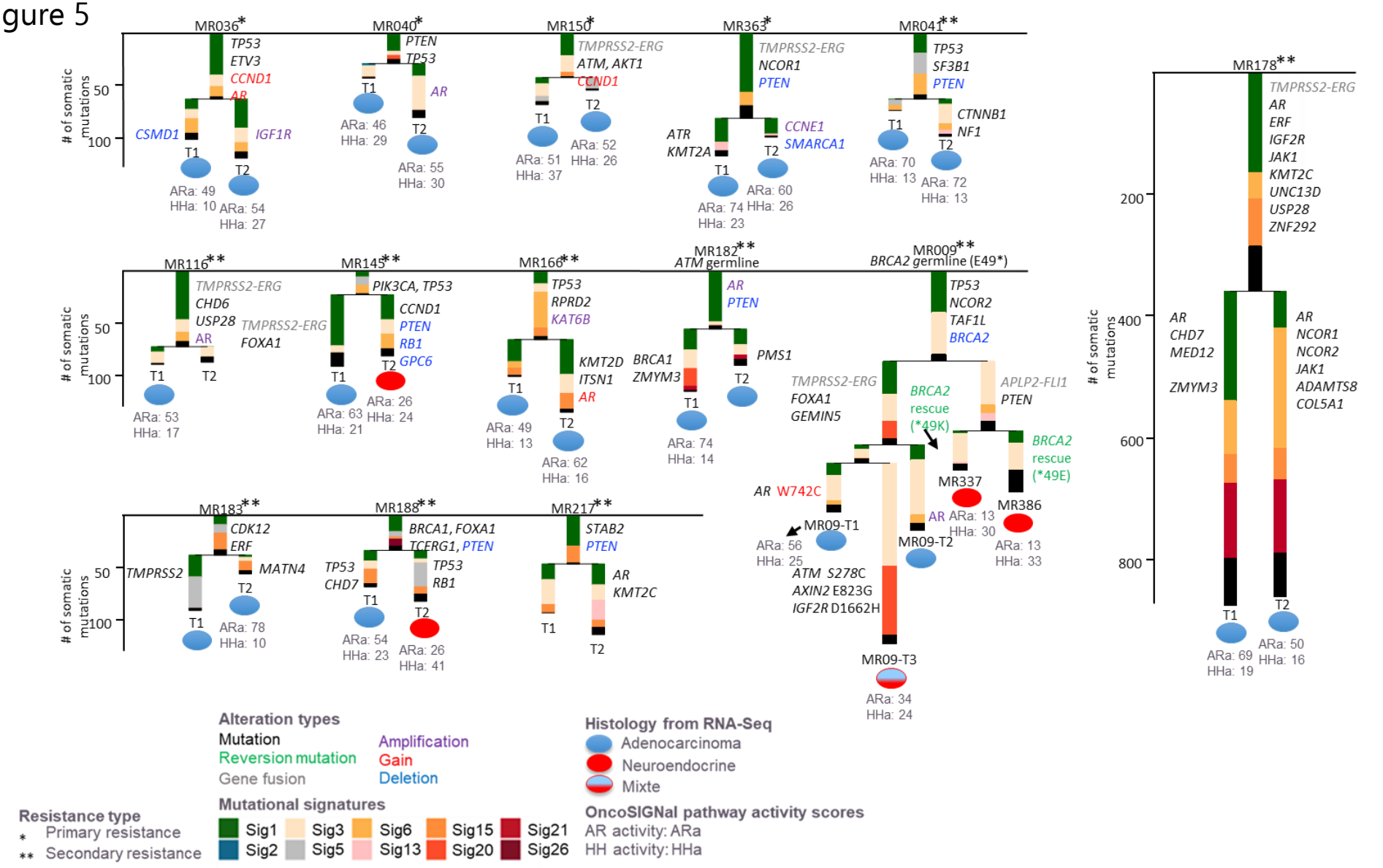
MR036*
TP53
ETV3
CCND1
AR
CSMD1
IGF1R
ARa: 49
HHa: 10
ARa: 54
HHa: 27
MR040*
PTEN
TP53
AR
ARa: 46
HHa: 29
ARa: 55
HHa: 30
MR150*
TMPRSS2-ERG
ATM, AKT1
CCND1
ARa: 51
HHa: 37
ARa: 52
HHa: 26
MR363*
TMPRSS2-ERG
NCOR1
PTEN
ATR
KMT2A
CCNE1
SMARCA1
ARa: 74
HHa: 23
ARa: 60
HHa: 26
MR041**
TP53
SF3B1
PTEN
CTNNB1
NF1
ARa: 70
HHa: 13
ARa: 72
HHa: 13
MR116**
TMPRSS2-ERG
CHD6
USP28
AR
TMPRSS2-ERG
FOXA1
ARa: 53
HHa: 17
MR145**
PIK3CA, TP53
CCND1
PTEN
RB1
GPC6
ARa: 63
HHa: 21
ARa: 26
HHa: 24
MR166**
TP53
RPRD2
KAT6B
KMT2D
ITSN1
AR
ARa: 49
HHa: 13
ARa: 62
HHa: 16
MR182**
ATM germline
AR
PTEN
BRCA1
ZMYM3
PMS1
ARa: 74
HHa: 14
MR009**
BRCA2 germline (E49*)
TP53
NCOR2
TAF1L
BRCA2
TMPRSS2-ERG
FOXA1
GEMIN5
BRCA2
rescue
(*49K)
APLP2-FLI1
PTEN
BRCA2
rescue
(*49E)
AR W742C
MR09-T1
ARa: 56
HHa: 25
MR337
AR ARa: 13
HHa: 30
MR386
ARa: 13
HHa: 33
MR09-T2
ATM S278C
AXIN2 E823G
IGF2R D1662H
MR09-T3
ARa: 34
HHa: 24
MR183**
CDK12
ERF
TMPRSS2
MATN4
ARa: 78
HHa: 10
MR188**
BRCA1, FOXA1
TCERG1, PTEN
TP53
CHD7
TP53
RB1
ARa: 54
HHa: 23
ARa: 26
HHa: 41
MR217**
STAB2
PTEN
AR
KMT2C
MR178**
TMPRSS2-ERG
AR
ERF
IGF2R
JAK1
KMT2C
UNC13D
USP28
ZNF292
AR
CHD7
MED12
ZMYM3
AR
NCOR1
NCOR2
JAK1
ADAMTS8
COL5A1
ARa: 69
HHa: 19
ARa: 50
HHa: 16
# of somatic mutations
50
100
200
400
600
800
Alteration types
Mutation
Reversion mutation
Gene fusion
Amplification
Gain
Deletion
Histology from RNA-Seq
Adenocarcinoma
Neuroendocrine
Mixte
Mutational signatures
Sig1
Sig2
Sig3
Sig5
Sig6
Sig13
Sig15
Sig20
Sig21
Sig26
OncoSIGNal pathway activity scores
AR activity: ARa
HH activity: HHa
Resistance type
* Primary resistance
** Secondary resistance

Figure 6

A

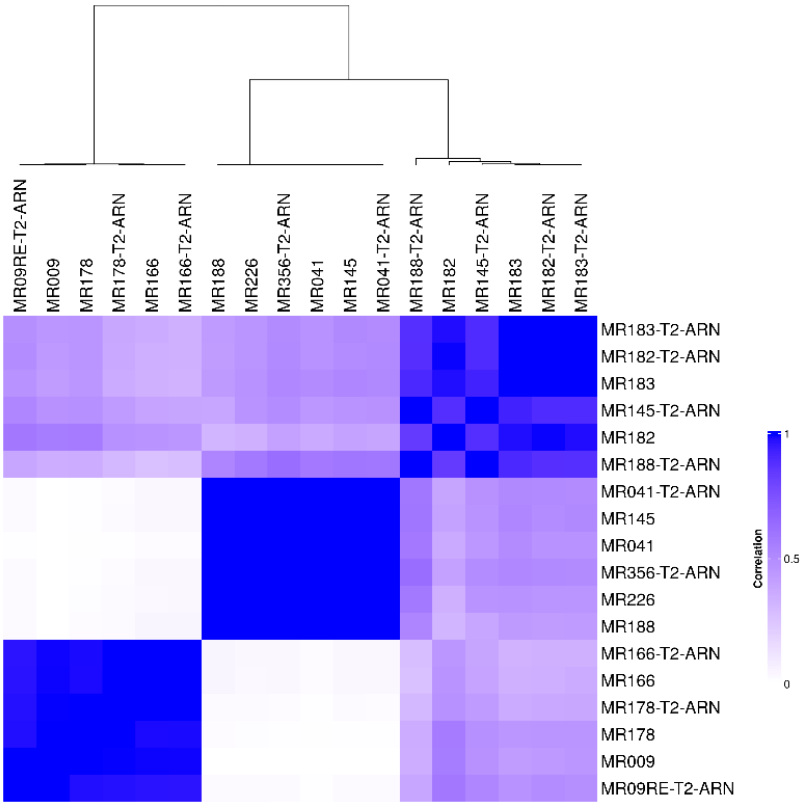
MR09RE-T2-ARN
MR009
MR178
MR178-T2-ARN
MR166
MR166-T2-ARN
MR188
MR226
MR356-T2-ARN
MR041
MR145
MR041-T2-ARN
MR188-T2-ARN
MR182
MR145-T2-ARN
MR183
MR182-T2-ARN
MR183-T2-ARN
MR183-T2-ARN
MR182-T2-ARN
MR183
MR145-T2-ARN
MR182
MR188-T2-ARN
MR041-T2-ARN
MR145
MR041
MR356-T2-ARN
MR226
MR188
MR166-T2-ARN
MR166
MR178-T2-ARN
MR178
MR009
MR09RE-T2-ARN
Correlation
1
0.5
0

B

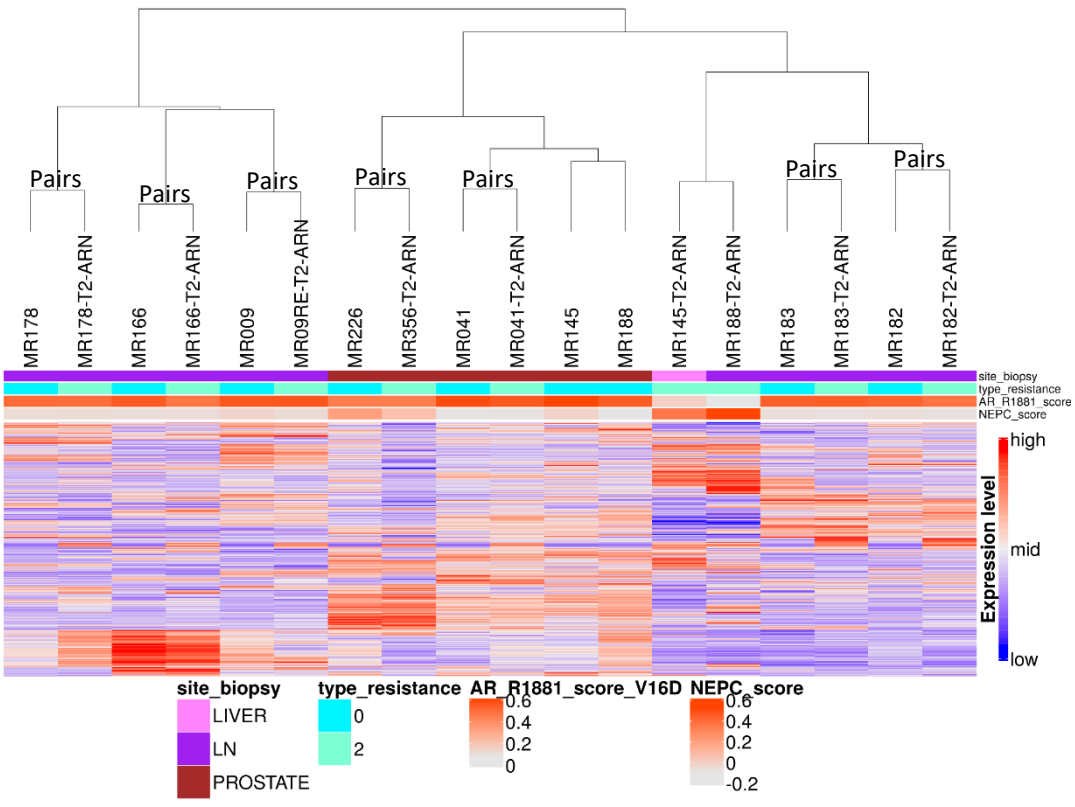
Pairs
Pairs
Pairs
Pairs
Pairs
Pairs
Pairs
MR178
MR178-T2-ARN
MR166
MR166-T2-ARN
MR009
MR09RE-T2-ARN
MR226
MR356-T2-ARN
MR041
MR041-T2-ARN
MR145
MR188
MR145-T2-ARN
MR188-T2-ARN
MR183
MR183-T2-ARN
MR182
MR182-T2-ARN
site_biopsy
type_resistance
AR_R1881_score
NEPC_score
high
mid
low
Expression level
site_biopsy
LIVER
LN
PROSTATE
type_resistance
0
2
AR_R1881_score_V16D
0.6
0.4
0.2
0
NEPC_score
0.6
0.4
0.2
0
-0.2

C

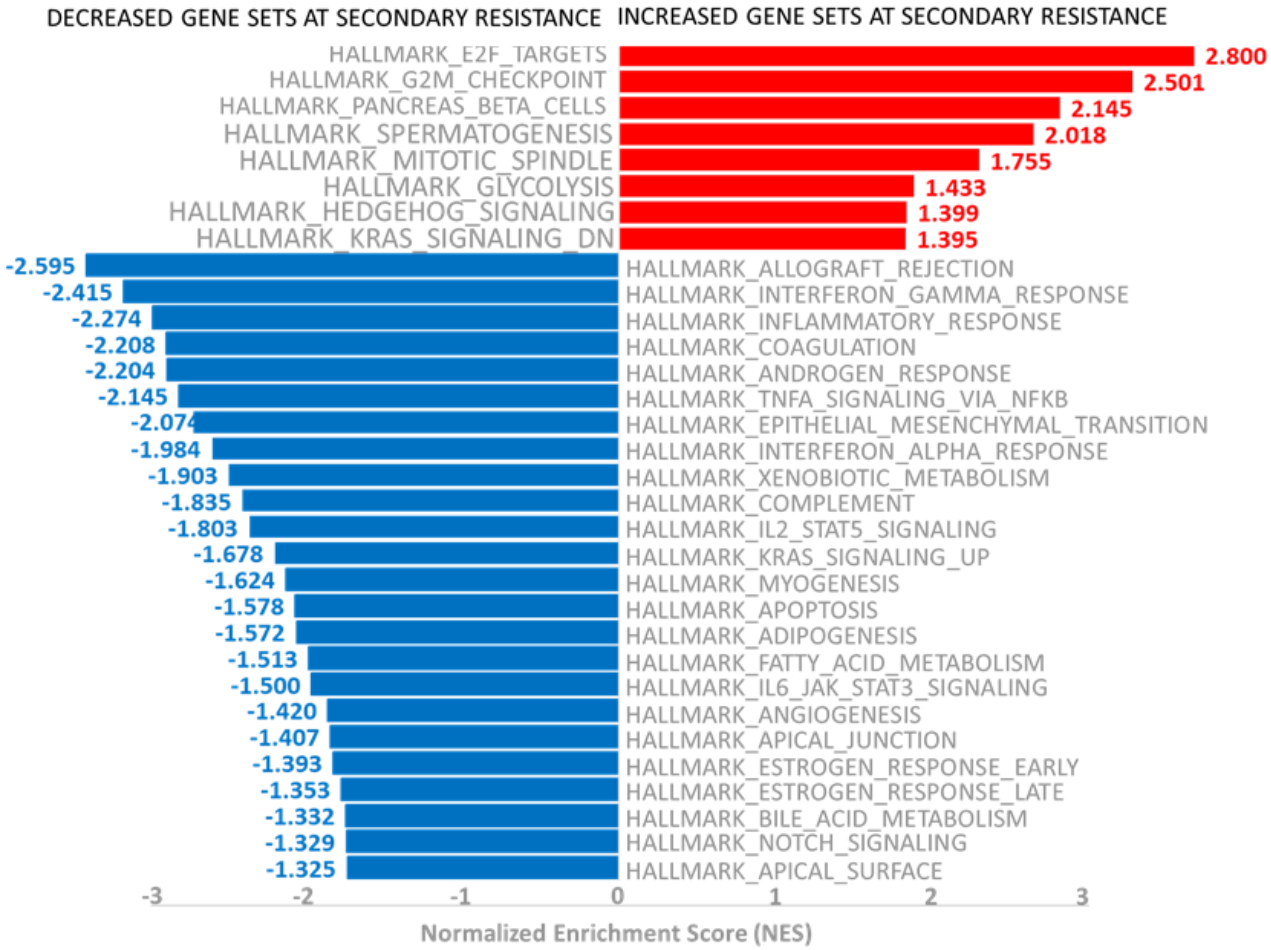
DECREASED GENE SETS AT SECONDARY RESISTANCE
INCREASED GENE SETS AT SECONDARY RESISTANCE
HALLMARK_E2F_TARGETS
HALLMARK_G2M_CHECKPOINT
HALLMARK_PANCREAS_BETA_CELLS
HALLMARK_SPERMATOGENESIS
HALLMARK_MITOTIC_SPINDLE
HALLMARK_GLYCOLYSIS
HALLMARK_HEDGEHOG_SIGNALING
HALLMARK_KRAS_SIGNALING_DN
2.800
2.501
2.145
2.018
1.755
1.433
1.399
1.395
-2.595
-2.415
-2.274
-2.208
-2.204
-2.145
-2.074
-1.984
-1.903
-1.835
-1.803
-1.678
-1.624
-1.578
-1.572
-1.513
-1.500
-1.420
-1.407
-1.393
-1.353
-1.332
-1.329
-1.325
HALLMARK_ALLOGRAFT_REJECTION
HALLMARK_INTERFERON_GAMMA_RESPONSE
HALLMARK_INFLAMMATORY_RESPONSE
HALLMARK_COAGULATION
HALLMARK_ANDROGEN_RESPONSE
HALLMARK_TNFA_SIGNALING_VIA_NFKB
HALLMARK_EPITHELIAL_MESENCHYMAL_TRANSITION
HALLMARK_INTERFERON_ALPHA_RESPONSE
HALLMARK_XENOBIOTIC_METABOLISM
HALLMARK_COMPLEMENT
HALLMARK_IL2_STAT5_SIGNALING
HALLMARK_KRAS_SIGNALING_UP
HALLMARK_MYOGENESIS
HALLMARK_APOPTOSIS
HALLMARK_ADIPOGENESIS
HALLMARK_FATTY_ACID_METABOLISM
HALLMARK_IL6_JAK_STAT3_SIGNALING
HALLMARK_ANGIOGENESIS
HALLMARK_APICAL_JUNCTION
HALLMARK_ESTROGEN_RESPONSE_EARLY
HALLMARK_ESTROGEN_RESPONSE_LATE
HALLMARK_BILE_ACID_METABOLISM
HALLMARK_NOTCH_SIGNALING
HALLMARK_APICAL_SURFACE
-3
-2
-1
0
1
2
3
Normalized Enrichment Score (NES)

9. List of tables

The following Excel tables (.xlsx) are included in the article:

Suppdata 1 : Clinical data

Suppdata 2 : WES features

Suppdata 3 : Fusion transcripts for all samples

Suppdata 4 : Exposure of mutational signatures

Suppdata 5 : DNA repair genes and germline variants

Suppdata 6 : RNA-seq features

Suppdata 7 : Statistics on genomic characteristics on primary resistance groups

Suppdata 8 : GSEA between non-responders and responders at primary resistance

Suppdata 9 : Pathway activity scores from OncoSIGNal tool

Suppdata 10 : Statistics on genomic characteristics of secondary resistance groups

Suppdata 11 : GSEA between paired secondary resistance groups

Suppdata 12 : GSEA between secondary resistance group and baseline group becoming resistant

Suppdata 13 : GSEA between secondary resistance group and baseline group becoming resistant NEPC

Suppdata 14 : GSEA between secondary resistance group and baseline group becoming resistant, excluding NEPC samples

10. Supplemental figure legends

Supplementary figure 1: CONSORT flow diagram of patients enrolled in the study

Overall, 30 patients were excluded due to insufficient tumor cell proportion or DNA/RNA amount and 1 patient was excluded due to unknown response status.

Supplementary figure 2: Patient and sample list for acquired resistance analysis

Whole exome sequencing (WES) and whole transcriptome sequencing (RNA-seq) data from baseline and resistant samples. Five patients with primary resistance underwent two sequential biopsies (baseline and at time of diagnosis of disease progression). MR009 patient underwent five sequential biopsies (MR009, MR009-T2, MR009-T3, MR337, and MR386). "*": samples with sufficient quality for phylogenetic tree construction. "!": samples from the same patient (MR009). "( )": baseline sample.

Supplementary figure 3: Genomic landscape of the whole cohort

A. Whole exome sequencing (WES) results of the whole cohort. An OncoPrint reflecting the copy number alteration and mutation status for the indicated genes in baseline and resistant samples (n = 74) is shown. FAG: Fraction of altered genome. Treatment response (0: response, 1: primary resistance, 2: secondary resistance).

B. Mutational signatures. The proportion of selected mutational signatures is reported for each baseline and resistant samples (n = 74).

Supplementary figure 4: Transcriptomic analysis of the whole cohort

A. Unsupervised clustering of of 69 RNA-seq samples (including baseline and resistant samples) using the 1000 most variable genes identified four clusters. AR: Androgen receptor. NEPC: Neuroendocrine prostate cancer. Resistance type (0: baseline sample from responding patient, 1: baseline sample from non-responding patient, 2: sample collected at time of resistance).

B. Contribution of different component of unsupervised clustering. AR: Androgen receptor. ARPI: Androgen receptor pathway inhibitor.

C. Lymph node biopsies from mCRPC patients with AR (left column) and CD56 (right column) stainings from IHC analysis. Phenotype: (a-b) high luminal (MR064), (c-d) low luminal (MR178), (e-f) mixed (MR009), and (g-h) neuroendocrine (MR191). (At X40 scale enlargement).

Supplementary figure 5: Correlation between Hh pathway, AR and NEPC scores

A. Scatter plot of association between AR activity score and Hh activity score determined from OncoSIGNal analysis, analysed by Pearson's correlation. B: Scatter plot of association between Hh activity score and NEPC score. r: Pearson correlation coefficient. AR: Androgen receptor. Hh: Hedgehog pathway. NEPC: Neuroendocrine prostate cancer.

Supplementary figure 6: Kaplan–Meier curves stratified by AR activity

Tick marks indicate censoring events. P values were determined using the log-rank test to compare outcome measures between patients with high versus low AR activity scores (< median versus ≥ median). PFS: Probability that patients are alive and without evidence of disease progression during follow-up in months. AR: Androgen receptor.

Supplementary figure 7: Unsupervised clustering of baseline and resistant samples

Unsupervised clustering of baselines samples and resistant samples using the 1000 most variable genes. AR: Androgen receptor. ARPI: Androgen receptor pathway inhibitor. NEPC: Neuroendocrine prostate cancer.

11. Supplemental figures

Supplementary figure1

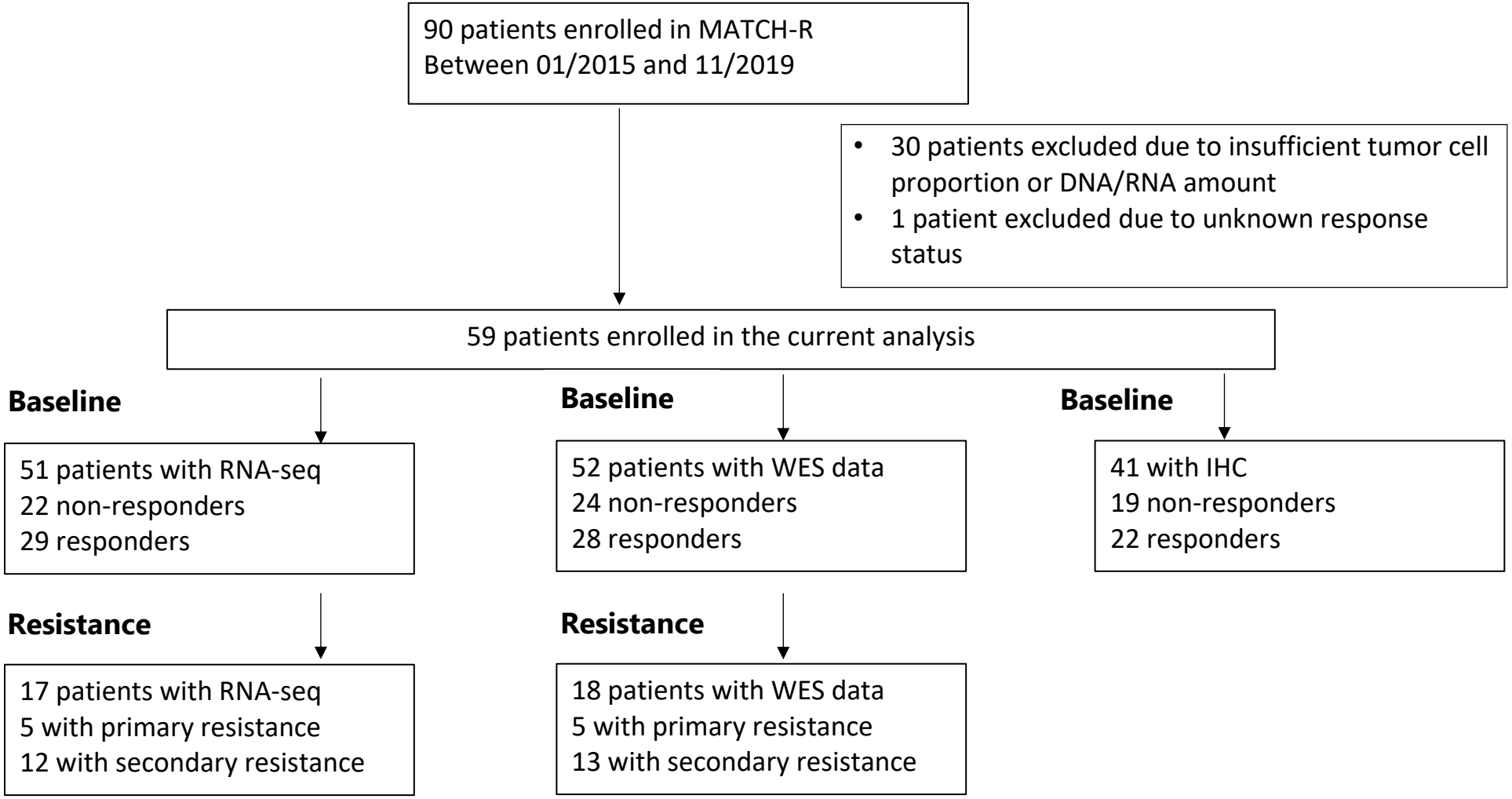

Supplementary figure 2

1. WES data for resistance analysis

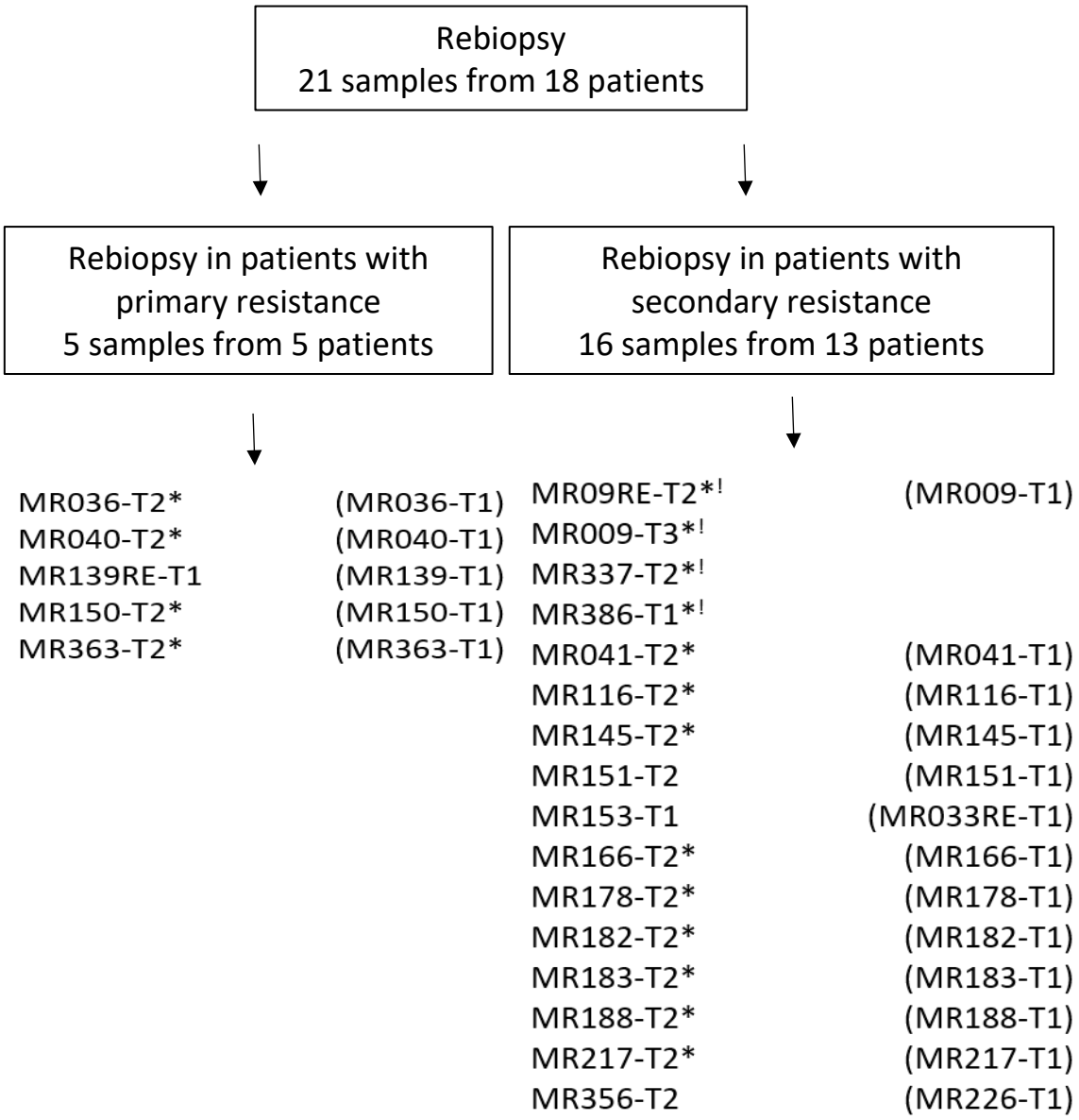

2. RNA-seq data for resistance analysis

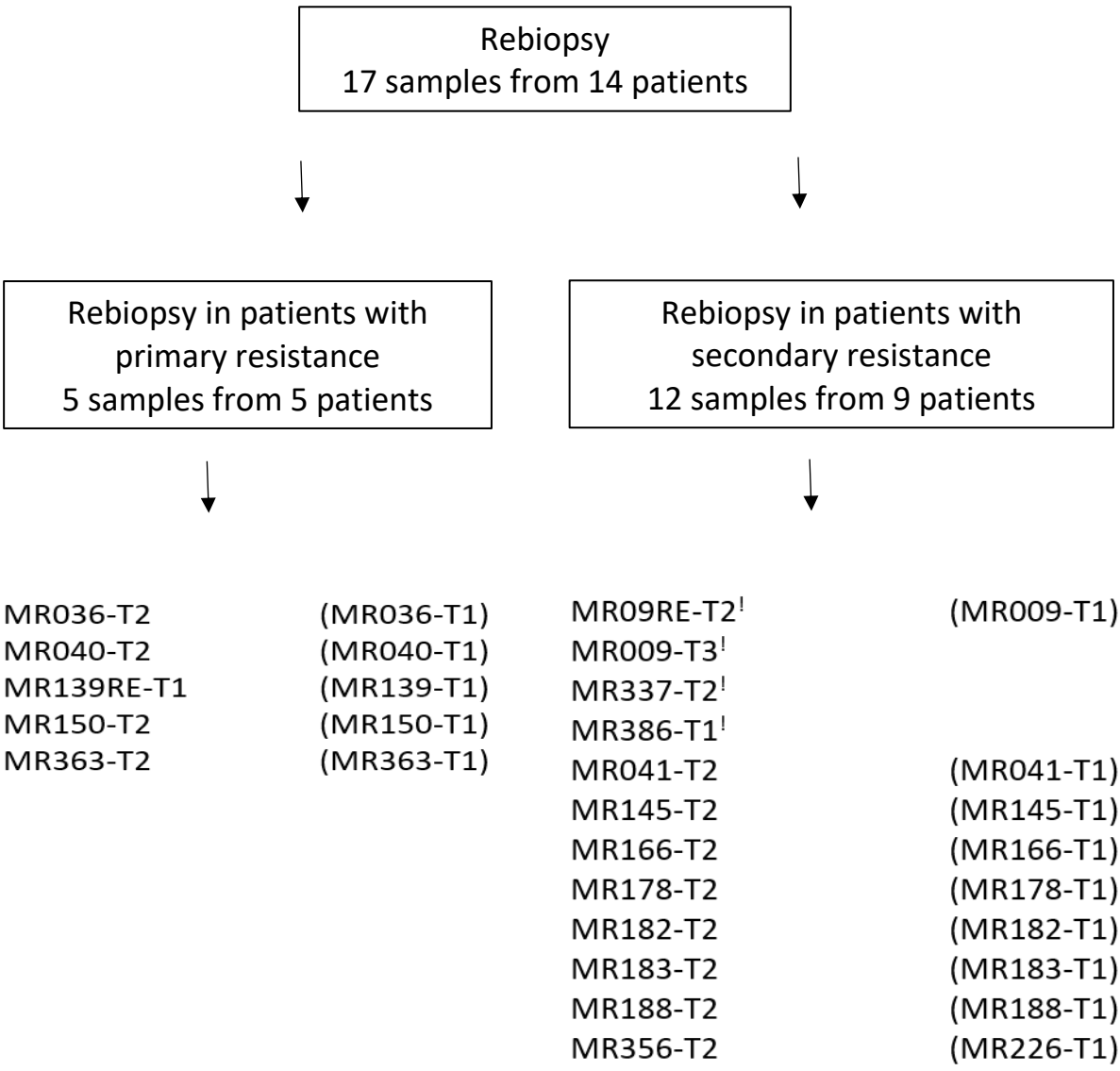

Supplementary figure 3

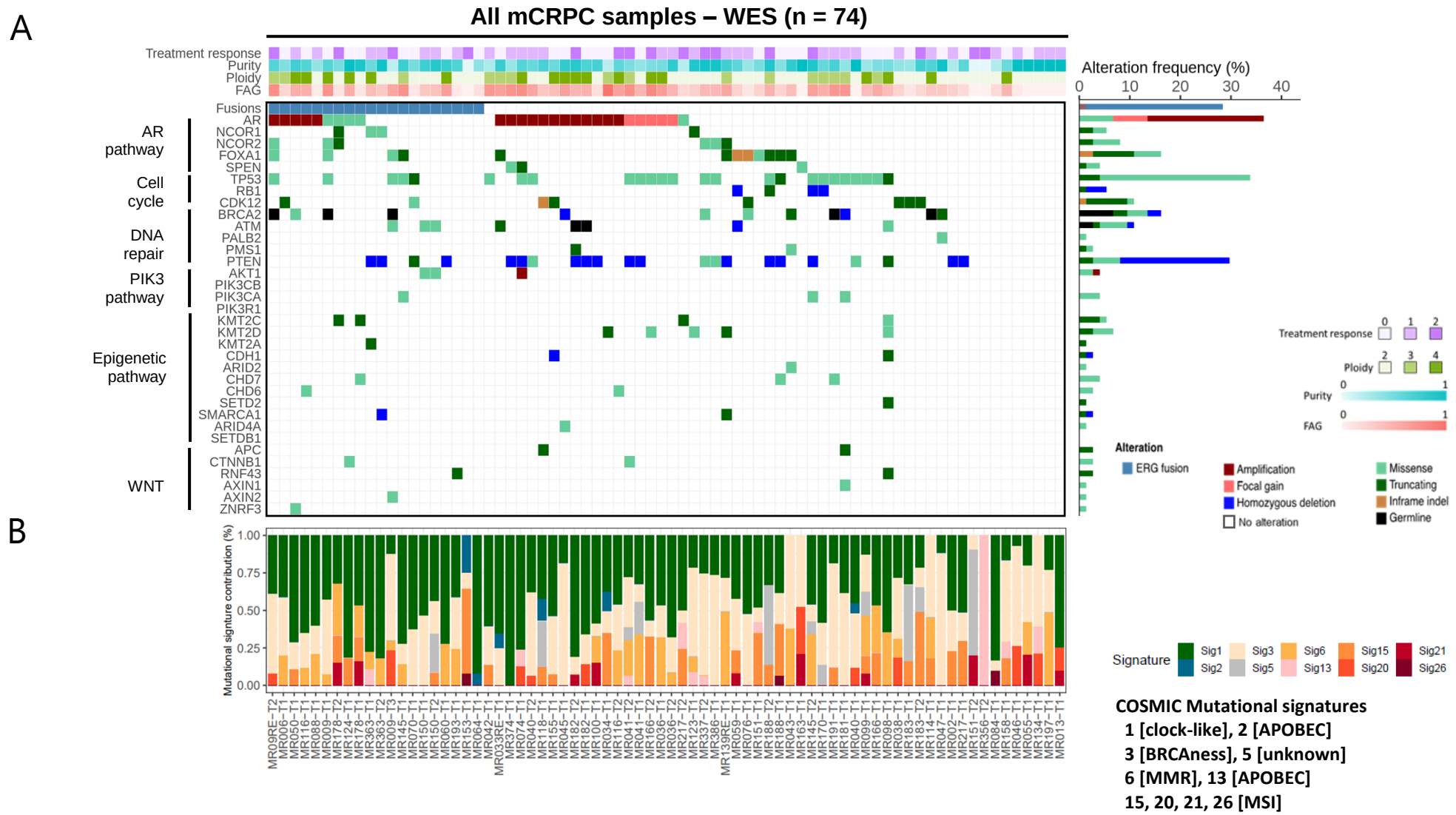

Supplementary figure 4

A

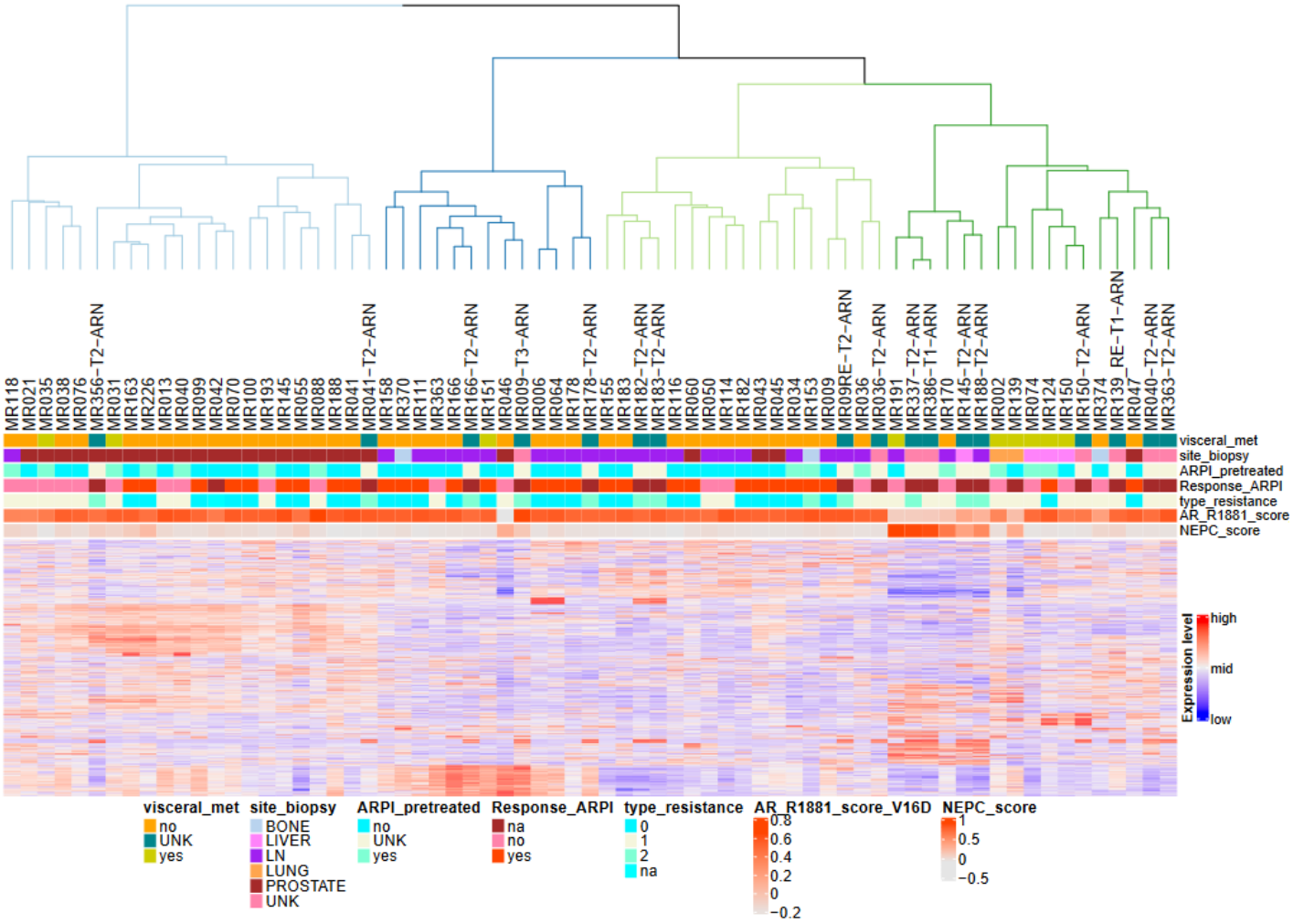

B

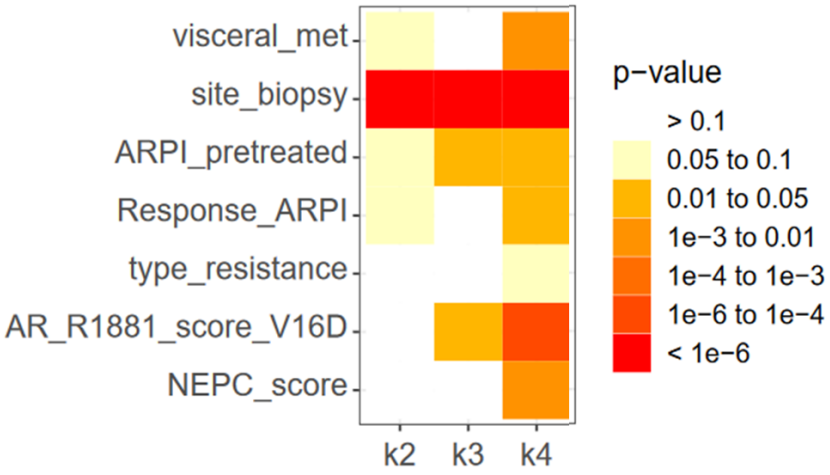

C

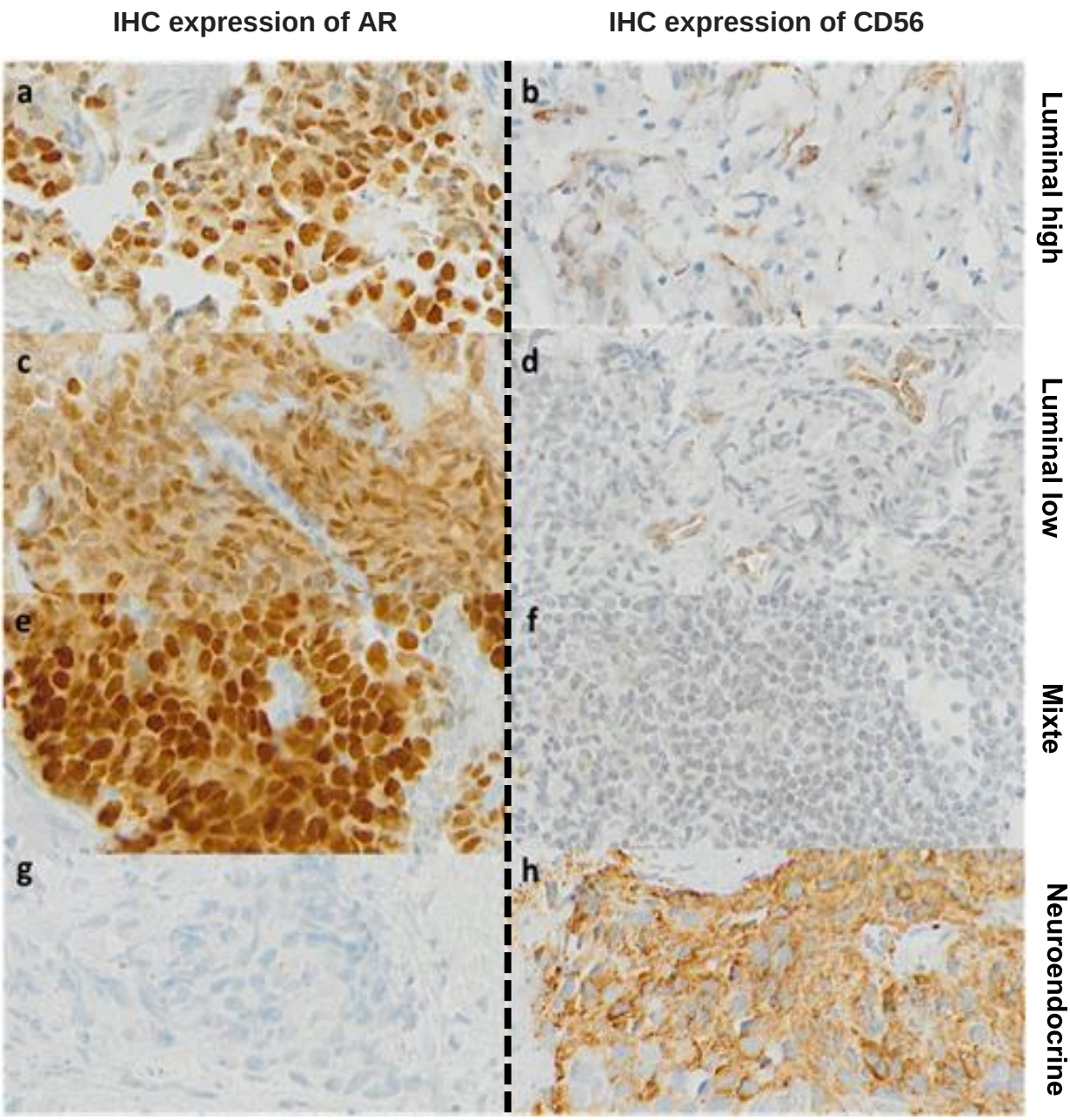
IHC expression of AR
IHC expression of CD56
a
b
c
d
e
f
g
h
Luminal high
Luminal low
Mixte
Neuroendocrine

Supplementary figure 5

A

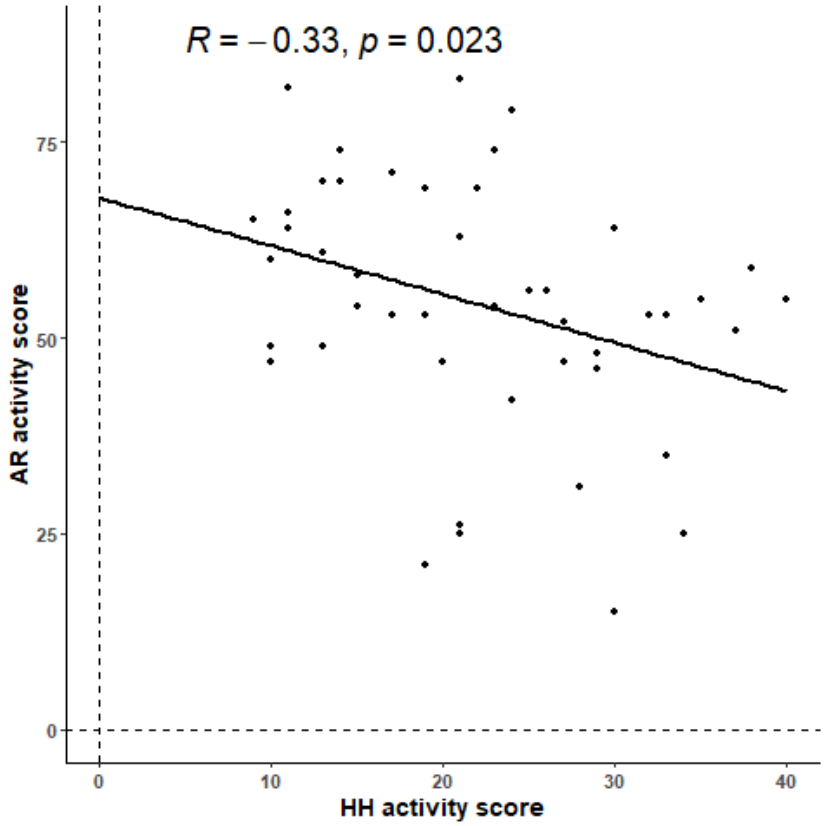

B

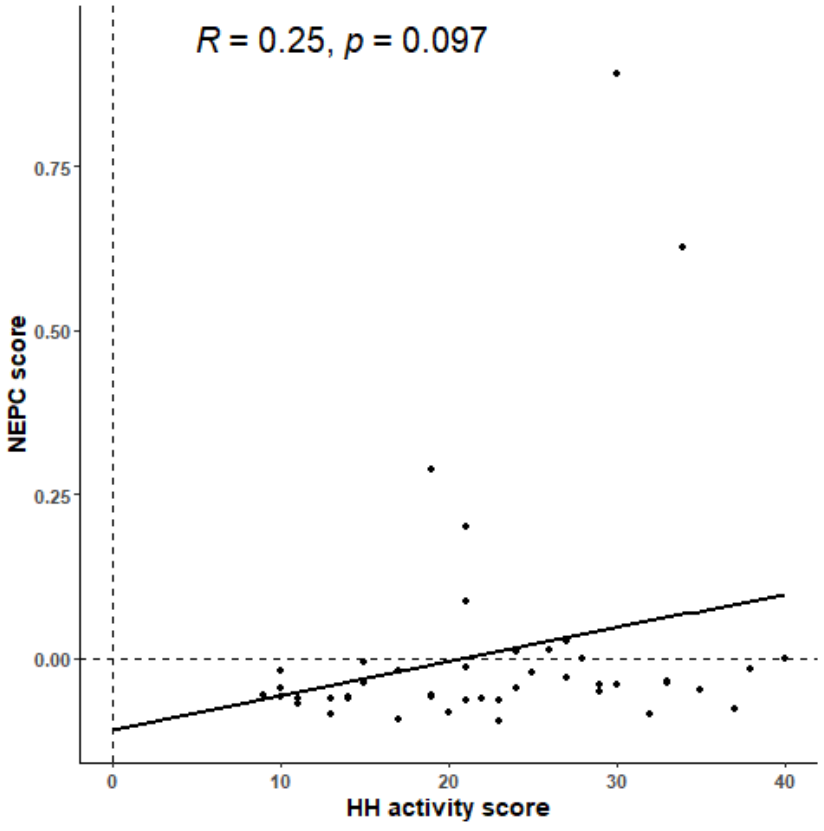

Supplementary figure 6

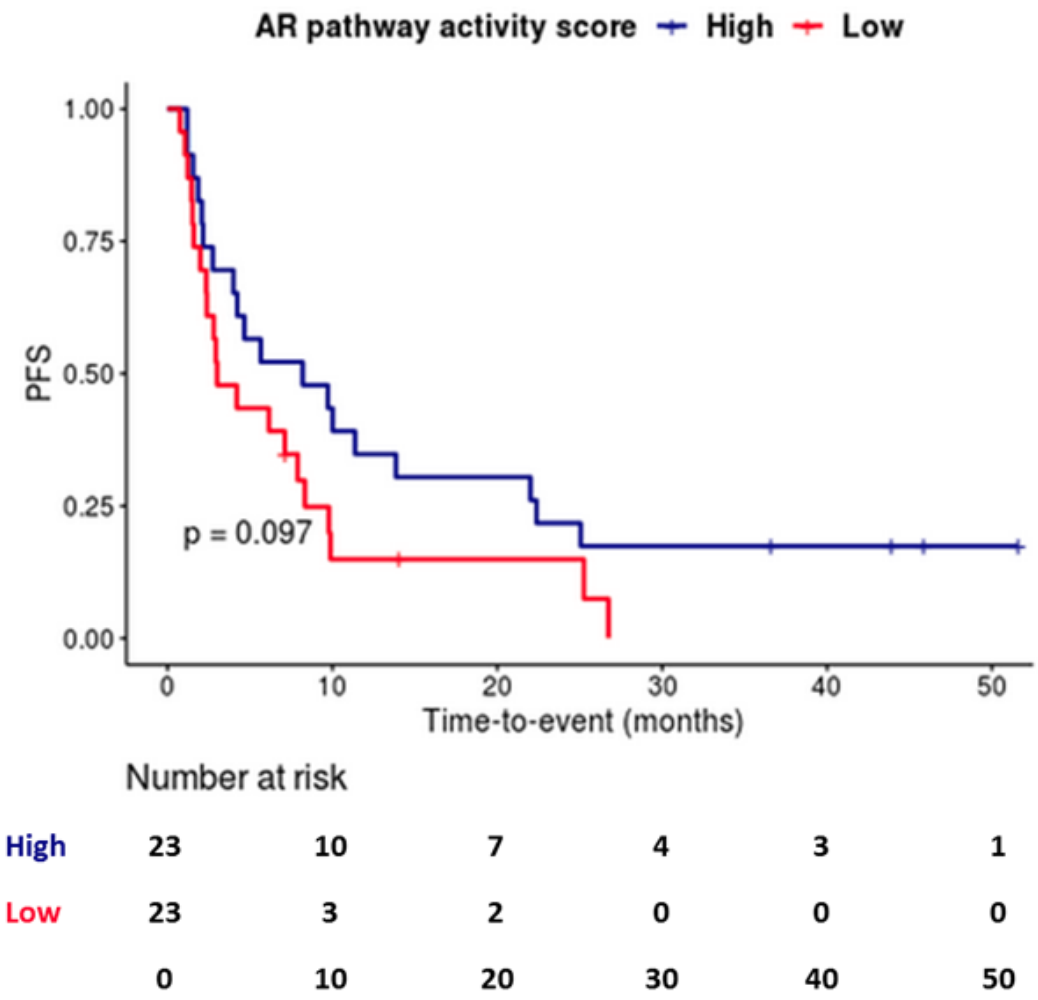

Supplementary figure 7

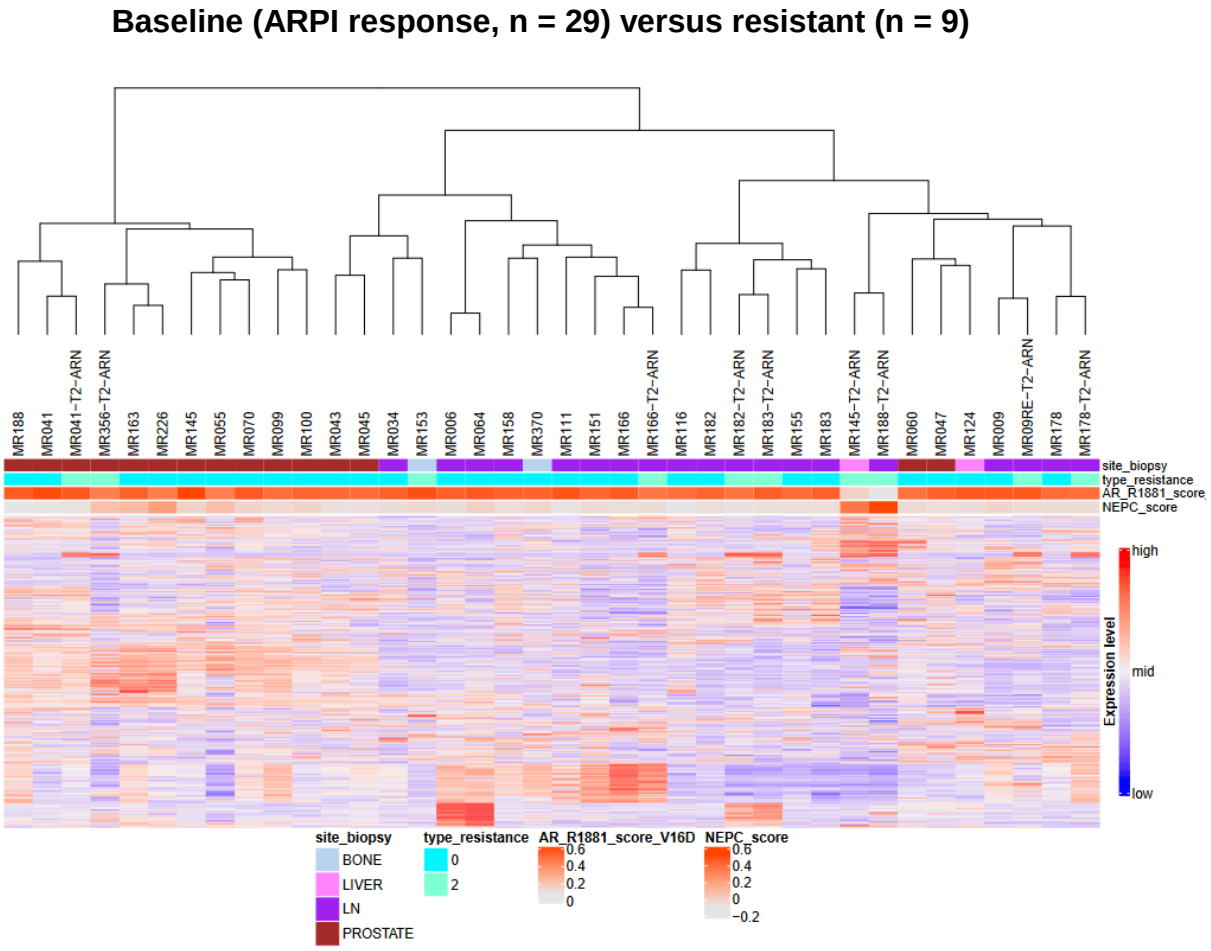

12. Supplementary methods

12.1 Whole exome analysis

12.1.1 DNA extraction and sequencing

The DNA sequencing analysis was performed on tumor DNA samples and paired constitutive DNA, on Illumina NextSeq500 system and HiSEQ2000. Clinical Research Exome – Agilent, Clinical Research Exome V2 – Agilent, SureSelect Human All Exon V5 – Agilent and Human Core Exome - TWIST with custom baits IntegraGen were used as capture of DNA. The expected mean coverage was at least 100X. The Paired-end 75 reads were generated according to the manufacturer's instructions. The quality of raw sequences was evaluated using the FastQC (v0.11.4).

12.1.2 Sequence alignment and variant calling

Base calling was performed using the Real-Time Analysis (RTA) software sequence pipeline (v2.7.7) from Illumina with default parameters. Reads were then aligned to the human genome build hg38/GRCh38.p7 using the Burrows-Wheeler Aligner (BWA) tool[1] (v0.7.15). Duplicated reads were removed using Sambamba[2] (v0.6.5). Variant calling of single nucleotide variants (SNVs) and small insertions/deletions (indels) was performed using the Broad Institute's GATK[3,4] Haplotype-Caller tool (v3.7) for germline variants and MuTect2[5] tool (v2.0) with default parameters (except for: --max_alt_alleles_in_normal_count = 2; --max_alt_allele_in_normal_fraction = 0.04) for somatic variants. Somatic variants called as "clustered_event" or *"multi_event_alt_allele_in_normal"* were further validated with VarScan2[6,7] (v2.3.9). Ensembl's Variant Effect Predictor[8] (VEP, release 87) was used to annotate variants with respect to functional consequences (type of mutation and prediction of the functional impact on the protein by SIFT v2.2 and PolyPhen v2.2.2), frequencies in public (dbSNP v147, 1000 Genomes phase 3, ExAC r3.0, and COSMIC v79), and in-house databases.

12.1.3 Detection of germline and somatic variants

To investigate germline variants, we used the following filters for more accurate identification: "PASS" filter, depth ≥ 10, and variant allele fraction (VAF) ≥ 0.25% were retained. The rare variants were selected, with a frequency < 0.001 in GnomAD non-Finnish Europeans (v2.1.1) and < 0.01 in house database. We then categorized the variants in genes known to predispose to cancer as defined by Zhang et al.[9], into the following three tiers: (1) truncating variants (nonsense, frameshift, and splice sites), (2) missense variants predicted to be "damaging" or "possibly damaging" by SIFT and Polyphen2, including in-frame indels and splice region variants, and (3) other variants.

To explore somatic alterations detected by MuTect2, we retained the most reliable somatic variants that passed following thresholds: (1) coverage ≥ 8 X in paired tumor and constitutive samples, (2) QSS score ≥ 20 (the average base quality of variant bases), and (3) VAF in the tumor (VAF_T) ≥ 0.05% with ≥ 3 mutated reads, VAF in the constitutive sample (VAF_N) < 0.04% with < 2 mutated reads, and $VAF_N < VAF_T/5$. The set of 120 prostate cancer driver genes from Armenia et al.[10] was highlighted. For patients biopsied at multiple time points, we considered a variant with a VAF ≥ 0.05 in at least one biopsy to be equally "present" in any biopsy from the same patient.

12.1.4 Copy number analysis

To reconstruct the copy number profiles of each tumor, we performed two distinct and complementary approaches.

In the first approach, we applied the Genome Alteration Print (GAP)[11] which uses germline polymorphisms and considers both log-ratio (LRR) and B-Allele Frequency (BAF) signals. The GAP method determines the absolute copy number of each segment, the ploidy of the sample and the level of contamination by normal cells. The second approach, called "Coverage", uses the coverage ratio for each capture amplicon between tumor and matched normal. The profiles are smoothed, discretized, and thresholds are applied to the log-ratio values to classify each aberration as

homozygous deletion, loss, normal, gain or high amplification. The chromosomal instability of the tumors was evaluated, by measuring two parameters which are FAG (fraction of aberrant genome) and FAA (fraction of aberrant chromosome arms) which represents the proportion of aberrant chromosome arms over ≥ 60% of their length.

The "Coverage" method uses the entire signal (> 200,000 amplicons on the capture kits used). It is therefore preferred for detecting focal aberrations (homozygous deletions and amplicons). The GAP method uses only heterozygous germline polymorphisms (~ 20,000 per sample). In addition, this approach provides the ability to study the clonality of mutations. It is preferred for large aberrations.

12.1.4.1 A genotype-based approach

For each sample, the germline single-nucleotide polymorphisms (SNPs) were determined, the LRR and BAF were estimated at every SNP site. We obtained the homogeneous segments according to genomic profiles by using the circular binary segmentation (CBS) algorithm from DNAcopy[12] package (v1.60.0), on both LRR and BAF values. We then used the GAP approach[11] to identify: (1) the ploidy per sample, which is calculated as the median copy number across the genome, (2) the contamination level with normal cells, and (3) the allele-specific copy number per segment. Therefore, we considered empirical thresholds for copy gain: copy number > ploidy + 0.5 and copy loss: copy number < ploidy - 0.5, to define chromosome aberrations. For each segment, we estimated the loss of heterozygosity (LOH).

12.1.4.2 A coverage-based approach

To identify locations of abnormal copy number, for each exome bait from the capture kit, we first estimated the coverage LRR between the tumor and matched normal sample.

Secondly, we smoothed the obtained log-ratio profiles with the circular binary segmentation algorithm from DNAcopy[12] package that is part of Bioconductor. We supposed that the zero level was the most common smoothed value per sample. The

used thresholds for copy gains: segments with a smoothed log ratio over zero + 0.15 and under zero - 0.15 for copy deletions. Furthermore, we used average + 5 s.d. (standard deviation) of smoothed log ratios in regions with gains to define high-level amplification. We also use average + 5 s.d. of smoothed log ratios in regions with deletions to define homozygous deletion.

This method shows higher resolution than approach based on genotype data, because it includes the use of more exon capture baits than germline polymorphisms. However, it does not allow the absolute copy number quantification. In fact, a coverage-based approach is most suited to study focal aberration such as high-level amplifications and homozygous deletions.

12.1.5 Clonality analysis

We used the R package *Palimpsest*[13] to estimate the cancer cell fraction (CCF), e.g. the proportion of tumor cells harboring each somatic mutation. *Palimpsest* allows calculating the CCF and its confidence interval from the VAF while accounting for tumor purity and copy number changes, as previously described[14]. Mutations were classified as subclonal when the upper bound of the 95% confidence interval of the CCF was < 0.95.

12.1.6 Mutational signatures

To provide a complementary knowledge of understanding the pathological physiology of metastatic prostate cancer, we applied the Palimpsest[13] approaches to identify potential mutational signatures across all the cohort. This R package allows: (1) either perform a *de novo* analysis of mutational signatures, allowing the discovery of new signatures and (2) to quantify the contribution to each tumor of a predefined set of signatures. We firstly carried out a *de novo* analysis based on exome data. Through this approach, we identified two signatures, which correspond to a combination of 6 signatures already found in prostate cancer via whole genome sequencing (WGS)[15]. Then, we achieved an extraction of two known series of signatures in prostate cancer,

and their contribution to each sample in our series. Both series' signatures are COSMIC (v2) signatures 1, 2, 3, 5, 6 and 13[15] and signatures 15, 20, 21 and 26 associated with Microsatellite instability[16]. We assessed the evolution of mutational processes from the baseline to resistance. From clonal and subclonal mutations, we extracted the signatures separately.

12.1.7 Pathways analysis

A pathway analysis was performed using AR, cell cycle, DNA repair, PI3K, WNT, and epigenetic pathways from Armenia et al.[10]. Gene alterations present in more than 10 % of the cohort (≥ 5 patients) were grouped by pathway. A pathway was considered as altered when at least one of the genes in the pathway was altered.

12.1.8 Tumor progression trees

To analyze the molecular history of tumoral progression, we reconstructed the oncogenetic trees for patients sequenced at least twice. We applied package *phangorn*[17] (v2.3.1) implemented in R, with the "parsimony ratchet"[18] method to reconstruct the tree implicating the smallest number of events. We annotated driver mutations, gene fusions, high-level amplifications and homozygous deletions across every branch of the trees, along with the contribution of each mutational signature assessed with *Palimpsest*[13]. Any variant detected by MuTect2 or having a VAF > 0.05 was considered "present" in a sample. For baseline-progression pairs, we distinguished between common or specific alterations to each sample. Whereas for patient MR009 (with 5 biopsies), we reconstructed the most parsimonious tree with the *phangorn*[17] package, then assigned each mutation to each branch. Four samples with poor quality were excluded (**Supplementary figure 2**).

12.1.9 Genomic aberration analysis methods

The following genomics characteristics were selected to test association with response and resistance: tumor mutational burden (number of clonal and subclonal mutations), tumor heterogeneity (proportion of subclonal variations), chromosomal instability

(Fraction of Altered Genome (FAG) and Fraction of Chromosome Arms Altered (FAA)), ploidy, frequency of driver genes alterations and mutational signatures. We performed three different analyses: (1) patients grouped by response status (response [n = 28] versus primary resistance [n = 24]), (2) patients grouped by resistance (baseline samples from responding patients who never received prior ARPIs [n = 24] versus samples with acquired resistance [n = 13], and (3) patients with paired samples (baseline versus samples with acquired resistance [n = 12]). For each comparison, the frequency of single alteration or pathway alterations between each group was calculated. We represented on an oncoprint plot (http://www.cbioportal.org/faq#what-are-oncoprints) the most relevant genes altered in a large number of patients.

12.2 RNA extraction and sequencing

RNA libraries were prepared with TruSeq Stranded mRNA kit for Illumina protocol according supplier instructions. In brief, the poly-A containing mRNA was converted from total RNA (1000ng engaged in the process) into a cDNA library using poly-T oligo-attached magnetic beads. The purified mRNA was chemically fragmented prior to reverse transcription and cDNA generation. RNA-seq library that comprises inserts of ~400mers was results from fragmentation step. The repair process was performed for the cDNA ends, and a single 'A' base was added to its 3'end. Then the adapters were ligated. To create the final double stranded cDNA library, the products were purified and enriched with the polymerase chain reaction (PCR). The libraries were then purified and quantified by QPCR. The sequencing of each transcriptome library was performed using Illumina NextSeq500 as paired-end 75b reads.

12.2.1 Quality control (QC), mapping, and quantification of gene expression

The quality assessment of raw sequences was performed using the FastQC tool (v0.11.4). Raw sequences were then aligned against GRCh38 version of the Human

genome using STAR[19] (v2.5.3a) with the following parameters: --twopassMode Basic --outReadsUnmapped None --chimSegmentMin 12 --chimJunctionOverhangMin 12 --alignSJDBoverhangMin 10 --alignMatesGapMax 200000 --alignIntronMax 200000 --chimSegmentReadGapMax parameter 3 --alignSJstitchMismatchNmax 5 -1 5 5 --quantMode GeneCounts --outWigType wiggle –sjdbGTFtagExonParentGene gene_name.

Sequences that map at more than one genomic position were not considered. The full annotation of Gencode v26 (GRCh38) was used in the quantification of gene expression. To get the number of reads related to each gene in the Gencode v26 database (restricted to protein-coding genes, antisense, and lincRNA), we also used STAR. The Integrative Genomics Viewer (IGV [20], http://www.broadinstitute.org/igv/) was used for mapping visualization and quality control. Throughout the mapping, STAR calculated the number of reads associated with each transcript from the Gencode annotation. To prepare a count data for further analysis, we used the Bioconductor *DESeq* package [21] (v1.38.0) to import raw HTSeq counts for each sample into R software and extract matrix of read counts. The TPM (Transcripts Per Million) normalization was used to compare gene expression levels across samples.

12.2.2 Gene expression-based scoring

We established androgen receptor (AR) and neuroendocrine prostate cancer (NEPC) scores in order to examine more deeply the role of androgenic and neuroendocrine gene expression in response to ARPI. These scores were based on set of genes used previously to distinguish NEPC versus adenocarcinoma patient tumors. To calculate the AR score, we considered AR transcriptomic signature (30 genes) from Beltran et al.[22] and the V16D prostate cancer cell line, derived from the LNCaP cell line, as reference sample to show AR pathway activation. V16D cell line was provided by Vancouver Prostate Cancer Centre[23]. V16D cell line was used with R1881 (testosterone) treatment, which induces intense AR binding in the model. We first performed the

alignment of the reference sample and patients' samples reads on the hg38 genome to estimate 30 genes' expression. Second, the AR score was calculated by computing Pearson correlation coefficient between the patients' samples and the reference sample on the expression of the 30 genes. The NEPC score was calculated using the 70 genes of NEPC transcriptomic signature and 13 patients' samples with neuroendocrine prostate cancer from Beltran et al.[22] Then, we calculated a metasample expression, which corresponded to the mean expression of the 13 samples for each of the 70 genes. Then, for each sample, the NEPC score was calculated by computing Pearson correlation coefficient between the patients' samples and the metasample reference on the expression of the 70 genes.

12.2.3 Gene fusion detection

To explore the impact of gene fusions in prostate cancer, we performed gene fusion identification with STAR-Fusion[24] (v1.8.0) and FusionCatcher[25] (v1.20) using paired-end RNA-seq data. The results of two fusion calling algorithms are merged, giving confidence to the detected fusions. FusionInspector[26] (v2.2.1), a part of the Trinity Cancer Transcriptome Analysis Toolkit (CTAT)[27] was used to validate the predicted fusion events. FusionInspector approach based on a supervised analysis of fusion predictions, by re-evaluating and re-scoring evidence for these found gene fusions. For each predicted fusion, we retained for a further analyses fusions that were not found in healthy and artifact databases (table 2, https://github.com/ndaniel/fusioncatcher/blob/master/doc/manual.md#output-data) and with at least 2 pairs of read spanning and overlapping the gene fusion partners.

12.2.4 AR isoform analysis

AR-V7 expression has been considered as one of the mechanisms of resistance to androgen deprivation therapy. Therefore, we looked closely at the expression of AR splice variants and more particularly AR-V7 in our cohort. To this purpose, we assigned AR mapped reads to each reference transcript based on pseudoalignment,

for a rapidly determination of the compatibility of reads to a transcriptome, without the need for alignment, using kallisto[28] (v0.44.0). The expression of each transcript was normalized by library size and transcript length to compare expression levels between transcripts and samples.

12.2.5 OncoSIGNal pathway activity analysis

The paired-end RNA-seq data (FASTQ files) were blinded and sent to InnoSIGN for OncoSIGNal pathway activity analysis[29]. The RNA-seq pipeline starts with mapping the raw reads to the reference genome (human genome assembly GrCH38.95) using STAR (v.2.6.1). Transcripts are quantified using RSEM (v1.3.1) (RNA-seq by Expectation-Maximization)[30]. Data are normalized as protein-coding TPM. This shows the proportion of exonic reads with a protein-coding label that is being mapped to which gene, eliminating variation in mRNA selection (such as rRNA removal efficiency). A proprietary method for additional normalization is performed such that the normalized data is library prep kit independent, e.g. compatible with both rRNA depletion (such as TruSeq Stranded Total RNA) and polyA (such as TruSeq Stranded mRNA) library prep kits.

A quality control (QC) pass/fail judgment is made for each sample based on a multitude of predefined QC criteria (e.g. ratio of mapped reads to total number of reads; reference gene expression; transcript integrity number). Samples with poor performance are excluded from further analysis.

For the MATCH-R cohort, five baseline samples (MR031, MR055, MR139, MR183, and MR282) failed QC due to poor library complexity. Two resistant samples (MR074 and MR182) failed QC due to a low transcript integrity number and poor gene body coverage. One resistant sample (MR09RE-T2) had a significant 3' bias and was therefore excluded. The normalized gene expression values are the input for the OncoSIGNal pathway activity analysis.

Each pathway assay is based on the concept of a Bayesian network computational model to measure signal transduction pathway activity, as described before[29]. In brief, the computational network model for signaling pathways is constructed to infer the probability that the pathway-driving transcription factor is actively transcribing mRNA of its target genes. The Bayesian network describes the causal relationship where the measured intensity of microarray probesets is dependent on the activity of target gene transcription, which is, in turn, causally related to the activity of the transcription complex. These relations are probabilistic in nature. Selection of target genes of the pathway-driving transcription factors has been based on insights from *in vitro* and *in vivo* studies assessing if the gene promoter region contains a transcription factor response element, if the transcription factor binds to this response or enhancer element, the promotor functionality, and differential expression upon pathway activation. The models are calibrated based on samples with ground truth information about their pathway activity state. The model calculates, from mRNA levels of the selected target genes of the pathway-associated transcription factor, a probability score for the pathway activity. The probability is translated to the log2 value of the transcription factor odds. The pathway activity score is then normalized to a 0-100 scale; inferred from the log2(odds) that the pathway is active, 0 corresponding to the lowest and 100 corresponding to the highest odds in favor of an active pathway that the computational model can theoretically infer. Practically this means that the actual range of pathway activity scores for a signaling pathway assay, when performed on a specific cell/tissue type, covers only part of this 0-100 scale depending on the biologically lowest and highest possible activity in this cell/tissue type.

12.3 Internal validation with Immunohistochemistry (IHC)

To define AR phenotype, we used antibodies directed against AR (Cell Signaling, clone D6F11) staining. To determine NEPC phenotype, we stained with Synaptophysin (DAKO, DAK-SYNAPTO), Chromogranin A (DAKO, DAK-A3), and CD56 (Roche, MRQ-42). Tumor biopsies were stained with the Ventana Benchmark Ultra platform (Roche

Diagnostics, Mannheim, Germany). Routine hematoxylin and eosin (H&E) staining was performed for morphological examination of the tumor. The immunohistochemical characterization was double read by two pathologists to obtain a high level of certainty. Four different phenotypes were defined: luminal high (strong AR nuclear staining), luminal low (low AR nuclear staining or cytoplasmic staining), neuroendocrine phenotype (NEPC), and mixed phenotype (both luminal and NEPC component within the same biopsy).

13. Supplementary references

1. Li H, Durbin R. Fast and accurate short read alignment with Burrows-Wheeler transform. Bioinformatics. 2009; 25(14): 1754-60.

2. Tarasov A, Vilella AJ, Cuppen E, Nijman IJ, Prins P. Sambamba: fast processing of NGS alignment formats. Bioinformatics. 2015; 31(12): 2032-4.

3. DePristo MA, Banks E, Poplin R, Garimella KV, Maguire JR, et al. A framework for variation discovery and genotyping using next-generation DNA sequencing data. Nat Genet. 2011; 43(5): 491-8.

4. Van der Auwera GA, Carneiro MO, Hartl C, Poplin R, Del Angel G, Levy-Moonshine A, et al. From FastQ data to high confidence variant calls: the Genome Analysis Toolkit best practices pipeline. Curr Protoc Bioinformatics. 2013; 43(1110): 11.10.1-11.10.33.

5. Cibulskis K, Lawrence MS, Carter SL, Sivachenko A, Jaffe D, Sougnez C, et al. Sensitive detection of somatic point mutations in impure and heterogeneous cancer samples. Nat Biotechnol. 2013; 31(3): 213-9.

6. Koboldt DC, Larson DE, Wilson RK. Using VarScan 2 for Germline Variant Calling and Somatic Mutation Detection. Curr Protoc Bioinformatics. 2013; 44: 15.4.1-17.

7. Koboldt DC, Zhang Q, Larson DE, Shen D, McLellan MD, Lin L, et al. VarScan 2: somatic mutation and copy number alteration discovery in cancer by exome sequencing. Genome Res. 2012; 22(3): 568-76.

8. McLaren W, Gil L, Hunt SE, Riat HS, Ritchie GR, Thormann A, et al. The Ensembl Variant Effect Predictor. Genome Biol. 2016; 17(1): 122.

9. Zhang J, Walsh MF, Wu G, Edmonson MN, Gruber TA, Easton J, et al. Germline Mutations in Predisposition Genes in Pediatric Cancer. N Engl J Med. 2015; 373(24): 2336-2346.

10. Armenia J, Wankowicz SAM, Liu D, Gao J, Kundra R, Reznik E et al. The long tail of oncogenic drivers in prostate cancer. Nat Genet. 2018; 50(5): 645-651.

11. Popova T, Manié E, Stoppa-Lyonnet D, Rigaill G, Barillot E, Stern MH. Genome Alteration Print (GAP): a tool to visualize and mine complex cancer genomic profiles obtained by SNP arrays. Genome Biol. 2009; 10(11): R128.

12. Venkatraman ES, Olshen AB. A faster circular binary segmentation algorithm for the analysis of array CGH data. Bioinformatics. 2007 Mar 15; 23(6): 657-63.

13. Shinde J, Bayard Q, Imbeaud S, Hirsch TZ, Liu F, Renault V, et al. Palimpsest: an R package for studying mutational and structural variant signatures along clonal evolution in cancer. Bioinformatics. 2018; 34(19): 3380-3381.

14. Letouzé E, Shinde J, Renault V, Couchy G, Blanc JF, Tubacher E, et al. Mutational signatures reveal the dynamic interplay of risk factors and cellular processes during liver tumorigenesis. Nat Commun. 2017; 8(1): 1315.

15. Gerhauser C, Favero F, Risch T, Simon R, Feuerbach L, Assenov Y, et al. Molecular Evolution of Early-Onset Prostate Cancer Identifies Molecular Risk Markers and Clinical Trajectories. Cancer Cell. 2018; 34(6): 996-1011.e8.

16. Alexandrov LB, Nik-Zainal S, Wedge DC, Aparicio SA, Behjati S, Biankin AVet al. Signatures of mutational processes in human cancer. Nature. 2013; 500(7463): 415-21.

17. Schliep KP. phangorn: phylogenetic analysis in R. Bioinformatics. 2011; 27(4): 592-3.

18. Nixon KC. The Parsimony Ratchet, a New Method for Rapid Parsimony Analysis. Cladistics. 1999; 15(4): 407-414.

19. Dobin A, Gingeras TR. Mapping RNA-seq Reads with STAR. Curr Protoc Bioinformatics. 2015; 51: 11.14.1-11.14.19.

20. Robinson JT, Thorvaldsdóttir H, Winckler W, et al. Integrative genomics viewer. Nat Biotechnol. 2011; 29(1): 24-6.

21. Anders S, Huber W. Differential expression analysis for sequence count data. Genome Biol. 2010; 11(10): R106.

22. Beltran H, Prandi D, Mosquera JM, Benelli M, Puca L, Cyrta J, et al. Divergent clonal evolution of castration-resistant neuroendocrine prostate cancer. Nat Med. 2016; 22(3): 298-305.

23. Yamamoto Y, Loriot Y, Beraldi E, Zhang F, Wyatt AW, Al Nakouzi N, et al. Generation 2.5 antisense oligonucleotides targeting the androgen receptor and its splice variants suppress enzalutamide-resistant prostate cancer cell growth. Clin Cancer Res. 2015; 21(7): 1675-87.

24. Haas BJ. STAR-Fusion code and documentation on GitHub 2019. Available from: https://github.com/STAR-Fusion/STAR-Fusion/wiki.

25. Nicorici D, Satalan M, Edgren H et al. FusionCatcher - a tool for finding somatic fusion genes in paired-end RNA-sequencing data. bioRxiv 011650. 2014; 10.1101/011650.

26. Haas B, Dobin A, Ghandi M et al Targeted in silico characterization of fusion transcripts in tumor and normal tissues via FusionInspector. bioRxiv 2021; 08.02.454639; doi: https://doi.org/10.1101/2021.08.02.454639.

27. Haas B; Tickle T; Pochet N et al. Fast and accurate fusion transcript detection using the Trinity Cancer Transcriptome Analysis Toolkit. Cancer Res. 2016; 76 (14_Supplement): 5266.

28. Bray, N., Pimentel, H., Melsted, P. et al. Near-optimal probabilistic RNA-seq quantification. Nat Biotechnol 2016; 34, 525–527.

29. Verhaegh W, van Ooijen H, Inda MA, Hatzis P, Versteeg R, Smid M, Martens J, Foekens J, van de Wiel P, Clevers H, van de Stolpe A. Selection of personalized patient therapy through the use of knowledge-based computational models that identify tumor-driving signal transduction pathways. Cancer Res. 2014; 74(11): 2936-45.

30. Li, B., & Dewey, C. N. RSEM: accurate transcript quantification from RNA-Seq data with or without a reference genome. BMC bioinformatics, 2011; 12(1):1-16.

DISCUSSION AND PERSPECTIVES

Global view of this contribution among studies on resistance

Unveiling the biological mechanisms responsible for resistance to ARPIs is a fundamental step in the goal for better survival outcomes for patients with metastatic PCa and also localized prostate cancer. Landscape studies on resistance, dealing with large and homogeneous cohorts of patients, allowed the identification of recurrent patterns of resistance, thus allowing generalizations on the most frequent events responsible for resistance. Understanding how specific cancers progress on these targeted agents is inform their optimal use, and to develop novel therapies and strategies to overcome resistance. Consortium like the Prostate Cancer Dream Team had the power to collect samples from hundreds of patients previously treated with ARPIs[153]. Nevertheless, our study distances itself from previous experiences in the field, limited to case reports and case series, or preclinical studies representing an intermediate strategy between these latter and a landscape approach. Here we move from global, general findings to more granular data on patients prospectively monitored with collection well clinically-annotated human samples. This type of strategy is usual in the field of precision oncology, as isolated experiences can be extremely informative on biological and clinical behaviors of diseases at resistance. However, in metastatic PCa, few prospective studies[159,160] on the topic were reported far, due to the challenge of obtaining biopsy of metastases, especially paired pre and post therapy biopsies. In the first study[158], targeted DNA sequencing and whole transcriptome analysis were performed while in the second study[159] only bone metastases were collected before DNA and RNA sequencing. In both studies, mechanisms of acquired resistance were not studied. Even if the number of samples obtained in the context of acquired resistance was limited, our results provided insights into how acquired resistance to ARPIs occurs in prostate cancer. Overall, we think that our clinical approach can distinguish itself from previous experiences, in providing a useful clinical-genomic dataset to understand, and hopefully overcome, resistance in

the clinical setting. Our study is one of the largest prospective clinical trials examining molecular predictors of ARPIs response from metastatic tumor biopsies, and we look forward to the results of other studies with novel AR-targeting agents that may help to validate our results.

Relevance of genomic assays for the understanding of resistance to ARPIs

Mutational profiling primarily consisted of whole exome sequencing rather than targeted DNA-seq allowing a high number of genes examined across all patients. Thus, our panel did include key genes previously linked to ARPIs resistance or EMT/lineage plasticity (*TP53*, *RB1*, and *PTEN*), and no significant differences were found. We cannot rule out that loss of function of these genes or others through epigenetic or post-transcriptional mechanisms could have also contributed to *de novo* ARPI resistance. Next step will be to use epigenetics and/or proteomics assays to better explore this field. Also, WES had limited power to detect structural variants or mutational signatures associated with resistance. *De novo* analysis of mutational signatures was not possible and we used a strategy based extraction of previously reported active mutational signature in prostate cancer. Thus, we cannot rule out that new mutational signature was associated with either primary or secondary resistance to ARPIs. To this end, WGS analysis may be necessary to clarify theses issues.

Another potential limitation of our study is that only a single metastatic site was biopsied prior to treatment, although it remains challenging to collect biopsies from multiple sites at the same time point. However, despite only obtaining a biopsy from a single site, we did determine, using RNA sequencing, that the site sampled had molecular features strongly correlated with primary resistance. This suggests that a single-site biopsy—if it contains adequate material for sequencing—may be sufficient

to identify markers of ARPIs response. Furthermore, a recent study[161] using digital spatial profiling technology to quantitate transcript and protein abundance in spatially-distinct regions of mPCs reported a high level of intra-patient homogeneity with respect to tumor phenotype even tough there were notable exceptions including tumors displaying regions with high and low AR and neuroendocrine activity. In another analysing multiple tumors from men with disseminated prostate cancer through whole-exome sequencing, array comparative genomic hybridization (array-CGH) and RNA transcript profiling, there was limited diversity among metastases within an individual[162]. These data indicate that although exceptions exist, evaluating a single metastasis provides a reasonable assessment of the major oncogenic driver alterations that are present in disseminated tumors.

Dealing with heterogeneous mechanisms of primary resistance

We hypothesized that a detailed characterization of the genomic landscape of baseline CRPC samples in patients beginning ARPIs treatment would clarify determinants of *de novo* resistance. We did not detect any statistically significant differences in mutations or genetic alterations found between non-responders and responders. Other studies observed a trend toward statistical significance for *TP53* mutations that were more common in non-responders[159]. This was consistent with findings from a study which used cfDNA-seq of enzalutamide- or abiraterone-naïve patients and determined that alterations in *TP53* were associated with poor outcomes[163]. However, contradictory results were found in other studies that did not find any recurrent genetic alterations associated with primary resistance[160]. In all prospective studies including ours, the relatively limited number of samples precludes any definitive conclusion. In the largest (retrospective) study reported so far among 128 patients treated with a first-line ARPIs,

the association of 18 recurrent DNA- and RNA-based genomic alterations, including AR variant expression, AR transcriptional activity, and NE expression signatures with clinical outcomes were examined. Of these, only *RB1* alteration was significantly associated with poor survival, whereas alterations in *RB1*, *AR*, and *TP53* were associated with shorter time on treatment with an ARPIs. The next step to adress this question would be to pool all the data available to expand the sample size and/or to analyse prospectively collected samples in large clinical trials, especially in castration-naive prostate cancer patients where the lack of prior therapy will allow correct analysis of the mutational landscape.

Because AR pathway is the target of ARPIs, we examined alterations in the *AR* gene itself as well as measurements of AR transcriptional function. We did not observe statistically significant differences in *AR* gene alterations between non-responders and responders, although this may be due to sample size limitations. Levels of *AR* mRNA and protein expression were also similar between the two groups, suggesting that AR genomic or AR expression changes are not good predictors of ARPIs response. We found that lower AR transcriptional activity was associated with ARPIs primary resistance. Because AR is the final target of ARPIs, this result holds a strong biological rationale and strongly suggests that cancer with lower AR activity are less AR pathway dependent and thus, less likely to respond to ARPIs therapy. Low AR activity has been linked to lineage plasticity, EMT, or stemness. Previous studies reported that the IL-6–JAK-STAT3 signaling pathway was activated in tumors resistant to AR pathway inhibition and that IL-6–JAK-STAT3 promotes stem-like properties, EMT, and lineage plasticity[164]. GSEA also implicated activation of the transforming growth factor-β (TGF-β) signaling pathway that is upstream of SMAD3 in non-responders[165], with a role in regulating gene activity and cell proliferation.

One important finding of our study was the potential role of Hh pathway in promoting ARPIs resistance. The exact mechanisms leading to Hh pathway activation is unclear. We did not find any genetic alteration of genes associated with Hh pathway (e.g.

PTCH1, *GLI1*, and *GLI3*). Elucidading these mechanisms will be important to test rational pathway inhibition. We took advantage of PDX from samples obtained in patients enrolled in MATCH-R. We selected one PDX with high Hh pathway activity and at time of writing the manuscript, experiments in mice investigating Hh pathway inhibition are ongoing. One important question is to determine whether all the pathways associated with resistance are active in the same patients. To adress this question, single-cell RNA sequencing (scRNA-seq) analysis would be helpful.

Dealing with mechanisms of acquired resistance

Our study provides some new aspects to understand mechanisms of acquired resistance. Limited data are currently available mainly due to the difficulty to obtain biopsy at time of resistance. Previous studies reported multiple mechanisms of resistance suh as *AR* amplification[163], AR splice variants[166], increased WNT/β-catenin signaling[167], increased TGF-β signaling[167], EMT or increased stemness, and lineage plasticity[167,159]. However, these prior studies were largely restricted to DNA mutational analysis, compared baseline and progression samples from different patients, used limited numbers of matched samples, or did not focus on transcriptional changes. We hypothesized that comparing gene expression profiles between matched CRPC tumor biopsy samples prior to ARPIs and at the time of progression would identify pre-treatment and treatment-induced resistance mechanisms in individual patients. Our study adresses these limitations by analysing paired biopsies from the same patients and did include transcriptome analysis. Our work suggests that most CRPC tumors resistant to ARPIs continue to depend on the AR as most tumors exhibit either *AR* amplification of *AR* mutations in a model of branched evolution where subclones emerged at time of resistance. Importantly, we determined that most progressive tumors clustered with their baseline pair and that most tumors did not change their

transcriptional cluster designation between baseline and progression. Many patients' matched tumors expressed a similar gene expression program, regardless of whether a different lesion or tissue type was biopsied, suggesting homogeneity of many lesions within the same patient. In a recent study[168] that analysed serial cfDNA from mCRPC patients treated with ARPIs, the analysis found no regions that contained recurrent mutations, structural rearrangements, or copy number changes that were acquired at treatment progression on ARPIs. This strongly suggest that mCRPC evolution is continually dependent on AR genotype, reinforcing the need for new therapies that target AR pathway, and proposing a minimally invasive practical tool for detecting emerging genomic mechanisms of resistance.

In other patients, AR activity was reduced at progression, suggesting other AR-independent resistance mechanisms or activation of a non-canonical AR program. Pathway analysis of progression demonstrated upregulation of several inflammatory pathways found previously to be activated in cancer stem cells such as IFNα, IFN-γ response, allograft rejection, IL6/JAK/STAT signaling, and TNF-α signaling via NFKB. Interestingly, these pathways were found to be associated with primary resistance. These results suggest that ARPIs treatment may contribute to a stem-like state even in tumors that did not yet have evidence of lineage plasticity (assessed with a low NEPC score) contributes to resistance.

Open questions and perspectives

The main objective of this project is to provide therapeutic suggestions to overcome resistance to ARPIs in patients with metastatic PCa and improve their overall health. Several key findings from this and other work in a coherent clinical approach to overcoming resistance to ARPIs:

The data shown here indicate that, indeed, most tumors that acquired resistance to ARPIs remain dependent on AR signaling. Two strategies may be therefore envisioned to optimize outcomes in patients with mCRPC treated with ARPIs.

1. The first would be to develop new AR pathway inhibitors. Several drugs that inhibit other players in the steroidogenesis are currently investigated in phase 1 and phase 2 trials. For example, CYP11A1 inhibitors such as ODM-208 may rescue the resistance to ARPIs mediated by activation of upstream androgen. CYP11A1 inhibition might halt the synthesis of all steroid hormones, since CYP11A1 is the only enzyme that catalyses the first step of steroid hormone biosynthesis. ODM-208 suppresses the production of all steroid hormones and their precursors that may activate the AR signaling pathway. This is particularly relevant in patients with AR ligand binding domain activating somatic point mutations, a mechanism of resistance to hormone-based therapies in mCRPC[169]. Another strategy will be to inhibit N-terminal domain with highly specific inhibitors. This strategy would have the advantage to overcome the resistance mediated by *AR* LBD mutations and *AR* amplifications. Selective inhibition of the N-terminal domain of the AR can inhibit its' transcriptional activity even in the presence of LBD-driven resistance[170].
2. Another strategy would be to early detect AR-mediated resistance by analysing serial cfDNA in order to offer patient combination therapy or other drugs (e.g. chemotherapy) when these mechanisms occur. A recent study showed the

feasibility of this approach[168]. Our work has not focused on cfDNA analysis. However, plasma and serum were collected over time and next step will be to focus on how liquid biopsies can be used to better characterize clonal evolution of resistant prostate cancers and to evaluate the concordance between genomic alterations observed in tissue and liquid biopsies to assess reliability of the latter.

Another challenge will be to envision how non-AR mediated mechanisms of resistance can be addressed. Around 15%-20% of prostate cancers with acquired resistance have NE features. Currently, there is no specific drug that has been shown to be highly active against this phenotype. Beyond the genetic alterations associated with NE differentiation (*TP53*, *RB1*, and *PTEN*), other mechanisms have been reported to play a role in this phenomenon such as upregulation of SOX2[171], BRN2[172], and PEG10[173]. Currently, these mechanisms involved in both primary and acquired resistance are difficult to inhibit and much work is needed to better understand how to efficiently target these adaptive mechanisms of resistance. We showed also that other mechanisms are associated with resistance in the absence of clear association with NE differentiation such as Hh and immune-related pathways. Whether or not these pathways are active in all tumors and are mutually exclusive is difficult to address today. Single-cell analysis can be helpful in the future to address this question. Recently, a study[166] using scRNA-seq analysis showed that resistance to enzalutamide was associated with cancer cell-intrinsic EMT and TGF-β signaling. Small cell carcinoma cells exhibited divergent expression programs driven by transcriptional regulators promoting lineage plasticity such as HOXB5, HOXB6, and NR1D2. Additionally, a subset of patients had high expression of dysfunction markers on cytotoxic CD8+ T cells undergoing clonal expansion following enzalutamide treatment. In this context where cooperation between different cell population (e.g. tumor cells, immune cells, normal cells, and stroma cells), spatial transcriptomic analysis may be helpful to better understand the contribution of intratumoral heterogeneity.

Finally, ARPIs are now used in earlier stage, especially in patients with *de novo* metastatic PCa in combination with androgen deprivation therapy. It will be important to analyse whether these mechanisms of resistance of both primary and acquired are also found in this context. The PEACE-1 trial will be an opportunity to address this question in the future[40].

CONCLUSION

In conclusion, the study of resistance to ARPIs in mCRPC turned out to be quite a challenging goal. The interplay between the clinical outcomes observed and the molecular correlates of resistance from human samples was the real backbone of this translational project and manuscript. As a bioinformatician, I see this translational and multidisciplinary approach as the most successful and satisfactory one in trying to understand and overcome resistance to drugs in solid tumors. Starting from a clinical question, the real meaning of these intellectual questions is to provide new hope for patients.

OTHER RELATED PROJECTS AND COLLABORATIONS

Supplementary data – How does AR inhibitors remodel the immune landscape?

In addition to the genomic and transcriptomic profiling of the mCRPC tumor done in this thesis, the transcriptomic profiling showed us that the immune system is involved in the resistance to ARPIs in these patients. Thus, we decided to focus on the study of the immune response to ARPIs in advanced prostate cancer with the aim of bringing to these patients existing immune therapies that are effective in the fight against certain types of cancer like melanoma.

Furthermore, as we know, tumor progression does not only originate from the epithelial cells but also from the tumor environment (TME). It encompasses several cells that either form a wall surrounding the tumor or may be in diffused forms. This environment includes stromal cells (epithelial cells, mesenchymal stem cells, fibroblasts, adipocytes supported by the extracellular matrix, and blood and lymphatic vascular cells) and immune cells (e.g. B-cells, dendritic cells, macrophages, T-cells, monocytes and natural killer cells). Both their proportions and their specific roles will depend greatly on the type and stage of the cancer. The inter-communication between epithelial cells and cells in the tumor environment via signaling pathways promotes tumor spread from the prostate cancer primary site to metastatic sites and play a role in patient's response to treatment. Since prostate cancer metastases preferentially reach the skeleton, it makes it more challenging to understand the specific interaction between prostate cancer epithelial cells and the surrounding biological environment has followed. Even if immune therapies are growing and successful treatments in other cancer types, mainly due to a low mutational burden of mCRPC, this field is still under-investigated in mCRPC.

In order to extend the study for further analysis of the tumor microenvironment, solid biopsies from patients participating in the MOSCATO (Molecular Screening for CAncer

Treatment Optimization) (NCT01566019) and MATCH-R trials (n = 100 samples) were considered for this study.

To start assessing the abundance of different immune cell populations in the mCRPC microenvironment, specific and complementary algorithms like Cibersort and MCP-counter[174] implemented in R package were used on RNA-seq data from biopsies from the prospective MATCH-R trial. Indeed, the Cibersort approach allows comparison between cells and the MCP-counter approach allows comparison between samples. Based on a gene expression matrix normalized by TPM, MCP-counter provides abundance scores for 11 immune cell types: CD3+ T cells, CD8+ T cells, cytotoxic lymphocytes, Natural Killer (NK) cells, B cells, macrophage/monocyte-derived cells, myeloid dendritic cells, neutrophils, endothelial cells, and cancer-associated fibroblasts (CAF) for each sample. While Cibersort estimates abundance scores for 22 human hematopoietic populations of T-cell types, naive and memory B-cells, plasma cells, NK cells and myeloid subpopulations.

Interestingly, preliminary results from the characterisation of the immune landscape of mCRPC tumors showed that mCRPC tumors reveal heterogeneity in the inference of immune cell populations (**Supplementary figures 1-2**).

Macrophages are the most involved immune cell population with the M2 population being the most represented compared to the M1 (**Supplementary figure 1**). This is likely to be associated with immunosuppressive TME in PCa where the outcome is expected to be poor[175].

In addition, cancer-associated fibroblasts (CAFs) are also highly present in mCRPC patients. CAF abundance, effectively plays a causal role in treatment resistance and tumour progression in PCa, as reported in previous studies[176,177].

Overall, CD8+ T scores and inferred cytotoxicity are low (**Supplementary figure 2**). Moreover, AR and NEPC transcriptomic scores, as described above, were significantly negatively and positively associated with the immune infiltration score, respectively

(**Supplementary figure 3 A-B).** This may suggest that neuroendocrine differentiation can trigger an immune response in PCa, more work is needed to make this evident.

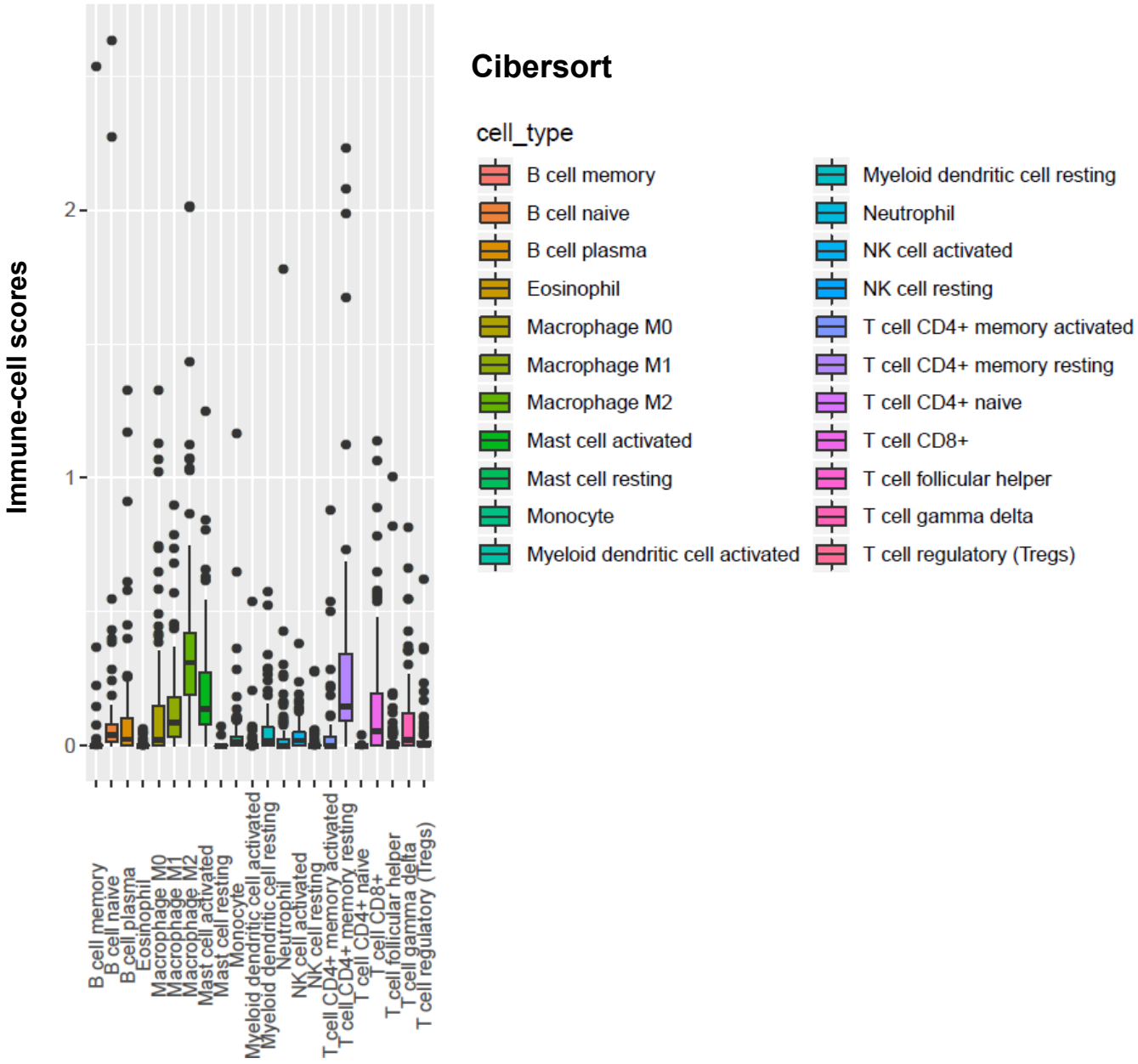

Supplementary figure 1: Global variation in immune infiltrate transcripts.

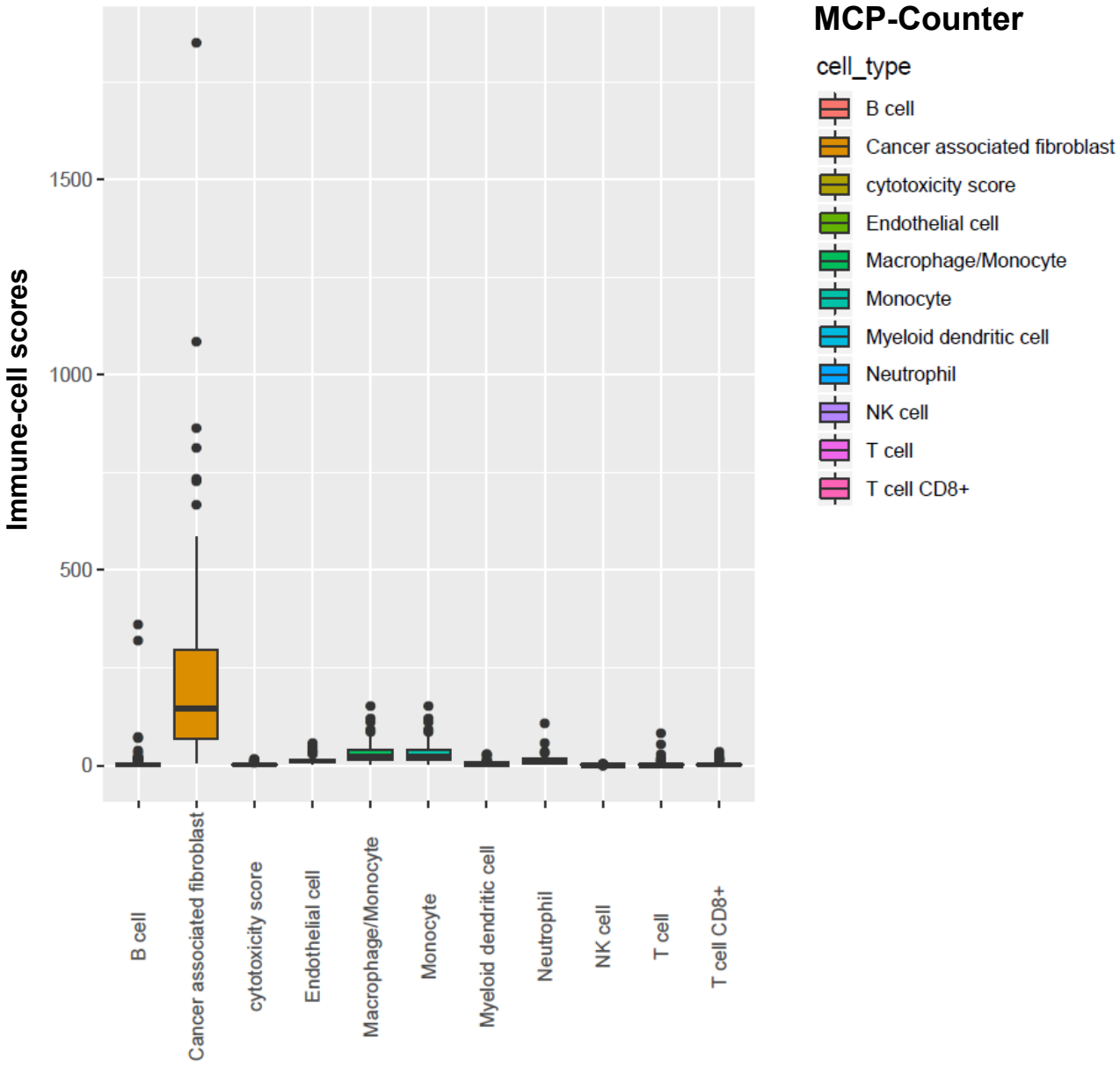

Supplementary figure 2: Immune landscape of mCRPC by using MCP-Counter.

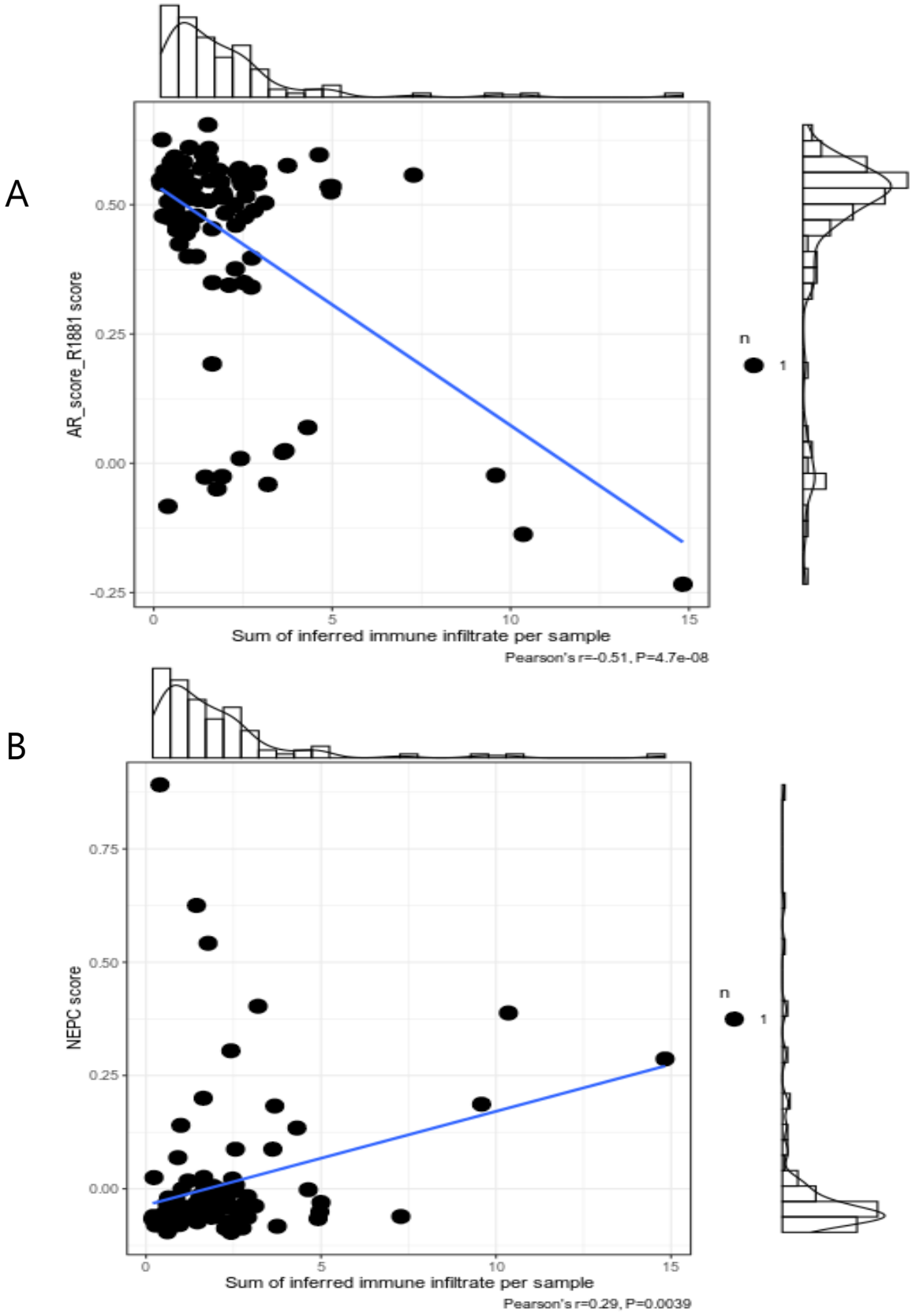

Supplementary figure 3: Association between mCRPC immune infiltrations estimated by Cibersort, vesus AR (A) and NEPC (B) scores.

These results are promising and offer new insights into how to identify immune populations in the mCRPC that may play a crucial role in resistance to ARPI treatment. This project is still ongoing to try to understand the integrated immunogenomic landscape of metastatic prostate tumours. The association of immune, genomic, transcriptomic and clinical portraits will be studied in depth in the future. Moreover, PDX and organoid models obtained from MATCH-R patient biopsies were collected to better model the tumor environment of mCRPC. We hope to identify specific subsets of patients who could benefit from immunotherapy. To achieve this goal, specific computational pipelines will be developed, some of which will need to be further refined.

MANUSCRIPT 2: Development of novel models of aggressive variants of castrate-resistant prostate cancer

Authors

Ludovic Bigot[1], Jonathan Sabio[1], Loïc Poiraudeau[1], Maxime Annereau[2], **Naoual Menssouri**[1], Carole Hellisey [3], Olivier Déas[4], Marine Aglave[5], Tony Ibrahim[1], Cédric Pobel1, Catline Nobre[1], Claudio Nicotra[6], Maud Ngo-Camus[6], Ludovic Lacroix[7,8], Etienne Rouleau[7,8], Lambros Tselikas[9], Jean-Gabriel Judde[4], Anne Chauchereau[1], Alice Bernard-Tessier[10], Anna Patrikidou[10], Natacha Naoun[10], Ronan Flippot[10], Emeline Colomba[10], Alina Fuerea[10], Laurence Albiges[10], Pernelle Lavaud[10], Christophe Massard[1], Luc Friboulet[1], Karim Fizazi[1,10], Benjamin Besse[1,10], Jean-Yves Scoazec[7,8], Yohann Loriot[1,6,10]

Affiliations

1 Université Paris-Saclay, Gustave Roussy Cancer Campus, INSERM U981, Biomarqueurs prédictifs et nouvelles stratégies thérapeutiques en oncologie, 94800, Villejuif, France

2 Pharmacy, Gustave Roussy Cancer Campus, Université Paris-Saclay, Villejuif, France

3 Clinical Research Unit, Department of Oncology, Military Hospital Begin, Saint-Mandé, France

4 XenTech, Evry, France

5 Gustave Roussy Cancer Campus, Plateforme de Bioinformatique, F-94805, Villejuif, France

6 Drug Development Department (DITEP), Gustave Roussy Cancer Campus, Villejuif, France

7 Experimental and Translational Pathology Platform (PETRA), Genomic Platform – Molecular Biopathology Unit (BMO) and Biological Resource Center, AMMICA, INSERM, Villejuif, France

8 Department of Medical Biology and Pathology, Gustave Roussy Cancer Campus, Villejuif, France

9 Department of Interventional Radiology, Gustave Roussy Cancer Campus, Villejuif, France

10 Department of Medical Oncology, Gustave Roussy Cancer Campus, Villejuif, France

Statement of translational relevance

Clinical and genomic studies have identified new subsets of metastatic prostate cancer with poor outcome such as PCa resistant to androgen receptor inhibitor pathway, NEPC, and/or PCa with specific molecular alterations. Clinically relevant models are essential for preclinical and translational studies aimed at testing novel therapeutics and identifying mechanisms of resistance. To this end, we have established a broad panel of metastatic PCa patient-derived xenograft (PDX) and PDX-derived organoids (PDXOs) models and characterized its genomic and phenotypic features. The established PDX models reflect patient characteristics and capture the most frequent aggressive variants of PCa, with representation of most major genetic driver alterations (e.g. *BRCA2*, *CDK12* alterations) and molecular subgroups (e.g. neuroendocrine PCa). Our PDX panel constitutes a useful tool to test new compounds and to study mechanisms of resistance in metastatic PCa field.

Publication: Submitted to journal *Clinical Cancer Research* in September 2022

Structured abstract

Purpose

Genomic studies have identified new subsets of aggressive prostate cancer (PCa) with poor prognosis (e.g. neuroendocrine prostate cancer (NEPC), PCa with DNA Damage Response (DDR) alterations or PCa resistant to androgen-receptor pathway inhibitors (ARPI)). Development of novel therapies relies on the availability of relevant preclinical models.

Experimental Design

NEPC (n = 5), DDR (n = 7), MSI-high (n = 1) patient-derived xenografts (PDXs) were established from 51 patients with metastatic PCa enrolled in MATCH-R trial (NCTNCT02517892). PDX-derived organoids (PDXO) (n = 16) and patient-derived

organoids (PDO) (n = 6) were developed to perform drug screening. Histopathology and treatment response were characterized. Molecular profiling was performed by whole-exome sequencing (WES, n = 13), RNA sequencing (n = 13), and single-cell RNA sequencing (n = 14). WES and RNA-seq data from patient tumors were compared with the models.

Results

Our PDXs captured both common and rare molecular phenotypes as well as their molecular drivers, including alterations of BRCA2, CDK12, MSI-high status and NEPC. RNA sequencing profiling demonstrated broad representation of PCa subtypes. scRNA-seq indicate that PDXs reproduce the cellular and molecular intra tumor heterogeneity. WES of matched patient tumors showed preservation of most genetic driver alterations. PDXOs and PDOs preserve drug sensitivity of the matched tissue and can be used to determine drug sensitivity.

Conclusions

Our models reproduce the phenotypic and genomic features of both common and aggressive PCa variants and capture their molecular heterogeneity. Successfully developed aggressive-variants PCa preclinical models provide an important preclinical tool to predict tumor response to anti-cancer therapy and study mechanisms of resistance.

1. Introduction

Prostate cancer (PCa) is the second most commonly diagnosed cancer type and the fifth leading cause of cancer death in men worldwide[1,2]. Androgen deprivation therapy (ADT) is the backbone of treatment for patients with metastatic prostate cancer (mPCa) who are not candidates for definitive locoregional therapy[3]. Although most men benefit from ADT, nearly all patients experience disease progression on ADT and mPCa reoccurs as castration-resistant prostate cancer (CRPC). New agents have been developed and approved in mPCa over the last 5 years such as the new androgen-receptor pathway inhibitor (ARPI) (e.g. abiraterone, enzalutamide, darolutamide), radiopharmaceuticals (radium-223, Lu-PSMA radioligand) and Poly(ADP-ribose) polymerase (PARP) inhibitor (olaparib)[3]. However, acquisition of resistance still limits their efficiency on the long-term perspective and now constitutes an important area of research.

In the last few years, molecular studies have led to better understanding of the genomic landscape of mPCa and identified a subset of tumors with poor outcomes. These include among others, CDK12-altered[4,5], BRCA2-mutated[6], Microsatellite instability-high (MSI-H) PCa[7] and neuroendocrine prostatecancer (NEPC)[8]. CDK12-altered PCa defined a genomic subtype of PCa with a unique copy-number alteration profile and involvement of distinct oncogenic pathway alterations, including cell-cycle pathway genes[9]. From a clinical standpoint, CDK12-altered PCa constitutes an aggressive subtype with poor outcomes to hormonal and taxane therapies as well as PARP inhibitors[4,5]. In addition, PCa with a germline BRCA2 mutation are associated with higher rates of lymph node involvement, metastases, and prostate cancer-specific death[10]. PCa that are BRCA2-deficient have aggressive genomic profiles that may contribute to worse outcomes observed in this subset[6]. Finally, NEPC is another aggressive variant of PCa that may arise *de novo* or in patients previously treated with hormonal therapies for prostate adenocarcinoma as a mechanism of resistance, leading

to a worse overall survival[8]. The lack of available experimental models of these aggressive variants is a major restriction in preclinical PCa research.

Patient-derived xenografts (PDX) are used to study tumor features and drug response since they reproduce the matched human tumor they are derived from. Even though important efforts have been provided to improve engraftment success and xenograft tumor growth, the establishment of PCa PDXs is still challenging. Cohorts of available PCa PDXs have expanded in recent years[11,12] for both localized and metastatic disease. It should be noted however that PDXs are time, money, and energy consuming, requiring sacrificing mice, which strongly limits their ability to test drug combinations[13].

Tumor-derived organoids are new preclinical model with fewer constraints than PDX. A body of evidence indicates that organoids can reproduce tumor-tissue characteristics such as phenotype (structure and expression patterns), *in vivo* drug sensitivity as well as cancer heterogeneity while maintaining genetic and lineage specificity[14,15]. Organoids could be derived from PDX (PDXO) or directly from the patients (PDO). Organoid culture is still in its nascent stage with very few prostate cancer biobanks established till date[16-18].

In this study, we describe the development of PDX models derived from patients with aggressive variants mPCa that reproduce the human tumor phenotype, genomics and sensitivity to approved drugs in prostate cancer. Using PDXO from different models, we developed a workflow for an organoid drug screen on these models and implemented the use of *in vitro* testing from PDO derived directly from patients with aggressive mPCa.

2. Methods

Methods for tissue collection, PDX and organoids development, molecular and cellular experiments are described in the supplementary methods.

3. Results

Establishment of models for aggressive PCa

All tissue PCa samples were derived from patients with mPCa enrolled in the MATCH-R study[19] (NCT02517892), a prospective institution trial, designed to identify mechanisms of resistance in patients with advanced cancer treated with molecular targeted agents and immunotherapy (**Figure 1a**). Seventy-five patients with mCRPC were enrolled in the study. Overall, 61 tumor biopsies were performed from 51 mCRPC patients. As shown in **Figure 1b**, sixteen biopsies derived from thirteen patients were successfully engrafted in mice leading to an overall success rate of 26.2%. Forty-six biopsies were performed at baseline (e.g. before initiation of drug of interest) and eleven PDX models were successfully obtained (success rate: 23.9%). Fifteen biopsies were collected at time of acquired resistance to a drug of interest with an overall intake rate of 33.3% (resistance to ARPI (n = 14), resistance to PD-L1 inhibitor (n = 1) and resistance to PARP inhibitor (n = 1)). In addition, we have successfully established three PDX models from a single patient (MR-0009) during the course of his disease (as refereed to MR-009, MR-009RI and MR-009RO).

The clinical characteristics of these 13 patients are summarized in **Table 1**. All patients had mCRPC at time of biopsy. Five patients (MR-0009, MR-0041, MR-0151, MR-0178, MR-0182) did not receive any prior treatment (except ADT) for the mCRPC phase before the inclusion in MATCH-R, while the others received either chemotherapy (n = 2) or ARPI (n = 3) or both (n = 3). Most had lymph nodes (n = 12) and bone metastases (n = 10) before the baseline biopsy. Visceral metastases were detected in five patients at time of biopsy.

The biopsy site was associated with *in vivo* tumor take rate. Biopsies derived from prostate tissue had a lower success rate of engraftment than biopsies derived from

metastases (1/27 vs 12/34, p < 0.01 Khi2 test) (**Supplementary Figure 1a**). Tumor growth properties in response to castration, were addressed *in vivo* in six models. The PDXs (at passage 6) were implanted subcutaneously and surgical castration was performed when tumor reached a volume of ≈ 150 mm^3. Four PDXs were resistant to castration (MR-0059, MR-0191, MR-0084, and MR-0077) while two still responded to surgical castration (MR-0041 and MR-0123) (**Figure 2**). We next sought to evaluate the tumor growth properties in response to several approved drugs to assess the concordance between PDX and clinical response. The mice bearing six different models (used for assessing the response to castration above) were treated with either enzalutamide or docetaxel. The three models (MR-0059, MR-0191, and MR-0084) demonstrated resistance to enzalutamide and limited response to docetaxel which was consistent with the clinical data (**Figure 2, Table 1**). Two PDXs, MR-0041 and MR-0123 achieved response and limited response to enzalutamide respectively while MR-0077 was resistant to enzalutamide which again was in line with the clinical disease history (clinical progression on ARPI).

To further explore the *in vitro* characteristics of the PDX tumor cells and to perform a drug screening assay, we next developed PDXO from all our PDXs models (n = 16) (**Figure 2b**). We developed an organoid culture method from bulk tumor tissue that allows organoids to grow non adherent conditions, with no requirement for extracellular matrix support (see Methods). The median cells number obtained after digestion was 6.02 $x10^6$ (Interquartile range (IQR): 2.2 - 12.8 $x10^6$) with an average of 59% (IQR: 47-76) of live cells (**Supplementary data S1**). Median passage for PDXO was 3 (IQR: 2-4). A long-term culture of PDXO lines defined by a minimum of five passage (**Supplementary data S1**) was obtained in two out of nine PDXO. After 7 days in culture, we observed a disorganized and irregular structure with invading cells migrating outside the organoid, confirming the potential aggressiveness of PDXO generated (**Supplementary figure 2**). We then developed a rapid drug-screening test using PDXO. Seven days after cell seeding, the drugs were added and the cell viability

was assessed after 14 days of culture. We tested ten different compounds that have demonstrated activity or potential activity in PCa. Approved drugs included an *AR*-antagonist (enzalutamide), a taxane chemotherapy (docetaxel) and a PARP inhibitor (olaparib). Investigational therapies included EZH2 inhibitor (GSK343), BRAF inhibitor (dabrafenib), MEK inhibitor (trametinib), MTOR inhibitor (everolimus), PI3K inhibitor (alpelisib) and CD4/CDK6 inhibitor (Palbociclib) and a platinum agent (carboplatin). The *in vitro* responses (defined as when at least 50% cell mortality was achieved compared to the control) were compared with responses observed in patients', to the treatment administered just before (e.g. at time of resistance) and after the biopsy. High concordances (78%) between the PDX and the patients as well as a high concordance (83.3%) between the PDXO and the patients were observed (**Supplementary data S2**). As an example, the patient MR-0059 underwent a biopsy at time of resistance to ADT and docetaxel. The patient was then treated with enzalutamide with disease progression as best response (**Supplementary figure 3**). As expected the PDX and the PDXO derived from MR-0059 mimicked the clinical resistance to docetaxel and enzalutamide as only the dose at 10 x Cmax (215 µmol/L) induced cell death in PDXO. The PDXO from MR-0009, MR-0150, MR-0182-R, and MR-0191 demonstrated a sensitivity to docetaxel, a standard therapy used in PCa. No efficacy was observed with dabrafenib, trametinib, everolimus, palbociclib in all the PDXO, however treatment of PDXO MR-0009, MR-0009-RI, MR-0009-RO, MR-0077, MR-0084, MR-0170. MR-0182-R, and MR-0191 had good response to GSK343 EZH2 inhibitor (**Figure 2c**). These data demonstrate that our PDXO constitute robust models for drug screening.

Morphological and histological features of PDX and PDXO were compared to their original human tissues by hematoxylin and eosin (H&E) staining and immunohistochemistry (IHC). The H&E staining showed that PDXs and PDXOs retained the major histopathologic characteristics of their matched patient tumor (**Figure 1c**). Several markers such as Androgen Receptor (AR), Prostate-Specific Antigen (PSA) and Synaptophysin (SYP) used in daily practice were then used to define the subtype. Three

different cell populations were found: (i) the pure luminal phenotype, the NEPC phenotype and a mixed phenotype. MR-0123 is an illustrative example of pure luminal phenotype with *AR* positive expression and SYP negative expression (**Figure 1c**). The patient MR-0084 was diagnosed as a pure NEPC with negative *AR* expression and positive *SYP* expression on both derived PDX and PDXO. MR-0009 model finally illustrates the mixed phenotype with a co-expression of *AR* and *SYP* marker within the biopsy, PDXs and PDXOs. The IHC analysis highlights that PDX and PDXO retain the microscopic features of the original patient sample across a range of histology. The NEPC phenotype was associated with a higher take rate than the luminal phenotype (p = 0.021) (**Supplementary figure 1b**).

PDO

While PDXO can be successfully derived from PDX, developing organoids directly from needle human biopsies may become even more relevant for decision-making. Thus, we aimed to derive PDO from nine additional patients enrolled in MATCH-R following the same methods we used for PDXO (**Figure 2b**). The PDO were used for drug testing at Day 7. The clinical characteristics of these patients are summarized in **Supplementary table 1**. A drug screening with one to nine drugs (median: 5) was successfully performed in 6 (66%) patients at day 7 (**Supplementary table 1**). The median number of cells obtained after mechanical and enzymatically digestion was 191,000 cells (IQR: 109,000 to 268,000 cells) with median of 16% of alive cells (IQR: 12-21). As expected, the PDO maintained the pharmacological characteristics of their matched patients when we compared the treatment given before or after the biopsy (**Supplementary table 1**, concordance 5/5). For example, the PDO MR-0182-R was resistant to enzalutamide which was consistent with the clinical profile of the matched patient who experienced an acquired resistance to enzalutamide at time of the biopsy. A docetaxel-based chemotherapy was initiated after the biopsy and the patient achieved a partial response, which was consistent with the observed *in vitro* sensitivity observed with the

matched PDO (**Figure 2d**). Another patient, MR-363 was treated with ADT and then abiraterone at time of castration resistance. He underwent a first biopsy before starting abiraterone. At time of resistance, a second biopsy was performed. PDO was derived from the second biopsy. The drug screening indicate that the MR-0363-R PDO (MR-0363) was potentially resistant to another ARPI enzalutamide (here enzalutamide). The patient started docetaxel-based chemotherapy just after the second biopsy, but experienced disease progression confirmed on the CT-scan performed 6 weeks after treatment initiation.

Patient MR-0183-R was treated with enzalutamide in MATCH-R. WES performed on tissue sample obtained at time of resistance revealed a bi-allelic CDK12 mutation. The patient was included in a clinical trial investigating the combination of a Checkpoint Inhibitor (CPI) and a PARP inhibitor, on which the patient experienced tumor progression. The matched PDO established from the tissue sample obtained prior to the administration of the experimental association also indicated a resistance to olaparib.

Genetic preservation

We then studied the genomic and transcriptomic landscapes of PDXs (at serial time points, e.g. early stage: passage P0 or P1 and late stage: passage P3 or P4), PDXOs models and matched tissues by whole exome sequencing (WES) to assess overall genomic stability across multiple samples. For seven samples, we compared four samples from the same patient: the biopsy, the PDX at P0, PDX at P4/ PDXO. For three patients, we compared the biopsy and the PDX at P0 and at P4. The Single Nucleotide Variation (SNV), and Copy Number Variation (CNV) analysis of 124 driver genes (**Supplementary data S3**) involved in CRPC showed high genetics conservation between the preclinical models (PDXs and PDXOs) and the biopsies (**Figure 3a**). Overall, the somatic mutation analysis showed that each model exhibits a large number

of mutations common to all samples from each patient, and frequently a pool of mutations common to all (**Supplementary figure 4**). We found genetic alterations commonly found in CRPC affecting the AR pathway, the cell cycle pathway, the DNA Damage Response (DDR) pathways, the PI3K pathways and the epigenetics pathways (**Figure 3a**). These data suggest that PDXs recapitulate the genomic landscape of the initial tumor tissue. Nevertheless, they exhibit non-shared alterations resulting either from clonal selection or from tumor adaptation to the new microenvironment (e.g. angiogenic pathways and cell-to-cell adhesion pathways which may be needed for tumor engraftment and growth in the mice-tissue microenvironment). An example of clonal selection, in MR 182, two genomic alterations with a low VAF (variant allele frequency) were detected on the primary tissue sample collected before enzalutamide treatment (*BRCA1* missense mutation VAF 5.6% and *ZMYM3* VAF 8.2%) but not on the second biopsy collected at time of resistance. Neither of these alterations were detected on the preclinical models established from the first biopsy.

NEPC models

Differentiation into NEPC is one of the mechanisms of resistance to ARPI. NEPC are highly aggressive variants of prostate cancer and outcomes associated with NEPC remains dismal. There is a lack of approved therapies for patients with NEPC. Principal component analysis (PCA) and unsupervised hierarchical cluster analysis of RNA-seq data indicated a high transcriptomic correlation among tumors from PDXs, PDXOs and human samples (**Figure 3b**). All our models and their matched patient samples clustered together except the MR-0178-R samples. Two clusters were obtained by unsupervised hierarchical cluster analysis: one cluster including almost all NEPC samples characterized by high NEPC transcriptomic score and low *AR* transcriptomic score and one cluster with luminal samples. The luminal cluster includes five patients with their associated models (MR-0009, MR-0009-T3, MR-0041, MR-0178-R, MR-0182, and MR-0283) along with the PDX/PDXO of MR-0123 and MR-0077 (no RNA-seq

available from these human samples). NEPC PDXs clustered based on their shared expression of CRPC-NE signature genes, including overexpression of *AURKA*, *PEG10*, *SYP*, *SYT11*, and *CHGA* and low expression of AR signaling genes such as *AR*, *KLK2*, *KLK3*, and *TMPRSS2*. The RNA-seq analysis did not identify the subgroup of patients and models identified with a mixed phenotype previously identified by IHC. Gene set enrichment analysis (GSEA) using Hallmark gene sets found, as previously reported[20], a significant upregulation (log2FC(NES) ≥ | 1 , FDR < 0.05) of pathways involved in cell growth (E2F targets, G2M checkpoint) and androgen-regulated pathways (androgen response) (**Supplementary data S4**) in the NEPC cluster. For most samples, the matched PDX and PDXO tissues clustered with human samples. The high gene expression correlation scores between PDXs and PDXOs (**Supplementary Figure 6**) such as MR-191 model (**Figure 3c**) supported this.

These models can recapitulate some mechanisms of NE differentiation. As an example, patient MR-0009 was diagnosed with a pure luminal prostate cancer in 2014 with a germline *BRCA2* mutation (p.E49*) and was treated with several therapies including ADT, enzalutamide and atezolizumab (**Figure 4a**). A total of five biopsies were performed overtime. The AR expression along with luminal markers and a small contingent of cells that express NEPC markers were observed in the first and the third biopsy (MR-0009 and MR-0009-RI) (**Figure 4b**). On the fourth biopsy (MR-0009-RO) obtained at time of resistance to olaparib, the tumor cells expressed only the SYP and did not express AR, suggestive of a complete phenotypic switch from luminal to neuroendocrine tumors. WES indicated that a couple of alterations in driver genes were shared, including somatic mutation of *TP53*, *NCOR2*, *TAF1L* and a *BRCA2* germline mutation (**Figure 4c**). In the NEPC samples (MR-0009-RO), a *PTEN* missense mutation was found which is consistent with prior reports indicating that a double mutation affecting both *TP53* and *PTEN* was associated with NE differentiation[21,22]. RNA-seq analysis showed that the first three biopsies (MR-0009, MR-0009-T2, and MR-0009-T3) and their matched models (MR-0009/MR-0009-RI) had a high AR score and lower

NEPC score (**Figure 3b**). By contrast, in the fourth sequential biopsy (MR-0337-T2) and the matched PDX (MR-0009-RO), a complete phenotypic change was observed with a high neuroendocrine score and a low expression of AR score (**Figure 3b**). As expected, the NEPC PDXs and most PDXO models exhibited resistance to enzalutamide (**Figure 2a,c**). In addition, as previously reported[23], we found that an EZH2 inhibitor (here GSK343 compound) was active on NEPC PDXOs such as MR-0009-RO, MR-0084, MR-0170, and MR-0191 (**Figure 2c**) and in models with a mixed phenotypes (MR-0009, MR-0009-RI, and MR-0077).

In order to study intratumor heterogeneity in the NEPC PDXs, we performed a single-cell RNA sequencing (scRNA-seq) of 15 PDX (luminal and NEPC PDXs). Overall, 14 passed the quality control and were deemed available for scRNA-seq analysis. To determine NEPC/luminal scores per cell, we used MR-0041 as reference for pure luminal PDX and MR-0084 as one reference for NEPC PDX based on RNA-seq and IHC staining (see Methods). The results obtained in the group of luminal PDXs revealed the presence of few cells with a high NEPC score and cells with a positive expression of both NEPC and luminal genes (**Figure 4d, Supplementary figure 7**). As observed by histological analysis, scRNA-seq results of PDXs with a mixed phenotype confirmed the intra-tumoral heterogeneity observed in the luminal PDX. The cells can be divided into 4 different groups: (i) a group of cells with high luminal scores; (ii) a group of cells with both low luminal score and NEPC score (double negative cells); (iii) a group of cells with high NEPC scores and (iv) a group of cells with mixed phenotype with both high luminal and NEPC scores; and (iv) a group of cells with high NEPC scores (**Figure 4d**). This intra-tumoral heterogeneity observed in PDXs with luminal and mixed phenotypes highlights the possible transdifferentiation phenomenon observed in the context of resistance to ARPI. Future work will focus on epigenetic features of the models to study lineage plasticity. In NEPC PDXs, the data indicated a high homogeneity with a vast majority of cells having a high NEPC score. In PDX with a luminal (MR-0123) and a mixed phenotype (MR-0009-RI), a majority of cells expressing AR, PSA and PSMA and few

cells with a SYP expression while in the NEPC PDX (MR-0084), only cells with an expression of SYP were found (**Supplementary figure 8**). In the four NEPC PDXs (MR-0059, MR-0084, MR0170, and MR-0191), we found that a high proportion (mean: 34.7%) of NE cells express DLL3 which is relevant in the context of clinical investigation of DLL3-directed therapies[24,25].

DDR models

The DNA Damage Repair (DDR) pathways alterations such as BRCA2, ATM or CDK12 mutations are associated with distinct prostate cancer subsets and are found in 10-15% of mCRPC[4-7]. Although some progress has been made to manage patients with *BRCA2*, *BRCA1* or *ATM* alterations with the approval of PARP inhibitors[26-27], most of these patients eventually develop disease progression. To provide material for further exploratory research in DDR-altered PCa, we sought to develop PDXs from patients with DDR alterations. We established seven PDXs from five patients. Three genes involved in DDR pathway were found altered: biallelic *CDK12* (MR-0151-R) mutation, *ATM* (MR-0059, MR-0182) and germline *BRCA2* mutation (MR-0191, MR-0009). In addition, the MR-0178-R models exhibited a MSI profile associated with MLH1 deletion (**Figure 3a**) (812 mutations in MR-0178R, 958 mutations in MR-0178R PDX P1 and 1025 in MR-0178R PDXO). The drug testing performed in PDXOs with *CDK12* and *ATM* alteration did not show any consistent efficacy of PARP inhibitor and carboplatin (**Figure 2c**). The patient MR-0191 with a germline mutation of *BRCA2* (c.6373dup), was enrolled in the MATCH-R trial after disease progression to carboplatin (**Figure 5a**). The molecular analysis identified an emergence of contingent of cells harboring a mutation restoring the frameshift of *BRCA2* (c.6352_6367delins16). This *BRCA2* reversion mutation was not found in the PDX and PDXO models possibly due to the clonal selection. The PDX and PDXO were sensitive to carboplatin and olaparib (**Figure 5b, c**). The patient MR0009 exhibited germline p.E49* *BRCA2* mutation and underwent multiple biopsies during disease history (**Figure 4a**). The patient was treated with

olaparib and achieved clinical response for one year. A PDX was derived at baseline (before olaparib therapy, MR-0009-RI) and another at time of resistance (MR-0009-RO). At time of resistance, the tumor acquired a *PTEN* missense R159S mutation along with a *BRCA2* reversion mutation that restores that corrects the open reading frame of germline alteration (**Figure 4c**). The PDX MR-0009 that harbors the p.E49* *BRCA2* mutation was sensitive to both olaparib and carboplatin (**Figure 5d**). However, results of MR-0009 RI PDXO and MR-0009 RO PDXO experiments provided conflicting data (**Figure 2c**). Exome sequencing were not performed on PDXO due to the low number of cells.

4. Discussion

The emergence of new drugs in cancer research over the last years have made it possible to identify new therapeutic strategies and to improve the outcome of patients with metastatic cancer. Unfortunately, the few preclinical models available in prostate cancer and the challenge to recapitulate the clinical and molecular heterogeneity observed among patients are a major hurdle to the development of new and effective strategies for metastatic prostate cancer, especially for patients with a highly aggressive cancer such as NEPC and cancers with resistance to approved drugs. In this study, we describe the establishment of PCa PDX models from patients with aggressive metastatic PCa such as NEPC, *BRCA2*-mutated or MSI PCa. We then established organoid cultures from these models to develop an organoid-based drug screening workflow. Finally, we adapted further organoid cultures to patient-derived biopsy, implementing clinically relevant organoids for drug screening experiments.

NEPC are highly aggressive tumors with poor prognosis[8]. No specific therapies have been approved in NEPC. In our study, we developed several models from patients with NEPC and showed that PDX and the PDXO retained the molecular and the histological features of their matched patients and maintained similar drug responses. Recent data

shows that there is a substantial genomic overlap between castration-resistant tumors that were histologically characterized as prostate adenocarcinomas and NEPC[20]. NEPC tumors appear clonal in origin with a clonal ancestry traceable back to a CRPC-Adenocarcinoma precursor in a model of divergent clonal evolution of metastatic CRPC towards neither an AR-driven or AR-indifferent. Our data supports this hypothesis since we showed that the MR-0009 model provides clear evidence of neuroendocrine transdifferentiation as a phenomenon of resistance to ARPI. Our drug screening suggested the efficacy of EZH2 inhibitor as previously reported[18,23]. Furthermore, the scRNA-seq analysis found frequent DLL3 expression on the cell surface of NEPC cells opening the way to antibody drug conjugates, radioligand therapies and bispecific antibodies against NEPC[24,25]. Importantly, our models maintain the intratumor heterogeneity which is relevant in the context of resistance to systemic therapies. While RNA sequencing lacks sufficient depth to assess accurately both luminal and NEPC populations, the scRNA sequencing technology applied to PDX models demonstrated the coexistence of small contingent of neuroendocrine cells with luminal cells even in adenocarcinoma models. These NEPC models may be helpful to decipher the disease evolution and to envision new therapeutic strategies to early inhibit the molecular switch from luminal to NEPC cells.

Several models display alteration in DDR pathways, especially *BRCA2* and *CDK12* mutation. Clinical data indicates that patients with germline *BRCA2* alterations have earlier prostate cancer onset and a poor survival compared to non-carriers[6]. Tumors with BRCA1/2 defects and defective DNA repair mechanisms are sensitive to DNA damaging agents such as PARP inhibitors currently approved in metastatic CRPC. Even though the patients benefit from olaparib, most of these patients experienced disease progression[26]. MR-0009 and MR-0191 exhibited a germline frameshift mutation in the *BRCA2* gene. We were able to develop PDX from the patient MR009 at the time of resistance to olaparib that resulted from *BRCA2* reversion mutation that has been shown to lead to re-expression of the wild-type BRCA2 protein. Interestingly, MR-191

model was also derived from patients with germline *BRCA2* mutation but treated with platinum-based chemotherapy. The mechanisms of resistance again identified an emergence of contingent of cells harboring a mutation restoring the frameshift of *BRCA2* (c.6352_6367delins16) suggesting common mechanisms of resistance between PARP inhibitor and platinum agents. In addition, *CDK12* mutations define another subset of aggressive prostate cancer subgroup, with a high rate of metastases and short overall survival with poor outcomes to hormone therapies, taxane therapies as well as to PARP inhibitors[4]. The MR-0151-R models exhibit *CDK12* biallelic mutations, a well-described genomic alteration associated with *CDK12* alteration[27]. The drug testing performed on PDXO models did not find any efficacy of PARP inhibitor and carboplatin consistent with previously reported clinical cases[4]. Immune checkpoint inhibitors may be effective in a minority of these patients[28], but we are unable to test Checkpoint Inhibitor (CPI) in MR-151R so far. Finally, we reported one MSI-H case of metastatic prostate cancer (MR-0178-R) associated with *MLH1* deletion. High MSI is associated with poorly differentiated stage[29] but with response to CPI[30]. However, the lack of relevant immune system, in both PDX and PDXO, could make it difficult to study the role of this pathway PCa. Humanized mice models[31], co-culture organoids[21] and microfluidics culture[33] can serve as useful tools to assess more accurately the role of immunotherapy in prostate cancer.

The implementation of PCa organoids in translational assays could facilitate the identification of effective therapies in aggressive forms of PCa such as NEPC, BRCA2 or CDK12 altered PCa. In our experience, PDXO and PDO can be used for a few passages only. The pharmacological concordance between the organoids and the clinical disease history matched, make the organoids useful tools for the development of new drugs in CRPC. Indeed, the overall molecular concordance between PDX and PDXO will enable PDXO in early drug screening, while PDX models provide a large amount of tissue sample for molecular and phenotype analysis. This approach makes rapid drug-screening tests possible at a lower cost, also reducing the number of animals required

for preclinical experiments. We further developed a PDO-based drug screening in a small number of mPCa patients, demonstrating the feasibility of the approach. The developed PDO-based drug assay was designed to test PDO seven days following the biopsy, which is relevant for further clinical decision-making. The drug response overall matched with the clinical history of the patient, highlighting the relevance of this assay. However, optimization of workflow is needed, notably culture protocol, organoids amplification, and the use of an automatic device for more robust and accurate results.

In summary, we developed a translational workflow to obtain several models of aggressive metastatic PCa. These models provide useful material to better understand the biology of clinically relevant aggressive PCa and the mechanisms of resistance to recently approved drugs in metastatic PCa.

5. Figures and legends

Figure 1: Study design

A: Patients were enrolled in MATCH-R trial[18] (NCT02517892). A tissue biopsy was performed prior to commencing a new systemic therapy, and at time of acquired resistance. The biopsy samples were used for whole-exome sequencing, RNA-seq and pathological analyses. For some patients, additional biopsies were used to develop patient-derived xenografts and/or Patient-derived organoids.

B: Study flowchart of the study.

C: Representative pictures of tissue slides of native tumor tissue (Patient), the matched PDX at passage 4 and patient-derived organoids (PDXO). Tissue samples were stained with hematoxylin-and-eosin (H&E) and immunohistochemistry (IHC) was performed to assess the expression of androgen receptor (AR), Prostate Specific Antigen (PSA) and synaptophysin (SYP). Three examples are provided: a pure luminal phenotype (left panel, MR-0123); a pure neuroendocrine (NE) phenotype (centre panel, MR-0084) and a mixed phenotype combining both luminal and NE phenotypes (right panel, MR-0009).

Figure 2: Pharmacological preservation of PDX and organoid models

A: *In vivo* pharmacological evaluation of vehicle (black color), castration (green color), enzalutamide 60 mg/kg p.o (red color) and docetaxel 20 mg/kg i.p 3 doses/week (blue color) in luminal and NEPC PDXs. Grafts were established subcutaneously in testosterone-supplemented mice until tumor volume reached 80-200 mm^3, at which point host mice were castrated or treated with (n = 8 per group) aforementioned drugs; data shown as mean ± SEM of tumor volume. Tumor growth inhibition (ΔT/ΔC value) was calculated as following: ΔT/ΔC (%) = [(median TDayY – median TDayX)/(median CDayY - median CDayX)] x 100 (where DayY is the day of evaluation, and DayX is the

day of initiation of therapy for treated [T] and control [C] tumor volumes). NEPC: neuroendocrine prostate cancer. PDX: patient-derived xenograft. Tumor volume was measured with calipers twice weekly throughout the treatment period. In some cases, tumor volume reached the maximum ethical limit of 1000 mm^3 during the treatment period and tumors were harvested earlier to comply with animal ethics approvals.

B: Scheme of experimental protocol for organoid (Patent-derived xenograft (PDXO) or patient-derived organoid (PDO)) drug screens from. Created with BioRender.com.

C: Organoid drug screen heatmap of viability values (over vehicle, for each PDXO/PDO model). Seven days after cell seeding, the drugs were added and the cell viability was assessed with the CellTiter-Glo (Promega, G7573) after 14 days of culture. The CellTiter-Glo 3D assay was used to measure ATP levels as a proxy for cell viability. The cell viability readout was performed according to manufacturer's instructions using the automation equipment. DMSO at 0.05% was used as negative control and DMSO at 10% was used as positive control. Ten compounds were evaluated and response status was indicated as following: Resistance in red (IC50 > 10 x Cmax); Potential Resistance in orange (Cmax < IC50 ≤ 10 x Cmax); Potential sensitivity in light green (Concentration of sensitivity < IC50 ≤ Cmax); Sensitivity in green (concentration of hypersensitivity IC50 ≤ concentration of sensitivity). Concentration associated with resistance as the concentration 10-fold above the Cmax and the concentration associated with sensitivity as the concentration of 10-fold below the Cmax for intravenous drugs or in the case of drug associated with an equilibrium plateau (such as oral drugs or monoclonal antibody) as the minimal concentration observed just before the next dosing at equilibrium. Finally, a concentration of hypersensitivity was defined as the concentration 2 log below the Cmax.

The drug screening was performed using 96 wells plates (Nunc™ Edge™ 96-Well, Nunclon Delta-Treated, Flat-Bottom Microplate, Thermo Fisher Scientific, 167425) coated with PohyHema. The cells were added to each well at the density of 5000 cells

per well. Seven days after cell seeding, the drugs were added and the cell viability was assessed with the CellTiter-Glo (Promega, G7573) after 14 days of culture. Drug concentrations ranged from 10nM to 1000µM depending on the individual properties of the drug. The dose for the targeted agents had been selected to capture Cmax (human serum level) values. A chemogram was provided for each PDXO/PDO tested. IC50 (Half-maximal inhibitory concentration) was calculated as the concentration needed to induce cell death of at least 50% of the tumor cells. Four categories were defined: Drug resistance: IC50 > 10 x Cmax; Potential resistance: Cmax <IC50<10 x Cmax; Potential sensitivity: Concentration associated with sensitivity <IC50<Cmax; Sensitivity: concentration associated with hypersensitivity <IC50 < concentration associated with sensitivity.

D: Results of PDO drug screen assay on two metastatic PCa cases (MR-0182, MR-0363). Cells were treated with incremental concentrations of Enzalutamide (pink), Docetaxel (yellow), EZH2 inhibitor (brown), carboplatine (red), olaparib (dark green), everolimus (green), trametinib (grey), palbociclib (dark), dabrafenib (blue). Control (light blue) is representative of PDO treated with DMSO at 0.05%, used as negative control. Horizontal lines represent the different concentrations for each compound. The vertical line represents the percentage of cell viability assessed with the CellTiter-Glo kit. All samples are normalized with the control; the black line represents the threshold to determine the drug response (50% cell viability).

Figure 3: Genomic features of PDXs and PDXOs match the clinical landscape

A: Summary of key somatic alterations in PDXs, PDXOs and matched tumor tissue based on whole exome sequencing based on copy number variation and single nucleic variation of 120 prostate cancer driver genes defined by Armenia et al.[40] and 5 genes to defined the MSI status. Rows represent samples Patients, PDX at passage P0 and P4 or P5 and organoids, columns represent genomics aberration. Two complementary approaches were used to reconstruct the copy-number profiles of the tumors: copy-number analysis using genotype data and copy-number analysis based on coverage. With the first approach, chromosome aberrations were defined using empirically determined thresholds as follows: gain, copy number > ploidy + 0.5; loss, copy number < ploidy − 0.5. We considered a segment to have undergone loss of heterozygosity (LOH) when the copy number of the minor allele was equal to 0. With the second approach, segments with a smoothed log ratio above zero + 0.15 or below zero − 0.15 were considered to have gains and deletions, respectively. High-level amplification and homozygous deletion thresholds were defined as the mean +5 s.d. of smoothed log ratios in regions with gains and deletions, respectively.

(Focal amplification—pink; amplification—red; deep deletion—dark blue; frameshift mutations—orange; truncating mutation: dark green; missense mutation—light green; germline mutation - black)

B: Hierarchical clustering of PDX, PDXO and human samples based on RNA-seq analysis. The 5000 most variant genes (based on standard deviation) was used to classify the samples according to their gene expression. The red barplot on the top of the heatmap represents the NEPC score calculated according to methodologies described in Beltran et al[19] and the AR score (range from -0.5, low to 1, high) calculated with luminal cell lines (V16D) as reference (see methods).

C: Correlation plots of gene expression from RNA-seq data between tissue and matched PDX (left panel) and between PDX and PDXO (right panel) for PCa case MR-

0191 in log2(FPKM) (fragments per kilobase of transcript per million fragments mapped). Pearson correlation coefficient, r: 0.92 and 0.98, respectively.

Figure 4: NEPC Models

A: Patient MR-0009 clinical course between 2014 and 2018.

B: Histological slides images of tumor biopsy tissue (Patient, Pt) and the corresponding PDX models at passage 4 for the 3 paired of samples collected overtime –biopsy 1, 3 and 4). Samples are stained with haematoxylin-and-eosin (H&E) and immunohistochemistry (IHC) for AR, synaptophysin (SYP).

C: Heatmap plot of SNV and CNV based on WES on tumor samples from MR-0009 patient, the corresponding PDX at P0 and P4 and PDXO collected overtime. D: Pie charts of single-cell RNA-seq data from the 14 PDX at passage P2 to P4. Three phenotypes were analysed: luminal PDX models (MR-0041, MR-0123, MR-0182, MR-0151-R, and MR-0178-R) (top panel); mixed phenotype PDX models (MR-0009, MR-0009-RI, MR-0077, MR-0150, and MR-0283); and neuroendocrine PDX models (MR-0059, MR-0084, MR-0170, and MR0191) (medium panel) (bottom panel). Dark blue color represents cells with high luminal phenotype defined as luminal score ≥ 0.4 and neuroendocrine score ≤ 0.1; light blue color represents cells with a low luminal phenotype defined as luminal score ≤ 0.4 and neuroendocrine ≤ 0.1; red color represents cells with neuroendocrine phenotype defined as a luminal score ≤ 0.4 et neuroendocrine score ≥ 0.1; green color represents cells with a mixed phenotype defined as a luminal score ≥ 0.4 and a neuroendocrine score ≥ 0.1 or a luminal score of 0 ≥ luminal score ≤ 0.4 and a neuroendocrine score of 0 ≥ neuroendocrine score≤0.1.

Figure 5: DDR models

A: Patient MR-0191 clinical course. *BRCA2* status from sequencing of sample collected at diagnosis, at MATCH-R study inclusion and from PDX and PDXO samples. IGV view of the *BRCA2* (c.6373dup) and *BRCA2* (c.6352_6367delins16) mutations found in human sample collected after carboplatin treatment and from its corresponding models (PDX/PDXO).

B: *In vivo* evaluation of vehicle (black), olaparib 50 mg/kg (dark green) i.p QD (15% captisol/Phosphate Buffer Saline), and carboplatin 50 mg/kg (red) i.p once a week (Phosphate Buffer Saline) in MR-0191 PDX models. Mice were treated for 17 days and tumor volume was measured with calipers twice weekly throughout the treatment period. Tumor volumes mean+/-SEM (n = 8 per group). Tumor growth inhibition (ΔT/ΔC value) was calculated as following: ΔT/ΔC (%) = [(median TDayY - median TDayX)/ (median CDayY - median CDayX)] x 100 (where DayY is the day of evaluation, and DayX is the day of initiation of therapy for treated [T] and control [C] tumor volumes).

C: Results of MR-0191 PDXO drug screen assay. The experiment was performed as in figure 2b and c. Horizontal lines represent the different concentrations for each compound. The vertical line represent the percentage of cell viability assessed with the with the CellTiter-Glo kit. All samples are normalized with the control; the black line represents the threshold to determine the drug response (50% cell viability).

D: *In vivo* evaluation of vehicle (black), olaparib 50 mg/kg (dark green) i.p QD (15% captisol/Phosphate Buffer Saline), carboplatin 50 mg/kg (red) i.p once a week (Phosphate Buffer Saline) and enzalutamide 60 mg/kg p.o QD (5% chromophore/Phosphate Buffer Saline) 5 doses/week in MR-0009 PDX model. Mice were treated for 18 days and tumor volume was measured with calipers twice weekly throughout the treatment period. Tumor volumes mean+/-SEM (n = 8 per group). Tumor volumes mean+/-SEM (n = 8 per group). Tumor growth inhibition (ΔT/ΔC value) was calculated as following: ΔT/ΔC (%) = [(median TDayY - median TDayX)/(median

CDayY – median CDayX)] x 100 (where DayY is the day of evaluation, and DayX is the day of initiation of therapy for treated [T] and control [C] tumor volumes).

Table 1. Patient's characteristics

ID	Age at inclusion	Phenotype at diagnosis	Stage at diagnosis	Gleason score	PSA (ng/ml) at diagnosis	Chemotherapy before inclusion	Chemotherapy response	ARPI	Response to ARPI	Site of metastasis	Site of biopsy	Nb successful PDX/total biopsies	Nb successful PDXO
MR009	62	Ad	TxN1M1	8	51	no	NA	Enza	CR	LN, Visc	LN x 2, Visc x 1	3/4	3
MR041	57	Ad	TxN3M0	9	NA	no	NA	Abi	CR	LN	Prostate x 2	1/2	1
MR059	71	Ad	TxN0M1	8	1653	D	PR	Enza	PD	Bone, Visc	Visc	1/1	1
MR077	66	Ad	T3N0M0	8	5	D	PD	Abi, Enza	CR, PD	LN, bone, Visc	Visc	1/1	1
MR084	61	Ad	T4N1M1	8	6	D	PD	Enza	PD	LN, Bone	LN	1/1	1
MR123	73	Ad	TxN0M0	8	91	D, Cab	PD	Abi	PD	LN, Bone	LN	1/1	1
MR150	67	Ad	T2N0M1	9	13	D, Cab, Carbo	PD, PD, PD	Abi	PD	LN, Bone, Visc	Visc	1/1	1
MR151	67	Ad	T3N1M0	9	4	no	NA	Abi, Enza	PR PD	LN, Visc	Visc	1/2	1
MR170	52	Ad	T2N1M1	9	11	D, Carbo	PR, PR	Enza	PD	LN, Bone	LN	1/1	1
MR178	71	Ad	T3N0M0	7	NA	no	NA	Enza	CR	LN, Bone	LN	1/1	1
MR182	70	Ad	T2N0M0	7	7	no	NA	Enza	CR	LN, Bone, Visc	LN	2/2	2
MR191	36	Ad	TxN1M0	8	140	D, Carbo	CR, PD	Enza	PD	LN, Bone	LN	1/1	1
MR283	70	Ad	T3N0M0	9	NA	no	NA	Enza	PR	LN, Bone	LN	1/1	1

Abi: Abiraterone; Ad: Adenocarcinoma, ARPI: Androgen receptor pathway inhibitor; Cab: Cabazitaxel, Carbo: Carboplatin; CR: complete response; D: Docetaxel, Enza: enzalutamide; ID: identification number; LN: Lymph node; NA: Not available; Nb: number; NEPC: neuroendocrine Prostate cancer; PD: Progressive disease; PDX: Patient-derived xenograft; PDXO: Patient-derived xenograft organoid; PR: partial response; PSA: Prostate specific antigen; Visc: visceral metastasis

Figure 1. Study description

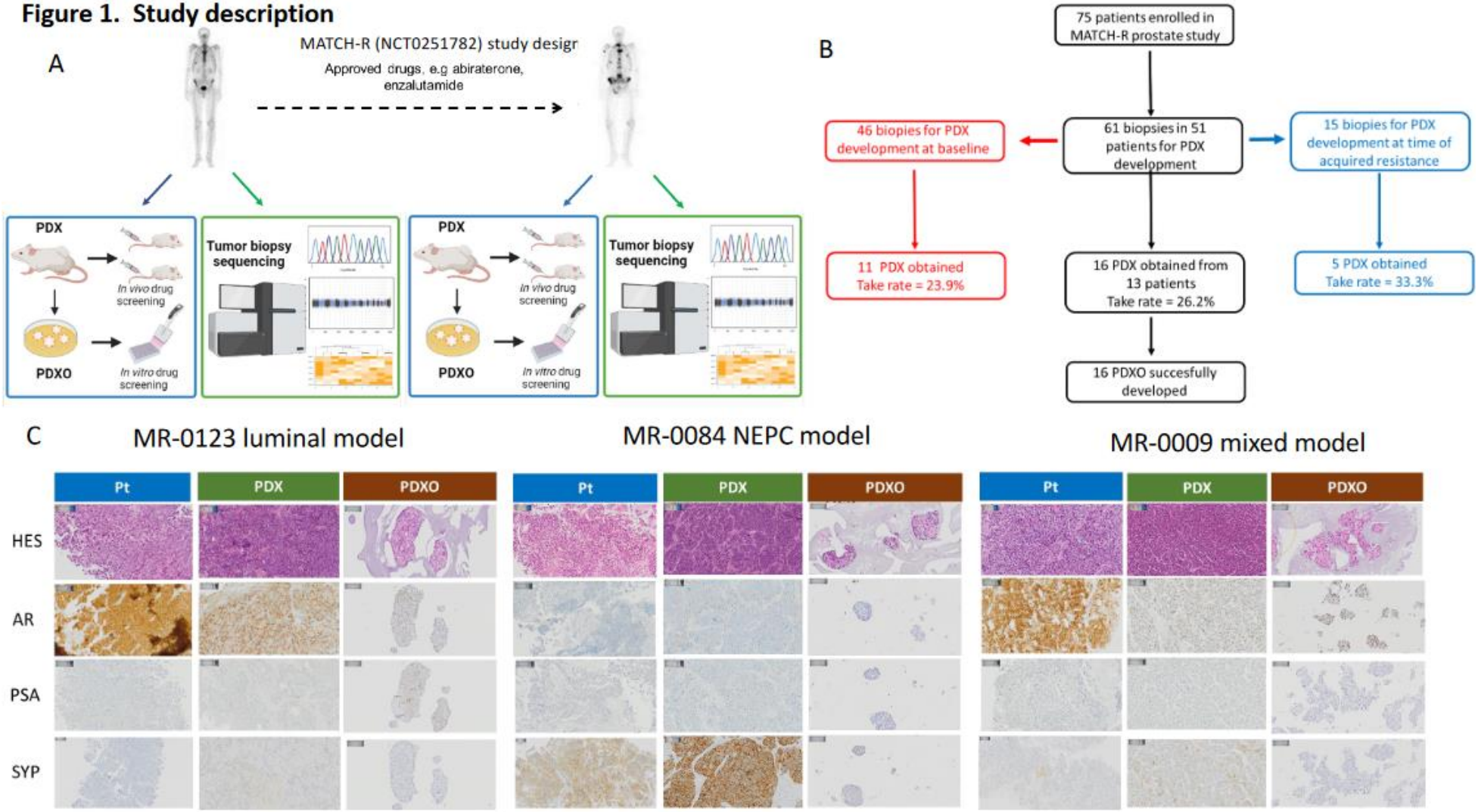

Figure 2

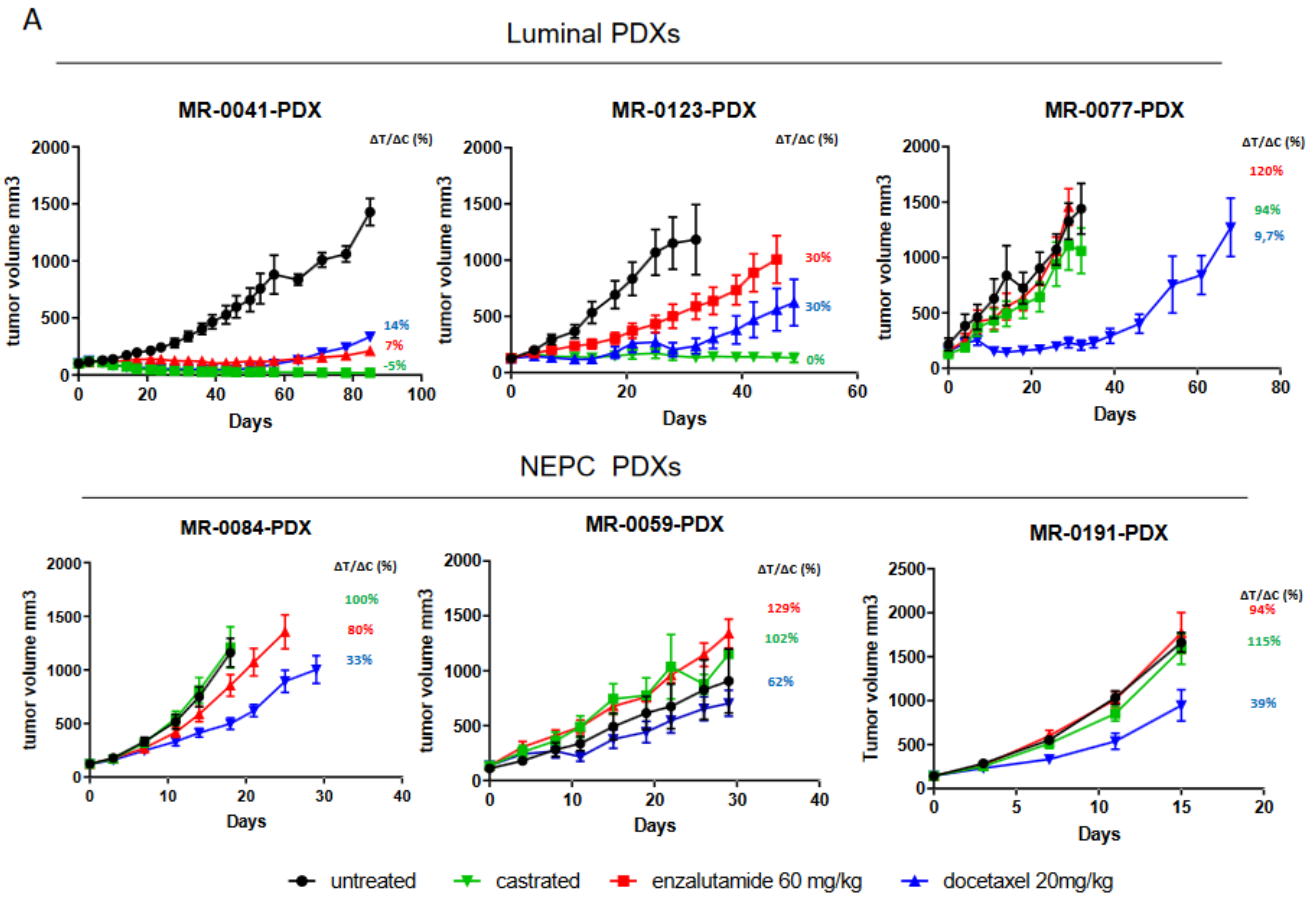
A
Luminal PDXs
MR-0041-PDX
MR-0123-PDX
MR-0077-PDX
tumor volume mm3
Days
ΔT/ΔC (%)
14%
7%
-5%
30%
30%
0%
120%
94%
9,7%
NEPC PDXs
MR-0084-PDX
MR-0059-PDX
MR-0191-PDX
100%
80%
33%
129%
102%
62%
94%
115%
39%
untreated
castrated
enzalutamide 60 mg/kg
docetaxel 20mg/kg

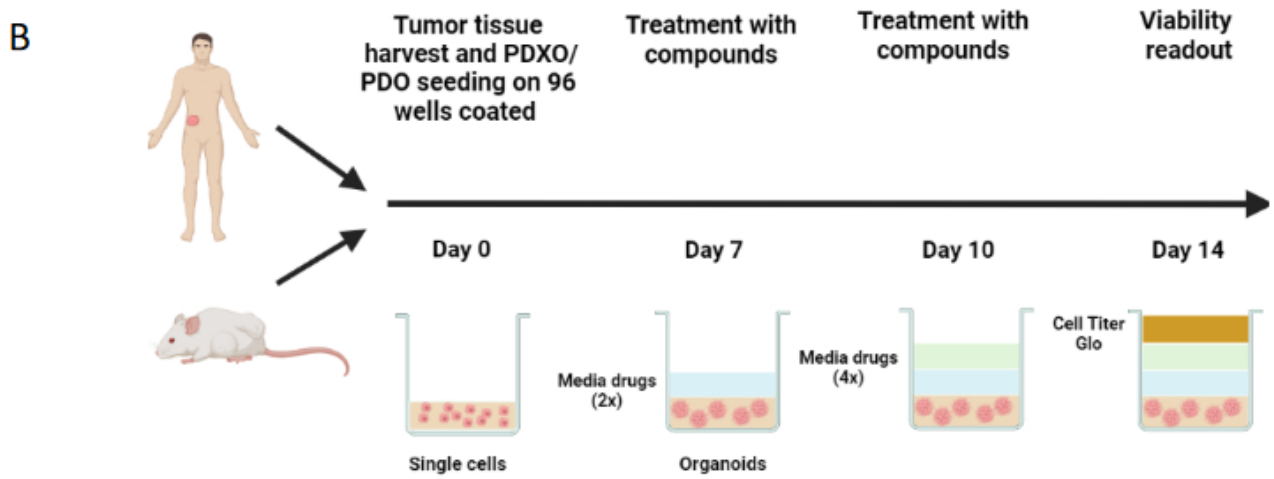
B
Tumor tissue harvest and PDXO/ PDO seeding on 96 wells coated
Treatment with compounds
Treatment with compounds
Viability readout
Day 0
Day 7
Day 10
Day 14
Media drugs (2x)
Media drugs (4x)
Cell Titer Glo
Single cells
Organoids

C

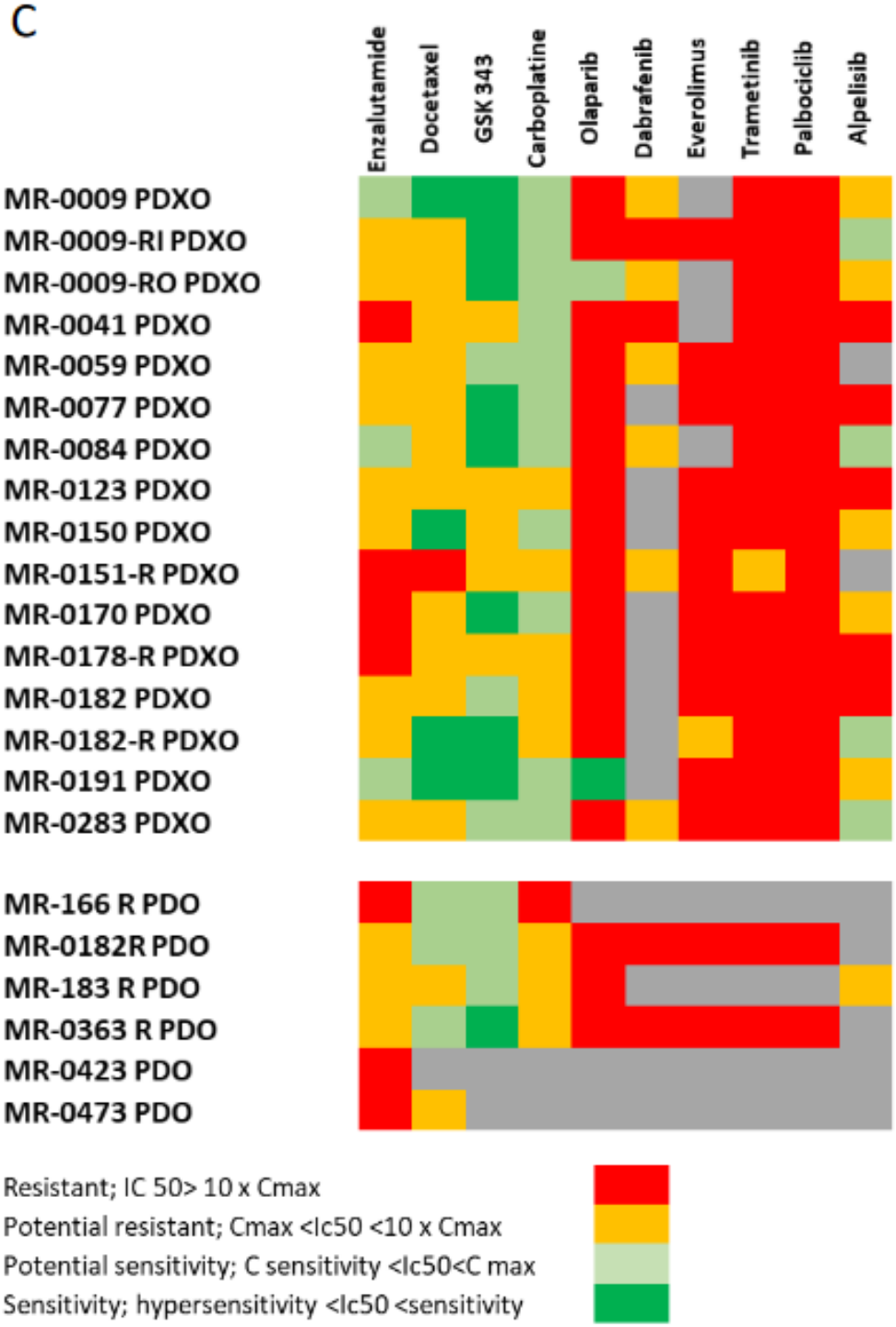
Enzalutamide
Docetaxel
GSK 343
Carboplatine
Olaparib
Dabrafenib
Everolimus
Trametinib
Palbociclib
Alpelisib
MR-0009 PDXO
MR-0009-RI PDXO
MR-0009-RO PDXO
MR-0041 PDXO
MR-0059 PDXO
MR-0077 PDXO
MR-0084 PDXO
MR-0123 PDXO
MR-0150 PDXO
MR-0151-R PDXO
MR-0170 PDXO
MR-0178-R PDXO
MR-0182 PDXO
MR-0182-R PDXO
MR-0191 PDXO
MR-0283 PDXO
MR-166 R PDO
MR-0182R PDO
MR-183 R PDO
MR-0363 R PDO
MR-0423 PDO
MR-0473 PDO
Resistant; IC 50> 10 x Cmax
Potential resistant; Cmax <Ic50 <10 x Cmax
Potential sensitivity; C sensitivity <Ic50<C max
Sensitivity; hypersensitivity <Ic50 <sensitivity

D

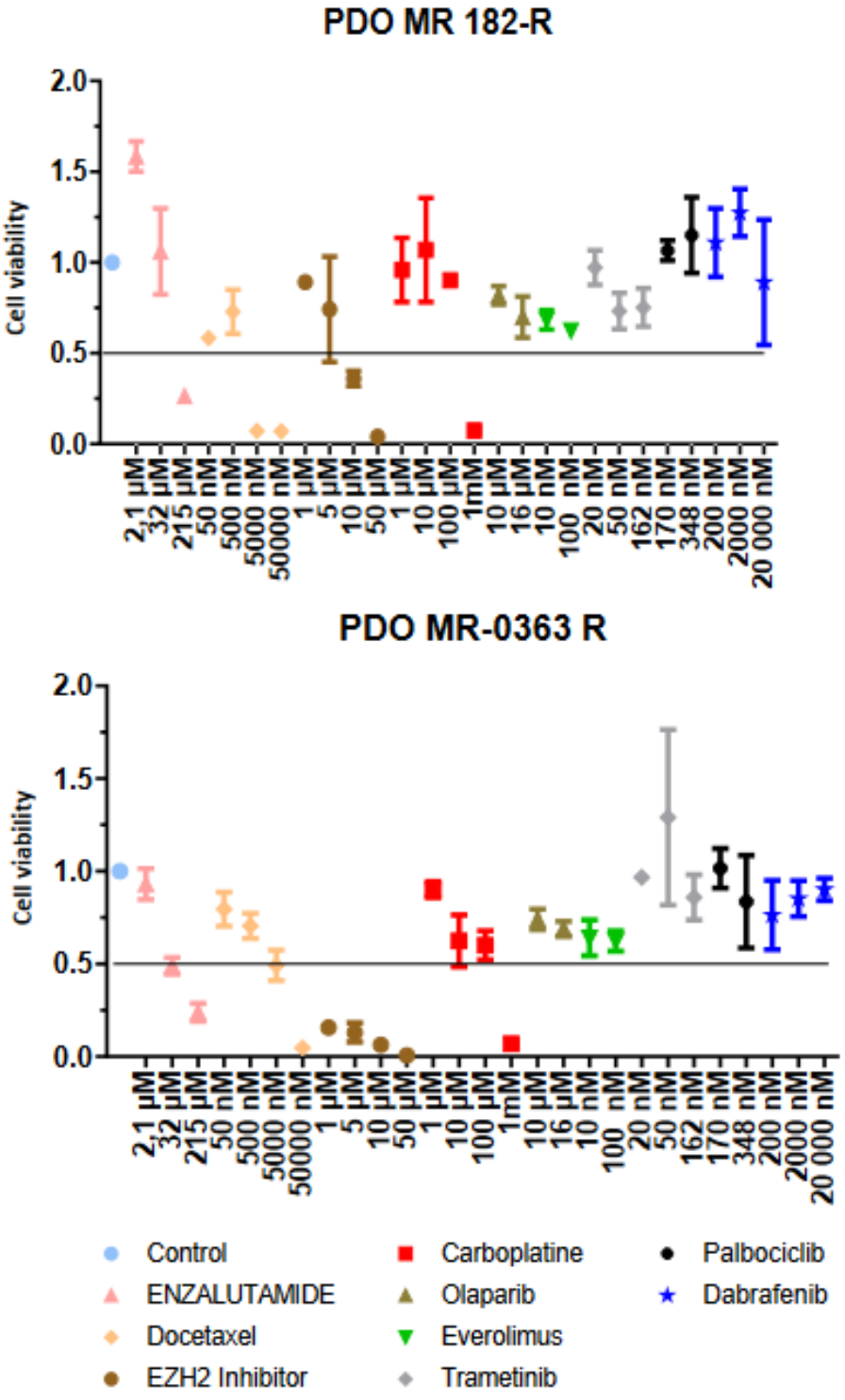
PDO MR 182-R
Cell viability
2.0
1.5
1.0
0.5
0.0
2,1 µM
32 µM
215 µM
50 nM
500 nM
5000 nM
50000 nM
1 µM
5 µM
10 µM
50 µM
1 µM
10 µM
100 µM
1mM
10 µM
16 µM
10 nM
100 nM
20 nM
50 nM
162 nM
170 nM
348 nM
200 nM
2000 nM
20 000 nM
PDO MR-0363 R
Cell viability
2.0
1.5
1.0
0.5
0.0
2,1 µM
32 µM
215 µM
50 nM
500 nM
5000 nM
50000 nM
1 µM
5 µM
10 µM
50 µM
1 µM
10 µM
100 µM
1mM
10 µM
16 µM
10 nM
100 nM
20 nM
50 nM
162 nM
170 nM
348 nM
200 nM
2000 nM
20 000 nM
Control
ENZALUTAMIDE
Docetaxel
EZH2 Inhibitor
Carboplatine
Olaparib
Everolimus
Trametinib
Palbociclib
Dabrafenib

Figure 3

A

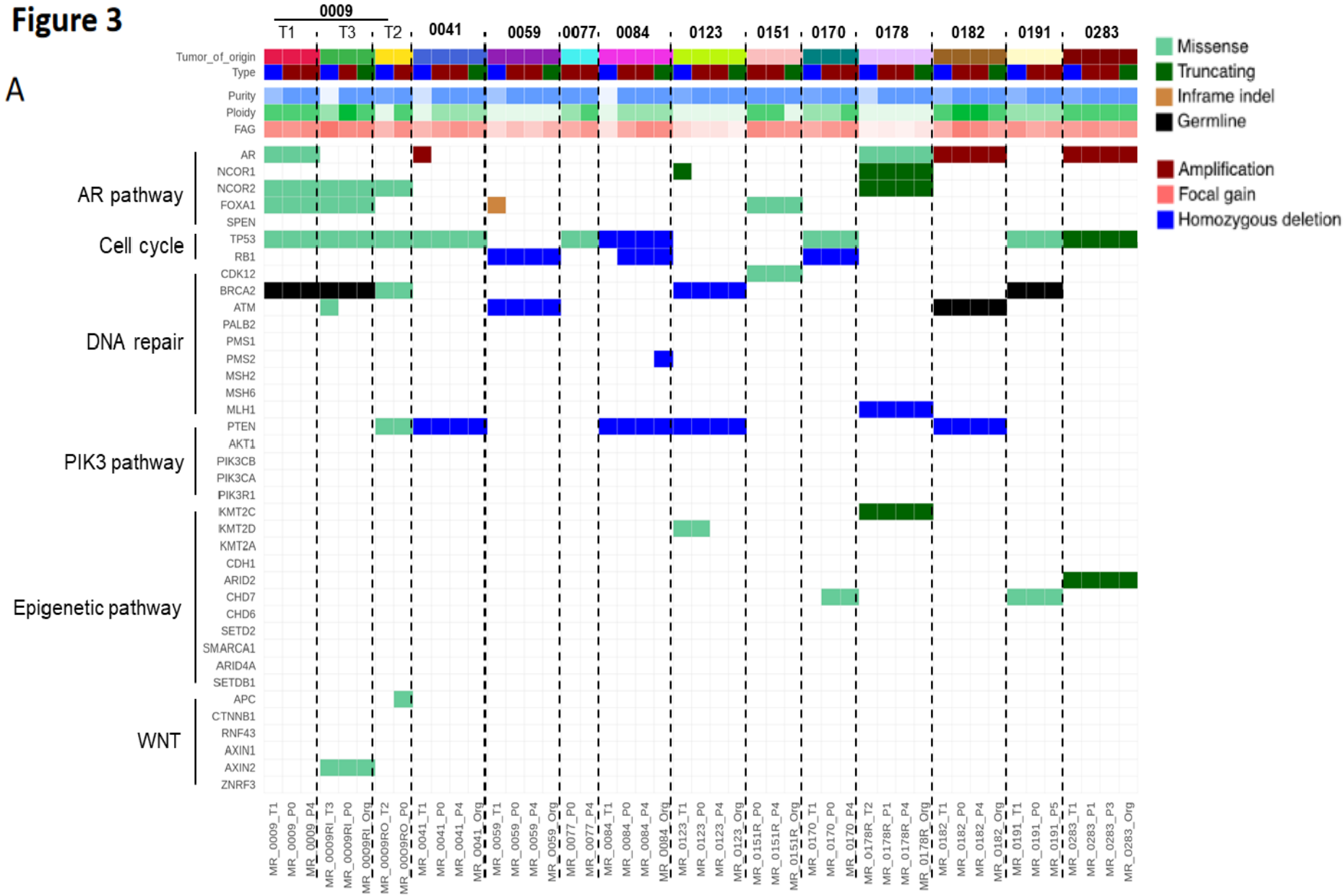
0009
T1
T3
T2
0041
0059
0077
0084
0123
0151
0170
0178
0182
0191
0283
Tumor_of_origin
Type
Purity
Ploidy
FAG
AR pathway
Cell cycle
DNA repair
PIK3 pathway
Epigenetic pathway
WNT
AR
NCOR1
NCOR2
FOXA1
SPEN
TP53
RB1
CDK12
BRCA2
ATM
PALB2
PMS1
PMS2
MSH2
MSH6
MLH1
PTEN
AKT1
PIK3CB
PIK3CA
PIK3R1
KMT2C
KMT2D
KMT2A
CDH1
ARID2
CHD7
CHD6
SETD2
SMARCA1
ARID4A
SETDB1
APC
CTNNB1
RNF43
AXIN1
AXIN2
ZNRF3
Missense
Truncating
Inframe indel
Germline
Amplification
Focal gain
Homozygous deletion

B

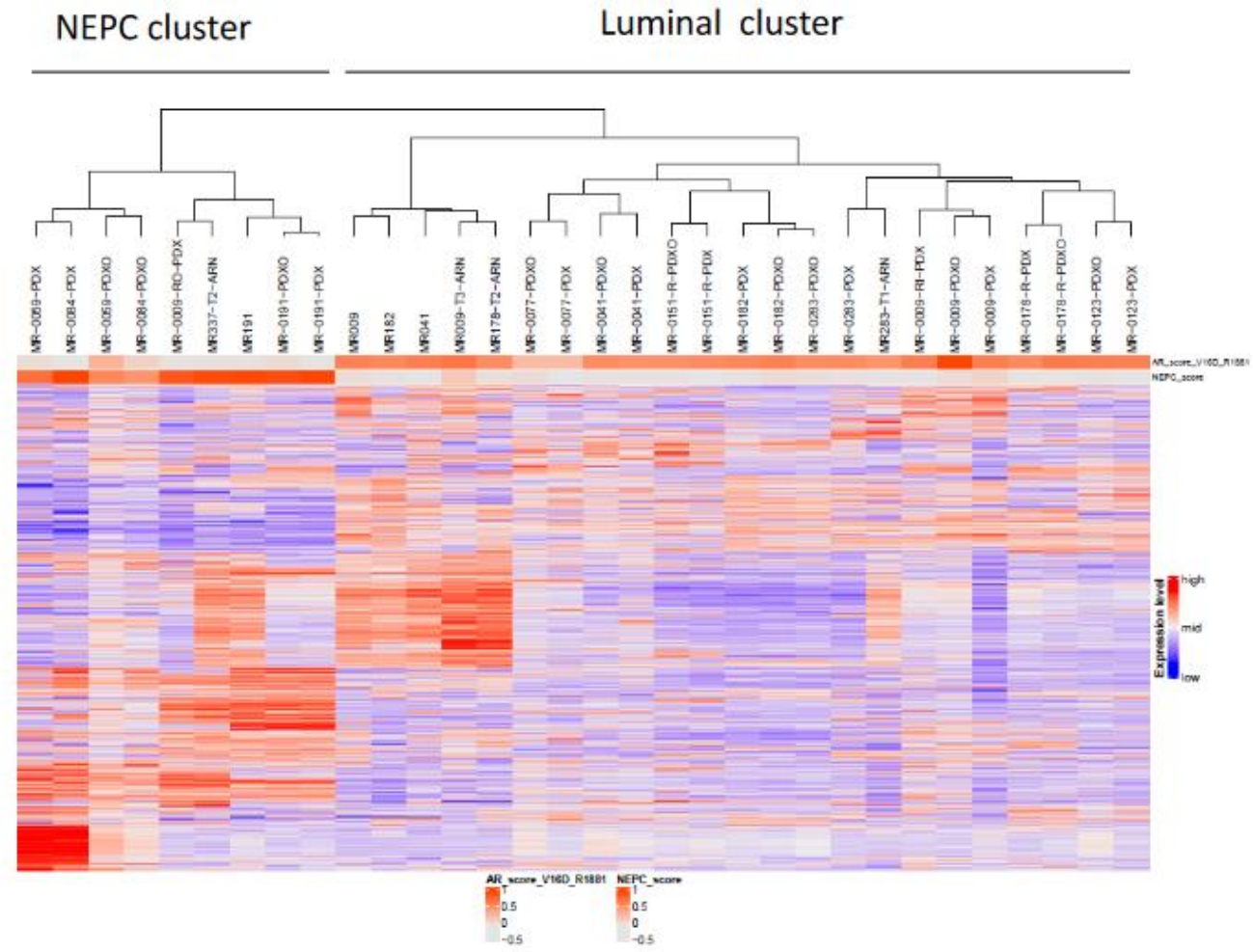
NEPC cluster
Luminal cluster
MR-0069-PDX
MR-0084-PDX
MR-0059-PDXO
MR-0084-PDXO
MR-0009-RD-PDX
MR337-T2-ARN
MR191
MR-0191-PDXO
MR-0191-PDX
MR009
MR182
MR041
MR009-T3-ARN
MR178-T2-ARN
MR-0077-PDXO
MR-0077-PDX
MR-0041-PDXO
MR-0041-PDX
MR-0151-R-PDXO
MR-0151-R-PDX
MR-0182-PDX
MR-0182-PDXO
MR-0283-PDXO
MR-0283-PDX
MR283-T1-ARN
MR-0009-RI-PDX
MR-0009-PDXO
MR-0009-PDX
MR-0178-R-PDX
MR-0178-R-PDXO
MR-0123-PDXO
MR-0123-PDX
AR_score_V16D_R1881
NEPC_score
Expression level
high
mid
low

C

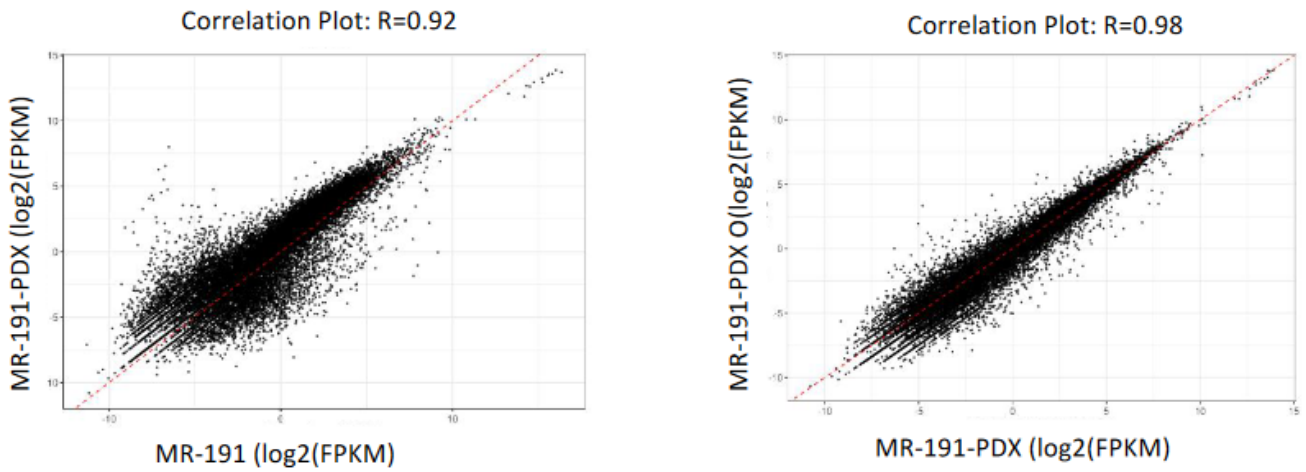
Correlation Plot: R=0.92
MR-191-PDX (log2(FPKM)
MR-191 (log2(FPKM)
Correlation Plot: R=0.98
MR-191-PDX O(log2(FPKM)
MR-191-PDX (log2(FPKM)

Figure 4

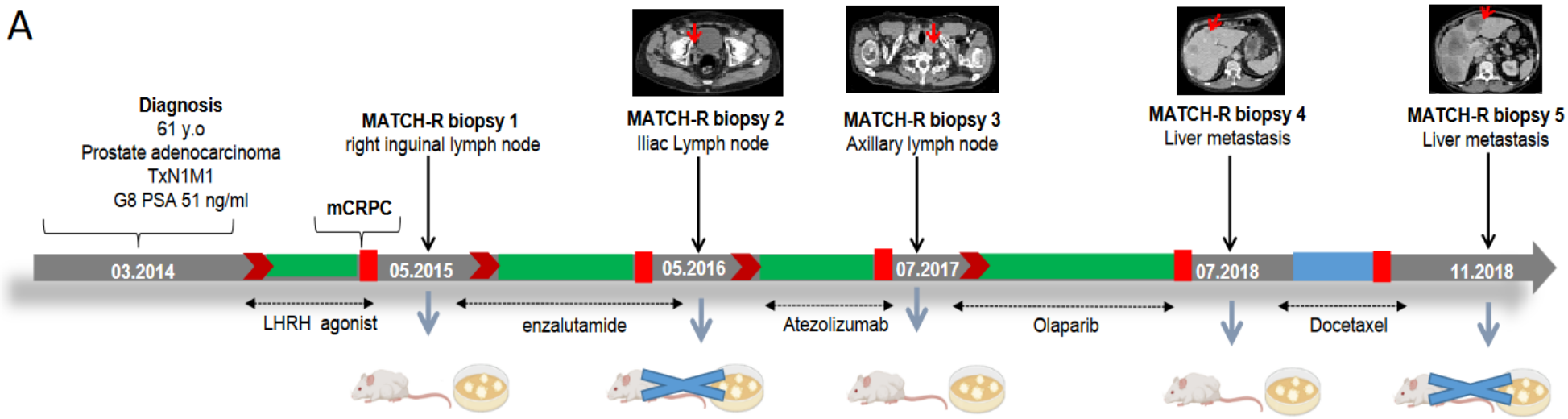
A
Diagnosis
61 y.o
Prostate adenocarcinoma
TxN1M1
G8 PSA 51 ng/ml
mCRPC
MATCH-R biopsy 1
right inguinal lymph node
MATCH-R biopsy 2
Iliac Lymph node
MATCH-R biopsy 3
Axillary lymph node
MATCH-R biopsy 4
Liver metastasis
MATCH-R biopsy 5
Liver metastasis
03.2014
05.2015
05.2016
07.2017
07.2018
11.2018
LHRH agonist
enzalutamide
Atezolizumab
Olaparib
Docetaxel

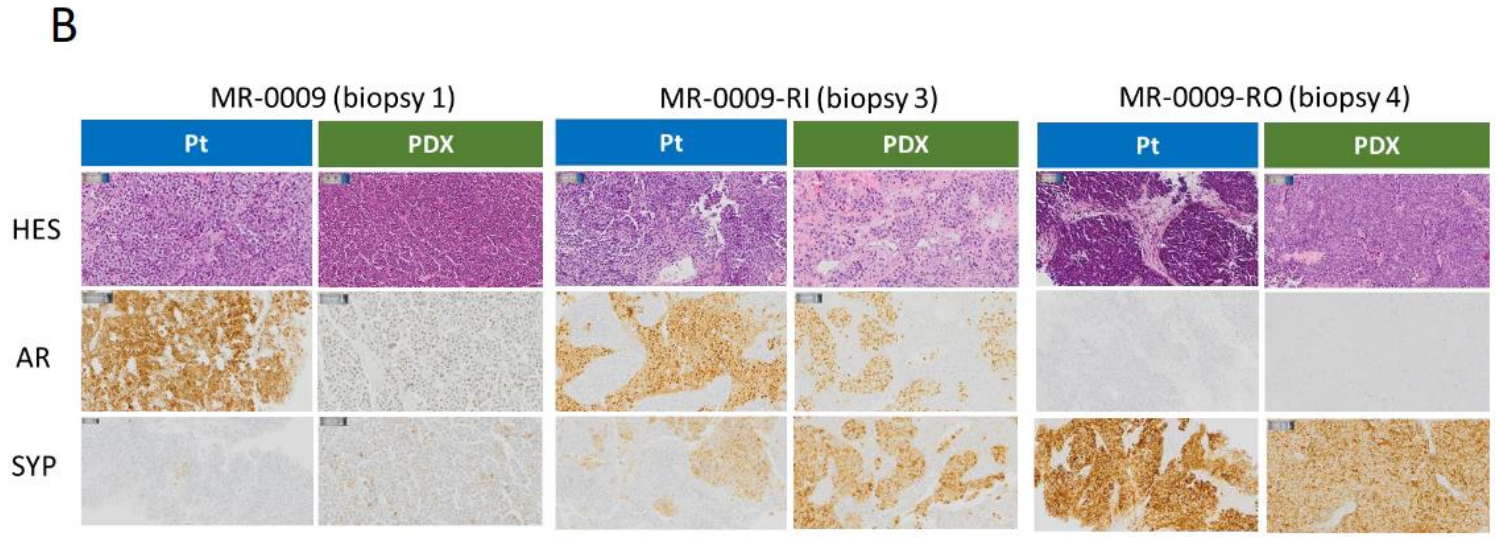
B
MR-0009 (biopsy 1)
MR-0009-RI (biopsy 3)
MR-0009-RO (biopsy 4)
Pt
PDX
HES
AR
SYP

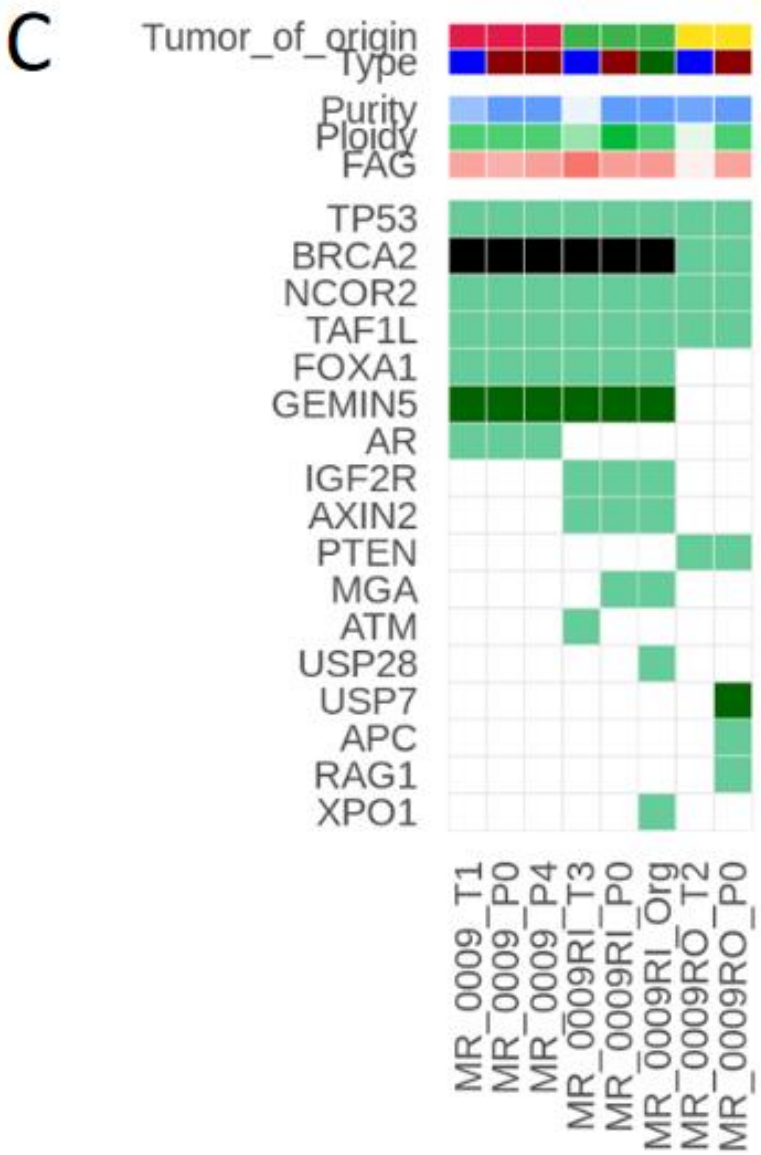
C
Tumor_of_origin
Type
Purity
Ploidy
FAG
TP53
BRCA2
NCOR2
TAF1L
FOXA1
GEMIN5
AR
IGF2R
AXIN2
PTEN
MGA
ATM
USP28
USP7
APC
RAG1
XPO1
MR_0009_T1
MR_0009_P0
MR_0009_P4
MR_0009RI_T3
MR_0009RI_P0
MR_0009RI_Org
MR_0009RO_T2
MR_0009RO_P0

D

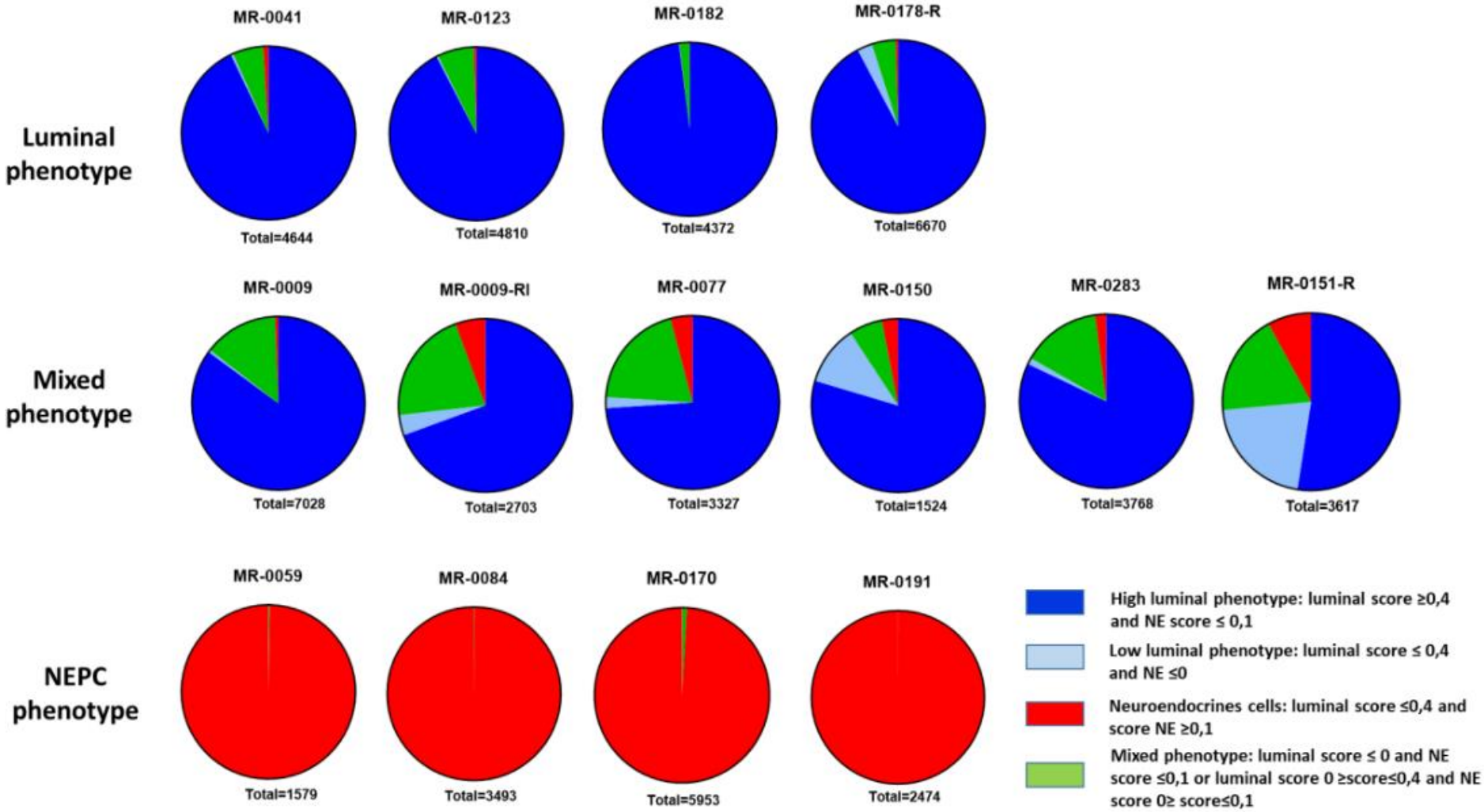
Luminal phenotype
MR-0041
Total=4644
MR-0123
Total=4810
MR-0182
Total=4372
MR-0178-R
Total=6670
Mixed phenotype
MR-0009
Total=7028
MR-0009-RI
Total=2703
MR-0077
Total=3327
MR-0150
Total=1524
MR-0283
Total=3768
MR-0151-R
Total=3617
NEPC phenotype
MR-0059
Total=1579
MR-0084
Total=3493
MR-0170
Total=5953
MR-0191
Total=2474
High luminal phenotype: luminal score ≥0,4 and NE score ≤ 0,1
Low luminal phenotype: luminal score ≤ 0,4 and NE ≤0
Neuroendocrines cells: luminal score ≤0,4 and score NE ≥0,1
Mixed phenotype: luminal score ≤ 0 and NE score ≤0,1 or luminal score 0 ≥score≤0,4 and NE score 0≥ score≤0,1

Figure 5

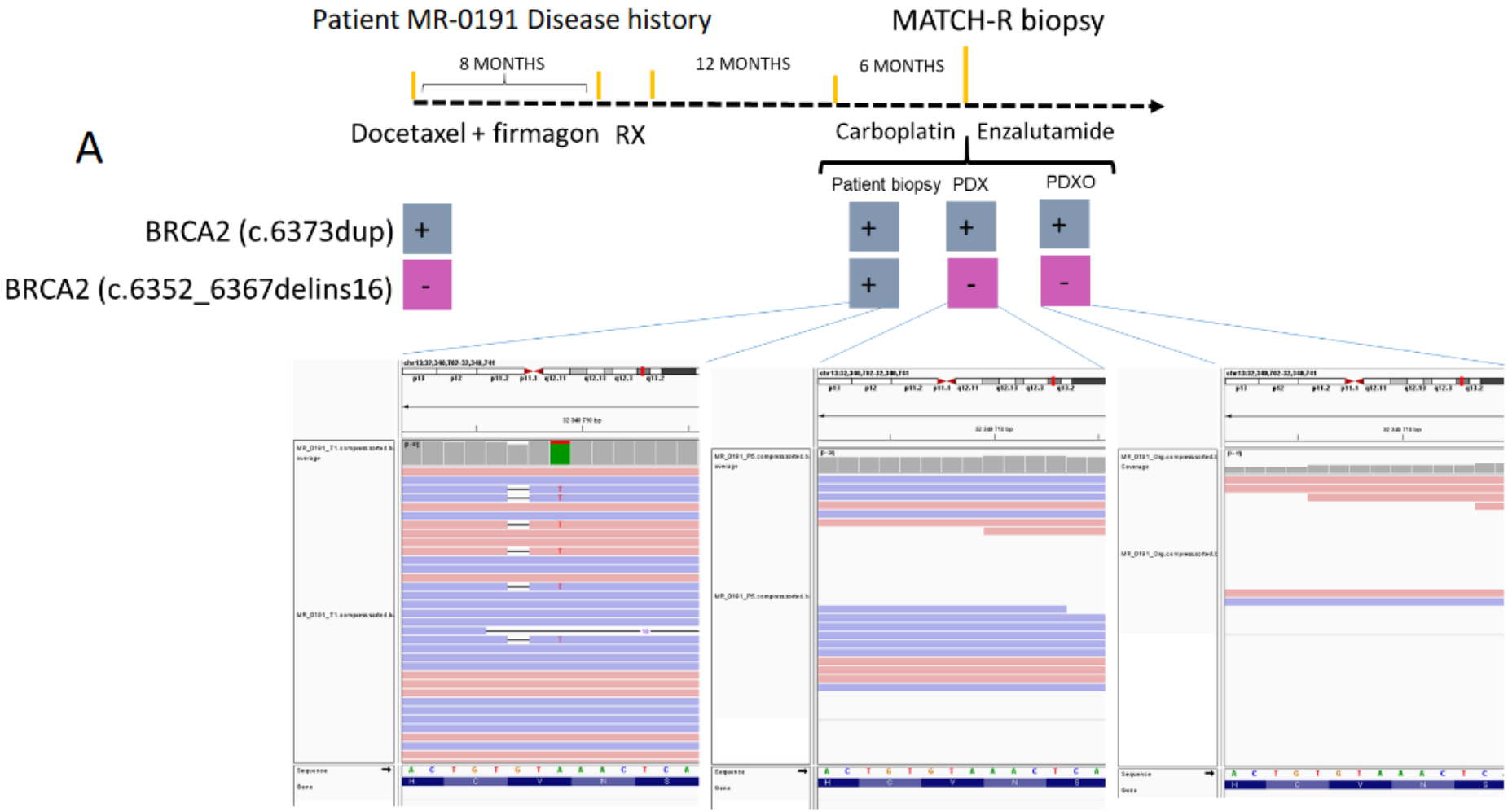
A
Patient MR-0191 Disease history
MATCH-R biopsy
8 MONTHS
12 MONTHS
6 MONTHS
Docetaxel + firmagon RX
Carboplatin
Enzalutamide
Patient biopsy
PDX
PDXO
BRCA2 (c.6373dup)
BRCA2 (c.6352_6367delins16)
+
+
+
+
+
-
-

B

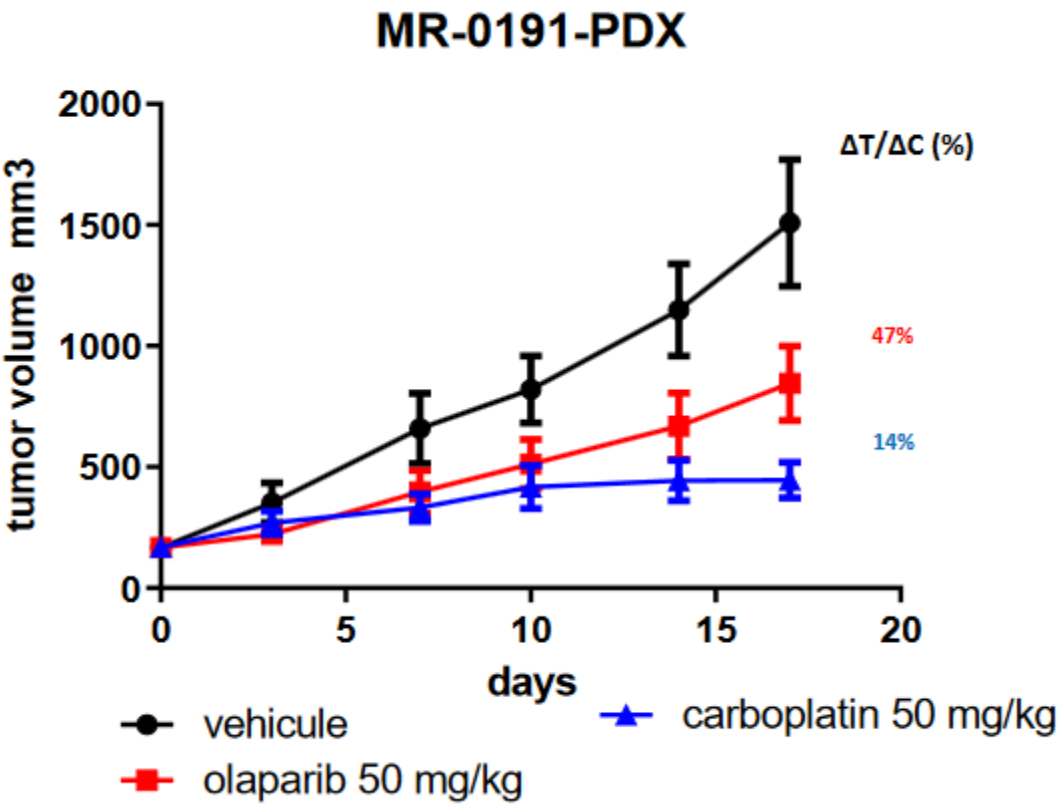
MR-0191-PDX
tumor volume mm3
2000
1500
1000
500
0
0
5
10
15
20
days
ΔT/ΔC (%)
47%
14%
vehicule
olaparib 50 mg/kg
carboplatin 50 mg/kg

C

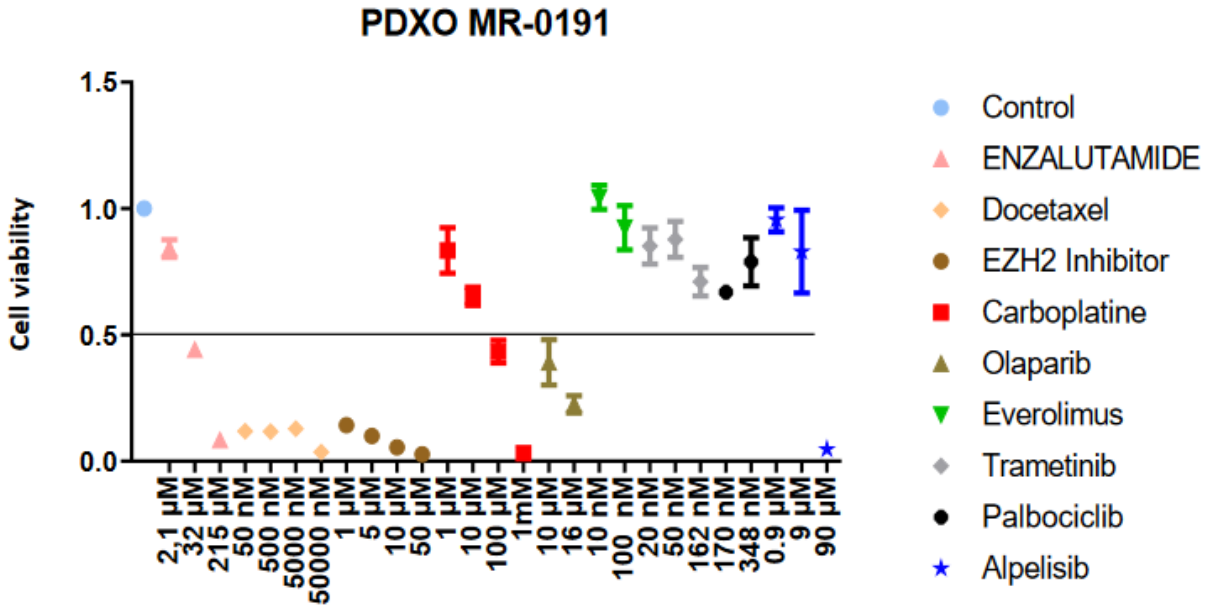
PDXO MR-0191
Cell viability
1.5
1.0
0.5
0.0
2,1 µM
32 µM
215 µM
50 nM
500 nM
5000 nM
50000 nM
1 µM
5 µM
10 µM
50 µM
1 µM
10 µM
100 µM
1mM
10 µM
16 µM
10 nM
100 nM
20 nM
50 nM
162 nM
170 nM
348 nM
0.9 µM
9 µM
90 µM
Control
ENZALUTAMIDE
Docetaxel
EZH2 Inhibitor
Carboplatine
Olaparib
Everolimus
Trametinib
Palbociclib
Alpelisib

D

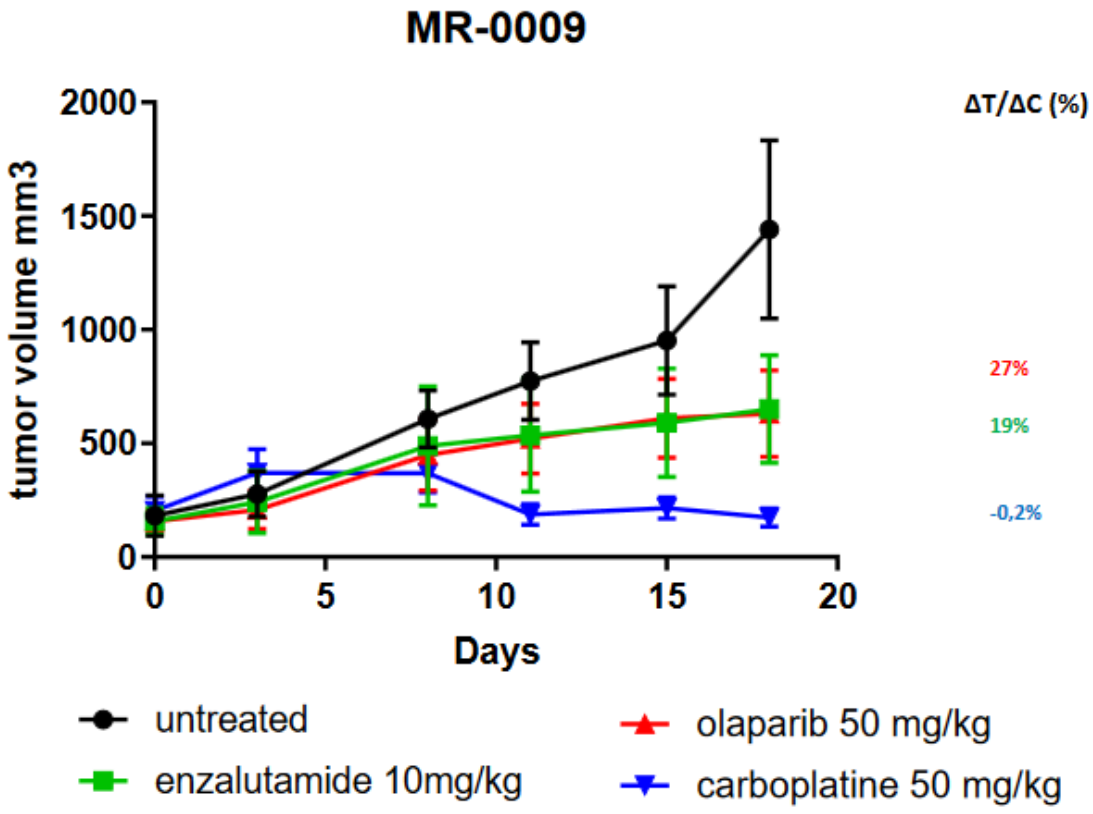
MR-0009
ΔT/ΔC (%)
tumor volume mm3
2000
1500
1000
500
0
0
5
10
15
20
Days
27%
19%
-0,2%
untreated
olaparib 50 mg/kg
enzalutamide 10mg/kg
carboplatine 50 mg/kg

Supplementary Table 1

ID	Site of biopsy	Established PDX	number of cells	Percent of alive cells	PDO obtained	nb of drug tested	pre biopsy treatment	patient status	PDO response	Post biopsy treatment	Patient response	PDO response	Potential therapy response
MR-0166 R	LN	No	250,000	43	Yes	4	Cabo + Atezo+ADT	PD	Not tested	Abi	PR	Enza Resistance	EZH2 inhibitor
MR-0182-R	LN	Yes	459,000	15	Yes	9	Enza +ADT	PD	Enza Potential resistance	D	PR	D Potential sensible	no
MR-0183-R	LN	No	393,000	11	Yes	6	Enza+ADT	PD	Enza Potential resistance	PARP inhibitor +ICI	PD	Olaparib resistance	no
MR-0363 R	LN	No	268,000	21	Yes	9	ADT+abi	PD	Enza Potential resistance	D	PD	D Potential Resistance	EZH2 inhibitor
MR-0386 (MR-0009)	LIVER	No	109,000	16	No	NA	D+ADT	PD	NA		NA		
MR-0413	LIVER	No	191,000	8	No	NA	ADT	PD	NA	abi	PR	NA	no
MR-0423	LN	No	92,900	12	Yes	1	D+ Nivolumab+ ADT	PD	Not tested	abi	PD	Resistance Enza	no
MR-0473	LN	No	184,000	20	Yes	2	ADT	PD	NA	abi	PR	Resistance Enza	no
MR-0539	LN	No	32,800	80	No	NA	ODM-201+ADT	PD	NA	abi	SD	NA	no

6. Supplementary figures and legends

Supplementary figure 1

A: The biopsy site was associated with *in vivo* tumor take rate. The success rate of engraftment when the biopsy was performed in prostate (1/27) was lower than the success rate when the biopsy was performed in metastases (12/34, $p < 0.01$ Khi2 test), especially in the lymph nodes (10/24 vs prostate; $p = 0.03$ Khi2 test). B: The NEPC phenotype was associated to higher take rate that the luminal phenotype ($p = 0.021$, Khi2 test)

Supplementary figure 2

Representative pictures of organoids taken after 7 days cultures of 6 PDXO (MR-0123, MR-0283, MR-0191, MR-0009, MR-0009-RI, and MR-0041) that show disorganized and irregular structures with invading cells migrating outside the organoid. Fresh harvested PDX tissue were placed in culture medium. Tissue sample were dissociated by mechanical dissection and digested using Collagenase type II. The cells were individually separated into single cells or cluster of 2 or 3 days. Created with BioRender.com.

Supplementary figure 3

A. Patient MR-0059 clinical course between 2015 and 2016.

B. *In vivo* evaluation of vehicle (black), castration (green), Enzalutamide 60 mg/kg oral gavage QD (5% chromophore/Phosphate Buffer Saline) 5 doses/week (red) and Docetaxel 20 mg/kg i.p 3 doses/week (Phosphate Buffer Saline) (blue) in MR-0059 PDX models. Tumor volumes mean+/-SEM (n = 8). Mice were treated for 29 days and tumor volume was measured with calipers twice weekly throughout the treatment period. Tumor volumes mean+/-SEM (n = 7 pergroup). Tumor growth inhibition (ΔT/ΔC value) was calculated as following: ΔT/ΔC (%) = [(median TDayY - median TDayX)/(median

CDayY - median CDayX)] x 100 (where DayY is the day of evaluation, and DayX is the day of initiation of therapy for treated [T] and control [C] tumor volumes).

C. Results of MR-0059 PDXO drug screen assay. Cells were treated with incremental concentrations of Enzalutamide (pink), Docetaxel (yellow), EZH2 inhibitor (brown), carboplatine (red), olaparib (dark green), everolimus (green), trametinib (grey), palbociclib (dark), dabrafenib (blue). Control (light blue) is representative of PDO treated with DMSO at 0.05%, used as negative control.

Horizontal lines represent the different concentrations for each compound. The vertical line represent the percentage of cell viability assessed with the with the CellTiter-Glo kit. All samples are normalized with the control; the black line represents the threshold to determine the drug response (50% cell viability).

Supplementary figure 4

Mutations in human sample and the corresponding PDX and/or PDXO for each model. The number of mutations shared by all models (pink) or by all samples from the same patient (e.g. shared by the human tumor and the PDX and/or the PDXO, green) or mutation shared by at least 2 out of 3 samples (blue) or private to one sample (purple) are represented.

Supplementary figure 5

Heatmap plot of SNV and CNV based on WES on tumor samples from MR-0182 patient (T1), the corresponding PDX at P0 and P5 and PDXO.

Supplementary figure 6

Correlation plots of gene expression from RNA-seq data between human tissue and the corresponding PDX and between PDX and PDXO for PCa case MR-0182, MR-0178R,

MR-0123, MR-0151R, MR-0059, MR-0009, MR-0077, MR-0041, and MR-0084. For MR-0009, three human samples have been analysed (MR-0009, MR-0337, and MR-0009-T3). Pearson correlation coefficient, are provided on top of each correlation plot.

Supplementary figure 7

scRNA-seq for dissociated PDXs was performed using 10X genomics technology. Expression of specific genes expressions (AR, PSA, SYP, PSMA, and DLL3) are projected on t-SNE plot for 14 PDXs. Cells are projected into t-SNE space, but are colored by the relative expression: colors span a gradient from dark blue (high expression) to yellow (low expression).

Supplementary figure 8

scRNA-seq for dissociated PDXs was performed using 10X genomics technology in three different type of PDX: luminal PDX (MR-0123), Mixed phenotype (MR-0009-RI) and Neuroendocrine PDX (MR-084). Expression of specific genes expressions (AR, PSA, SYP, PSMA, and DLL3) are projected on t-SNE plot. Cells are projected into t-SNE space, but are colored by the relative expression: colors span a gradient from dark blue (high expression) to yellow (low expression).

Supplementary figure 1

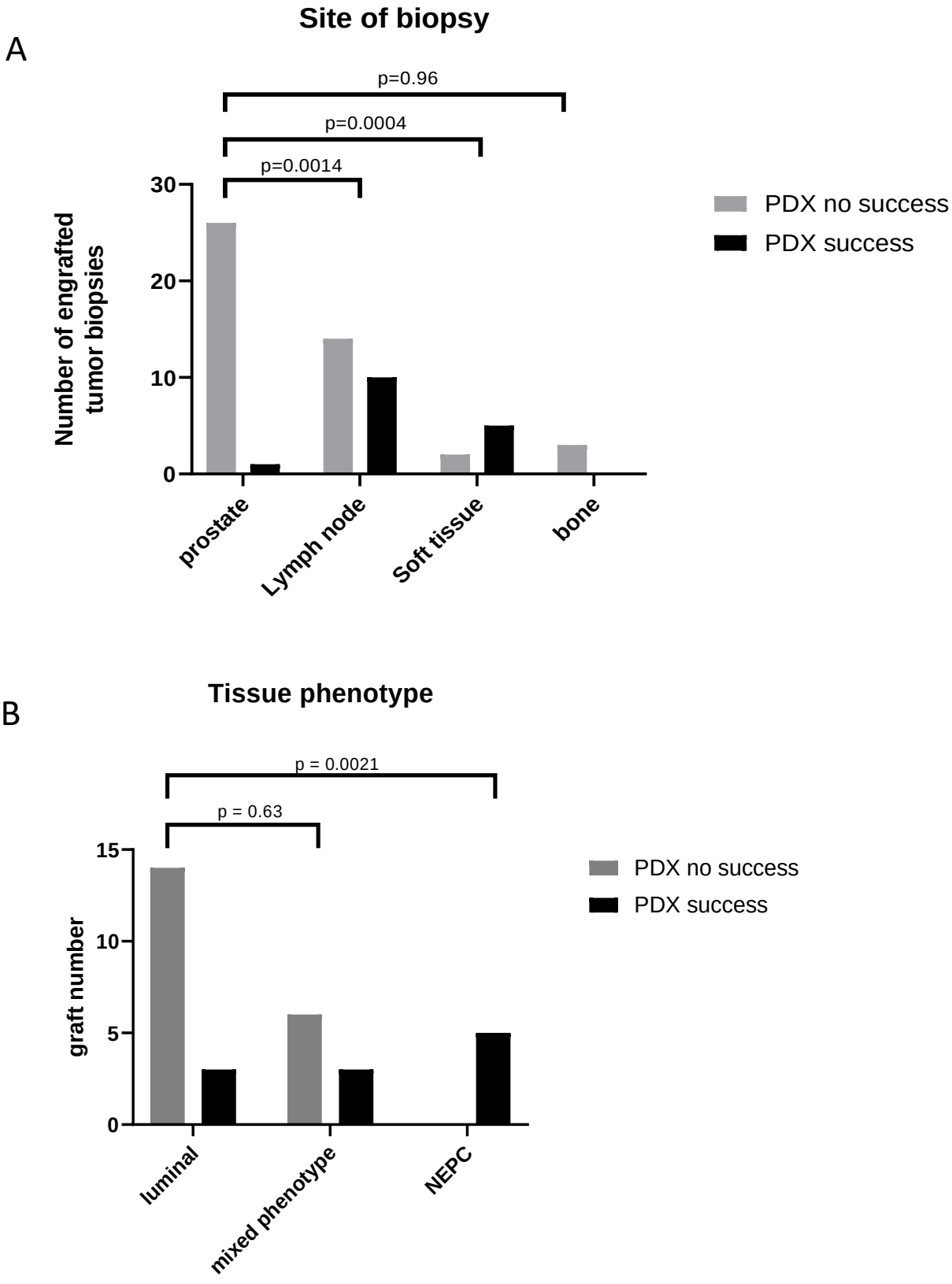

Supplementary figure 2

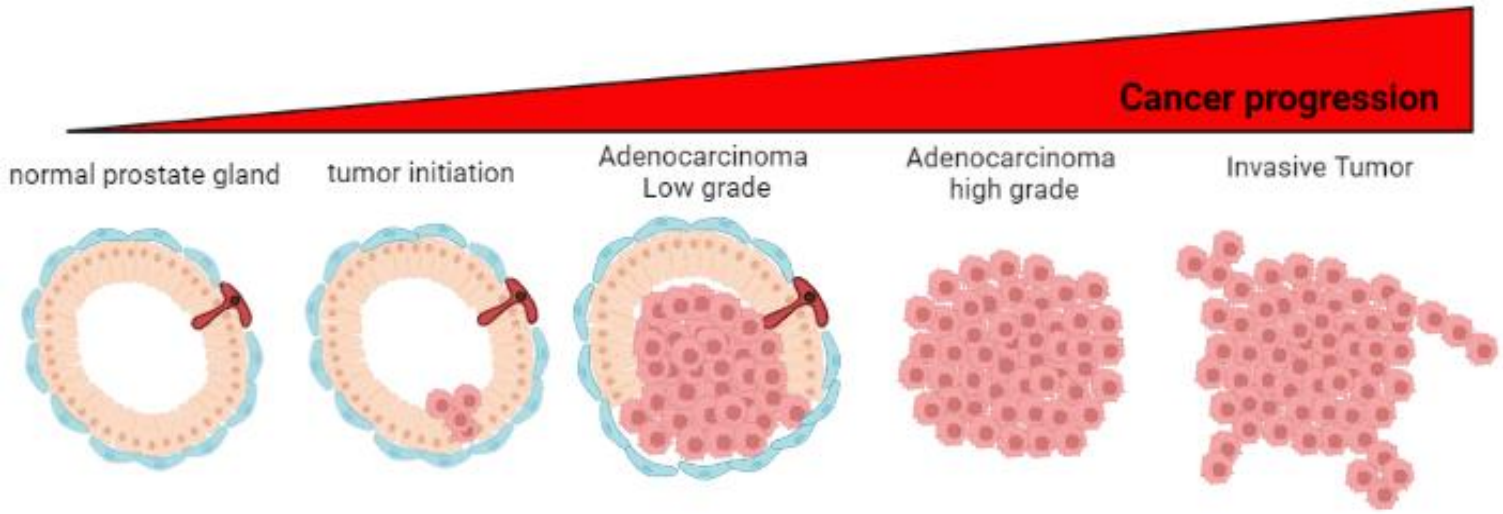

PDXO

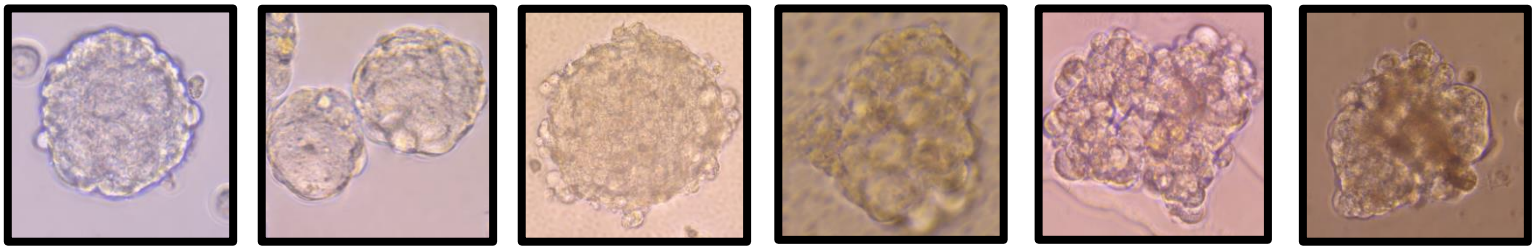

MR-0123 Day 7 | MR-0283 Day 7 | MR-0191 Day 7 | MR-0009 Day 7 | MR-0009-RI Day 7 | MR-0041 Day 7

Supplementary figure 3

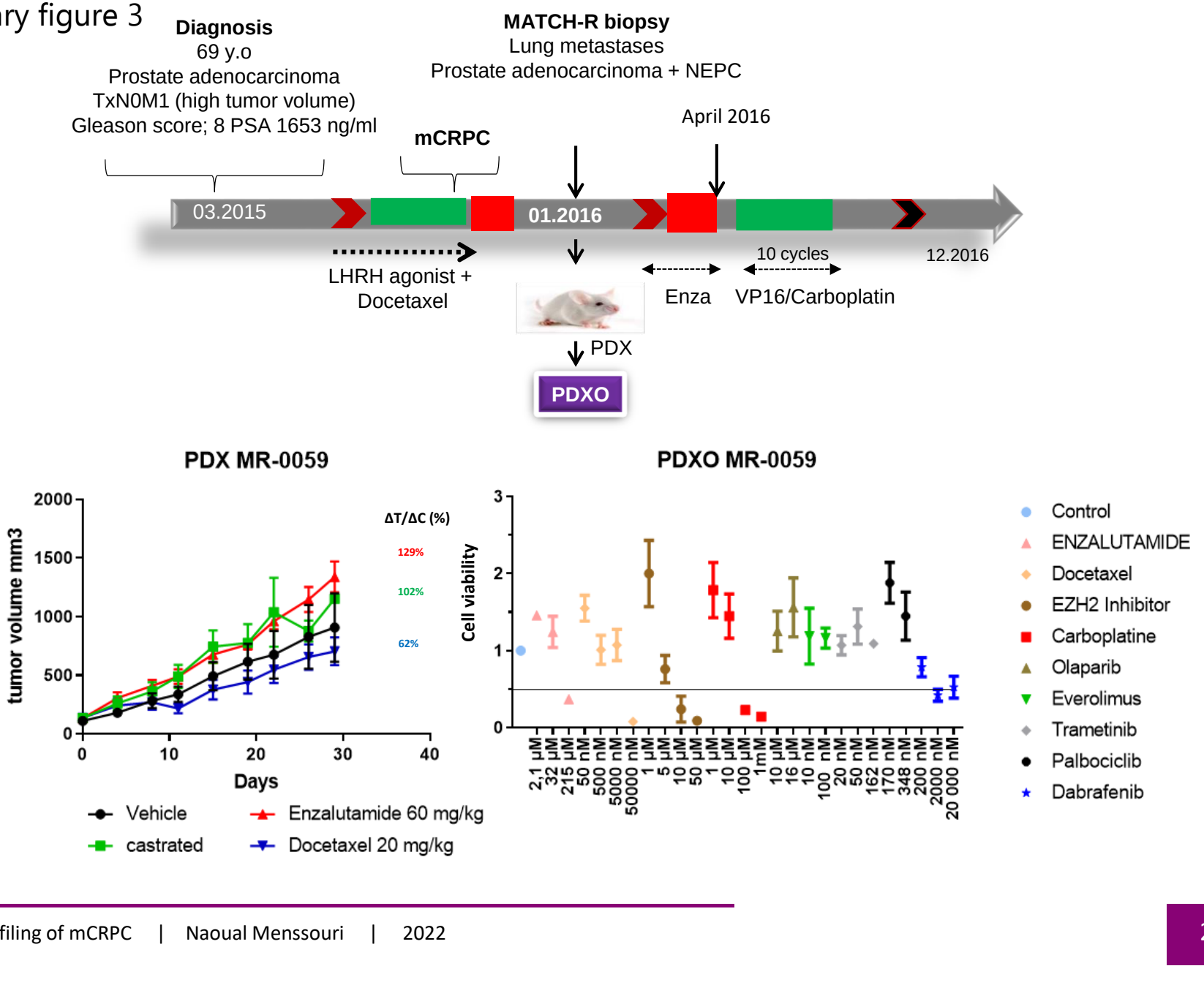

Supplementary figure 4

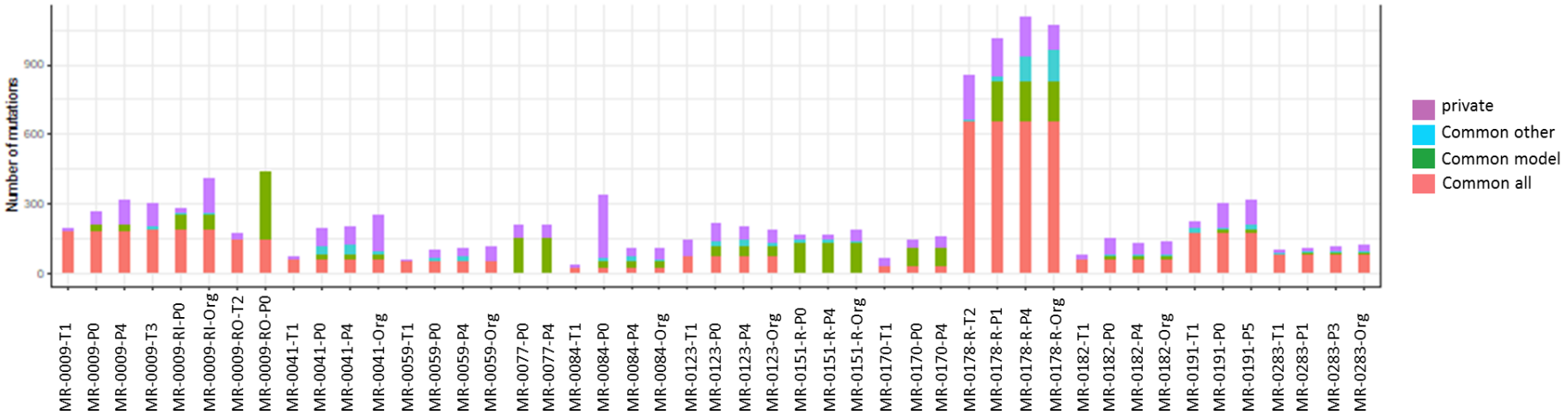

Supplementary figure 5

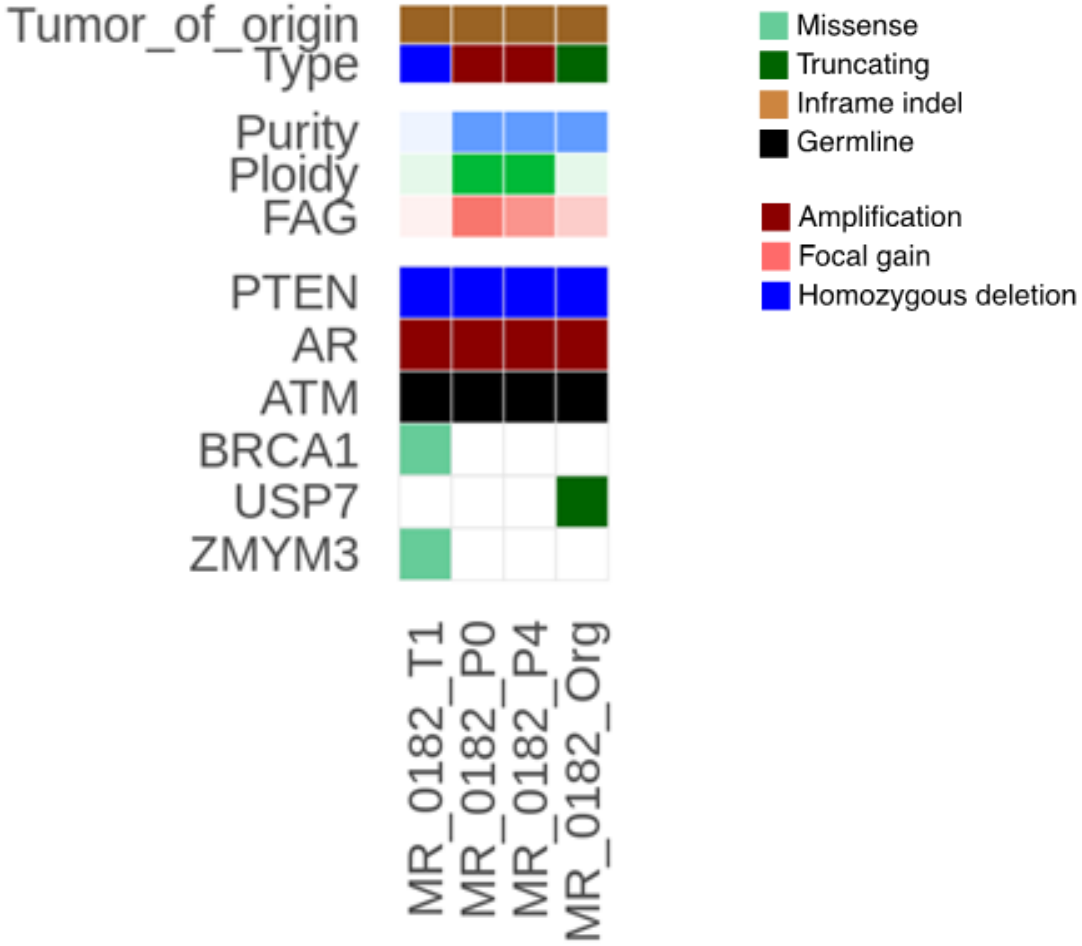

Supplementary figure 6

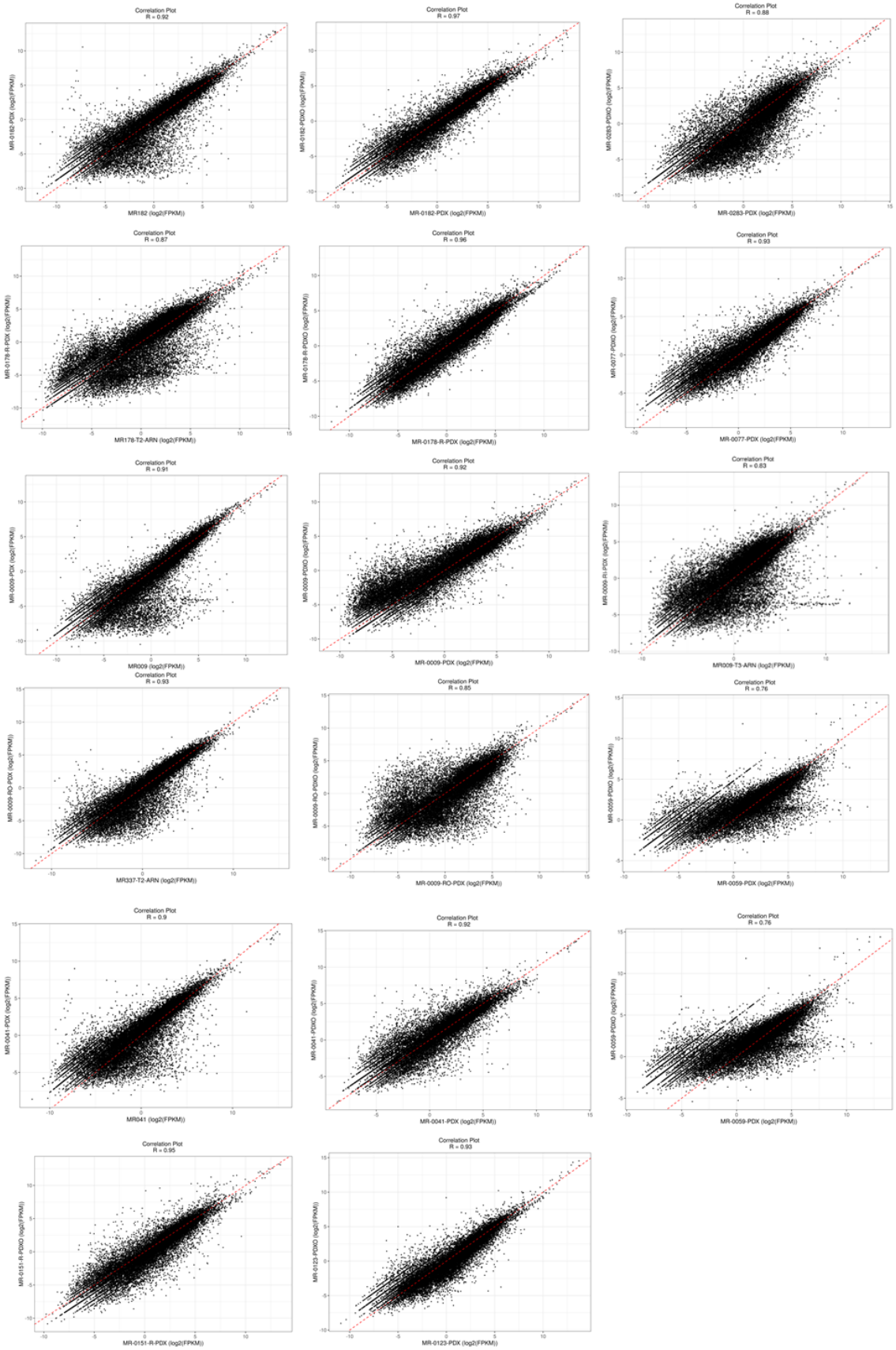

Supplementary figure 7

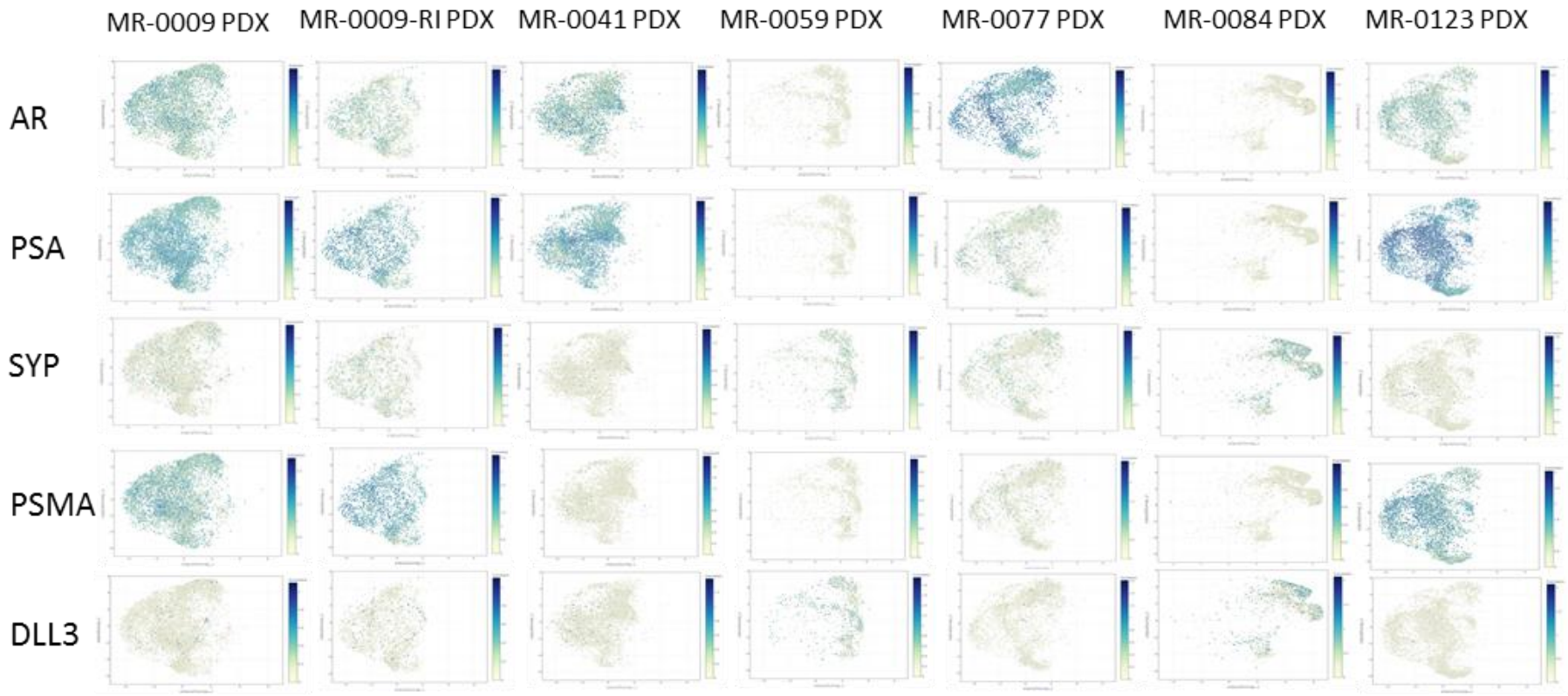

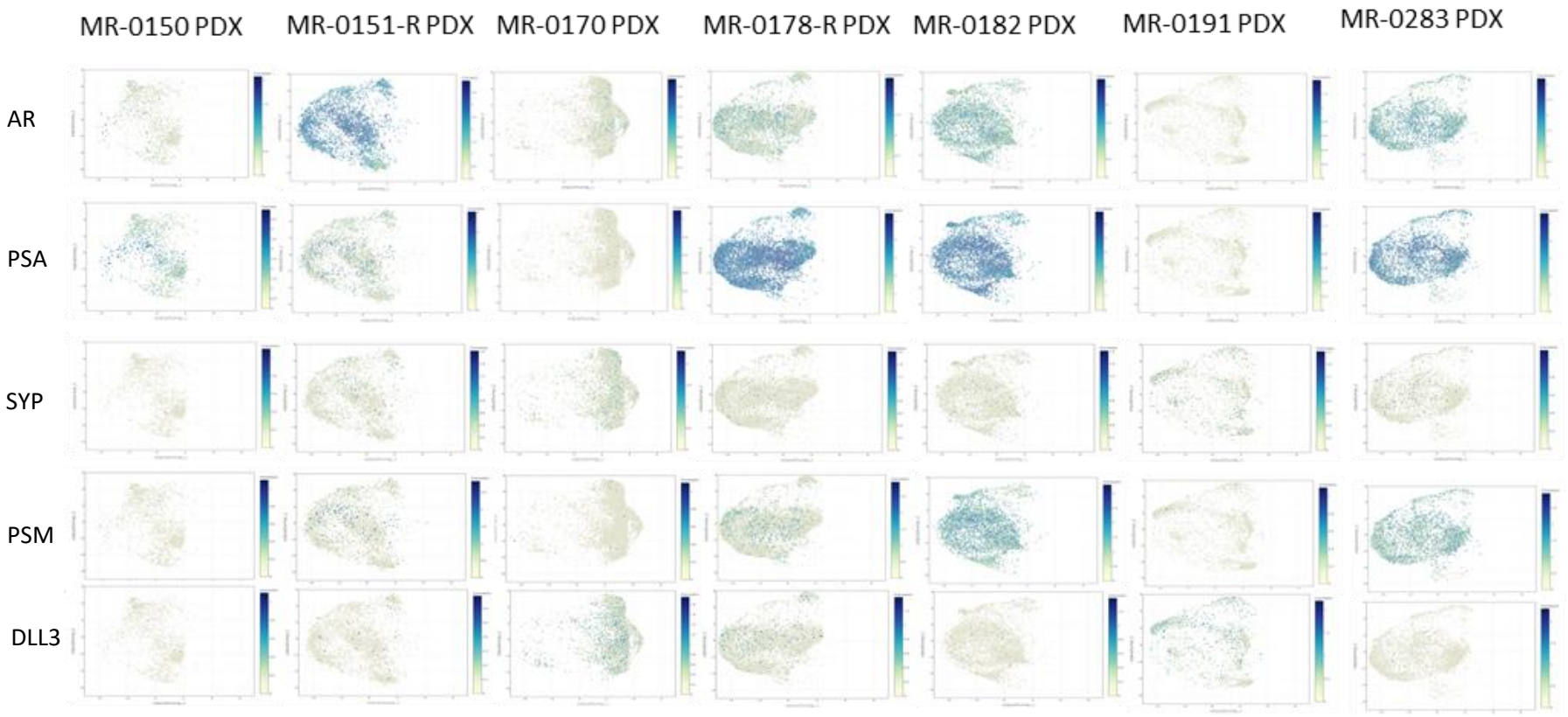
MR-0150 PDX
MR-0151-R PDX
MR-0170 PDX
MR-0178-R PDX
MR-0182 PDX
MR-0191 PDX
MR-0283 PDX
AR
PSA
SYP
PSM
DLL3

Supplementary figure 8

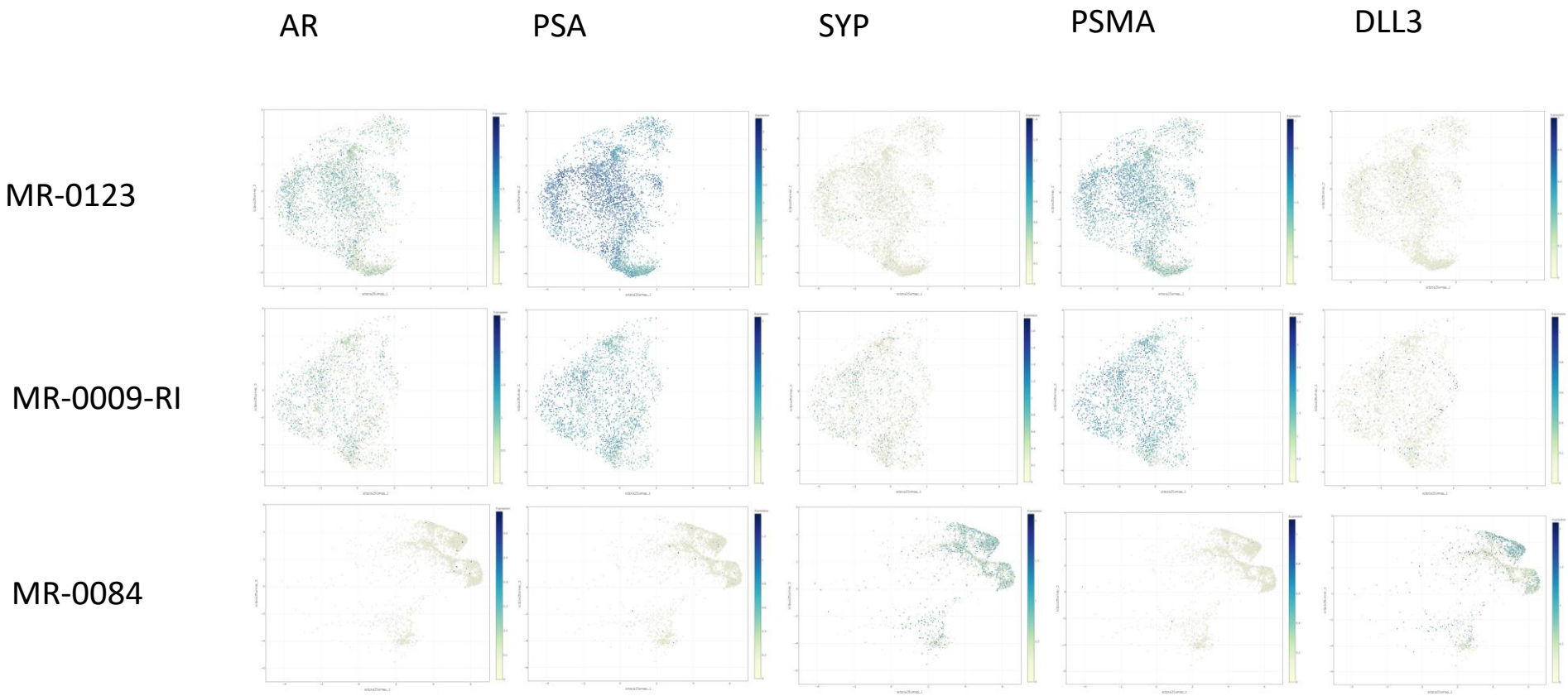

7. Supplementary methods

Patient samples

All PCa fresh tumor biopsy specimens were collected prospectively from the MATCH- R clinical trial (NCT0251782). MATCH-R is a prospective, institutional study ongoing since 2015 at Gustave Roussy to identify molecular mechanisms of acquired resistance to therapies[19]. Patients underwent biopsy at diagnosis and later when the disease develops resistance. All specimens were obtained with consent. (ANSM 141022B-12 and human ethics committee Ile de France III 2014-A01147-40). Clinicopathological features of each patient included in the current analyses are presented in **Table 1**. Tissue viability and tumor content were assessed by haematoxylin and eosin (H&E) staining by dedicated pathologist. Tumor samples were transported to INSERM U981 laboratory in transport medium (Roswell Park Memorial Institute (RPMI) 1640 medium (Life technologies, California, USA) supplemented with 10% (vol/vol) fetal calf serum, 100 UI/ml penicillin, 100 µg/ml streptomycine (Gibco).

Development of patients-derived xenografts (PDX)

All animal procedures and studies were performed in accordance with the approved guidelines for animal experimentation by the ethics committee at University Paris Sud (CEEA 26, Project 2014_055_2790) following EU regulation. Animals were housed under pathogen-free conditions with food and water ad libitum. After 1 to 12 hours following the patient biopsy, fresh tumors fragments were implanted under the renal capsule of 6 to 8-week-old male NOD scid gamma (NSG) mice obtained from Charles River Laboratories. A testosterone pellet of 10 mg (sigma, T1500) was added under the neck of mice. Mice were monitored at least once a week for signs of tumor growth. If grafts were observed to increase in volume, grafts tissues were dissected from the kidneys using a sterile scalpel blade. Grafts were then transferred to the sub-cutaneous site of host mice to allow external monitoring of tumor size using calipers (Passage P0). Over

time, subcutaneous grafts were then transferred to four new host mice. Once tumors reached a volume of 750-1000 mm^3, they were re-grafted directly into four new mice. This occurred between generations 0-12 for each PDX. After the first engraftment, the tumor was implanted subcutaneously on the flank of the mice when the tumors reached a volume of 750 to 1000 mm^3. PDXs were screened for lymphoma using immunohistochemistry with a combination of markers to confirm the phenotype of human prostate epithelial cells (AR, PSA, and CK) and exclude the presence of lymphoma (CD45).

***In vivo* drug response studies**

For each PDX model, PDXs were established subcutaneously (1 graft/mouse) in nude or NSG mice (from Charles River) until tumor volume reached a volume of 80-200 mm^3. Then, they were randomized to be allocated to treatment and vehicle groups. Mice were treated with enzalutamide, 10 or 60 mg/kg, oral gavage QD (5% chromophore/Phosphate Buffer Saline) 5 doses/week or with olaparib, 50 or 100 mg/kg IP QD (15% captisol/Phosphate Buffer Saline) or with Docetaxel 20 mg/kg 3 doses/week (Phosphate Buffer Saline) or with Carboplatin 50 mg/kg once a week (Phosphate Buffer Saline). Tumor volume was measured with calipers twice weekly throughout the treatment period. In some cases, tumor volume reached the maximum ethical limit of 1000 mm^3 during the treatment period and tumors were harvested earlier to comply with animal ethics approvals.

Organoids development

Fresh harvested PDX tissue were placed in media DMEM (Invitrogen) with GlutaMAX (1×, Invitrogen), 100 U/ml penicillin, 100 µg/ml streptomycin (Gibco). Tissue samples were dissociated by mechanical dissection (by using scalpel and pipetting), trimmed of excess connective tissue, finely minced with scalpels and digested using Collagenase

type II (Thermo Fisher Scientific, 17101-015) mix in DMEM/F-12, GlutaMAX Supplement (Thermo Fisher Scientific,31331028) containing 10 mM HEPES (1M) (Thermo Fisher Scientific, 15630056), 1% of Penicillin-Streptomycin (10,000 U/mL) (Thermo Fisher Scientific, 5140122) and 10 µM of Y-27632 dihydrochloride Rock inhibitor (AbMole BioScience, M1817) at 37 °C for 30-45 min. After tissue digestion, DMEM media containing 10% FBS was added to the suspension to inactivate collagenase IV and the mixture was centrifuged at 300 rcf for 5 min. The cells were individually separated into single cells or a cluster of 2 or 3 cells using the TrypLE™ Express Enzyme (1X), phenol red (Thermo Fisher Scientific, 12605036) and 10 µM of Rock inhibitor for 5 min. The cells were then washed twice with DMEM media containing 10% FBS and centrifuge at 300 rcf for 5 min.

The pellet was resuspended with prostate-specific culture media composed of Advanced DMEM/F-12 (Dulbecco's Modified Eagle Medium/Nutrient Mixture F-12) containing 10 µM Y-27632 dihydrochloride Rock inhibitor, 1X B27 supplement serum free (Thermo Fisher Scientific, 17504044), 10 mM Nicotinamide (Sigma-Aldrich, N0636), 500 ng/ml Recombinant human R-spondin-1 (PeproTech, 120-38), 100 ng/ml Recombinant human Noggin (PeproTech, 120-10C), 1.25 mM N-acetyl-cysteine (Sigma-Aldrich, A9165), 10 µM SB 202190 monohydrochloride hydrate (Sigma-Aldrich, S7076), 500 nM A83-01 (Tocris, 2939), 1 nM DHT (Sigma-Aldrich, A8380), 5 ng/mL Animal-Free Recombinant Human EGF (PeproTech, AF-100-15), 5 ng/mL Recombinant Human FGF-basic (PeproTech, 100-18B), 10 ng/ml Recombinant Human FGF10 (PeproTech, 100-26), 1 µM Prostaglandin E2 (Tocris, 2296)[34].

The cells were then seeded in low attachment plates coated with Poly (2-hydroxyethyl methacrylate) at a final concentration of 5 mg/ml (PolyHema) (Santa Cruz, SC-253284). The prostate-specific culture media was added every 2 or 3 days. The organoids obtained were then passaged after 14 days of culture.

To develop PDO, the protocol followed the same steps described for PDXO establishment with few modifications regarding the enzymatic digestion: Collagenase type II was used for 30 minutes only at 37 °C and the separation into single cells with TrypLE™ Express Enzyme (1X) was performed for 5 minutes only.

Drug screening with PCa organoids

The drug screening was performed using 96 wells plates (Nunc™ Edge™ 96-Well, Nunclon Delta-Treated, Flat-Bottom Microplate, Thermo Fisher Scientific, 167425) coated with PohyHema. The cells were added to each well at the density of 5000 cells per well. After cell seeding, plates were shaken for 2 min, incubated for 1 h at room temperature and subsequently transferred to a 37 °C incubator with 95% humidity and 5% CO2. Seven days after cell seeding, the drugs were added and the cell viability was assessed with the CellTiter-Glo (Promega, G7573) after 14 days of culture. The CellTiter-Glo 3D assay was used to measure ATP levels as a proxy for cell viability. The cell viability readout was performed according to manufacturer's instructions using the automation equipment. We used the following approach to define the drugs concentration. Drug concentrations ranged from 10nM to 1000 µM depending on the individual properties of the drug. The dose for the targeted agents have been selected to capture Cmax (human serum level) values. The dose for chemotherapy were derived from the clinical dosage recommendations, one log above and two log below of the assumed average body surface area of 1.8 m^2 based on the data available in the literature. Within the selected ranges, we defined several levels of sensitivity or resistance to the drug based on the response to the drug tested. A response was defined when at least 50% cell mortality was achieved compared to the control. We defined the concentration associated with resistance as the concentration 10-fold above the Cmax and the concentration associated with sensitivity as the concentration of 10-fold below the Cmax for intravenous drugs or in the case of drug associated with an equilibrium plateau (such as oral drugs or monoclonal antibodies) as the minimal

concentration observed just before the next dosing at equilibrium. Finally, a concentration of hypersensitivity was defined as the concentration 2 log below the Cmax.

A chemogram was provided for each PDXO/PDO tested. IC50 (Half-maximal inhibitory concentration) was calculated as the concentration needed to induce cell death of at least 50% of the tumor cells. Four categories of were defined: Drug resistance: IC50 > 10 x Cmax; Potential resistance: Cmax < IC50 <10 x Cmax; Potential sensitivity: Concentration associated with sensitivity < IC50 <Cmax; Sensitivity: concentration associated with hypersensitivity < IC50 < concentration associated with sensitivity.

The drug panel was compiled based on demonstrated or potential activity against PCa and included: Enzalutamide (ARPI, MedChemExpress, HY-70002) at final concentrations of: 2.1; 32 and 215µmol/L. Docetaxel (TAXOTERE 160 mg/8 ml, Sanofi, France) at final concentration of: 50; 500, 5000 and 50 000 nmol/L. GSK343 (Histone Methyltransferase inhibitor, Selleckchem, S7164) at final concentration of: 1; 5; 10 and 50 µmol/L. Carboplatin 10 mg/ml (chemotherapy, Accord Healthcare) at final concentration of: 1; 10; 100 and 1000 mmol/L. Olaparib (PARP inhibitor, MedChemExpress, HY-10162) at final concentration of: 10; 16; 32 µmol/L. Everolimus (mTOR1 inhibitor, MedChemExpress, HY-10218) at final concentration of: 10 and 100 nmol/L. Dabrafenib (BRAF inhibitor, Selleckchem, S2807) at final concentration of: 200; 2000 and 20 000 nmol/L. Alpelisib (PI3Kα inhibitor, MedChemExpress, HY-15244) at final concentration of: 0.9; 9 and 90 µM. Trametinib (dimethylsulfoxyde) 0.5 mg (MEKINIST) (MEK inhibitor) at final concentration of: 20; 50 and 162 nmol/L. Palbociclib (IBRANCE) (Aromatase inhibitor) at final concentration of: 170 and 348 nmol/L.

All of these drugs are diluted in Dimethyl sulfoxide (DMSO, Sigma-Aldrich, D4540). The DMSO was used as positive [0.05%] and negative [10%] control conditions in this drug screening.

Immunohistochemistry

Patient specimens and PDXs were fixed using 4% paraformaldehyde for 1 to 4 hours at room temperature. The organoids were fixed using 4% paraformaldehyde for 45 min at room temperature. Then, samples were sectioned into 3 µM serial sections. All tissues were stained using H&E for pathological assessment. Immunohistochemistry was performed on deparaffinized FFPE sections (xenograft or patient tissue) using Ventana Discovery ULTRA by Roche. Heat-mediated antigen retrieval was performed using the Bond Epitope Retrieval solution (Citrate at Ph 6, Citrate at Ph 8 or EDTA at pH9). The following antibodies and conditions were used for human and PDX samples: PSA/KLK3(ER-PR8) (Roche, 07239327001); AR (D6F11) XP® Rabbit mAb (1:100, Cell Signaling, 5153S); SYP/Synaptophysin (DAK-A3) (1:200, Roche, M731501-2). For PDXO, the following antibodies were used: PSA/KLK3 (D11E1) XP® Rabbit mAb (1:2000, Cell Signaling, 2475); AR (N-20) (1:200, Santa Cruz, sc-816); SYP/Synaptophysin (D-4) (1:2000, Santa Cruz, sc-17750).

Sequencing analysis and bioinformatics

Methods for DNA and RNA extraction, whole exome and RNA sequencing, tissue preparation for ScRNA-seq and bioinformatics analysis are described in the supplementary methods.

Statistical analysis

GraphPad Prism 7.0 software (GraphPad Software, California, United States of America) was used for all analyses. The take rate of different sources of tissues or different phenotypes were compared using a chi-squared test. Experiments were not blinded. For *in vivo* experiments, all data are expressed as mean +/- standard of the mean (SEM). When comparisons were performed, tumor volume between treatment arms were compared using two-way ANOVA with Tukey's multiple comparison correction.

Statistical significance was set at p < 0/05. The *in vivo* response was performed using the tumor growth inhibition (ΔT/ΔC value). Because tumors were measurable at the start of therapy, the initial tumor burden was taken into account in the calculation of the tumor growth inhibition (ΔT/ΔC value): ΔT/ΔC (%) = [(median TDayY - median TDayX)/(median CDayY - median CDayX)] x 100 (where DayY is the day of evaluation, and DayX is the day of initiation of therapy for treated [T] and control [C] tumor volumes). Resistance was defined as ΔT/ΔC (%) ≥ 50; Potential resistance as 50< ΔT/ΔC (%) > 30; Potential sensitivity as 30 < I ΔT/ΔC (%) >10 and sensitivity as ΔT/ΔC (%) ≤10.

Whole exome sequencing

DNA extraction and whole exome sequencing

DNA extraction from patient samples, PDX (from early passage P0 and from passage 3 to 5) and PDXOs were performed using DNeasy Blood and Tissue Kit (QIAGEN). A total of 200 ng of genomic DNA was sheared with the Covaris E220 system (LGC Genomics / Kbioscience). DNA fragments were end-repaired, extended with an 'A' base on the 3' end, ligated with paired-end adaptors with the Bravo Platform (Agilent) and amplified (ten cycles). Exome-containing adaptor-ligated libraries were hybridized for 40 h with biotinylated oligo RNA baits using SureSelect Clinical Research 2 (Agilent), and enriched with streptavidin-conjugated magnetic beads. The final libraries were indexed, pooled and sequenced using the onboard cluster method, as paired-end sequencing (2x100 bp reads) on Illumina NovaSeq-6000 sequencer at Gustave Roussy.

Sequence alignment and variant calling

Base calling was performed using the Real-Time Analysis software sequence pipeline (2.7.7) from Illumina with default parameters. Raw reads were aligned to the human hg38/GRCh38.p7 and the mouse mm10 genomes using the Burrows-Wheeler Aligner (BWA)[35]. Reads were classified depending on their species of origin (graft or host) with XenofilteR[36]. Only reads corresponding to the human species were considered for the rest of the analysis. Duplicated reads were removed using Sambamba[37]. Variant calling

of single nucleotide variants (SNVs) and small insertions/deletions (indels) was performed using the Broad Institute's GATK[38] Haplotype Caller GVCF tool (3.7) for germline variants and MuTect2[39] (2.0, --max_alt_alleles_in_normal_count = 2; --max_alt_allele_in_normal_fraction = 0.04) for somatic variants. For the 3 samples of MR_0077, no matched normal counterpart was available hence somatic variants were called against a panel of normal samples. Ensembl's Variant Effect Predictor[40] (VEP, release 99) was used to annotate variants with respect to functional consequences (type of mutation and prediction of the functional impact on the protein by SIFT5.2.2 and PolyPhen 2.2.2) and frequencies in public (dbSNP153, GnomAD 2.1) and in-house databases.

Somatic variant filtering

To keep only reliable somatic variants, we applied the following post-filtering steps: Coverage ≥ 8 in the tumor and matched normal sample. QSS score ≥ 20 (the average base quality of variant bases). Variant allele fraction in the tumor (VAFT) ≥ 0.05 with ≥ 3 mutated reads, variant allele fraction in the normal sample (VAFN) < 0.04 with < 2 mutated reads and VAFN < VAFT/5.

Located in coding regions

For the three samples of MR_0077, no matched normal counterpart was available hence we excluded referenced germline variants with a frequency ≥ 1e-5 in GnomAD (global AF) or a frequency ≥ 0.01 in IntegraGen proprietary database. We highlighted genes belonging to the list of 120 prostate cancer drivers defined by Armenia et al.[41] and 5 genes to defined the MSI status. For patients with multiple samples, the VAF of each variant detected by MuTect2 in one sample was calculated in all other samples using BamReadCount (https://github.com). Mutations detected by MuTect2 in at least one sample were considered to be also present in any sample from the same patient with a variant allele fraction (VAF) ≥ 0.05.

Copy-number analysis

We used two complementary approaches to reconstruct the copy-number profiles of the tumors:

*** Copy-number analysis using genotype data**

We identified germline single-nucleotide polymorphisms (SNPs) in each sample and we calculated the coverage log-ratio (LRR) and B allele frequency (BAF) at each SNP site. Genomic profiles were divided into homogeneous segments by applying the circular binary segmentation algorithm, as implemented in the Bioconductor package DNAcopy[42], to both LRR and BAF values. We then used the Genome Alteration Print (GAP) method[43] to determine the ploidy of each sample, the level of contamination with normal cells and the allele-specific copy number of each segment. Ploidy was estimated as the median copy-number across the genome. Chromosome aberrations were then defined using empirically determined thresholds as follows: gain, copy number > ploidy + 0.5; loss, copy number < ploidy – 0.5. We considered a segment to have undergone loss of heterozygosity (LOH) when the copy number of the minor allele was equal to 0.

*** Copy-number analysis based on coverage**

We calculated the coverage log ratio in each bait of the exon capture kit between the tumor and matched normal sample (or panel of normals for samples of MR_0077). Log-ratio profiles were then smoothed using the circular binary segmentation algorithm as implemented in the Bioconductor package DNAcopy [41]. The most frequent smoothed value was considered to be the zero level of each sample. Segments with a smoothed log ratio above zero +0.15 or below zero -0.15 were considered to have gains and deletions, respectively. High-level amplification and homozygous deletion thresholds were defined as the mean +5 s.d. of smoothed log ratios in regions with gains and deletions, respectively. This approach does not provide absolute copy-number estimates but has a higher definition than the previous one as there are more exon

capture baits than germline polymorphisms. It was used to characterize focal aberrations like high-level amplifications and homozygous deletions.

RNA seq analysis

Data processing mRNA was extracted from organoids and PDXs using phenol chloroform method (Sigma, TRI reagent ref 93289). The RNA integrity (RNA Integrity Score ≥ 7.0) was checked on the Agilent 2100 Bioanalyzer (Agilent) and quantity was determined using Qubit (Invitrogen). SureSelect Automated Strand Specific RNA Library Preparation Kit was used according to manufacturer's instructions with the Bravo Platform. Briefly, 50 to 200 ng of total RNA sample was used for poly-A mRNA selection using oligo(dT) beads and subjected to thermal mRNA fragmentation. The fragmented mRNA samples were subjected to cDNA synthesis and were further converted into double stranded DNA using the reagents supplied in the kit, and the resulting dsDNA was used for library preparation. The final libraries were bar-coded, purified, pooled together in equal concentrations and subjected to paired-end sequencing on Novaseq 6000 sequencer (Illumina) at Gustave Roussy. Sequence alignment and quantification of gene expression are processed as following. Raw reads were aligned to the human hg38/GRCh38.p7 and the mouse mm10 genomes using STAR. Reads were classified depending on their species of origin (graft or host) with XenofilteR tool[36]. Fusion Detection in RNA-seq data were initially detected by STAR-Fusion[44] and FusionCatcher (https://github.com) were validated and annotated using FusionInspector (https://github.com).

Quantification of gene expression

STAR was used to obtain the number of reads associated to each gene in the Gencode v26 annotation (restricted to protein-coding genes, antisense and lincRNAs). Raw counts for each sample were imported into R statistical software. Extracted count matrix was normalized for library size and coding length of genes to compute FPKM (Fragments per kilo base of transcript per million mapped fragments) expression levels.

Unsupervised analysis

The Bioconductor edgeR package was used to import raw counts into R statistical software, and compute normalized log2(CPM) (counts per millions of mapped reads) using the TMM (weighted trimmed mean of M-values) as normalization procedure. The normalized expression matrix from the 5000 most variant genes (based on standard deviation) was used to classify the samples according to their gene expression patterns using principal component analysis (PCA), hierarchical clustering and consensus clustering. PCA was performed by FactoMineR::PCA function with "ncp = 10, scale.unit = FALSE" parameters. Hierarchical clustering was performed by stats::hclust function (with Dispearson distance and ward.D method). Subsequently, for visualizing the expression patterns, the CPM expression were scaled for plotting onto a heatmap. Scatter plots of corresponding human samples, PDX and organoids samples were also plotted and the Pearson correlation was calculated to assess the similarity of the transcriptomes.

Differential expression analysis

The Bioconductor edgeR package was used to import raw counts into R software. Differential expression analysis was performed using the Bioconductor limma package and the voom transformation. To improve the statistical power of the analysis, only genes expressed in at least one sample (FPKM ≥ 0.1) were considered. A qval threshold of ≤ 0.05 and a fold change ≤ 1.2 were used to define differentially expressed genes.

Pathway enrichment analysis – GSEA

Gene list from the differential analysis was ordered by decreasing log2(fold change). Gene set enrichment analysis was performed by clusterProfiler::GSEA function using the fgsea algorithm. Gene sets from MSigDB v7.4 database were selected among the Hallmark classes, keeping only gene sets defined by 10-500 genes.

Androgen receptor and neuroendocrine prostate cancer transcriptomic scores

One AR score and one NEPC score were calculated from the RNA-seq data. The AR score was calculated by calculating the Pearson correlation score between the patient

samples and the reference sample (a V16D prostate cancer cell line[45] treated with R1881 (testosterone) (AR_R1881 score) on the expression of the 30 genes from Beltran et al. 2016[20]. The NEPC score was calculated by averaging the expression of the 13 neuroendocrine patient samples, as a reference, for each of the 70 genes from Beltran et al. 2016[20]. Then, for each sample, the Pearson correlation score was calculated between each patient sample and the reference.

Single-cell RNA transcriptome analysis

Tissue dissociation

Single cells were isolated from frozen vials with DMEM, 10% DMSO and 1% penicillin/streptomycine using the tumor dissociation kit human (MACS Milteny biotec, 130-095-929) and Mouse cell depletion kit (MACS Milteny biotec, 130-104-694). Tissue were placed in gentleMACS™ C Tubes (MACS Milteny biotec, 130-096-334) with media without EDTA and magnesium and dissociation kit Enzyme. After the completed dissociation, the cells suspension was filtered by MACS Smart Strainers (100 µM) then MACS Smart Strainers (30 µM) and centrifuged at 300 rcf for 10 minutes. The mouse cell depletion kit was adding to the cells for 15 min at 4 °C then the human cells were isolated with autoMACS® Pro Separator (MACS Milteny biotec). The single cells isolated were place on media without EDTA and magnesium on ice at 0.7 to 1.2 million cells/ml.

Single-cell RNA-sequencing

scRNA-seq for dissociated PDXs was performed using 10X genomics technology. 3' Single-cell RNA-seq: Sample preparation was done at room temperature. Single-cell suspensions were loaded into a Chromium Single Cell Chip (10x Genomics) according to the manufacturer's instructions for co-encapsulation with barcoded Gel Beads at a target capture rate of ~10,000 individual cells per sample. Captured mRNAs were barcoded during cDNA synthesis using the Chromium Next GEM Single Cell 3' GEM, Library & Gel Bead Kit v3.1 (10X Genomics) according to the manufacturer's

instructions. All samples were processed simultaneously with the Chromium Controller (10X Genomics) and the resulting libraries were prepared in parallel in a single batch. We pooled all of the libraries for sequencing in a single SP Illumina flow cell. All of the libraries were sequenced with an 8-base index read, a 28-base Read1 containing cell-identifying barcodes and unique molecular identifiers (UMIs), and a 91-base Read2 containing transcript sequences on an Illumina NovaSeq 6000.

Quality control, Pseudo-mapping and quantification

Raw BCL-files were demultiplexed and converted to Fastq format using bcl2fastq (Illumina). Human reads were isolated from mouse reads using the Xenome tool gossamer patch (ref: https://github.com/data61/gossamer). Seqkit was used to match RNA to barcodes-UMI. Reads quality control was performed using fastqc and assignment to the expected genome species evaluated with fastq-screen. Reads were pseudo-mapped to the Ensembl reference transcriptome v99 corresponding to the GRCh38 homosapiens build with kallisto using its « bus » subcommand and parameters corresponding to the 10X Chromium 3′ scRNA-seq v3 chemistry. The index was made with the kb-python wrapper of kallisto. Barcode correction using white list provided by the manufacturer (10XGenomics) and gene-based reads quantification was performed with BUStools[46].

Quality control data on each sample

Cell barcode by symbol count table were loaded in R (v3.6.3) using the BUSpaRse package (R package version 1.4.1, https://github.com/BUStools/BUSpaRse). To call real cells from empty droplets, we used the emptyDrops[47] function from the dropletUtils[48] package, which assesses whether the RNA content associated with a cell barcode is significantly distinct from the ambient background RNA present within each sample. Barcodes with p-value < 0.001 (Benjamini–Hochberg-corrected) or 1000 UMI (retain parameter) were considered as legitimate cells for further analysis. The count matrix was filtered to exclude genes detected in less than 5 cells, cells with less than 1000

UMIs or less than 200 detected genes, as well as cells with mitochondrial transcripts proportion higher than 20%. The proportion of ribosomal gene counts and the proportion of mechanical stress-response gene counts were also estimated but not used to filter cells. Cell cycle scoring of each cell was performed using two methods: the CellCycleScoring function from the Seurat package[49], and the cyclone function from Scran. Barcodes corresponding to doublet cells were identified and discarded using the union of two methods. First, scDblFinder using default parameters except for minClusSize (set to the minimum of 50, or the number of cells divided by 50) and dbr set to (number of cells)^2 / 1E+05. Second, scds with its hybrid method using default parameters. We manually verified that the cells identified as doublets did not systematically correspond to cells in G2M phase.

Merge Analysis

Seurat was applied for further data processing. Each dataset was normalized independently. The SCTransform normalization method[50] was used to normalize, scale, select 3000 Highly Variable Genes and regress out bias factors (number of detected genes, proportion of mitochondrial transcripts, proportion of ribosomal transcripts, and proportion of mechanical stress response transcripts). Then data were merged using the merge function from Seurat[48]. A common dimension reduction was performed by Principal Component Analysis (PCA). The number of PCA dimensions to keep for further analysis was evaluated by assessing a range of reduced PCA spaces using 3 to 49 dimensions, with a step of 2. For each generated PCA space, Louvain clustering of cells was performed using a range of values for the resolution parameter from 0.1 to 1.2 with a step of 0.1. The optimal space was manually evaluated as the one combination of kept dimensions and clustering resolution resolving the best structure (clusters homogeneity and compacity) in a Uniform Manifold Approximation and Projection space (UMAP). Additionally, we used the clustree method to assess if the selected optimal space corresponded to a relatively stable position in the clustering results tested for these dimensions / resolution combinations.

Correlations scores

Spearman and Pearson correlations were calculated for each cell. Two PDXs for which phenotype was known (MR084-P4 for Neuroendocrine phenotype and MR041-P2 for luminal adenocarcinoma) were used as a reference. The normalized expression means of the genes from the signatures of each phenotype (signature genes from Beltran et al[20]) was compared to the normalized expression of these same genes for each cell (reference cells included). Only the results with a p-value greater than 5% have been kept.

8. References

1. Bray F, Ferlay J, Soerjomataram I, Siegel RL, Torre LA, Jemal A. Global cancer statistics 2018: GLOBOCAN estimates of incidence and mortality worldwide for 36 cancers in 185 countries. CA Cancer J Clin. 2018;68(6):394-424.

2. Ferlay J, Colombet M, Soerjomataram I, Dyba T, Randi G, Bettio M, et al. Cancer incidence and mortality patterns in Europe: Estimates for 40 countries and 25 major cancers in 2018. Eur J Cancer. 2018;103:356-387.

3. Gillessen S, Armstrong A, Attard G, Beer TM, Beltran H, Bjartell A, et al. Management of Patients with Advanced Prostate Cancer: Report from the Advanced Prostate Cancer Consensus Conference 2021. Eur Urol. 2022 Jul;82(1):115-141.

4. Antonarakis ES, Isaacsson Velho P, Fu W, Wang H, Agarwal N, Sacristan Santos V, et al. CDK12-Altered Prostate Cancer: Clinical Features and Therapeutic Outcomes to Standard Systemic Therapies, Poly (ADP-Ribose) Polymerase Inhibitors, and PD-1 Inhibitors. JCO Precis Oncol. 2020;4:370-381.

5. Schweizer MT, Ha G, Gulati R, Brown LC, McKay RR, Dorff T, et al. CDK12-Mutated Prostate Cancer: Clinical Outcomes With Standard Therapies and Immune Checkpoint Blockade. JCO Precis Oncol. 2020;4:382-392.

6. Decker B, Karyadi DM, Davis BW, Karlins E, Tillmans LS, Stanford JL, et al. Biallelic BRCA2 Mutations Shape the Somatic Mutational Landscape of Aggressive Prostate Tumors. Am J Hum Genet. 2016;98(5):818-829.

7. Sokol ES, Jin DX, Fine A, Trabucco SE, Maund S, Frampton G, et al. PARP Inhibitor Insensitivity to BRCA1/2 Monoallelic Mutations in Microsatellite Instability-High Cancers. JCO Precis Oncol. 2022;6:e2100531.

8. Conteduca V, Oromendia C, Eng KW, Bareja R, Sigouros M, Molina A, et al. Clinical features of neuroendocrine prostate cancer. Eur J Cancer. 2019;121:7-18.

9. Nguyen B, Mota JM, Nandakumar S, Stopsack KH, Weg E, Rathkopf D, et al. Pan-cancer Analysis of CDK12 Alterations Identifies a Subset of Prostate Cancers with Distinct Genomic and Clinical Characteristics. Eur Urol. 2020;78(5):671-679.

10. Castro E, Goh C, Olmos D, Saunders E, Leongamornlert D, Tymrakiewicz M, et al. Germline BRCA mutations are associated with higher risk of nodal involvement, distant metastasis, and poor survival outcomes in prostate cancer. J Clin Oncol. 2013;31(14):1748-57.

11. Navone NM, van Weerden WM, Vessella RL, Williams ED, Wang Y, Isaacs JT, et al. Movember GAP1 PDX project: An international collection of serially transplantable prostate cancer patient-derived xenograft (PDX) models. Prostate. 2018;78(16):1262-1282.

12. Risbridger, G.P., Clark, A.K., Porter, L.H. et al. The MURAL collection of prostate cancer patient-derived xenografts enables discovery through preclinical models of uro-oncology. Nat Commun 2021;12, 5049.

13. Hidalgo M, Amant F, Biankin AV, Budinská E, Byrne AT, Caldas C,et al. Patient-derived xenograft models: an emerging platform for translational cancer research. Cancer Discov. 2014;4(9):998-1013.

14. Drost J, Clevers H. Organoids in cancer research. Nat Rev Cancer. 2018;18(7):407-418.

15. Fatehullah A, Tan SH, Barker N. Organoids as an *in vitro* model of human development and disease. Nat Cell Biol. 2016;18(3):246-54.

16. Beshiri ML, Tice CM, Tran C, Nguyen HM, Sowalsky AG, Agarwal S, et al. A PDX/Organoid Biobank of Advanced Prostate Cancers Captures Genomic and Phenotypic Heterogeneity for Disease Modeling and Therapeutic Screening. Clin Cancer Res 2018;24(17):4332-45.

17. Gao D, Vela I, Sboner A, Iaquinta PJ, Karthaus WR, Gopalan A, et al. Organoid cultures derived from patients with advanced prostate cancer. Cell 2014;159(1):176-87.

18. Puca L, Bareja R, Prandi D, Shaw R, Benelli M, Karthaus WR, et al. Patient derived organoids to model rare prostate cancer phenotypes. Nat Commun. 2018;9(1):2404.

19. Recondo G, Mahjoubi L, Maillard A, Loriot Y, Bigot L, Facchinetti F, et al. Feasibility and first reports of the MATCH-R repeated biopsy trial at Gustave Roussy. NPJ Precis Oncol. 2020;4:27.

20. Beltran H, Prandi D, Mosquera JM, Benelli M, Puca L, Cyrta J, et al. Divergent clonal evolution of castration-resistant neuroendocrine prostate cancer. Nat Med. 2016;22(3):298-305.

21. Faugeroux V, Pailler E, Oulhen M, Deas O, Brulle-Soumare L, Hervieu C, et al. Genetic characterization of a unique neuroendocrine transdifferentiation prostate circulating tumor cell-derived eXplant model. Nat Commun. 2020;11(1):1884.

22. Zou M, Toivanen R, Mitrofanova A, Floch N, Hayati S, Sun Y, et al. Transdifferentiation as a Mechanism of Treatment Resistance in a Mouse Model of Castration-Resistant Prostate Cancer. Cancer Discov. 2017 Jul;7(7):736-749.

23. Davies A, Nouruzi S, Ganguli D, Namekawa T, Thaper D, Linder S, ET AL. An androgen receptor switch underlies lineage infidelity in treatment-resistant prostate cancer. Nat Cell Biol. 2021 Sep;23(9):1023-1034.

24. Puca L, Gavyert K, Sailer V, Conteduca V, Dardenne E, Sigouros M, et al. Delta-like protein 3 expression and therapeutic targeting in neuroendocrine prostate cancer. Sci Transl Med. 2019;11(484):eaav0891.

25. Korsen JA, Gutierrez JA, Tully KM, Carter LM, Samuels ZV, Khitrov S, et al. Delta-like ligand 3-targeted radioimmunotherapy for neuroendocrine prostate cancer. Proc Natl Acad Sci U S A. 2022 ;119(27):e2203820119.

26. Hussain M, Mateo J, Fizazi K, Saad F, Shore N, Sandhu S, et al; PROfound Trial Investigators. Survival with Olaparib in Metastatic Castration-Resistant Prostate Cancer. N Engl J Med. 2020 ;383(24):2345-2357.

27. Abida W, Patnaik A, Campbell D, Shapiro J, Bryce AH, McDermott R, et al. Rucaparib in Men With Metastatic Castration-Resistant Prostate Cancer Harboring a BRCA1 or BRCA2 Gene Alteration. J Clin Oncol. 2020;38(32):3763-3772.

28. Wu YM, Cieślik M, Lonigro RJ, Vats P, Reimers MA, Cao X, et al. Inactivation of CDK12 Delineates a Distinct Immunogenic Class of Advanced Prostate Cancer. Cell. 2018 Jun 14;173(7):1770-1782.e14. doi: 10.1016/j.cell.2018.04.034. PMID: 29906450; PMCID: PMC6084431.

29. Uchida T, Wada C, Wang C, et al. Microsatellite instability in prostate cancer. Oncogene. 1995;10(5):1019-1022.

30. Petrylak DP, Loriot Y, Shaffer DR, Braiteh F, Powderly J, Harshman LC, et al. Safety and Clinical Activity of Atezolizumab in Patients with Metastatic Castration-Resistant Prostate Cancer: A Phase I Study. Clin Cancer Res. 2021;27(12):3360-3369.

31. Yao L-C, Aryee K-E, Cheng M, Kaur P, Keck JG, Brehm MA. Creation of PDX-Bearing Humanized Mice to Study Immuno-oncology. Methods Mol Biol. 2019;1953:241-52.

32. Dijkstra KK, Cattaneo CM, Weeber F, Chalabi M, van de Haar J, Fanchi LF, et al. Generation of Tumor-Reactive T Cells by Co-culture of Peripheral Blood Lymphocytes and Tumor Organoids. Cell. 2018;174(6):1586-1598.e12.

33. Sontheimer-Phelps A, Hassell BA, Ingber DE. Modelling cancer in microfluidic human organs-on-chips. Nat Rev Cancer. 2019;19(2):65-81.

34. Drost J, Karthaus WR, Gao D, Driehuis E, Sawyers CL, Chen Y, Clevers H. Organoid culture systems for prostate epithelial and cancer tissue. Nat Protoc. 2016;11(2):347-58.

35. Li H, Durbin R. Fast and accurate short read alignment with Burrows-Wheeler transform. Bioinformatics. 2009;25(14):1754-60.

36. Kluin RJC, Kemper K, Kuilman T, de Ruiter JR, Iyer V, Forment JV, et al. XenofilteR: computational deconvolution of mouse and human reads in tumor xenograft sequence data. BMC Bioinformatics. 2018 ;19(1):366.

37. Tarasov A, Vilella AJ, Cuppen E, Nijman IJ, Prins P. Sambamba: fast processing of NGS alignment formats. Bioinformatics. 2015;31(12):2032-4.

38. Van der Auwera GA, Carneiro MO, Hartl C, Poplin R, Del Angel G, Levy-Moonshine A, et al. From FastQ data to high confidence variant calls: the Genome Analysis Toolkit best practices pipeline. Curr Protoc Bioinformatics. 2013;43(1110):11.10.1-11.10.33.

39. Cibulskis K, Lawrence MS, Carter SL, Sivachenko A, Jaffe D, Sougnez C, Gabriel S, Meyerson M, Lander ES, Getz G. Sensitive detection of somatic point mutations in impure and heterogeneous cancer samples. Nat Biotechnol. 2013;31(3):213-9.

40. McLaren W, Gil L, Hunt SE, Riat HS, Ritchie GR, Thormann A, et al. The Ensembl Variant Effect Predictor. Genome Biol. 2016 ;17(1):122.

41. Armenia J, Wankowicz SAM, Liu D, Gao J, Kundra R, Reznik E, et al. The long tail of oncogenic drivers in prostate cancer. Nat Genet. 2018;50(5):645-651.

42. Venkatraman ES, Olshen AB. A faster circular binary segmentation algorithm for the analysis of array CGH data. Bioinformatics. 2007;23(6):657-63.

43. Popova T, Manié E, Stoppa-Lyonnet D, Rigaill G, Barillot E, Stern MH. GenomeAlteration Print (GAP): a tool to visualize and mine complex cancer genomic profiles obtained by SNP arrays. Genome Biol. 2009;10(11):R128.

44. Haas BJ, Dobin A, Li B, Stransky N, Pochet N, Regev A. Accuracy assessment of fusion transcript detection via read-mapping and *de novo* fusion transcript assembly-based methods. Genome Biol. 2019 ;20(1):213.

45. Toren P, Kim S, Johnson F, Zoubeidi A. Combined AKT and MEK Pathway Blockade in Pre-Clinical Models of Enzalutamide-Resistant Prostate Cancer. PLoS One. 2016 Apr 5;11(4):e0152861.

46. Melsted P, Ntranos V, Pachter L. The barcode, UMI, set format and BUStools. Bioinformatics. 2019 ;35(21):4472-4473.

47. Lun ATL, Riesenfeld S, Andrews T, Dao TP, Gomes T; participants in the 1st Human Cell Atlas Jamboree, Marioni JC. EmptyDrops: distinguishing cells from empty droplets in droplet-based single-cell RNA sequencing data. Genome Biol. 2019;20(1):63.

48. Griffiths JA, Richard AC, Bach K, Lun ATL, Marioni JC. Detection and removal of barcode swapping in single-cell RNA-seq data. Nat Commun. 2018 ;9(1):2667.

49. Butler A, Hoffman P, Smibert P, Papalexi E, Satija R. Integrating single-cell transcriptomic data across different conditions, technologies, and species. Nat Biotechnol. 2018;36(5):411-420.

50. Hafemeister C, Satija R. Normalization and variance stabilization of single-cell RNA-seq data using regularized negative binomial regression. Genome Biol. 2019 ;20(1):296.

OVERALL REFERENCES

OVERALL REFERENCES

1. Sung, H. *et al.* Global cancer statistics 2020: GLOBOCAN estimates of incidence and mortality worldwide for 36 cancers in 185 countries. *CA: a cancer journal for clinicians* **71**, 209–249 (2021).
2. Ferlay, J. *et al.* Cancer incidence and mortality patterns in Europe: Estimates for 40 countries and 25 major cancers in 2018. *European journal of cancer* **103**, 356–387 (2018).
3. Carioli, G. *et al.* European cancer mortality predictions for the year 2020 with a focus on prostate cancer. *Annals of Oncology* **31**, 650–658 (2020).
4. Siegel, D. A., O'Neil, M. E., Richards, T. B., Dowling, N. F. & Weir, H. K. Prostate Cancer Incidence and Survival, by Stage and Race/Ethnicity — United States, 2001–2017. *MMWR Morb. Mortal. Wkly. Rep.* **69**, 1473–1480 (2020).
5. Dong, L., Zieren, R. C., Xue, W., de Reijke, T. M. & Pienta, K. J. Metastatic prostate cancer remains incurable, why? *Asian journal of urology* **6**, 26–41 (2019).
6. Ferlay, J. *et al.* Global Cancer Observatory: Cancer Tomorrow. Lyon, France: International Agency for Research on Cancer, 2018. (2019).
7. Verze, P., Cai, T. & Lorenzetti, S. The role of the prostate in male fertility, health and disease. *Nature Reviews Urology* **13**, 379–386 (2016).
8. Rebello, R. J. *et al.* Prostate cancer. *Nat Rev Dis Primers* **7**, 1–27 (2021).
9. McNeal, J. E. The zonal anatomy of the prostate. *The prostate* **2**, 35–49 (1981).
10. Timms, B. G. Prostate development: a historical perspective. *Differentiation* **76**, 565–577 (2008).
11. Zlotta, A. R. *et al.* Prevalence of prostate cancer on autopsy: cross-sectional study on unscreened Caucasian and Asian men. *Journal of the National Cancer Institute* **105**, 1050–1058 (2013).
12. Abate-Shen, C. & Shen, M. M. Molecular genetics of prostate cancer. *Genes & development* **14**, 2410–2434 (2000).
13. Lamb, A. D., Warren, A. Y. & Neal, D. E. Pre-malignant Disease in the Prostate. in *Pre-Invasive Disease: Pathogenesis and Clinical Management* 467–491 (Springer, 2011).
14. Thompson, I. M. *et al.* Assessing prostate cancer risk: results from the Prostate Cancer Prevention Trial. *Journal of the National Cancer Institute* **98**, 529–534 (2006).
15. D'Amico, A. V. Combined-modality staging for localized adenocarcinoma of the prostate. *Oncology (Williston Park, NY)* **15**, 1049–59 (2001).
16. Loeb, S. *et al.* Overdiagnosis and overtreatment of prostate cancer. *European urology* **65**, 1046–1055 (2014).
17. Parker, C. *et al.* Prostate cancer: ESMO Clinical Practice Guidelines for diagnosis, treatment and follow-up. *Annals of Oncology* **31**, 1119–1134 (2020).

18. Montironi, R. *et al.* Narrative review of prostate cancer grading systems: will the Gleason scores be replaced by the Grade Groups? *Translational Andrology and Urology* **10**, 1530 (2021).

19. Amin, M. B. *et al.* The eighth edition AJCC cancer staging manual: continuing to build a bridge from a population-based to a more "personalized" approach to cancer staging. *CA: a cancer journal for clinicians* **67**, 93–99 (2017).

20. Albertsen, P. C., Hanley, J. A. & Fine, J. 20-year outcomes following conservative management of clinically localized prostate cancer. *Jama* **293**, 2095–2101 (2005).

21. Johansson, J.-E. *et al.* Natural history of early, localized prostate cancer. *Jama* **291**, 2713–2719 (2004).

22. Pound, C. R. *et al.* Natural history of progression after PSA elevation following radical prostatectomy. *Jama* **281**, 1591–1597 (1999).

23. Smith, M. R. *et al.* Natural history of rising serum prostate-specific antigen in men with castrate nonmetastatic prostate cancer. *Journal of Clinical Oncology* **23**, 2918–2925 (2005).

24. Hirst, C. J., Cabrera, C. & Kirby, M. Epidemiology of castration resistant prostate cancer: a longitudinal analysis using a UK primary care database. *Cancer epidemiology* **36**, e349–e353 (2012).

25. Scher, H. I. *et al.* Design and end points of clinical trials for patients with progressive prostate cancer and castrate levels of testosterone: recommendations of the Prostate Cancer Clinical Trials Working Group. *Journal of clinical oncology: official journal of the American Society of Clinical Oncology* **26**, 1148 (2008).

26. Gandaglia, G. *et al.* Distribution of metastatic sites in patients with prostate cancer: a population-based analysis. *The Prostate* **74**, 210–216 (2014).

27. Hess, K. R. *et al.* Metastatic patterns in adenocarcinoma. *Cancer* **106**, 1624–1633 (2006).

28. Nafissi, N. N. *et al.* Evolving Natural History of Metastatic Prostate Cancer. *Cureus* **12**, (2020).

29. Chu, K. C., Tarone, R. E. & Freeman, H. P. Trends in prostate cancer mortality among black men and white men in the United States. *Cancer: Interdisciplinary International Journal of the American Cancer Society* **97**, 1507–1516 (2003).

30. Ryan, C. J., Elkin, E. P., Small, E. J., Duchane, J. & Carroll, P. Reduced incidence of bony metastasis at initial prostate cancer diagnosis: Data from CaPSURE™. in *Urologic Oncology: Seminars and Original Investigations* vol. 24 396–402 (Elsevier, 2006).

31. Kaisary, A. V., Tyrrell, C. J., Peeling, W. B. & Griffiths, K. Comparison of LHRH analogue (Zoladex) with orchiectomy in patients with metastatic prostatic carcinoma. *British journal of urology* **67**, 502–508 (1991).

32. Nesbit, R. M. & Baum, W. C. Endocrine control of prostatic carcinoma: clinical and statistical survey of 1,818 cases. *Journal of the American Medical Association* **143**, 1317–1320 (1950).

33. Murphy, G. P. *et al.* Treatment of newly diagnosed metastatic prostate cancer patients with chemotherapy agents in combination with hormones versus hormones alone. *Cancer* **51**, 1264–1272 (1983).

34. Hussain, M. *et al.* Intermittent (IAD) versus continuous androgen deprivation (CAD) in hormone sensitive metastatic prostate cancer (HSM1PC) patients (pts): Results of S9346 (INT-0162), an international phase III trial. (2012).

35. Ryan, C. J. *et al.* Interim analysis (IA) results of COU-AA-302, a randomized, phase III study of abiraterone acetate (AA) in chemotherapy-naive patients (pts) with metastatic castration-resistant prostate cancer (mCRPC). (2012).

36. Francini, E. *et al.* Impact of new systemic therapies on overall survival of patients with metastatic castration-resistant prostate cancer in a hospital-based registry. *Prostate Cancer and Prostatic Diseases* **22**, 420–427 (2019).

37. Ryan, C. J. *et al.* Androgens and Overall Survival in Patients With Metastatic Castration-resistant Prostate Cancer Treated With Docetaxel. *Clinical Genitourinary Cancer* **18**, 222-229.e2 (2020).

38. Sandhu, S. *et al.* Prostate cancer. *The Lancet* S0140673621009508 (2021) doi:10.1016/S0140-6736(21)00950-8.

39. Zoubeidi, A. & Ghosh, P. M. Celebrating the 80th anniversary of hormone ablation for prostate cancer. *Endocrine-related cancer* **28**, T1–T10 (2021).

40. Fizazi, K. *et al.* Abiraterone plus prednisone added to androgen deprivation therapy and docetaxel in de novo metastatic castration-sensitive prostate cancer (PEACE-1): a multicentre, open-label, randomised, phase 3 study with a 2$\times$ 2 factorial design. *The Lancet* **399**, 1695–1707 (2022).

41. Bul, M. *et al.* Active surveillance for low-risk prostate cancer worldwide: the PRIAS study. *European urology* **63**, 597–603 (2013).

42. Bruinsma, S. M. *et al.* Active surveillance for prostate cancer: a narrative review of clinical guidelines. *Nature Reviews Urology* **13**, 151–167 (2016).

43. Romero-Otero, J. *et al.* Active surveillance for prostate cancer. *International Journal of Urology* **23**, 211–218 (2016).

44. Young, H. H. The early diagnosis and radical cure of carcinoma of the prostate: Being a study of 40 cases and presentation of a radical operation which was carried out in four cases. *The Journal of urology* **167**, 939–946 (2002).

45. Saranchuk, J. W. *et al.* Achieving optimal outcomes after radical prostatectomy. *Journal of Clinical Oncology* **23**, 4146–4151 (2005).

46. Carlucci, J. R., Nabizada-Pace, F. & Samadi, D. B. Robot-assisted laparoscopic radical prostatectomy: technique and outcomes of 700 cases. *International journal of biomedical science: IJBS* **5**, 201 (2009).

47. Bagshaw, M. A., Kaplan, H. S. & Sagerman, R. H. Linear accelerator supervoltage radiotherapy: VII. Carcinoma of the prostate. *Radiology* **85**, 121–129 (1965).

48. Bolla, M. *et al.* Duration of androgen suppression in the treatment of prostate cancer. *New England Journal of Medicine* **360**, 2516–2527 (2009).

49. D'Amico, A. V., Chen, M.-H., Renshaw, A. A., Loffredo, M. & Kantoff, P. W. Androgen suppression and radiation vs radiation alone for prostate cancer: a randomized trial. *Jama* **299**, 289–295 (2008).

50. Wiegel, T. *et al.* Phase III postoperative adjuvant radiotherapy after radical prostatectomy compared with radical prostatectomy alone in pT3 prostate cancer with postoperative undetectable prostate-specific antigen. *Clinical Oncology* (2007).

51. Thompson, I. M. *et al.* Adjuvant radiotherapy for pathologically advanced prostate cancer: a randomized clinical trial. *Jama* **296**, 2329–2335 (2006).

52. Rogowski, P. *et al.* Radiotherapy of oligometastatic prostate cancer: a systematic review. *Radiation Oncology* **16**, 1–16 (2021).

53. Zelefsky, M. J., Fuks, Z. & Leibel, S. A. Intensity-modulated radiation therapy for prostate cancer. in *Seminars in radiation oncology* vol. 12 229–237 (Elsevier, 2002).

54. Morris, W. J. *et al.* Low-dose-rate brachytherapy is superior to dose-escalated EBRT for unfavourable risk prostate cancer: the results of the ASCENDE-RT* randomized control trial. *Brachytherapy* **14**, S12 (2015).

55. Stock, R. G., Cahlon, O., Cesaretti, J. A., Kollmeier, M. A. & Stone, N. N. Combined modality treatment in the management of high-risk prostate cancer. *International Journal of Radiation Oncology* Biology* Physics* **59**, 1352–1359 (2004).

56. Shore, N. D. *et al.* Oral relugolix for androgen-deprivation therapy in advanced prostate cancer. *New England Journal of Medicine* **382**, 2187–2196 (2020).

57. Balk, S. P. Androgen receptor as a target in androgen-independent prostate cancer. *Urology* **60**, 132–138 (2002).

58. Sweeney, C. J. *et al.* Chemohormonal therapy in metastatic hormone-sensitive prostate cancer. *New England Journal of Medicine* **373**, 737–746 (2015).

59. James, N. D. *et al.* Addition of docetaxel, zoledronic acid, or both to first-line long-term hormone therapy in prostate cancer (STAMPEDE): survival results from an adaptive, multiarm, multistage, platform randomised controlled trial. *The Lancet* **387**, 1163–1177 (2016).

60. James, N. D. *et al.* Abiraterone for prostate cancer not previously treated with hormone therapy. *New England Journal of Medicine* **377**, 338–351 (2017).

61. Fizazi, K. *et al.* Abiraterone plus prednisone in metastatic, castration-sensitive prostate cancer. *New England Journal of Medicine* **377**, 352–360 (2017).

62. Davis, I. D. *et al.* Enzalutamide with standard first-line therapy in metastatic prostate cancer. *New England Journal of Medicine* **381**, 121–131 (2019).

63. Attard, G., Reid, A. H., Yap, T. A., Raynaud, F. & Dowsett, M. Re: Phase I clinical trial of a selective inhibitor of CYP17, abiraterone acetate, confirms that castration-resistant prostrate cancer commonly remains hormone driven. *Journal of clinical oncology* **26**, 4563–4571 (2008).

64. Haidar, S., Ehmer, P. B., Barassin, S., Batzl-Hartmann, C. & Hartmann, R. W. Effects of novel 17α-hydroxylase/C17, 20-lyase (P450 17, CYP 17) inhibitors on androgen biosynthesis in vitro and in vivo. *The Journal of steroid biochemistry and molecular biology* **84**, 555–562 (2003).

65. De Bono, J. S. *et al.* Abiraterone and increased survival in metastatic prostate cancer. *New England Journal of Medicine* **364**, 1995–2005 (2011).

66. Fizazi, K. *et al.* Abiraterone acetate for treatment of metastatic castration-resistant prostate cancer: final overall survival analysis of the COU-AA-301 randomised, double-blind, placebo-controlled phase 3 study. *The lancet oncology* **13**, 983–992 (2012).

67. Logothetis, C. J., Efstathiou, E., Manuguid, F. & Kirkpatrick, P. Abiraterone acetate. *Nature Reviews Drug Discovery* **10**, 573 (2011).

68. Ryan, C. J. *et al.* Abiraterone in metastatic prostate cancer without previous chemotherapy. *New England Journal of Medicine* **368**, 138–148 (2013).

69. Scher, H. I. *et al.* Increased survival with enzalutamide in prostate cancer after chemotherapy. *New England Journal of Medicine* **367**, 1187–1197 (2012).

70. Fizazi, K. *et al.* Effect of enzalutamide on time to first skeletal-related event, pain, and quality of life in men with castration-resistant prostate cancer: results from the randomised, phase 3 AFFIRM trial. *The lancet oncology* **15**, 1147–1156 (2014).

71. Beer, T. M. *et al.* Enzalutamide in metastatic prostate cancer before chemotherapy. *New England Journal of Medicine* **371**, 424–433 (2014).

72. Beer, T. M. *et al.* Enzalutamide in men with chemotherapy-naive metastatic castration-resistant prostate cancer: extended analysis of the phase 3 PREVAIL study. *European urology* **71**, 151–154 (2017).

73. Tran, C. *et al.* Development of a second-generation antiandrogen for treatment of advanced prostate cancer. *Science* **324**, 787–790 (2009).

74. Watson, P. A., Arora, V. K. & Sawyers, C. L. Emerging mechanisms of resistance to androgen receptor inhibitors in prostate cancer. *Nature Reviews Cancer* **15**, 701–711 (2015).

75. Petrylak, D. P. *et al.* Docetaxel and estramustine compared with mitoxantrone and prednisone for advanced refractory prostate cancer. *New England Journal of Medicine* **351**, 1513–1520 (2004).

76. Berthold, D. R. *et al.* Docetaxel plus prednisone or mitoxantrone plus prednisone for advanced prostate cancer: updated survival in the TAX 327 study. *Journal of Clinical Oncology* **26**, 242–245 (2008).

77. De Bono, J. S. *et al.* Prednisone plus cabazitaxel or mitoxantrone for metastatic castration-resistant prostate cancer progressing after docetaxel treatment: a randomised open-label trial. *The Lancet* **376**, 1147–1154 (2010).

78. Oudard, S. *et al.* Cabazitaxel versus docetaxel as first-line therapy for patients with metastatic castration-resistant prostate cancer: a randomized phase III trial—FIRSTANA. *Journal of Clinical Oncology* **35**, 3189–3197 (2017).

79. Conteduca, V. *et al.* Clinical features of neuroendocrine prostate cancer. *European journal of cancer* **121**, 7–18 (2019).

80. Dunn, G. P., Bruce, A. T., Ikeda, H., Old, L. J. & Schreiber, R. D. Cancer immunoediting: from immunosurveillance to tumor escape. *Nature immunology* **3**, 991–998 (2002).

81. Kantoff, P. W. *et al.* Sipuleucel-T immunotherapy for castration-resistant prostate cancer. *New England Journal of Medicine* **363**, 411–422 (2010).

82. Sartor, O. *et al.* Survival of African-American and Caucasian men after sipuleucel-T immunotherapy: outcomes from the PROCEED registry. *Prostate cancer and prostatic diseases* **23**, 517–526 (2020).

83. Pol, J. G. *et al.* Trial Watch: Oncolytic viro-immunotherapy of hematologic and solid tumors. *Oncoimmunology* **7**, e1503032 (2018).

84. Kwok, G., Yau, T. C., Chiu, J. W., Tse, E. & Kwong, Y.-L. Pembrolizumab (Keytruda). *Human vaccines & immunotherapeutics* **12**, 2777–2789 (2016).

85. Le, D. T. *et al.* PD-1 blockade in tumors with mismatch-repair deficiency. *New England Journal of Medicine* **372**, 2509–2520 (2015).

86. Marcus, L., Lemery, S. J., Keegan, P. & Pazdur, R. FDA approval summary: pembrolizumab for the treatment of microsatellite instability-high solid tumors. *Clinical Cancer Research* **25**, 3753–3758 (2019).

87. Subbiah, V., Solit, D. B., Chan, T. A. & Kurzrock, R. The FDA approval of pembrolizumab for adult and pediatric patients with tumor mutational burden (TMB)≥ 10: a decision centered on empowering patients and their physicians. *Annals of oncology: official journal of the European Society for Medical Oncology* **31**, 1115–1118 (2020).

88. Antonarakis, E. S. *et al.* Pembrolizumab for treatment-refractory metastatic castration-resistant prostate cancer: multicohort, open-label phase II KEYNOTE-199 study. *Journal of Clinical Oncology* **38**, 395 (2020).

89. Parker, C. *et al.* Alpha emitter radium-223 and survival in metastatic prostate cancer. *New England Journal of Medicine* **369**, 213–223 (2013).

90. Yamada, Y. *et al.* Prognostic value of an inflammatory index for patients with metastatic castration-resistant prostate cancer. *The Prostate* **80**, 559–569 (2020).

91. Du, Y. *et al.* Practical recommendations for radium-223 treatment of metastatic castration-resistant prostate cancer. *European journal of nuclear medicine and molecular imaging* **44**, 1671–1678 (2017).

92. Litwin, M. S. & Tan, H.-J. The diagnosis and treatment of prostate cancer: a review. *Jama* **317**, 2532–2542 (2017).

93. xofigo-article-20-procedure-ema-restricts-use-prostate-cancer-medicine-xofigo_en-0.pdf.

94. Smith, M. *et al.* Addition of radium-223 to abiraterone acetate and prednisone or prednisolone in patients with castration-resistant prostate cancer and bone metastases (ERA 223): a randomised, double-blind, placebo-controlled, phase 3 trial. *The Lancet Oncology* **20**, 408–419 (2019).

95. Parker, C. *et al.* Alpha emitter radium-223 and survival in metastatic prostate cancer. *New England Journal of Medicine* **369**, 213–223 (2013).

96. Tan, N. *et al.* PSMA-targeted radiotracers versus 18F fluciclovine for the detection of prostate cancer biochemical recurrence after definitive therapy: a systematic review and meta-analysis. *Radiology* **296**, 44–55 (2020).

97. Yordanova, A. *et al.* Outcome and safety of rechallenge [177 Lu] Lu-PSMA-617 in patients with metastatic prostate cancer. *European journal of nuclear medicine and molecular imaging* **46**, 1073–1080 (2019).

98. Hofman, M. S. *et al.* [177Lu] Lu-PSMA-617 versus cabazitaxel in patients with metastatic castration-resistant prostate cancer (TheraP): a randomised, open-label, phase 2 trial. *The Lancet* **397**, 797–804 (2021).

99. Rahbar, K., Bodei, L. & Morris, M. J. Is the vision of radioligand therapy for prostate cancer becoming a reality? An overview of the phase III VISION trial and its importance for the future of theranostics. *Journal of Nuclear Medicine* **60**, 1504–1506 (2019).

100. Feuerecker, B. *et al.* Activity and adverse events of actinium-225-PSMA-617 in advanced metastatic castration-resistant prostate cancer after failure of lutetium-177-PSMA. *European Urology* **79**, 343–350 (2021).

101. Deegen, P. *et al.* The PSMA-targeting Half-life Extended BiTE Therapy AMG 160 has Potent Antitumor Activity in Preclinical Models of Metastatic Castration-resistant Prostate Cancer. *Clinical Cancer Research* **27**, 2928–2937 (2021).

102. Robinson, D. *et al.* Integrative clinical genomics of advanced prostate cancer. *Cell* **161**, 1215–1228 (2015).

103. Castro, E., Goh, C. & Olmos, D. Germline BRCA mutations are associated with higher risk of nodal involvement, distant metastasis, and poor survival outcomes in prostate cancer. *Journal of Clinical Oncology* **31**, 1748 (2013).

104. Lord, C. J. & Ashworth, A. PARP inhibitors: Synthetic lethality in the clinic. *Science* **355**, 1152–1158 (2017).

105. de Bono, J. *et al.* Olaparib for metastatic castration-resistant prostate cancer. *New England Journal of Medicine* **382**, 2091–2102 (2020).

106. Agarwal, N. *et al.* Talapro-2: A 2-part, placebo-controlled phase 3 study of talazoparib (TALA) with background enzalutamide (ENZA) in metastatic castration-resistant prostate cancer (mCRPC) with DNA damage repair deficiencies. (2018).

107. Schmid, S. *et al.* Activity of platinum-based chemotherapy in patients with advanced prostate cancer with and without DNA repair gene aberrations. *JAMA network open* **3**, e2021692–e2021692 (2020).

108. Janku, F., Yap, T. A. & Meric-Bernstam, F. Targeting the PI3K pathway in cancer: are we making headway? *Nature reviews Clinical oncology* **15**, 273–291 (2018).

109. Jamaspishvili, T. *et al.* Clinical implications of PTEN loss in prostate cancer. *Nature Reviews Urology* **15**, 222–234 (2018).

110. De Bono, J. S. *et al.* IPATential150: Phase III study of ipatasertib (ipat) plus abiraterone (abi) vs placebo (pbo) plus abi in metastatic castration-resistant prostate cancer (mCRPC). *Annals of Oncology* **31**, 1153–1154 (2020).

111. Abida, W. *et al.* Analysis of the prevalence of microsatellite instability in prostate cancer and response to immune checkpoint blockade. *JAMA oncology* **5**, 471–478 (2019).

112. Antonarakis, E. S. *et al.* CDK12-altered prostate cancer: clinical features and therapeutic outcomes to standard systemic therapies, poly (ADP-Ribose) polymerase inhibitors, and PD-1 inhibitors. *JCO precision oncology* **4**, 370–381 (2020).

113. Yamada, Y. & Beltran, H. The treatment landscape of metastatic prostate cancer. *Cancer Letters* (2021).

114. Joseph, D. B., Turco, A. E., Vezina, C. M. & Strand, D. W. Progenitors in prostate development and disease. *Developmental Biology* **473**, 50–58 (2021).

115. Cunha, G. R. *et al.* Development of the human prostate. *Differentiation* **103**, 24–45 (2018).

116. Collins, A. T., Habib, F. K., Maitland, N. J. & Neal, D. E. Identification and isolation of human prostate epithelial stem cells based on α2β1-integrin expression. *Journal of cell science* **114**, 3865–3872 (2001).

117. Goldstein, A. S. *et al.* Trop2 identifies a subpopulation of murine and human prostate basal cells with stem cell characteristics. *Proceedings of the National Academy of Sciences* **105**, 20882–20887 (2008).

118. Hudson, D. L., O'Hare, M., Watt, F. M. & Masters, J. R. Proliferative heterogeneity in the human prostate: evidence for epithelial stem cells. *Laboratory investigation* **80**, 1243–1250 (2000).

119. Karthaus, W. R. *et al.* Identification of multipotent luminal progenitor cells in human prostate organoid cultures. *Cell* **159**, 163–175 (2014).

120. Leong, K. G., Wang, B.-E., Johnson, L. & Gao, W.-Q. Generation of a prostate from a single adult stem cell. *Nature* **456**, 804–808 (2008).

121. Richardson, G. D. *et al.* CD133, a novel marker for human prostatic epithelial stem cells. *Journal of cell science* **117**, 3539–3545 (2004).

122. Karthaus, W. R. *et al.* Regenerative potential of prostate luminal cells revealed by single-cell analysis. *Science* **368**, 497–505 (2020).

123. Packer, J. R. & Maitland, N. J. The molecular and cellular origin of human prostate cancer. *Biochimica et Biophysica Acta (BBA)-Molecular Cell Research* **1863**, 1238–1260 (2016).

124. Shen, M. M. & Abate-Shen, C. Molecular genetics of prostate cancer: new prospects for old challenges. *Genes & development* **24**, 1967–2000 (2010).

125. DeMarzo, A. M., Nelson, W. G., Isaacs, W. B. & Epstein, J. I. Pathological and molecular aspects of prostate cancer. *The Lancet* **361**, 955–964 (2003).

126. Wang, G., Zhao, D., Spring, D. J. & DePinho, R. A. Genetics and biology of prostate cancer. *Genes & development* **32**, 1105–1140 (2018).

127. Henry, G. H. *et al.* A cellular anatomy of the normal adult human prostate and prostatic urethra. *Cell reports* **25**, 3530–3542 (2018).

128. Hudson, D. L. *et al.* Epithelial cell differentiation pathways in the human prostate: identification of intermediate phenotypes by keratin expression. *Journal of Histochemistry & Cytochemistry* **49**, 271–278 (2001).

129. Xue, Y., Smedts, F., Debruyne, F. M., de la Rosette, J. J. & Schalken, J. A. Identification of intermediate cell types by keratin expression in the developing human prostate. *The Prostate* **34**, 292–301 (1998).

130. Mills, I. G. Maintaining and reprogramming genomic androgen receptor activity in prostate cancer. *Nature Reviews Cancer* **14**, 187–198 (2014).

131. Tan, M. E., Li, J., Xu, H. E., Melcher, K. & Yong, E. Androgen receptor: structure, role in prostate cancer and drug discovery. *Acta Pharmacologica Sinica* **36**, 3–23 (2015).

132. Di Sant'Agnese, P. A. Neuroendocrine cells of the prostate and neuroendocrine differentiation in prostatic carcinoma: a review of morphologic aspects. *Urology* **51**, 121–124 (1998).

133. Shariff, A. H. & Ather, M. H. Neuroendocrine differentiation in prostate cancer. *Urology* **68**, 2–8 (2006).

134. Gelmann, E. P. Molecular biology of the androgen receptor. *Journal of Clinical Oncology* **20**, 3001–3015 (2002).

135. Verma, S. *et al.* Resistance to second generation antiandrogens in prostate cancer: pathways and mechanisms. *Cancer Drug Resistance* **3**, 742–761 (2020).

136. Chen, Y., Zhou, Q., Hankey, W., Fang, X. & Yuan, F. Second generation androgen receptor antagonists and challenges in prostate cancer treatment. *Cell Death & Disease* **13**, 1–11 (2022).

137. Beltran, H. *et al.* Targeted next-generation sequencing of advanced prostate cancer identifies potential therapeutic targets and disease heterogeneity. *European urology* **63**, 920–926 (2013).

138. Balbas, M. D. *et al.* Overcoming mutation-based resistance to antiandrogens with rational drug design. *elife* **2**, e00499 (2013).

139. Azad, A. A. *et al.* Androgen Receptor Gene Aberrations in Circulating Cell-Free DNA: Biomarkers of Therapeutic Resistance in Castration-Resistant Prostate CancerAR Gene Aberrations in Circulating Cell-Free DNA. *Clinical cancer research* **21**, 2315–2324 (2015).

140. Korpal, M. *et al.* An F876L Mutation in Androgen Receptor Confers Genetic and Phenotypic Resistance to MDV3100 (Enzalutamide) F876L Mutation in AR Confers Resistance to MDV3100. *Cancer discovery* **3**, 1030–1043 (2013).

141. Joseph, J. D. *et al.* A Clinically Relevant Androgen Receptor Mutation Confers Resistance to Second-Generation Antiandrogens Enzalutamide and ARN-509AR F876L Confers Enzalutamide and ARN-509 Resistance. *Cancer discovery* **3**, 1020–1029 (2013).

142. Lu, C. & Luo, J. Decoding the androgen receptor splice variants. *Translational Andrology and Urology* **2**, 9 (2013).

143. Watson, P. A. *et al.* Constitutively active androgen receptor splice variants expressed in castration-resistant prostate cancer require full-length androgen receptor. *Proceedings of the national academy of sciences* **107**, 16759–16765 (2010).

144. Antonarakis, E. S. *et al.* AR-V7 and Resistance to Enzalutamide and Abiraterone in Prostate Cancer. *N Engl J Med* **371**, 1028–1038 (2014).

145. Efstathiou, E. *et al.* Molecular characterization of enzalutamide-treated bone metastatic castration-resistant prostate cancer. *European urology* **67**, 53–60 (2015).

146. Arora, V. K. *et al.* Glucocorticoid receptor confers resistance to antiandrogens by bypassing androgen receptor blockade. *Cell* **155**, 1309–1322 (2013).

147. Beltran, H. *et al.* Divergent clonal evolution of castration-resistant neuroendocrine prostate cancer. *nature medicine* **22**, 12 (2016).

148. Aggarwal, R. *et al.* Clinical and Genomic Characterization of Treatment-Emergent Small-Cell Neuroendocrine Prostate Cancer: A Multi-institutional Prospective Study. *JOURNAL OF CLINICAL ONCOLOGY* 15.

149. Beltran, H. *et al.* The role of lineage plasticity in prostate cancer therapy resistance. *Clin Cancer Res* clincanres.1423.2019 (2019) doi:10.1158/1078-0432.CCR-19-1423.

150. Mosele, F. *et al.* Recommendations for the use of next-generation sequencing (NGS) for patients with metastatic cancers: a report from the ESMO Precision Medicine Working Group. *Annals of Oncology* **31**, 1491–1505 (2020).

151. Cortes-Ciriano, I., Lee, S., Park, W.-Y., Kim, T.-M. & Park, P. J. A molecular portrait of microsatellite instability across multiple cancers. *Nature communications* **8**, 1–12 (2017).

152. Abida, W. *et al.* Microsatellite instability in prostate cancer and response to immune checkpoint blockade. (2018).

153. Abida, W. *et al.* Genomic correlates of clinical outcome in advanced prostate cancer. *Proc Natl Acad Sci USA* **116**, 11428–11436 (2019).

154. de Bono, J. S. *et al.* Randomized Phase II Study Evaluating Akt Blockade with Ipatasertib, in Combination with Abiraterone, in Patients with Metastatic Prostate Cancer with and without PTEN LossIpatasertib in Prostate Cancer with and without PTEN Loss. *Clinical Cancer Research* **25**, 928–936 (2019).

155. Kotani, N. *et al.* Characterization of exposure–response relationships of ipatasertib in patients with metastatic castration-resistant prostate cancer in the IPATential150 study. *Cancer Chemotherapy and Pharmacology* 1–11 (2022).

156. Mateo, J. *et al.* DNA-repair defects and olaparib in metastatic prostate cancer. *New England Journal of Medicine* **373**, 1697–1708 (2015).

157. Crumbaker, M., Khoja, L. & Joshua, A. M. AR signaling and the PI3K pathway in prostate cancer. *Cancers* **9**, 34 (2017).

158. Recondo, G. *et al.* Feasibility and first reports of the MATCH-R repeated biopsy trial at Gustave Roussy. *NPJ precision oncology* **4**, 1–8 (2020).

159. Alumkal, J. J. *et al.* Transcriptional profiling identifies an androgen receptor activity-low, stemness program associated with enzalutamide resistance. *Proceedings of the National Academy of Sciences* **117**, 12315–12323 (2020).

160. Wang, L. *et al.* A prospective genome-wide study of prostate cancer metastases reveals association of wnt pathway activation and increased cell cycle proliferation with primary resistance to abiraterone acetate–prednisone. *Annals of Oncology* **29**, 352–360 (2018).

161. Brady, L. *et al.* Inter-and intra-tumor heterogeneity of metastatic prostate cancer determined by digital spatial gene expression profiling. *Nature communications* **12**, 1–16 (2021).

162. Kumar, A. *et al.* Substantial interindividual and limited intraindividual genomic diversity among tumors from men with metastatic prostate cancer. *Nature medicine* **22**, 369–378 (2016).

163. Annala, M. *et al.* Circulating Tumor DNA Genomics Correlate with Resistance to Abiraterone and Enzalutamide in Prostate Cancer. *Cancer Discov* **8**, 444–457 (2018).

164. Schroeder, A. *et al.* Loss of Androgen Receptor Expression Promotes a Stem-like Cell Phenotype in Prostate Cancer through STAT3 SignalingIL-6/STAT3 Signaling Enhances Prostate Cancer Stem-like Cells. *Cancer research* **74**, 1227–1237 (2014).

165. Pal, S. K. *et al.* Identification of mechanisms of resistance to treatment with abiraterone acetate or enzalutamide in patients with castration-resistant prostate cancer (CRPC). *Cancer* **124**, 1216–1224 (2018).

166. Armstrong, A. J. *et al.* Prospective multicenter study of circulating tumor cell AR-V7 and taxane versus hormonal treatment outcomes in metastatic castration-resistant prostate cancer. *JCO Precision Oncology* **4**, 1285–1301 (2020).

167. He, M. X. *et al.* Transcriptional mediators of treatment resistance in lethal prostate cancer. *Nature medicine* **27**, 426–433 (2021).

168. Herberts, C. *et al.* Deep whole-genome ctDNA chronology of treatment-resistant prostate cancer. *Nature* **608**, 199–208 (2022).

169. Fizazi, K. *et al.* Phase 1 results of the ODM-208 first-in-human phase 1-2 trial in patients with metastatic castration-resistant prostate cancer (CYPIDES). (2022).

170. Le Moigne, R. *et al.* EPI-7386 is a novel N-terminal domain androgen receptor inhibitor for the treatment of prostate cancer. *Annals of Oncology* **30**, v189–v190 (2019).

171. Ku, S. Y. *et al.* Rb1 and Trp53 cooperate to suppress prostate cancer lineage plasticity, metastasis, and antiandrogen resistance. 7 (2017).

172. Bishop, J. L. *et al.* The Master Neural Transcription Factor BRN2 Is an Androgen Receptor–Suppressed Driver of Neuroendocrine Differentiation in Prostate CancerBRN2 Is an AR-Suppressed Driver of NEPC. *Cancer discovery* **7**, 54–71 (2017).

173. Akamatsu, S. *et al.* The placental gene PEG10 promotes progression of neuroendocrine prostate cancer. *Cell reports* **12**, 922–936 (2015).

174. Becht, E. *et al.* Estimating the population abundance of tissue-infiltrating immune and stromal cell populations using gene expression. *Genome biology* **17**, 1–20 (2016).

175. Erlandsson, A. *et al.* M2 macrophages and regulatory T cells in lethal prostate cancer. *The Prostate* **79**, 363–369 (2019).

176. Chiarugi, P., Paoli, P. & Cirri, P. Tumor microenvironment and metabolism in prostate cancer. in *Seminars in oncology* vol. 41 267–280 (Elsevier, 2014).

177. Bonollo, F., Thalmann, G. N., Kruithof-de Julio, M. & Karkampouna, S. The role of cancer-associated fibroblasts in prostate cancer tumorigenesis. *Cancers* **12**, 1887 (2020).

178. Byrum, A. K., Vindigni, A. & Mosammaparast, N. Defining and modulating 'BRCAness'. *Trends in cell biology* **29**, 740–751 (2019).

PERSPECTIVES IN CARRER DEVELOPMENT

I am a bioinformatician, and since 2018, I have been working as a PhD student in Oncogenomics at the Doctoral School of Cancer/Biology/Medicine/Health of the Faculty of Medicine at the University of Paris Saclay under the direction of Dr Yohann Loriot and Pr Karim Fizazi. I belong to INSERM U981 "Molecular Predictors and New Targets in Oncology", directed by Pr Fabrice Andre at Gustave Roussy Cancer Campus.

The thesis proposal we developed with Dr Yohann Loriot, entitled "Genomic profiling of metastatic castration-resistant prostate cancer (mCRPC)", aimed to use innovative computational algorithms to characterize metastatic tumors resistant to standard and approved therapies in males with advanced aggressive prostate cancer. With this project, I had the opportunity to focus on research questions that will potentially have a major and direct impact on the management of patients with mCRPC, a growing patient population in need of optimal treatment for survival. My research brings new insight with high importance, as I am studying tumors from patients with very advanced, non-curable cancer who initially benefited from the latest lines of treatment, but resistance is emerging. For this, I used new and innovative bioinformatics approaches and big cross-sectional data of patients from a prospective clinical trial developed on our Cancer Campus. In addition to exploring the mechanisms of primary resistance, we explored those of secondary resistance, by studying baseline biopsy pairs and resistance in these patients. The focus was on characterising molecular and clinical factors and their relationship to these resistances in relation to treatment with the new androgen receptor inhibitors (Enzalutamide/ Abiraterone). This makes our study original and unique as the knowledge still lacks any effect on these kinds of treatments for prostate cancer. It is interesting for clinicians, researchers and patients to avoid resistance to previous treatments for a rapid diagnosis and genomic-based therapy.

I have specialised in the processing of genomic data from prostate cancer patients. I devoted a considerable part of my training to the methodology of bioinformatics and translational research. In addition, I have acquired programming and organisational skills. I have a particular interest in studying the integration of metadata from genomic, clinical, biological and biostatistical aspects of prostate cancer patients. In addition, I have collaborated on several projects aimed at evaluating other biological issues related to 1) a very aggressive form of prostate cancer (the neuroendocrine phenotype), 2) the relevance of xenograft models developed in the laboratory, from biopsies of prostate cancer patients, and 3) the evaluation of the relevance of data from liquid biopsies compared to solid biopsies in the diagnosis of bladder cancer, in order to favour liquid biopsies in hospital practice. At Gustave Roussy, I also had the opportunity to mentor young medical oncologists and biologists. I am committed to pursue my career in applied genomic oncology research in genitourinary cancers, especially prostate cancer.

In parallel to my thesis, I have been managing the Gustave Roussy Association for Young researchers, as president, since 2020. This position has allowed me to acquire skills in seminar organisation and scientific communication, and enrich my professional network. Furthermore, I have received a new entrepreneurship perspective specific to the field of oncology by following the Onco-Entreprenal programme on the Cancer Campus. My experience at Gustave Roussy was very important for this phase of my career, where I went from being a student to a fully qualified young bioinformatician. I thoroughly appreciated this opportunity, scientifically and personally.

My long-term project goals are to: 1) lead my own research group and move into a mentoring position with executive and teaching responsibilities; 2) conduct collaborative, interdisciplinary and patient-centred research; 3) be an implementer of research innovations in clinical practice, and in particular to be involved in relevant clinical stakeholder activities; and 4) promote the immediate and significant impact of research, in particular: design, experimentally test identified genetic alterations with bioinformatics analyses, exploite specific biological approaches.

GLOSSARY

Allele	There are two or more DNA sequences present at a particular genetic locus. Often, one allele ("normal" DNA sequence) is common, and the other alleles (mutations) are rare. They may be the same, but often contain small differences. Thus, alleles include all versions of a particular gene. These differences and similarities together can produce important effects in the body. https://www.cancer.gov/publications/dictionaries/genetics-dictionary/expand/A, accessed 13 November 2022
BRCAness	Concept of the pathogenesis and vulnerability of multiple cancers. The The concept of 'BRCAness' defines the pathogenesis and vulnerability of multiple cancers.The canonical definition of BRCAness is a defect in homologous recombination repair, mimicking *BRCA1* or *BRCA2* loss[178].
Cancer phenotype prediction	Study to predict different types of tumors based on molecular or morphological data allows for better treatment of cancer patients.
Clonal evolution	Evolution of a population of genetically identical cells or DNA molecules
Clonal mutation	Mutation of a population of genetically identical cells or DNA molecules in tumoral sample
Clustering	Method of unsupervised classification of data that are close together by distance or similarities.
Copy number variation (CNV)	Deletion or an amplification of a segment of DNA of a size larger than 1 kilobase (kb) of nucleotides, causing a gene or a part of gene, or even a whole chromosome to have respectively less or more than the normal 2 copies. CNV can have an important influence in the expression of the lost or gained genes.
Driver mutations	Changes in the DNA sequence of genes that cause cells to become cancer cells and grow and spread in the body. Checking tumor tissue for driver mutations may help plan treatment to stop cancer cells from growing, including drugs that target a specific mutation. https://www.cancer.gov/publications/dictionaries/cancer-terms/def/driver-mutation, accessed 13 November 2022.
Epigentics	Research field of heritable changes that do not affect the DNA sequence but influence gene expression. https://www.cancer.gov/publications/dictionaries/genetics-dictionary/expand/E
FDR	False discovery rate is a method of conceptualizing the rate of type I errors in null hypothesis testing when conducting multiple comparisons.
Focal gain	Copy number alterations of limited size, frequently enriched for cancer driver genes.
Gain or Amplification	Presence of multiple copies of a chromosome or chromosomal segment. An amplification is a high-level gain of a chromosomal segment (frequently defined as > 8 copies)
Gene expression	Gene expression is the process by which the information encoded in a gene is used to either make RNA molecules that code for proteins or to make non-coding RNA molecules that serve other functions. https://www.genome.gov/genetics-glossary/Gene-Expression, accessed 13 November 2022.
Genome	Complete set of DNA, including both the genes and non-coding sequences.

Germline variant	Gene change in a reproductive cell that becomes incorporated into the DNA of every cell in the body of the offspring. The germline alteration can be hereditary, as it can be carried from a parent to a progenitor. https://www.cancer.gov/publications/dictionaries/genetics-dictionary/search/germline/?searchMode=Begins, accessed 13 November 2022.
GSEA	Gene Set Enrichment Analysis is a computational method that determines whether an a priori defined set of genes shows statistically significant, concordant differences between two biological states (e.g. phenotypes). https://software.broadinstitute.org/cancer/software/gsea/wiki/index.php/Gsea_Algorithm, accessed 13 November 2022.
Hazard ratios	Measure of how often a particular event happens in one group compared to how often it happens in another group, over time. In cancer research, hazard ratios are often used in clinical trials to measure survival at any point in time in a group of patients who have been given a specific treatment compared to a control group given another treatment or a placebo. A hazard ratio of one means that there is no difference in survival between the two groups. A hazard ratio of greater than one or less than one means that survival was better in one of the groups.
Immunohisto-Chemistry (IHC)	Histological approach to detect protein expression levels
Inframe indel	Insertion or deletion of nucleotides in the same open reading frame
LOH	Also called loss of heterozygosity. If there is one normal and one abnormal allele at a particular locus, as might be seen in an inherited autosomal dominant cancer susceptibility disorder, loss of the normal allele produces a locus with no normal function. When the loss of heterozygosity involves the normal allele, it creates a cell that is more likely to show malignant growth if the altered gene is a tumor suppressor gene. https://www.cancer.gov/publications/dictionaries/genetics-dictionary/expand/L, accessed 13 November 2022.
Loss/deletion	Decrease in copy number of a chromosome or chromosomal segment.
Marker gene	DNA sequence with a known physical location on a chromosome. Genetic markers and genes that are close to each other on a chromosome tend to be inherited together. Genetic markers vary between individuals to the extent that they can be used to help find a nearby gene causing a certain disease or trait within a family. Examples of genetic markers are single polymorphism nucleotides (SNPs), restriction fragment length polymorphisms (RFLPs), variable number of tandem repeats (VNTRs), microsatellites, and copy number variants (CNVs). Genetic markers may or may not have a known function. https://www.cancer.gov/publications/dictionaries/genetics-dictionary/expand/G, accessed 13 November 2022.
Metasample	Aggregation of values for individual samples
Microsatellite	Repetitive segments of DNA scattered throughout the genome in noncoding regions between genes or within genes (introns). They are often used as markers for linkage analysis because of their naturally occurring high variability in repeat number between individuals. These regions are inherently genetically unstable and susceptible to mutations. https://www.cancer.gov/publications/dictionaries/genetics-dictionary/expand/M, accessed 13 November 2022.
Missense mutation	Genetic alteration in which a single base pair substitution alters the genetic code in a way that produces an amino acid that is different from the usual amino acid at that position.

	Some missense variants (or mutations) will alter the function of the protein. Also called missense variant. https://www.cancer.gov/publications/dictionaries/genetics-dictionary/expand/M, accessed 13 November 2022.
MSI	Cells feature that contain an abnormality in DNA mismatch repair. The presence of MSI can be a marker of a germline pathogenic variant in one of the DNA mismatch repair genes, as in the case of Lynch syndrome. MSI can also occur sporadically. Also called microsatellite instability. https://www.cancer.gov/publications/dictionaries/genetics-dictionary/expand/M, accessed 13 November 2022.
Mutational signature	Somatic mutations are present in all cells of the human body and occur throughout life. They are the consequence of multiple mutational processes, including the intrinsic slight infidelity of the DNA replication machinery, exogenous or endogenous mutagen exposures, enzymatic modification of DNA and defective DNA repair. Different mutational processes generate unique combinations of mutation types, termed "Mutational Signatures". https://cancer.sanger.ac.uk/signatures/, accessed 13 November 2022.
Nonsense mutation	Genetic alteration that causes the premature termination of a protein. The altered protein may be partially or completely inactivated, resulting in a change or loss of protein function. Also called nonsense variant. https://www.cancer.gov/publications/dictionaries/genetics-dictionary/expand/N, accessed 13 November 2022.
Omics	All fields of study in high-throughput molecular biology, commonly ending in -omics, such as genomics, proteomics or metabolomics.
Passengers genes	Each cancer is characterized by numerous aberrations in its genome. Only a subset of these aberrations contributes to the tumor initiation and progression. Contributing aberrations are referred to as 'drivers', the non-contributing aberrations as 'passengers'.
Phenotype	Measurable functional and structural characteristics of an organism as determined by the interaction of the genotype with the environment. https://www.ncbi.nlm.nih.gov/probe/docs/glossary/#s, accessed 13 November 2022.
Ploidy	Number of sets of chromosomes in a cell, or in the cells of an organism.
P-value	Statistical term used to show whether a difference found between groups being compared is due to chance. A small p-value usually means that the difference between groups is not due to chance alone, but is due to some other factor, such as a treatment one of the groups received. A large p-value usually means that the difference between groups is probably due to chance alone. https://www.cancer.gov/publications/dictionaries/cancer-terms/expand/P, accessed 13 November 2022.
RNA sequencing	Sequencing technique which uses next-generation sequencing (NGS) to reveal the presence and quantity of RNA in a biological sample at a given moment, analyzing the continuously changing cellular transcriptome.
Splicing	Process by which introns, the noncoding regions of genes, are excised out of the primary messenger RNA transcript, and the exons (e.g. coding regions) are joined together to generate mature messenger RNA. The latter serves as the template for synthesis of a specific protein.

	https://www.cancer.gov/publications/dictionaries/genetics-dictionary/expand/S, accessed 13 November 2022.
Silent mutation	Mutation occurs without a change in the protein sequence
SNP	Single Nucleotide Polymorphism. The most common form of DNA variation, alterations to a single base. If the SNP is in a gene, it can disrupt the gene's function. Most SNPs do not occur in genes but can be associated with other types of DNA variation and so are used effectively as markers. Typically, SNPs are biallelic, although very rarely tri- or tetraallelic forms can be found. The average frequency of SNPs in the human genome is approximately one per 1,000 bp https://www.ncbi.nlm.nih.gov/probe/docs/glossary/#s, accessed 13 November 2022.
Somatic variant	An alteration in DNA that occurs after conception and is not present within the germline. Somatic variants can occur in any of the cells of the body except the germ cells and therefore are not passed on to children. Somatic variants can (but do not always) cause cancer or other diseases
Subclonal mutation	Mutation of sub population of genetically identical cells in tumoral sample
Translocation	Chromosomal rearrangement in which a chromosomal segment breaks off and reattaches to a nonhomologous chromosome or a new site on the same chromosome. There are multiple types of translocations, including reciprocal and nonreciprocal translocations. Reciprocal translocations are when parts of two chromosomes exchange places. Nonreciprocal translocations are when a large part of one chromosome is transferred to another chromosome. https://gatk.broadinstitute.org/hc/en-us/articles/9022476791323-Structural-Variants, accessed 13 November 2022.
Truncating mutation	Mutation lead to a truncated protein
Tumor profiling	Laboratory test to check for certain genes or gene mutations (changes), proteins, or other biomarkers in a sample of tumor tissue. Tumor profiling may be used to help plan treatment and predict whether cancer will come back or spread to other parts of the body. A key step in the context of precision medicine is to identify actionable genomic alterations in the tumors of patients, allowing appropriate targeted therapies to be applied to patients targeting these specific alterations. https://www.cancer.gov/publications/dictionaries/cancer-terms/def/tumor-profiling, accessed 13 November 2022.
Tumor purity	Proportion of cancer cells in a tumor sample
Whole Exome sequencing	Exome sequencing is a high-throughput sequencing method that captures and selectively sequences the segment of the genome corresponding to protein coding. The exome represents less than 2% of the human genome and includes a majority of known disease-causing variants, particularly in cancer. For this reason, WES is a cost-effective option for identifying genetic alterations compared to whole genome sequencing.
Z-score	Score that indicates how many standard deviations a value is above or below the mean. https://www.cancer.gov/publications/dictionaries/genetics-dictionary/expand/Z, accessed 13 November 2022.

SYNTHÈSE EN FRANÇAIS

Le cancer de la prostate est le cancer le plus fréquent et consitue la troisième cause de décès par cancer chez l'homme dans les pays industrialisés. Le traitement systémique de première intention consiste en une thérapie de déprivation androgénique par castration chirurgicale ou médicamenteuse. Le cancer de la prostate métastatique résistant à la castration (mCRPC) est considéré comme incurable. Son traitement repose sur de la chimiothérapie ou des inhibiteurs de la voie du récepteur des androgènes (ARPIs) tels que l'enzalutamide ou l'abiratérone. Même si les ARPIs sont efficaces initialement chez la majorité des patients, environ 20% des patients n'en tirent pas bénéfice (résistance primaire) et ceux chez qui le traitement est efficace finissent par développer une maladie résistante aux ARPIs (résistance secondaire ou acquise). Les mécanismes de résistance sont multiples et extrêmement complexes. Plusieurs études se sont concentrées sur les mécanismes de résistance primaire, mais il existe très peu d'études axées sur les mécanismes de résistance secondaire. Des études antérieures, dont une majorité utilisant des modèles précliniques, ont suggéré que les altérations du récepteur aux androgènes lui-même telles que les variants d'épissage (en particulier AR-V7) sont associés à la résistance primaire et secondaire. Cependant, ce biomarqueur n'est pas utilisé en pratique courante. L'activation de voies de signalisation alternatives peut également être responsable de la résistance. D'autres mécanismes de résistance, encore peu connus et étudiés, incluent des modifications épigénétiques et l'activation d'autres facteurs de transcription. L'objectif de cette thèse était d'étudier les mécanismes de résistance aux ARPIs chez les patients atteints de mCRPC.

Pour cela, nous avons développé une étude prospective (MATCH-R) permettant de prélever des biopsies tumorales de patients traités par des ARPIs. Un séquençage de l'exome et du transcriptome ont été réalisés. Les relations entre les anomalies génomiques et la survenue de résistance aux ARPIs ont été analysées. Les résultats suggèrent que la résistance primaire aux ARPIs résulte de l'activation de plusieurs

phénomènes biologiques incluant (1) une réduction de l'activité de la voie de l'AR (2) une activation de la transition épithélio-mésenchymateuse (EMT) et de programme de cellules souches, et (3) l'activation du signal protéique de la voie de signalisation Hedgehog (Hh), suggérant un bénéfice potentiel de l'inhibition de la voie Hh chez les patients présentant une activation Hh. Aucune anomalie liée à l'ADN n'est associée à la résistance primaire. La collection de plusieurs échantillons au moment de la résistance secondaire a permis de caractériser l'évolution clonale de ces tumeurs qui suit essentiellement un modèle d'évolution « en branche » avec acquisition séquentielle de nouvelles altérations de gènes importantes (*AR*, *PTEN*, *RB1*). L'analyse du transcriptome montre l'activation de voie de signalisation impliquée dans la prolifération cellulaire et de voies conduisant à une différenciation neuro-endocrine. Les résultats de cette étude doivent être confirmés par des études indépendantes au stade mCRPC ou à des stades moins avancés compte-tenu de l'utilisation plus précoces des ARPIs en particulier dans la situation de cancer de la prostate hormono-sensible. Des travaux sont en cours au laboratoire pour valider fonctionnellement l'intérêt potentiel des inhibiteurs de Hh qui sont déjà utilisés dans le traitement du cancer épidermoïde de la peau.

Title : Genomic profiling of metastatic castration-resistant prostate cancer

Keywords: Prostate cancer, hormonotherapy, androgen receptor, resistance, translational research

Abstract: Prostate cancer is the second most common cause of cancer deaths in industrialized countries. First line systemic therapy is androgen-deprivation therapy using surgical or pharmacological castration. Metastatic castration-resistant prostate cancer (mCRPC) is treated by androgen receptor pathway inhibitors (ARPIs, Enzalutamide/Abiraterone), however a primay or acquired resistance will develop to ARPIs, thus mCRPC is still incurable. The mechanisms of resistance are still unknown and complex. Studies have focused on primary resistance mechanisms, but very few of them focused on mechanisms of secondary resistance.The aim of this thesis was to study mechanisms of resistance to the ARPIs in men with mCRPC. We proceeded to the assessment of genetic and protein abnormalities (WES,RNA-seq) as well as of clinical characteristics of patients included in the MATCH-R clinical trial. Then, we studied the relationships between these factors and primary or secondary treatment resistance and developed protein scores to predict those resistances. The results suggest that resistance to ARPIs results from multiple protein signatures that are already activated before the start of treatment, including those related to (1) a reduction in AR pathway activity (2) activation of the epithelial-mesenchymal transition and stem cell program, and (3) activation of the Hedgehog (Hh) signaling pathway protein, suggesting a potential benefit from the Hh pathway inhibition among patients with Hh activation. DNA abnormalities that may cause primary resistance have not yet been identified. Collection of multiple samples at the time of secondary resistance allowed characterization of the clonal evolution of these tumors, which essentially follows a "branching" evolutionary pattern with sequential acquisition of important new gene alterations (*AR*, *PTEN*, *RB1*). Transcriptome analysis shows the activation of signaling pathways involved in cell proliferation and pathways leading to neuroendocrine differentiation. Further researchs are needed to validate these results in larger cohorts, as well as in experimental preclinical models. Furthermore, as Hh inhibitor drugs are already used in the treatment of several cancers, the specific alterations in the Hh pathway in mCRPC that respond to Hh inhibitors need to be elucidated, in order to develop targeted therapeutic options.

Titre : Profilage génomique du cancer de la prostate métastatique résistant à la castration

Mots clés : Cancer de la prostate, hormonothérapie, récepteur aux androgènes, résistance, recherche translationnelle

Résumé : Le cancer de la prostate est la deuxième cause de décès par cancer dans les pays industrialisés. Le traitement systémique standard est une thérapie de déprivation androgénique par castration chirurgicale ou pharmacologique. Le cancer de la prostate métastatique résistant à la castration (mCRPC) est traité par les inhibiteurs de la voie du récepteur des androgènes (ARPIs, Enzalutamide/Abiraterone), cependant, une résistance primaire ou secondaire se développe et le mCRPC reste donc incurable. Les mécanismes de résistance sont encore inconnus et complexes. Des études se sont concentrées sur les mécanismes de résistance primaire, mais il en existe très peu axées sur les mécanismes de résistance secondaire. L'objectif de cette thèse était d'étudier les mécanismes de résistance aux ARPIs chez les hommes atteints de mCRPC. Nous avons procédé à l'évaluation des anomalies génétiques (exome) et protéiques (RNA-seq) ainsi que des caractéristiques cliniques des patients inclus dans l'essai clinique MATCH-R. Ensuite, nous avons étudié les relations entre ces facteurs et la résistance primaire ou secondaire au traitement et développé des scores protéiques pour prédire ces résistances. Les résultats suggèrent que la résistance aux ARPIs résulte de multiples signatures protéiques déjà activées avant le début du traitement, incluant (1) une réduction de l'activité de la voie de l'AR, (2) une activation d' « EMT » et de programme de cellules souches, et (3) l'activation du signal protéique de la voie de signalisation Hedgehog (Hh), suggérant un bénéfice potentiel de l'inhibition de la voie Hh chez les patients présentant une activation Hh. La collection de plusieurs échantillons au moment de la résistance secondaire a permis de caractériser l'évolution clonale de ces tumeurs qui suit un modèle d'évolution « en branche » avec acquisition de nouvelles altérations de gènes importantes (*AR, PTEN*, *RB1*). L'analyse du transcriptome montre l'activation de la prolifération cellulaire et de la différenciation neuro-endocrine. Des recherches supplémentaires sont nécessaires pour valider ces résultats dans des cohortes plus importantes, ainsi que dans des modèles expérimentaux précliniques. Les inhibiteurs de Hh sont utilisés dans le traitement de certains cancers, ainsi les altérations spécifiques de la voie Hh dans le mCRPC qui répondent aux inhibiteurs de Hh doivent être élucidées, afin de développer des options thérapeutiques ciblées.